Fall 2014

Simulations of diffusion driven phase evolution in heterogenous solids

Subramanya Gautam Sadasiva
Purdue University

Graduate School Form
(Revised /)

PURDUE UNIVERSITY
GRADUATE SCHOOL
Thesis/Dissertation Acceptance

This is to certify that the thesis/dissertation prepared

By Subramanya Gautam Sadasiva

Entitled
Simulations of Diffusion Driven Phase Evolution in Heterogenous Solids

For the degree of Doctor of Philosophy

Is approved by the final examining committee:

Ganesh Subbarayan

R. Edwin Garcia

Marisol Koslowski

Anil K. Bajaj

To the best of my knowledge and as understood by the student in the Thesis/Dissertation Agreement, Publication Delay, and Certification/Disclaimer (Graduate School Form 32), this thesis/dissertation adheres to the provisions of Purdue University's "Policy on Integrity in Research" and the use of copyrighted material.

Ganesh Subbarayan

Approved by Major Professor(s): _____

_____

Approved by: Ganesh Subbarayan 10/15/2014

Head of the Graduate Program Date

SIMULATIONS OF DIFFUSION DRIVEN PHASE EVOLUTION IN HETEROGENOUS SOLIDS

A Dissertation

Submitted to the Faculty

of

Purdue University

by

Subramanya Gautam Sadasiva

In Partial Fulfillment of the

Requirements for the Degree

of

Doctor of Philosophy

December 2014

Purdue University

West Lafayette, Indiana

Á les temps en récherche Purdue.

ACKNOWLEDGMENTS

This was much harder than I thought it would be. The past 6 years have seen a lot of ups and downs. I have a lot of people to be thankful for and I would like to mention a few of them here. I would like to thank my advisor, Prof. Subbarayan, for his support as well as the many opportunities for growth that he has provided over the past few years. I'd also like to thank Profs. Bajaj, Garcia and Koslowski for serving as members on my advisory committee. I'd also like to thank Prof. Anderson for having served on my advisory committee for having served on my committee prior to his retirement. A lot of this work was done in close collaboration with the people at Intel DTS/PTM/TMM. I would like to thank Dr. Daniel Pantuso, Dr. Lei Jiang and Dr. Boris Voinov at Intel for many helpful technical discussions. Also at Intel, I'd like to thank Dr. Ravi Mahajan for his encouragement and many kind words. I'd like to thank Prof. Bruce Murray of SUNY Binghamton for a chance meeting, that encouraged me to carry on with my PhD when I was very seriously wavering in my resolve. I'd also like to thank Prof. Brad Lucier for two classes that had a significant impact on how I view mathematics.

At my group at Purdue, I'd like to thank Anirudh for being a very nice audience for ideas and a great friend. I thank Kritika, Abhishek, Nikhil, Dennis and Yuvraj for being amazing friends and also for a lot of emotional support. Outside of the group, I'd like to thank my roommate Supradeepa for being a great friend. Santosh, Dharik, Rasika, Vinod and Anuradha, thanks for forming the bulk of my social life. I'd like to thank Renu aunty for giving me a place to call home these last few months. I'd like to thank Mohan for being a great friend over the past 10 years, and also for introducing me to Prof. Subbarayan and for encouraging me to finish.

A lot of my work has been made very easy thanks to the efforts of various open source projects. I'd like to thank the developers of `libMesh`and `Petsc`for eliminating

a lot of tedious programming, and also for maintaining amazing forums, where all questions are instantly answered. I am shocked by some of the hours at which I have received answers. I hope someday to make a contribution to these codebases, so that somebody else may benefit.

Most importantly, I'd like to thank my family, my mother and father for encouraging a questioning attitude towards everything and for supporting me emotionally over the last few years. My sister Sharanya for being a great sister, and a frequent voice of reason. I'd like to thank my uncle and aunt in Huntsville for being a great source of encouragement, and my cousins Maitreyi and Karthik for all the emotional support.

If the reader is wondering, the dedication is a nod to *Cherchez la F.E.M*, from Strang and Fish. Multilingual puns are the best. This one means "To the times lost in research", Purdue being homophonous to *perdu* which means lost. As with all multilingual puns, the grammar doesn't quite work.

Finally, I'd like to thank Purdue, Intel Corporation and the SRC for paying for all this.

TABLE OF CONTENTS

Page

Page

LIST OF TABLES

LIST OF FIGURES

ABSTRACT

Sadasiva, Subramanya Gautam Ph.D., Purdue University, December 2014. Simulations of Diffusion Driven Phase Evolution in Heterogenous Solids. Major Professor: Ganesh Subbarayan, School of Mechanical Engineering.

With reduction in size, ever greater operational demands are placed on electronics components at all levels of the device, starting from the transistor level to the level of the package and the solder interconnects. Concurrently, there has been a move to more complicated materials systems in order to meet health and environmental guidelines. These trends of reducing size, increasing loads have increased the necessity to understand the mechanisms of the failure.

As the length scales are reduced, it becomes increasingly important to consider interfacial and micro-structural effects that can be safely ignored at larger length scales owing to the randomness. It has become important to model the effect of interfacial motion and micro-structural evolution due to diffusion on the reliability of microelectronics components. Examples of interfacial motion phenomena in solids include crack propagation, grain boundary motion, diffusion driven void motion through surface and bulk diffusion. The presence and evolution of these over the life-cycle of electronics components such as metal lines and solder joints presents a significant reliability challenge. The mathematical models that describe the evolution of these interfaces are usually formulated as systems of non-linear equations and hence, numerical methods provide an important method to study and understand them. The primary challenge in the study of these moving boundary problems is the tracking of the moving boundary and the application of appropriate boundary conditions on the moving boundary.

The phase field method tracks through smooth approximations of the Heaviside step and Dirac δ functions, which are maintained through the solution of a system of

nonlinear differential equations. In this work, phase field approaches are developed for the study of diffusion driven phase evolution problems. First a phase field model for the evolution of voids in solder joints owing to electromigration and stress-migration both at the interface due to the surface gradients of the electric potential, temperature, curvature and strain energy, as well as self diffusion in the bulk on account of the chemical potential gradients as well as the electromigration force. This is modeled using a vacancy diffusion mechanism, while the growth of the voids is assumed to be due to the absorption of voids at the interface of pre-existing voids. A formal asymptotic analysis is performed to show the equivalence of the diffuse interface model to its sharp interface equivalents. Several numerical examples are presented.

Finally, an $n-$phase system of Cahn–Hilliard equations is developed to allow for the simulation of void evolution and growth in a multi-phase system. This is derived through a micro-force balance in order to eliminate the use of Lagrange multipliers that are commonly seen in such methods. A limited formal asymptotic analysis is performed to show the equivalence of the model to the standard surface diffusion model in regions where only two phase are present. This is numerically implemented and various numerical examples of phase evolution under simple surface diffusion, as well as surface diffusion with electromigration are demonstrated.

1. INTRODUCTION

Interfacial effects and phenomena play an important role in determining the behavior of systems in nature as well as in technology. They are probably the most important source for scale effects in nature. This is largely due to the fact that bulk quantities scale with the length scale l as l^3 while interfacial quantities scale as l^2 [1]. The study of these interactions between the surface and the bulk become more complex, when their evolution needs to be tracked, as this necessitates the application of boundary conditions on moving interfaces. A few of these phenomena are described here.

- **Tumor Growth:** The growth of malignant tumors is driven by the availability of nutrients and the surface area available for the absorption of nutrients [2]. Any drug absorption to reduce the growth rate or increase the death of the tumor cells at the surface of the tumor is also governed by the available surface area (Chapter 1). This surface changes as old cells on the surface of the tumor die or new cells are born to take their place.

- **Solidification:** Solidification processes play a very important part in nature, and display very intriguing structures such as the structure of snow-flakes (Fig. 1.2). The growth of different spokes on a snowflake is amongst a lot of other factors also affected by the size and length scales of perturbations at the solidification front.

- **Grain Boundary Motion:** Grain boundary motion (Fig. 1.3) plays an important part in the mechanical properties of solids at small length scales. Grain boundary motion can be driven by a variety of factors including simple free energy minimization to motion driven by the diffusion of species [4]. As engineering systems become smaller, the effect of grain boundaries become significantly more important.

1.1 Moving Boundary Problems in Engineering

A particular focus in this thesis is the study of the effect of moving boundaries on the reliability of solder interconnects in electronics packages. As the scale of

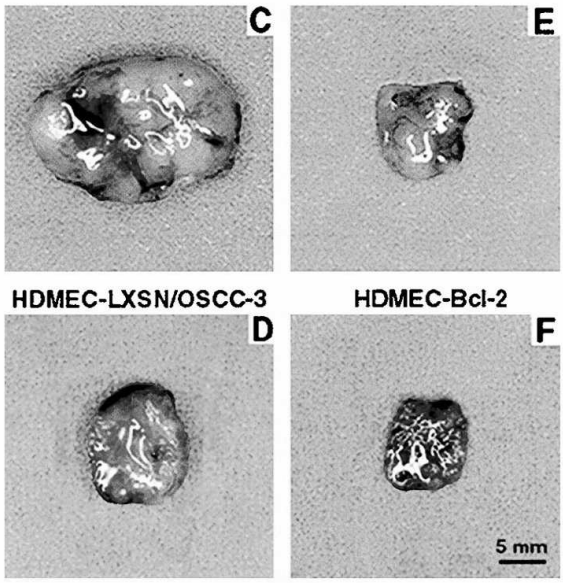

Figure 1.1. The degree to which blood vessels form in tumors depends on the surface area of the tumor, that changes as the tumor grows [3].

Figure 1.2. The formation of snowflakes is an example of dendritic solidification and the surface energy plays an important part *(by Wilson Bentley - Image in Public Domain)*.

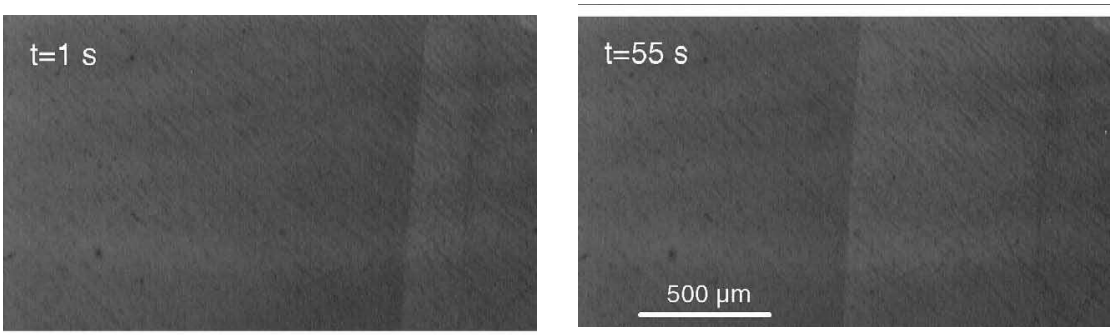

(a) t=1 sec (b) t=55 sec

Figure 1.3. Images of a 71°tilt grain boundary moving in a field of 12 T magnetic field at 410 °C after 1, 19, 37 and 55 s annealing [5].

these joints has shrunk, (from $> 100\mu m$ in previous generations to $\approx 10 - 15\mu m$ in the coming generations) the importance of interfacial effects for the prediction of behavior has increased. Also, the current densities have reached the order of $\approx 10^4 A\ cm^{-2}$ making electrically and thermally driven effects important. The recent move from PbSn solders to Pb-free solder has led to significantly more complicated material systems. These solder joints consist of 3-4 grains. This means that the averaging approximations that exist for larger solder joints are no longer valid for these small solder joints.

Moving boundaries play an important role in every stage of the manufacture of solder joints. The shape of the solder joints is largely determined by the minimization of the surface energy of the molten solder while the solder is being reflowed [6]. During this reflow process, buoyancy and thermocapillary recirculating flow is setup in the solder joints [7]. As the solder joint solidifies, bubbles of the flux gas in the solder joint rise to the interface and provide sites for further failure. The bubbles of the flux gas can also grow during this process due to the diffusion of the flux gas and the coalescence of dissolved flux gas at the surface of the void.

Once the solder joint is solidified, these voids can grow due to solid state diffusion effects. The shape and position of the voids can change due to spontaneous (chemical potential gradient driven as well as thermal, electrical and stress driven) surface

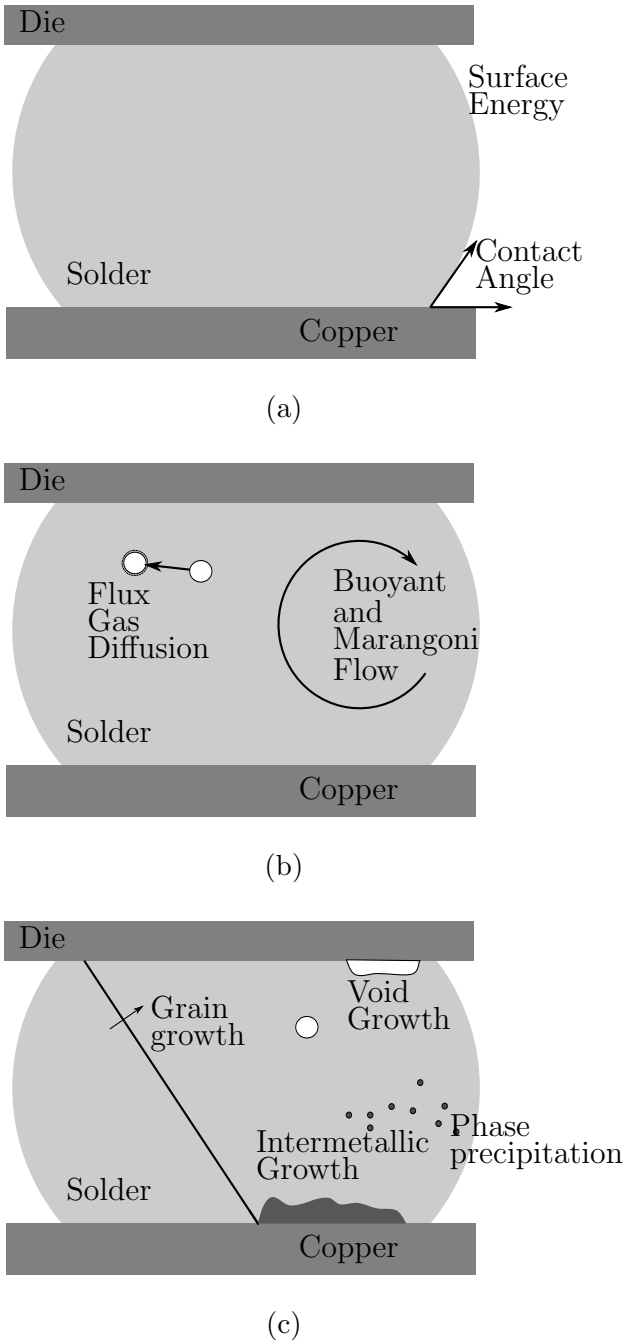

Figure 1.4. Moving boundary problems in Solder interconnects. (a): Solder bubble shape determination by surface energy minimization. (b): Formation and evolution of reflow voids. (c): Moving boundary problems in solder joints during use.

diffusion. While this progresses, self-diffusion (through a vacancy mechanism) and coalescence of vacancies at the void surface can cause the growth of these voids. Concurrent with the self-diffusion of tin, in Pb-Free solder joints, there is the added complication of the diffusion of silver and copper. These species can form precipitates of pure Ag, Cu or Cu−Sn and Ag−Sn intermetallics which affect the mechanical properties of the solder joint. The growth and evolution of these precipitates is also a phase evolution process and is governed by the surface energy and the local concentrations of Ag and Sn [8–10].

Recent designs for the solder interconnect possess large supplies of copper next to the solder material. Electrical and mechanical loading on the solder joints as well as the spontaneous chemical potential gradient across the copper-solder joint interface causes the copper to get consumed moving the interface. Some of this copper is consumed in the formation of intermetallic materials [11]. These intermetallic materials are brittle and provide paths for crack growth at the interface [12].

1.2 Literature Survey

In this section a short survey of the literature related to the thermodynamics of moving boundary problems, as well as the numerical methods used for their simulation is presented.

1.2.1 Thermodynamics of Diffusion Driven Moving Boundary Problems

To develop models for the evolution of voids and precipitates, it is important to develop an understanding of the non-equilibrium thermodynamics of moving boundary problems. The equilibrium thermodynamics for heterogenous systems was initially developed by Gibbs in his landmark work of 1877 [13]. This work developed equilibrium conditions for multi-species systems in fluid and gaseous systems. However, as solid state diffusion was an unknown phenomenon at this time, Gibbs did not consider these effects. In Gibbs' work, the chemical potential is defined (for the first time) as

a Lagrange multiplier ensuring constant mass/number density while maximizing the entropy or minimizing the energy. As this work exclusively deals with the determination of equilibrium conditions, it does not deal with evolution effects. The earliest developments of thermodynamics for non-equilibrium thermodynamics of heterogenous systems were in the work by Eckart [14, 15] and in Degroot and Mazur [16]. In this approach, the non-equilibrium effects are defined as consequences of gradients in the intensive quantities. In the classical non equilibrium treatment in [16], local equilibrium is used to define the value of the chemical potentials in terms of the other primary and secondary thermodynamic variables. The non-equilibrium fluxes are then defined as linear functions of the driving forces as,

$$\boldsymbol{J}_i = \sum_i L_{ij} F_j. \tag{1.1}$$

In Eq. (1.1), $\boldsymbol{J}_i$ is the irreversible flux of the $i-1$ components or of energy (as heat transfer). L_{ij} is a symmetric positive semi-definite matrix of coefficients and F_j is a vector containing the driving forces for irreversible processes ($\nabla\mu_i, \nabla T$ etc.).

A problem specific to the development of thermodynamics for solids is the treatment of non-hydrostatic equilibrium strains. In the classical Gibbs approach, the deformation variable is taken to be the volume or dilation and the conjugate variable is taken to be the pressure. At interfaces, the conditions of equilibrium at the interface in terms of equality of the chemical potential across the interface lead to the stress being hydrostatic on either side of the interface [17]. This is not reasonable in the case of solids. Another issue in the formulation of moving boundary problems in solids is that the kinematics is complicated by the existence of two ways in which the domain changes. The first being standard deformation processes of stresses and strains, the second the processes that correspond to the actual growth of the interfaces.

These issues were first dealt with accurately by Larché and Cahn [18, 19]. The Larché and Cahn approach has been extended for cases involving surface excess quan-

tities by several authors [20, 21]. The relations developed by these authors still fall within the framework of Gibbsian and classical non-equilibrium thermodynamics.

The limitations of this approach are largely in the fact that force-flux relations are a-priori limited to linear relations. Also equilibrium relations are used in the derivation of relations for non-equilibrium processes. For most engineering systems - this shortcoming is not very important. However in cases involving chemical reactions (formation of intermetallics) or where there are aging processes the assumption of local equilibrium is not valid, and the development of thermodynamics can feel logically incomplete.

To avoid these problems, an alternative approach was developed by Gurtin and co-authors starting 1989 onwards based on rational thermodynamics [22–27]. In rational thermodynamics [28], the Gibbs relations and the Maxwell relations are not assumed a priori, but are derived later as consequences of balance (as opposed to extremalization) laws. In this approach - no assumption of local equilibrium is explicitly made and hence it is better suited for the simulation of non-equilibrium processes involving chemical reactions and aging, where assuming local equilibrium is problematic. Another important factor in favor of rational thermodynamics is the existence of invariance principles for energetic quantities. The most important one is that the expression for the change of stored energy of the form

$$\frac{d}{dt}\int_{\Omega} E d\Omega = \int_{\Gamma} (\text{Energy Fluxes}) d\Gamma. \tag{1.2}$$

is invariant with respect to translational and rotational coordinate transformation. This is an extension of Noether's theorem used in classical mechanics, to allow for systems with dissipation. It can be shown that the balance equations (linear momentum, angular momentum) are consequences of invariance under these transformations [29]. The idea of the configurational force balance, an extension of earlier variational equilibrium arguments was originally introduced by Gurtin as the consequence of a similar invariance with respect to the velocity of material phase evolution processes. This

was later modified into a separate fundamental balance similar to the momentum balance. A more thorough review of the formulation of moving boundary problems through continuum thermodynamics can be found in Chapter 2.

Gradient Flow Approaches

In the approaches listed above, the equations of motion for the evolution of phase boundaries in solids are largely based on purely kinematical relations and corresponding conditions on driving force derived from thermodynamics. An alternative approach that is popular is the use of Gradient Flows [30–32]. Gradient flow approaches are based on the assumption that the evolution of the system near equilibrium proceeds in a way that the rate of entropy generation/free energy change is maximized/minimized. In this approach the first step is to determine a free energy function Ψ, which is being minimized while the process is in motion. Differentiating the free energy function with time leads to an expression of the form

$$\frac{d}{dt}\int_{\Omega}\Psi(\bullet)d\Omega = \int_{\Omega}\frac{d}{d\bullet}\Psi(\bullet)\mathcal{L}(\dot{\bullet})d\Omega. \tag{1.3}$$

In Eq. (6.6), the $\mathcal{L}$ is a linear operator that includes mobility terms for the change. The fastest rate of change is achieved when,

$$\dot{\bullet} = -\mathcal{L}^{-1}\frac{d}{d\bullet}\Psi(\bullet). \tag{1.4}$$

This approach is useful for deriving qualitative results, however there are a couple of issues. The approach is problematic when there are external supplies involved, and also when deriving the appropriate form of the linear operator $\mathcal{L}$ for various problems. The process of using gradient flows for deriving phase-field equations is shown in greater detail in Chapter 6.

1.2.2 Numerical Techniques for Moving Boundary Problems

In this subsection, the different numerical strategies that are available for the solution of moving boundary problems are discussed. In general, numerical methods for the solution of moving boundary problems can be divided into two general classes based on the representation and evolution strategy for the interface. These are,

- Explicit tracking methods,
- Implicit tracking methods.

These are described in greater detail in this section.

Explicit Tracking Methods

In explicit tracking methods, the moving boundary is explicitly discretized and has an independent parametrization, either with finite elements or other appropriate discretization. The surface is then evolved using this parametrized form. The motion of these surface nodes can cause excessive deformation in the elements which are close to the interface, leading to a loss in accuracy of solutions. To ameliorate these errors, an Arbitrary Lagrange Eulerian (ALE) [33] formulation of the governing equations is often used, in which a separate smoothing velocity field is specified for the motion of nodes in the bulk (Fig. 1.5). The transport theorems for quantities are modified by adding a convective term to time derivative quantities to account for the change in the mesh. For example, the time derivative in Lagrangian coordinates is written as,

$$\frac{d(\bullet)}{dt}|_{\mathrm{X}} = \frac{\partial(\bullet)}{\partial t}|_{\text{mesh point}} + \boldsymbol{v}_{\text{mesh}}\nabla(\bullet). \tag{1.5}$$

In Eq. (1.5), $\frac{d(\bullet)}{dt}$ is the Lagrangian time derivative, $\frac{\partial(\bullet)}{\partial t}$ is the rate of change of the quantity at the mesh point and $\boldsymbol{v}_{\text{mesh}}$ is the velocity of the mesh point itself. The need to construct special meshes which can benefit from the mesh smoothing also limits the domain of applicability of these methods. The existence of sharp boundaries allows

the application of complicated boundary conditions with relative ease, allowing the study of more complex physical phenomena with great accuracy. They have been used for a wide range of problems, including void electromigration [34, 35]. On the other hand, these methods are often impractical for simulations that involve topological changes.

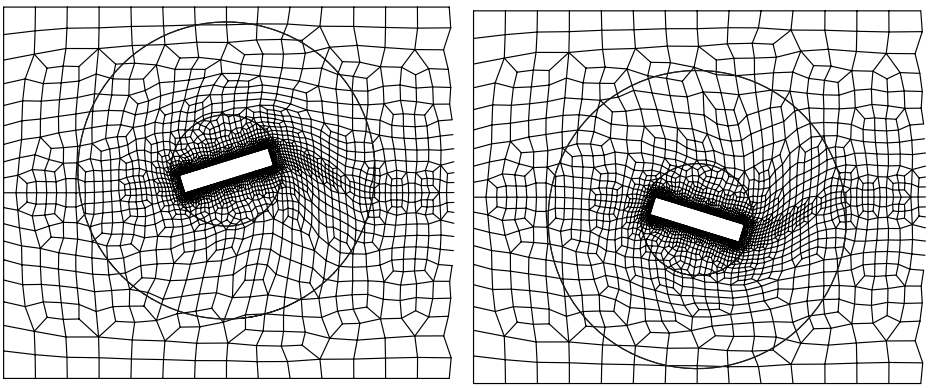

Figure 1.5. Arbitrary Lagrange Eulerian Meshes. The mesh is modified near the interface inside the circular region. As the rigid body in the fluid moves, the mesh is modified in such a way that the element distortion is minimized [33].

Implicit Tracking Methods

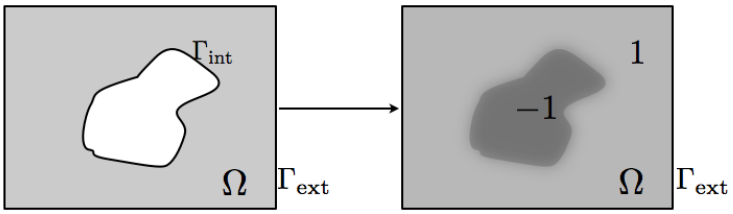

Figure 1.6. Implicit tracking methods.

Implicit methods track the interface by tracking the level set $\phi(\boldsymbol{x}) = c$ of a function that changes monotonically on either side of $\phi(\boldsymbol{x}) = c$ (Fig. 1.6). In addition to the governing equations in the bulk, an additional equation for the evolution of this function needs to be solved. The various implicit tracking methods are classified on the basis of this additional equation. The main Implicit Tracking Methods are listed below.

- **Level Set Method:** In the level set method [36], the function ϕ is taken to be the signed distance function, (usually indicated by ρ). The update to the interface is computed as a solution to the Hamilton Jacobi equation Eq. (1.6).

$$\frac{\partial \rho}{\partial t} + \boldsymbol{v}.\nabla\rho = 0 \tag{1.6}$$

  In Eq. (1.6) ρ is the exact signed distance function that is 0 at the interface and monotonically increases and decreases on opposite sides in the vicinity of the interface (Fig. 1.7). The normal velocity $\boldsymbol{v}.\boldsymbol{n}$ is explicitly computed based on the physics of the problem. Frequently, this is done by reconstructing the interface to compute the interfacial quantities. This reconstruction of the interface leads to this method frequently being called a sharp interface method. They are possibly the most popular technique for interface evolution problems and have been used for electromigration simulations as well [37].

- **Volume of Fluids Method:** In the volume of fluids method [39], the ϕ is the characteristic function. This is 0 on one side and +1 on the other. The update equation for the volume of fluid methods is very similar to the equation for the level set equation (Eq. (1.6)). However, in contrast with the distance function, the characteristic function is discontinuous and thus complicates the update procedure. Therefore, the solution of the equation in volume of fluid is by reconstructing the surface using linear polynomials and then updating the surface based on the velocity (Fig. 1.8). The characteristic function is then used

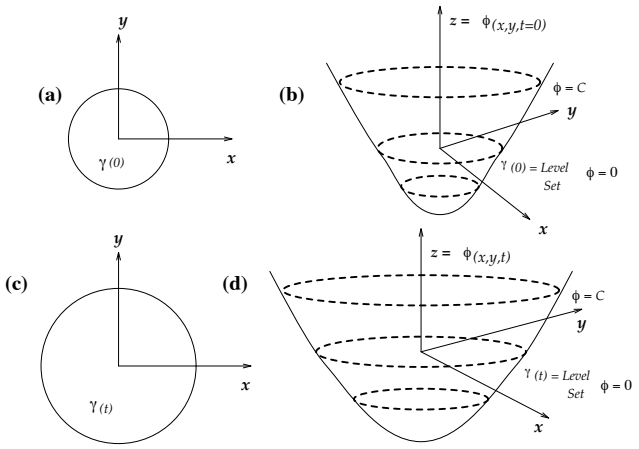

Figure 1.7. Level Set Function. The signed distance function is usually used to indicate the inside and outside of the interface are indicated by the sign of the distance function. The interface is evolved by evolving the distance function [36].

to localize the solution for the bulk problem, were the effect of the surface forces is captured through adding appropriate localized source terms.

- **Phase Field Methods:** The idea of treating interfaces with additional excess quantities as regions of space of finite thickness has a long history starting with van der Waals in 1893 [40, 41]. This insight is used for a more general study of problems with moving interface by various authors beginning with [42], where a smoothed characteristic function ϕ is set up over the domain, that transitions between two equilibrium values over a narrow region of thickness ϵ. However, in contrast to the volume of fluids and level set methods, the value of this characteristic function is not determined using an explicit representation of the surface but as the solution to a nonlinear diffusion equation. This nonlinear diffusion equation is usually obtained as the extremum of a functional that penalizes both non-constant values and forces the solution to one of two (in the simplest binary case) or more (in the general case) variables. The solution to the phase field equation thus involve updating the characteristic function while satisfying the extremum condition. The form of the functional being extremized

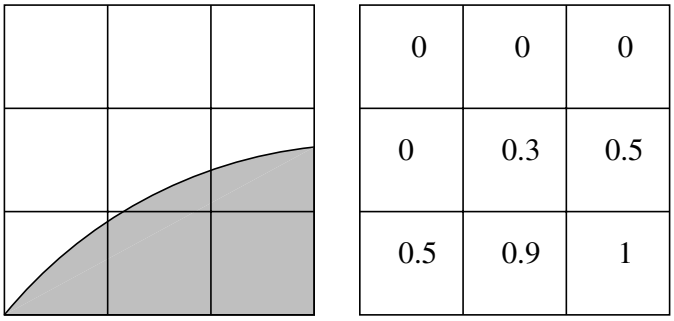

Volume of Fluids Method. The volume parameter indicates the fraction of each cell occupied by the fluid.

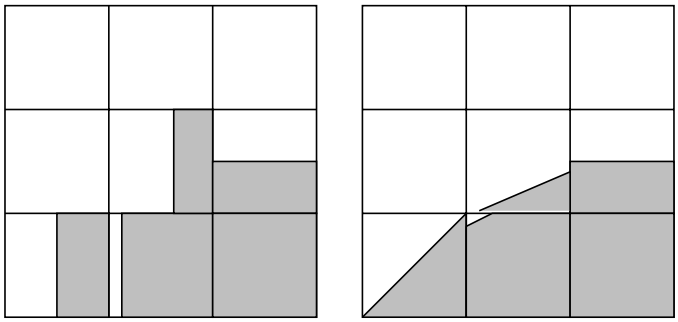

This information is then used to reconstruct the interface by either a method such as SLIC or linear interpolation.

Figure 1.8. Volume of Fluids Method [38].

determines the form of the function ϕ. While the computational demands of the phase field method are more significant compared to the other two methods described here, in requiring a denser mesh compared to the level-set or the volume of fluid methods, it provides a few unique advantages.

Both the level set and the volume of fluids equations are purely convective equations. As such, these equations are difficult to solve accurately using the Galerkin finite element method and some measure of stabilization is required through upwinding. This adds further complexity to the implementation of these methods. Another level of complexity is added due to the necessity of surface reconstruction and surface reinitialization. On the other hand, the phase field function is automatically reinitialized at every time-step. The diffusion-like nature of the equation also makes it

easier to solve the equation using standard Galerkin finite elements. A more detailed description of phase field methods is provided in the next section (§ 1.3).

1.3 Phase Field Methods

There are two ways of studying interface effects. The first is the method of van Der Waals and Korteweg [40, 41]. In this method of study, the interface is not a real physical entity. Instead, it is just a region of space where the fields show very sharp gradients. In thermodynamics, both variational [43, 44] and rational [45, 46], the behavior of the system can now be derived from the evolution of a volumetric functional with time. The equilibrium of the system under various sets of constraints on the system can now be obtained based on the extremum of this functional. This picture of interfacial effects is shown in Fig. 1.9. The free energy functional used in such models is a representation of the actual physics of the system. This idea is the inspiration behind the original Cahn-Hilliard model for spinodal decomposition [47], the Allen-Cahn model [48] for order-disorder transformation etc. Computationally, this approach has been widely used in the past 20 years. The approach has been used to study dendritic solidification [49, 50], diffusion driven changes in batteries [51, 52], and intermetallic growth [53, 54].

The principal challenge with numerical implementations of phase field models of this kind is discretization at the interfaces. All the fields in these models are physical. Hence, the problem has to be appropriately discretized at the smallest length scale in the problem. The interfaces in most physical systems are usually $\approx 10^{-8,9}m$ wide. This means that if the largest length-scales in the problem are of the order of $10\mu m$, the interface is 3-4 orders of magnitude smaller. This makes these models computationally quite prohibitive, especially when larger systems are under consideration.

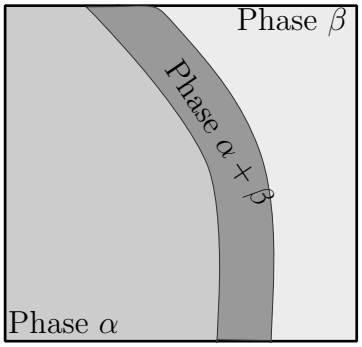

Figure 1.9. van der Waals, Korteweg idea of the interface. The interface is just a region of space, where the variables of the system display very sharp gradients. This picture is close to physical reality at atomic length scales.

The alternative picture of the interface is the Gibbs idea of the interface [13] which is shown in Fig. 1.10. In the Gibbs idea of the interface, the system is assumed to follow the evolution of an energy functional of the form,

$$\Psi = \int_{\Omega} \psi d\Omega + \int_{\Gamma} \psi_{\Gamma} d\Gamma \tag{1.7}$$

When using this approach to study the evolution of systems or the equilibrium of systems, the governing equations turn out to be a system of partial differential equations specified over the bulk of the system, with boundary conditions at the moving interface. This is the approach that leads to interfacial relations such as the classical Gibbs-Thomson, Thomson-Freundlich or Laplace-Young condition [13,55]. Geometric concepts, such as the *curvature* of the interface are meaningless in the Korteweg/van der Waals [41] idea of the interface, though they might be captured in alternate ways. For example, in Korteweg fluids, the classical Cauchy stress tensor is augmented by a term of the form, $\nabla\rho \otimes \nabla\rho$, where ρ is the density of the fluid. If the gradient of the densities are restricted to a very narrow region, the $\nabla\rho \otimes \nabla\rho$ is related to the geometrical surface projection tensor of the interface. When the divergence of such a tensor is computed Eq. (A.7), it leads to a force, normal to the interface, proportional to the curvature of the interface.

Sharp interface models for interface evolution usually use a Gibbs idea of the interface. Additionally, sharp interface equivalents are frequently derived to Korteweg type models for the interface [56].

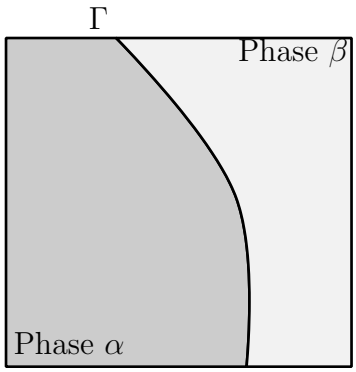

Figure 1.10. Gibbs idea of the Interface. The interface between two phases is indicated by a mathematically sharp interface, with interfacial excess quantities associated with them.

An alternative is to combine the two approaches. In this approach, energy functionals of the form Eq. (1.7) are modified into purely volumetric functionals [57]. This is done by introducing a phase field variable that does not correspond to any particular material property but just acts as a mathematical indicator for indicating the location of the phases. Hence, the integral Eq. (1.7) is modified by re-writing the surface integral as,

$$\int_{\Gamma} \psi_{\Gamma} d\Gamma \rightarrow \int_{\Omega} \psi_{\Gamma} \left(\epsilon \|\nabla \phi\|^2 + \frac{1}{\epsilon} f(\phi) \right) d\Omega \tag{1.8}$$

In the above, $f(\phi)$ is a positive function such that $f'(\phi)$ has roots at the values chosen to be the phase indicators. ϵ is a small number that acts as a measure of the interface thickness. This approach is illustrated in Fig. 1.11. An example of this approach is the regularization of the Mumford-Shah functional [58] for image segmentation. The Mumford-Shah functional is written as,

$$I(u, \nabla u) = \int_{\Omega} \alpha \|\nabla u\|^2 + \beta |u - g|^2 d\Omega + \int_{\Gamma} \gamma d\Gamma \tag{1.9}$$

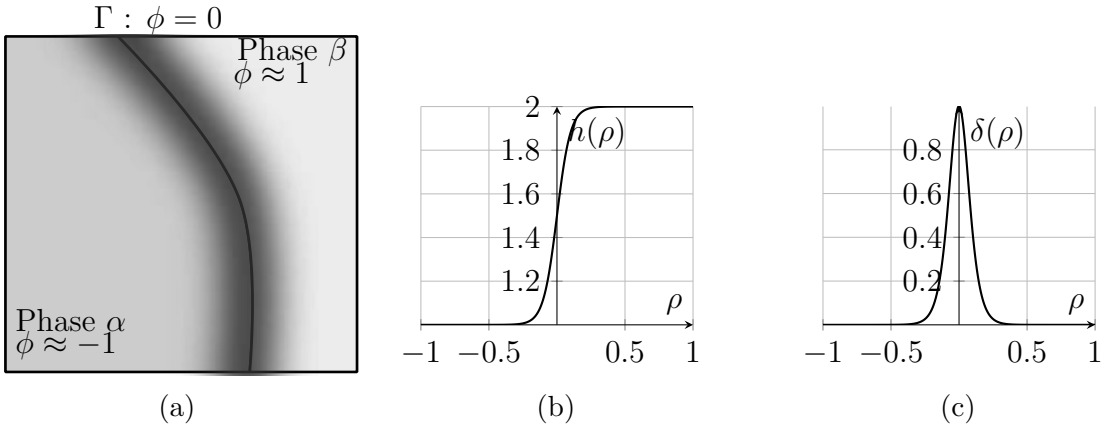

Figure 1.11. Numerical phase field. The physics is still determined by the Gibbsian idea of the interface. The properties between the phases are interpolated by a sigmoidal function (b), and properties at the interface are associated with a regularization of the Dirac δ function (c).

The gradient terms in Eq. (1.9) tend to remove noise from the data g, while the $\beta|u-g|^2$ ensures that the solution u fits the image. The surface integral in Eq. (1.9) divides the image into regions which have more or less constant values of u. Numerical solution of such problems is made difficult by the surface integral term. This is solved by using a modified *regularized* form of Eq. (1.9). This can be written as,

$$I(u,\nabla u,\phi,\nabla\phi)=\int_\Omega \left(\alpha(\phi)\|u-g\|^2+\beta(\phi)\|\nabla u\|^2\right)d\Omega+c\int_\Omega \epsilon\|\nabla\phi\|^2+\frac{\phi}{\epsilon}^2\,d\Omega. \tag{1.10}$$

This integral has the same information as Eq. (1.9), and can be shown to be rigorously the same as $\epsilon\to 0$. The same approach can be extended to physical problems. The standard energy functionals are modified to energies of the form Eq. (1.8) and a set of evolution equations is derived based on this energy functional either variationally or through rational thermodynamics. These evolution equations have ϵ as a parameter. Through a variety of methods, (asymptotic analysis [59], or $\Gamma-$convergence [60]), the equivalence of the modified partial boundary conditions can be shown to be equivalent

to the sharp-interface model. The solution scheme also leads to a regularized version of the Heaviside step function with different constant values in each of the phases, as well as various approximations to the Dirac δ function at the interface between the phases. These are determined by the choice of the phase field function and are described in § 1.3.2.

While exact reproduction of the physics by a numerical method still requires very dense discretization and ϵ has to be at the same length scale as the physical width of the interface, sufficiently good results can be obtained at much larger values of ϵ if very high accuracy is not required. This approach has been used for a variety of problems including phase field simulations of fracture [61, 62], multi-phase flows [63, 64], void electromigration [65, 66] and other problems.

1.3.1 Types of Phase Field Systems

Phase field systems can be broadly classified into two types based on the order of the differential equation being solved. These are:

- **Allen-Cahn Systems:** Allen-Cahn type systems are derived as simple gradient descents of Eq. (1.8) and lead to second order partial differential equations. They are not conservative (in terms of the phase field variable) and finally lead to the entire domain converging to either one of the roots of the function $f(\phi)$. These methods can be made conservative by adding a Lagrange multiplier to the functional (Eq. (1.11)). While this does make the method conserve the phase field variable, it also has the effect of making the system non-local which makes it unsuitable for modeling continuum physics [67].

$$\frac{\partial \phi}{\partial t} + \boldsymbol{v}\nabla\phi = M\left(\nabla^2\phi - f'(\phi) + \lambda(\phi - \phi_0)\right). \tag{1.11}$$

  In Eq. (1.11), $\phi_0 = \int_\Omega \phi(t=0)d\Omega$, and λ is a Lagrange multiplier that holds the value of ϕ_0 constant.

- **Cahn-Hilliard Systems:** The Cahn-Hilliard equation on the other hand uses the functional to define a chemical potential, and then tracks the minimization as a diffusive process driven by the gradient of this chemical potential. This process also minimizes the functional with a constraint on the integral of ϕ over the domain [68]. In contrast with the Allen-Cahn equation with a Lagrange multiplier, this approach is completely local - and hence more suitable for the simulation of continuum physics. The prototypical Cahn-Hilliard equation can be written as,

$$\frac{\partial \phi}{\partial t} + \boldsymbol{v}\nabla\phi = M\nabla^2\mu \tag{1.12a}$$

$$\mu = -\gamma\left(\epsilon\nabla\phi + \frac{1}{\epsilon}f'(\phi)\right) \tag{1.12b}$$

  The Cahn-Hilliard equation conserves the total value of the phase field variable over the entire domain.

1.3.2 Choice of the Phase Field Energy Function

An important consideration in the formulation of phase field equations is the form of the phase field energy function, $f(\phi)$. Traditionally, this function is derived from the phase diagram of the actual multi-phase system. This approach is frequently combined with a phase diagram generator such as CALPHAD [69]. This approach is useful for studying effects such as phase nucleation, where the precipitation of a secondary phase depends on the position of the system on the phase diagram. Various approximations to forms of the function $f(\phi)$ from the above approach have led to the various phase field functions that are commonly used in the phase field literature.

The oldest and the most commonly used version of the phase field function is the quartic energy function (Fig. 1.12). The motivation for the use of the biquadratic potential function is that it is the simplest polynomial that can have two distinct stable local extrema (quadratics and cubics only have one stable extremum). The

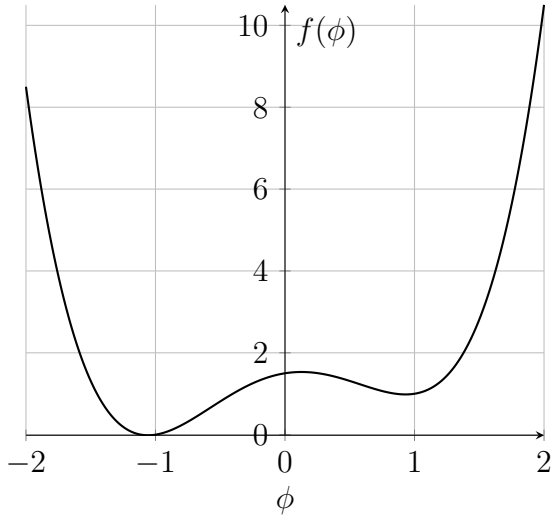

Figure 1.12. A quartic energy function.

coefficients of the quartic function are then determined via a fit to the phase diagram or another physical approach. In the mathematical phase field methods however, a biquadratic function is usually chosen with the minima at either 0 and 1 or ± 1. The primary advantage of using the biquadratic phase field functions is that they are smooth. This allows easy numerical solution by standard techniques for non-linear equations. The disadvantage is that the solutions lead to a hyperbolic tangent regularization of the Heaviside function (Fig. 1.14). These reach a constant value only asymptotically and hence there is no strictly defined interfacial region.

The second commonly used potential function type are the obstacle potentials (Fig. 1.13). The obstacle potentials were originally developed by Oono and Puri [70] to study phase separation dynamics. This can be written as,

$$f(\phi) = \begin{cases} -(\phi - a)(\phi - b) & \text{if } a \leq \phi \leq b \\ \infty & \text{otherwise.} \end{cases} \tag{1.13}$$

When solved, the solutions to the equations with the obstacle potentials lead to a localized sinusoidal regularization (Fig. 1.14) between the two extrema of the the potential function. In contrast with the quartic polynomials the obstacle potentials lead

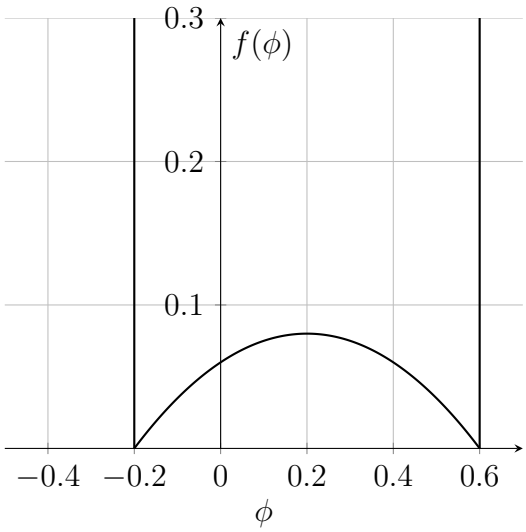

Figure 1.13. An obstacle potential function.

to a very sharp interfacial region. This often allows more accurate solutions. However, the solution to the phase field equations is no longer possible by the standard methods for non-linear equations, as the evolution equations are now variational inequalities. Most numerical methods for the solution of the phase field equations with obstacle potentials are able to restrict the solution to a narrow region around the interface, but this is not a significant advantage, especially if adaptive meshes are used.

1.3.3 Numerical Approaches

The primary numerical challenge with phase field models is on account of the fact that very dense discretizations are required to accurately capture interfacial effects. This implies fairly large memory requirements for the solution. The usual solution for time-stepping when the memory requirements are large is to use explicit time stepping schemes such as the forward Euler scheme. This proves problematic with the numerical solution of the Cahn-Hilliard equation as the CFL conditions for the Cahn-Hilliard equation for stable time-stepping, require very small time-steps ($\Delta t \approx O(h^4)$). Hence, in spite the large memory requirements, most of the numerical schemes

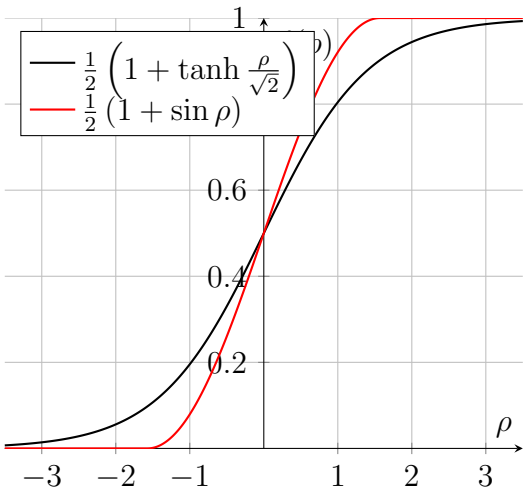

Figure 1.14. Regularizations of the Heaviside step function due to different forms of the function $f(\phi)$.

developed for the Cahn-Hilliard equations tend to focus on developing implicit or semi-implicit schemes [71–73].

A major challenge with fully implicit solutions of the phase field function is the fact that the phase field energies are non-convex. This is essential for the system to be able to evolve to different phases. Following Eyre in 1998 [72], various authors have developed techniques that depend on separating the system into a convex part and a concave part. The convex part is treated implicitly. The concave part is also treated implicitly and the values from the previous time-step are used to compute the effect. This allows the solution of every time-step to be the solution of a convex problem, which are much easier to solve. A further advantage of schemes of this kind is that the convex part can be designed to be linear. Eliminating non-linear problem solution saves approximately two matrix solutions, which is a significant saving when the problem sizes are very large. The approaches described in this paragraph are more suitable for phase field functions with smooth potential functions.

The solution to the phase field equations with the obstacle potentials tends to be more involved. The most successful methods tend to involve ideas from constrained optimization. The original solution schemes for this problem were dependent on a

projected Gauss-Seidel approach [74]. Later approaches were developed based on the Douglas Rachford operator splitting method. Recent research on the solution of the phase field equations of the variational inequalities focus on extending methods developed for the solution of constrained optimization problems to this class of problems [75–77].

1.3.4 Spatial Discretization

A numerical challenge that is specific to the numerical solution of the Cahn-Hilliard equations is the spatial discretization. As the Cahn-Hilliard equations are actually 4^{th} order differential equations, their direct solution by finite elements requires a discretization that is C^1 continuous. Various authors have developed schemes for the direct solution of the Cahn-Hilliard equations based on Hermite polynomials [78], NURBS [79], etc. The alternative approach is the use of a splitting scheme, where the equations are treated as a pair of coupled partial differential equations [80]. This is by far the most common method of discretization for the Cahn-Hilliard equation and the one adopted here. Numerical experiments have found that the C^1 elements have an advantage when it comes to solution accuracy, however, the additional cost of function evaluation for integration in these schemes keeps the standard C^0 approaches competitive [81].

1.4 Research Objectives

The primary objective of this research is to develop phase field methods and associated simulation tools for the simulation of diffusion driven moving boundary problems in heterogenous solids. A particular focus of the thesis is the study of problems of interest to the electronics packaging community, most importantly, void evolution growth in solder interconnect structures. In order to do this, it is essential to develop an understanding of the physics and thermodynamics of moving boundary problems in solids. This understanding is to be used to construct a continuum model

for the evolution of electromigration voids in solder interconnects (assuming a single material undergoing self-diffusion) owing to bulk and surface diffusion driven by the competing effects of surface energy, strain energy, stress, thermal and electrical potential gradients. Additionally, the effect of adhesion at interfaces and anisotropies in diffusivity need to be evaluated. Finally, approaches to study the evolution of phases under the action of electric fields in the presence of diffusive effects in more than two phases are studied.

1.5 Contributions

The main contributions of this thesis is the development of numerical methods and tools for the solution of moving boundary problems in electronics packages using a *numerical* phase field method. `DiffCode`, the numerical code developed in this research, takes arbitrary ABAQUS meshes with arbitrary material assignments and defines various initial void configurations. The evolution of these voids are tracked under the influence of surface energies, surface strain energies, electrical potential gradients and temperature gradients in the bulk and at the void interface. In addition, the void growth is modeled using a condition dependent on the local supersaturation of vacancies at every point at the interface. This code is used to demonstrate several cases of void evolution in line-type and solder type geometries. The numerical tool is also extended to study the effect of wetting at the interface between the solder joint and the die. The effect of anisotropy in the diffusivity on void growth rates is also studied. Finally, in order to simulate the growth and evolution of the voids at grain boundaries, an $n-$phase system of Cahn-Hilliard equations is developed. A numerical implementation of this $n-$phase system of Cahn-Hilliard equations is used to study the evolution of voids at grain boundaries.

1.6 Outline

This document is structured as follows. In Chapter 2, a comprehensive review of the thermodynamics required for the study of moving boundary problems is presented. Both variational and rational approaches are presented and contrasted. Methods to derive non-equilibrium relations from variational thermodynamics are discussed. Next, in Chapter 3, a phase field method for the evolution of voids is developed. Sharp interface equations are presented, followed by their diffuse interface equivalents. A formal asymptotic analysis is performed to show the equivalence of the diffuse interface equations to their sharp interface versions. The phase field model developed in Chapter 3 is solved using the finite element method. The numerical approach is described in Chapter 4 and several validation cases and a few applications are demonstrated. In Chapter 5, the model developed in Chapters 3 and 4 is extended to include the effects of diffusivity anisotropy as well as the effect of the adhesive energy due to wetting between the material of the interconnect and its surroundings. Several numerical examples are presented. In Chapter 6, an $n-$phase Cahn-Hilliard equation is developed for the solution of multi-phase problems based on the micro-force balance. This is modified in order to account for the effect of surface electromigration. An initial, formal asymptotic analysis is performed in order to determine the constants that relate the phase field model to it's sharp interface equations. A numerical method and several numerical examples for the $n-$phase Cahn-Hilliard equations is presented in Chapter 7. The research is summarized, and several avenues for future development are discussed in Chapter 8. The document has several appendices that provide additional information to aid with reading the dissertation. First, in Appendix A, the transport theorems and balance laws for systems with evolving interfaces are derived. Appendices B to D provide a short introduction to the mathematics of formal asymptotic analysis. Finally, the numerical tools developed in this thesis are described in Appendix E.

2. THERMODYNAMICS FORMULATION FOR MOVING BOUNDARY PROBLEMS

The thermodynamics of evolving phases in solids is made more involved by the fact that simple continuum thermodynamics is not sufficient to capture all the phenomena. Most importantly, the standard definition of phase equilibrium in terms of the equality of the chemical potential on either side of the interface is insufficient [17, 18] as this implies a spherical state of stress. This picture is insufficient for solids as the state of stress is not necessarily spherical. In this chapter, a review is presented of both the variational [18, 20] and rational thermodynamics [82, 83] approaches to the thermodynamics of moving boundary problems in solids. As phase evolution processes are non-equilibrium phenomena, the rational thermodynamics approach is the more rigorous one and involves fewer assumptions.

2.1 Extremum Principles for Equilibrium

The basic principles of variational thermodynamics arise from Gibb's landmark work [13]. Equilibrium of systems is defined through the stationarity of the internal energy or the entropy of the system. In case of the energy, it is postulated that all variations of the energy at constant entropy are non-negative,

$$\delta(E(S))|_{S=S_0} \geq 0. \tag{2.1}$$

This is essentially a statement of the minimization of total energy. Similarly for the entropy, it is postulated that all feasible variations of the entropy at constant energy are non-negative,

$$\delta(S(E))|_{E=E_0} \leq 0. \tag{2.2}$$

With the introduction of Lagrange multipliers T and β, Eqs. (2.1) and (2.2) can be stated as,

$$\delta\left(E - T(S - S_0)\right) \geq 0 \tag{2.3}$$

$$\delta\left(S - \beta(E - E_0)\right) \leq 0. \tag{2.4}$$

At strict equality, for a point system, the equilibrium conditions can be written as,

$$T = \frac{dE}{dS} \tag{2.5}$$

$$\beta = \frac{dS}{dE}. \tag{2.6}$$

β is therefore the inverse temperature. The above also points out a way to the definition of other intensive quantities as Lagrange multipliers to enforce the constancy of extensive quantities. Hence, the temperature of a system is defined as the Lagrange multiplier that ensures constant entropy at equilibrium when it is defined through the minimization of energy. Similarly the inverse temperature β is defined as the Lagrange multiplier that ensures constant energy when equilibrium is defined through the maximization of entropy. It can be shown that the two are equivalent [13]. The approach can be extended to systems where the primary variables are other extensive quantities. For example if the energy of the system is defined as $E(N)$, where N is a species that is held constant at equilibrium, the chemical potential μ is defined as the

Lagrange multiplier that holds the number constant, and the pressure p is defined as the Lagrange multiplier that holds the volume constant,

$$\mu = \frac{dE}{dN} \tag{2.7}$$

$$p = -\frac{dE}{dV}. \tag{2.8}$$

The above relations can be generalized to a system where the energy or the entropy has multiple arguments. For example, if the energy of a system is described by an energy function $E(S, N, V)$, the conditions for equilibrium at constant entropy, number and volume are as follows,

$$\mu = \frac{\partial E}{\partial N}|_{S,V} \tag{2.9a}$$

$$T = \frac{\partial E}{\partial S}|_{V,N} \tag{2.9b}$$

$$p = -\frac{\partial E}{\partial V}|_{S,N}. \tag{2.9c}$$

The above can also be used to write the so-called *Gibbs* relations which give incremental relation for the energy in terms of the changes in the arguments,

$$dE = -pdV + TdS + \mu dN. \tag{2.10}$$

2.1.1 Legendre Transforms for Changing Variables

It is often not convenient to determine the behavior of the system in terms of the variables of the energy. Depending on the type of the system and the conditions under which the experiments are performed, it might be more convenient to use other variables to define the system. For example, chemical reactions are often studied at constant atmospheric pressure, instead of at constant volume. This is accomplished through the Legendre transform [84,85]. The Legendre transform of a function allows

the transformation of the information contained in a function $y = f(x)$ into another function $g(f'(x))$.

The entropy of a system is hard to control in experiments, and hence determining $E(S)$ is difficult. On the other hand, systems can be kept at constant temperature easily by immersing the system in a large reservoir at a constant temperature. This is accomplished by taking the Legendre transform of $E(S, V, N)$ with respect to S to get a function $\Psi(\frac{\partial E}{\partial S}, V, N)$ or $\Psi(T, V, N)$. The function Ψ is determined as

$$\Psi = E - \frac{\partial E}{\partial S} S = E - TS. \tag{2.11}$$

The above function is also called the Helmholtz free energy. Minimizing the Helmholtz free energy at constant temperature, volume and species number determines the equilibrium of the system. The Helmholtz free energy can be used in the same way as E in the previous equation, and at equilibrium, the following relations are obtained,

$$\frac{\partial \Psi}{\partial T} = -S \tag{2.12a}$$

$$\frac{\partial \Psi}{\partial V} = -p \tag{2.12b}$$

$$\frac{\partial \Psi}{\partial N} = \mu. \tag{2.12c}$$

And a Gibbs relation can be written for Ψ as,

$$d\Psi = -SdT - pdV + \mu dN. \tag{2.13}$$

Another important condition that is frequently studied is when the system is maintained at constant pressure. This is achieved by a further Legendre transform of the Helmholtz free energy $\Psi(T, V, N)$ in terms of V. This function Φ is defined as follows by the same mechanism,

$$\Phi = \Psi - \frac{\partial \Psi}{\partial V} V = \Psi + pV. \tag{2.14}$$

Relations of the type Eq. (2.12) can now be written in terms of the enthalpy. Minimizing the enthalpy $\Phi(T, p, N)$ at constant temperature, pressure and species number also determines the equilibrium of the system. Functions of the type E, Φ and Ψ which can be minimized to determine the equilibrium are often referred to as thermodynamic potentials for the specific constraints that are active during the process of minimization. Another related interpretation of the idea of the thermodynamic potential is that they are a measure of the maximum reversible work that can be extracted from the system under different conditions [85].

It has to be noted that the term free energy is used in the literature for any function of the form $E - TS$, and the the term enthalpy is used for any function of the form $\Psi + pV$. The term enthalpy is also used for related functions in solids where p and V are replaced by appropriate variables of the same type. A very notable example which is very useful while determining the form of constitutive relations for systems with stress and diffusion is the enthalpy written as $\Psi - \sigma : \boldsymbol{\varepsilon}$.

2.1.2 Maxwell Relations between Derivatives

An important tool while determining the constitutive laws of systems are the Maxwell relations, that relate different thermal quantities at equilibrium. The basic idea is that the potential functions are smooth multi-variable functions. This implies that the order of differentiation doesn't matter. For example, consider the free energy function $\Psi(T, V, N)$. The equality of the mixed derivatives implies

$$\frac{\partial^2 \Psi}{\partial V \partial N} = \frac{\partial^2 \Psi}{\partial N \partial V} \tag{2.15}$$

$$\implies \frac{\partial \mu}{\partial V} = -\frac{\partial p}{\partial N}. \tag{2.16}$$

This equation can be integrated to derive a relation between the chemical potential and the volume. The above section and derivations are only valid for point systems and are not valid for systems with extent. For systems with extent, the extensive

variables are replaced with densities. The relations above are *assumed* to hold for every control volume that is of a sufficient size for thermodynamics to be meaningful.

2.2 Extension to Systems not at Equilibrium

The description of thermodynamics in the section above is strictly only valid for systems at equilibrium, and is not valid in systems where the system changes in any of the variables that describe it. Some authors [85] refer to the contents of the section above as thermostatics. The theory can be extended to study systems not in equilibrium by considering multiple systems that are individually at equilibrium and hence have a well defined T, μ and p. These systems can now be bought into contact with each other, and the equilibrium of the combined system can be considered. Consider two systems 1 and 2, described by entropy functions $S_1(E_1, N_1)$ and $S_2(E_2, N_2)$. Each of the systems is assumed to be at equilibrium at temperatures T_1 and T_2. While considering the equilibrium of the combined system, the following statements can be made about the system.

- Energy is conserved.

$$E_{1+2} = E_1 + E_2. \tag{2.17}$$

  This implies

$$dE_{1+2} = 0 \quad \text{or } dE_1 = -dE_2. \tag{2.18}$$

- Entropy of the total system increases.

$$S_{1+2} = S_1 + S_2 \tag{2.19}$$

$$dS_{1+2} = dS_1 + dS_2. \tag{2.20}$$

For the differentials,

$$dS_{1+2} \geq 0, dS_{1,2} \geq 0. \tag{2.21}$$

Considering the entropy of the total system,

$$dS_{1+2} = \frac{dE_1}{T_1} + \frac{dE_2}{T_2}. \tag{2.22}$$

The energy differential can be split into two parts $dE^o_{1,2}$, which is the energy supply from outside the system, and dE^I_{12}. Here, energy supply into the system is considered positive and dE_{12} is the energy flux from system 2 into system 1

$$dS_{1+2} = \frac{dE^o_1}{T_1} + \frac{dE^o_2}{T_2} + \frac{dE^I_{12}}{T_1} + \frac{dE^I_{21}}{T_2}. \tag{2.23}$$

As the system only changes by transferring energy from system 1 to system 2, $dE_{12} = -dE_{21}$. Substituting into Eq. (2.23),

$$dS_{1+2} = \frac{dE^o_1}{T_1} + \frac{dE^o_2}{T_2} + dE_{12}\left(\frac{1}{T_1} - \frac{1}{T_2}\right). \tag{2.24}$$

At this point, a form for the second law of thermodynamics for systems that are not in equilibrium is introduced as

$$dS^I_{1+2} \geq 0. \tag{2.25}$$

The above states that any internal change in the entropy during a non-equilibrium process is positive. The internal entropy change in Eq. (2.24) can be written as,

$$dS^I_{1+2} = dE_{12}\left(\frac{1}{T_1} - \frac{1}{T_2}\right) \geq 0. \tag{2.26}$$

Or,

$$dS^I_{1+2} = dE_{12}\left(\frac{T_2 - T_1}{T_1 T_2}\right) \geq 0. \tag{2.27}$$

In Eq. (2.27), if $T_2 = T_1$, the system is at equilibrium and there is no change in either of the systems 1 or 2. If $T_2 \geq T_1$, $dE_{12} \geq 0$ and system 2 loses energy to system 1. On the other hand if $T_2 \leq T_1$, the energy change is in the opposite direction. In systems that are able to exchange mass as well as energy, Eq. (2.26) is replaced by a more general relation of the form,

$$dS^I_{1+2} = dE_{12}\left(\frac{1}{T_1} - \frac{1}{T_2}\right) + dN_{12}\left(\frac{\mu_1}{T_1} - \frac{\mu_2}{T_2}\right) \geq 0. \tag{2.28}$$

Eq. (2.28) allows an easy extension to develop a variational thermodynamics for continuous systems.

1. Define the energy as a functional over the domain.

2. Assume that the smallest length scale relevant in the problem is large enough to be able to define a thermodynamically meaningful temperature, pressure and chemical potential

3. Minimize the energy functional with constraints of constant energy, volume and number over all possible variations, to determine the conditions of equilibrium and the values of the Lagrange multipliers.

4. If the Lagrange multiplier fields are constant over the domain of the problem, then the system is at equilibrium and there are no non-equilibrium effects, otherwise these effects are present (however slow) and the system will evolve towards equilibrium.

2.3 Larché Cahn Theory for Solids with Diffusion

In this section, the Larché Cahn [18,19] approach to the thermodynamics of solids with diffusion is reviewed. This is an isothermal variational approach where a constitutive energy functional is minimized over an arbitrary control volume under constraints of constant entropy and constant number density. The study of chemical equilibrium in solids is complicated by the presence of non-hydrostatic stresses and strains at equilibrium. Also, the standard definition of strain does not consider the presence of diffusing species, and only considers the transformations of line segments between arbitrarily defined material points. If needed, the points can be associated with atoms that form a part of the lattice. When considering a solid that allows evolution through diffusion, this picture is confused as shown in Fig. 2.1. There are two ways in which this issue has been addressed in the literature. The first is through the continuum theory of mixtures [86,87]. The continuum theory of mixtures defines a separate kinematics for each of the species that are present. The evolution of a mean quantity such as as the weighted mass density or the weighted volume occupied is then tracked as the primary deformation quantity. The difference between the kinematics for each of the species and this weighted mean is then treated as the diffusional evolution. This approach is very attractive in cases where there are deformation kinetics (acceleration - mixing reacting flows) to be considered. However, it leads to certain complications. While the definition of strain becomes easier, the definition of stress becomes more complicated as a separate partial stress is defined for each component. The definition of chemical potential also becomes more complex, with some authors arguing for the existence of tensor chemical potential [86,88].

The Larché-Cahn approach to equilibrium in solids avoids these by assuming that the strain corresponds to the strain of a hypothetical network, that is roughly the same as the lattice of the solid under consideration. The stress is now defined as a thermodynamic conjugate to this strain. The density of the diffusing species is also defined in terms of this back-ground lattice. The species are free to either move diffu-

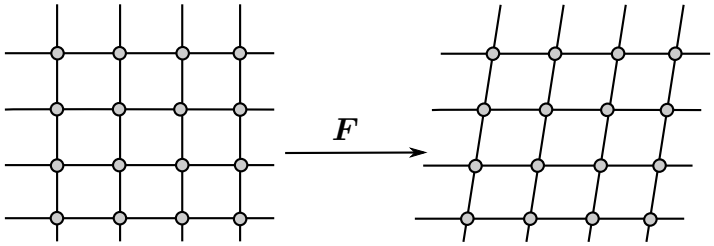

(a) Definition of strains in the absence of diffusion.

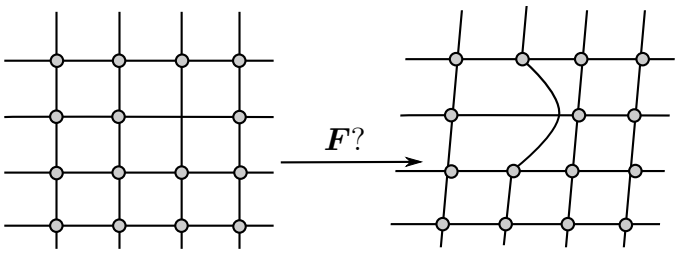

(b) Definition of strains in the presence of diffusive effects is not clear.

Figure 2.1. Definition of strains in crystals in the presence/absence of strain.

sively between the different sites on the network or they can also move interstitially in an unconstrained fashion.

The total energy of the system in the bulk is described using an energy density function as,

$$E_{\text{tot}} = \int_{\Omega_0} E(S, \boldsymbol{F}, \rho_{i,\ldots N}) d\Omega_0. \tag{2.29}$$

In the above, $\boldsymbol{F}$ is the deformation gradient between a reference domain and the current domain. This can be replaced by another appropriate variable such as the Euler or Green strain tensor. If the deformation is known to lead to small-strain, the symmetric small strain tensor ε can also be used. ρ_i is the number density of the i^{th} species. Introducing Lagrange multipliers T for the constancy of the total entropy, μ_i

for the constancy of the number density of each of the species, the following statement can be written for the stationarity of the energy,

$$\delta\left(\int_{\Omega_0} E(S,\boldsymbol{F},\rho_{i,\dots N})d\Omega_0 - T\left(\int_{\Omega_0} S d\Omega_0 - S_0\right) - \mu_i\left(\int_{\Omega_0}\rho_i d\Omega_0 - \rho_{i0}\right)\right) = 0. \tag{2.30}$$

The above integral is assumed to be defined over the reference domain, and hence the variation of the domain itself is zero. Expanding Eq. (2.30),

$$\int_{\Omega_0}\left(\left(\frac{\partial E}{\partial S} - T\right)\delta S + \left(\frac{\partial E}{\partial \boldsymbol{F}}\right) : \delta\boldsymbol{F} + \left(\frac{\partial E}{\partial \rho_i} - \mu_i\right)\delta\mu_i\right) d\Omega_0 = 0. \tag{2.31}$$

As the variations in the arguments are arbitrary,

$$T = \frac{\partial E}{\partial S}, \tag{2.32}$$

$$\mu_i = \frac{\partial E}{\partial \rho_i}. \tag{2.33}$$

Equilibrium is reached when T and μ_i are constant throughout the domain. For the middle term in Eq. (2.31), $\frac{\partial E}{\partial \boldsymbol{F}}$ is identified with the first Piola-Kirchhoff stress $\boldsymbol{\sigma}^I_{\mathrm{PK}}$. Using $\delta\boldsymbol{F} = \nabla_{\boldsymbol{X}}\delta\boldsymbol{x}$ and the identity,

$$\nabla(\boldsymbol{A}.\boldsymbol{v}) = (\nabla.\boldsymbol{A}).\boldsymbol{v} + \boldsymbol{A} : \nabla\boldsymbol{v}, \tag{2.34}$$

the middle term can be written as,

$$\int_{\Omega_0}\left(\nabla_{\boldsymbol{X}}(\boldsymbol{\sigma}^I_{\mathrm{PK}}.\delta\boldsymbol{x}) - \nabla_{\boldsymbol{X}}.\boldsymbol{\sigma}^I_{\mathrm{PK}}.\delta\boldsymbol{x}\right) d\Omega_0 = 0. \tag{2.35}$$

Applying the divergence theorem,

$$\int_{\Gamma}\boldsymbol{N}.\boldsymbol{\sigma}^I_{\mathrm{PK}}.\delta\boldsymbol{x}d\Gamma - \int_{\Omega_0}\nabla_{\boldsymbol{X}}.\boldsymbol{\sigma}^I_{\mathrm{PK}}.\delta\boldsymbol{x}d\Omega_0 = 0. \tag{2.36}$$

$\delta\boldsymbol{x} = 0$ on Γ, and the arbitrariness of $\delta\boldsymbol{x}$ in the domain leads to the condition for mechanical equilibrium

$$\nabla_{\boldsymbol{X}}.\boldsymbol{\sigma}^I_{\mathrm{PK}} = 0. \tag{2.37}$$

In a manner similar to Eq. (2.15), Maxwell relations can be written for the variables,

$$\frac{\partial \boldsymbol{\sigma}^I_{\mathrm{PK}}}{\partial \rho_i} = \frac{\partial \mu_i}{\partial \boldsymbol{F}}, \tag{2.38}$$

$$\frac{\partial \mu_i}{\partial \rho_j} = \frac{\partial \mu_j}{\partial \rho_i}. \tag{2.39}$$

An additional special case that is frequently encountered is the case of substitutional diffusion, where the species density can't be varied independently. Instead, there is a constraint on the sum of the species,

$$\sum_{i=1}^{N} \rho_i = \text{constant}. \tag{2.40}$$

For this case it can be shown that the individual chemical potentials can't be uniquely determined at equilibrium. Instead equilibrium for the species is determined by the constancy of the difference between chemical potentials. This can be done by adding a field of Lagrange multipliers to enforce Eq. (2.40) and then eliminating the Lagrange multiplier field. This is demonstrated for the purposes of developing a multi-phase system of Cahn-Hilliard equations in Chapter 6.

2.4 Variational Treatment of Interface Evolution Problems

The variational method in § 2.3 can be extended for the purposes of developing the equations of motion for systems with evolving interfaces. This has been done in [89] for systems without surface energetic excesses and in [20,21] for systems which possess a surface excess energy that depends on the concentration of species near the interface, the deformation of the energy and the entropy near the interface. In

this review, the interfacial strain energy is neglected as it is not expected to play an important role in the physics of interest and also in the interests of keeping the mathematics simple. Also, the effect of incoherence are neglected. (At incoherent interfaces, the tangential displacements at the phase interface are discontinuous - implying sliding. While developing the continuum mechanics of such systems, it is often necessary to define a separate reference domain for each of the phases [89].)

2.4.1 Geometric Definition of the Required Variation

The definition of the variations needed to develop the equilibrium relations is clearer in the large deformation context with mappings. Consider a control volume Ω_0 that is deformed to the current configuration Ω, with an intersecting interface Γ_0 in the reference configuration deformed in the current configuration to Γ. The interface Γ divides the domain into two phases α and β. The mapping from the reference to the current domain is described by a mapping $\boldsymbol{x} = \phi(\boldsymbol{X})$ and its deformation gradient $\boldsymbol{F} = \nabla_{\boldsymbol{X}}\phi(\boldsymbol{X})$. A geometric variation of this domain can be achieved in two ways.

1. The standard variation of the deformation. In the general large deformation case, this can be written as $\delta\boldsymbol{x}$. In small deformation cases, this is captured by the variation of the deformation ($\delta\boldsymbol{u}$).

2. In solids the interface can change by processes other than deformation. These include processes such as grain growth, boundary evolution by diffusion etc. To study the equilibrium of these processe an additional variation, $\delta\boldsymbol{y}$ is defined. This variation considers the variation of points on the interface. Only the normal component of $\delta\boldsymbol{y}$ can actually change the shape of the interface. Hence, this variation is written as,

$$\delta\boldsymbol{y} = \delta y\boldsymbol{N}, \tag{2.41}$$

where $\boldsymbol{N}$ is the normal to the interface in the reference configuration.

The total variation for points on the interface is the sum of the above two variations. As Eq. (2.41) is defined in the reference domain, it needs to be transformed into the current domain before they are added. Hence the total variation of points on the interface is given as,

$$\delta \boldsymbol{x}_{\text{total}} = \delta \boldsymbol{x} + (\boldsymbol{F}.\boldsymbol{N})\delta y. \tag{2.42}$$

Before considering the equilibrium relations for a energy functional with an interfacial component, the effect of a boundary variation of the type in Eq. (2.41) on a bulk functional of the type $\int_\Omega g(\boldsymbol{X})d\Omega$ needs to be specified as,

$$\delta \int_\Omega g(\boldsymbol{X})d\Omega = \int_\Omega \delta g(\boldsymbol{X})d\Omega + \int_\Gamma g(\boldsymbol{X})\delta y d\Gamma. \tag{2.43}$$

The last term in Eq. (2.43) is the change in the functional as additional material points are added to the control volume over which the functional is specified (Fig. 2.2).

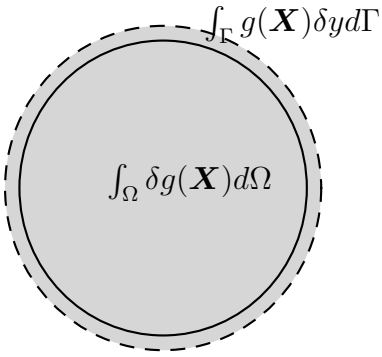

Figure 2.2. Variation associated with change in the domain.

2.4.2 Total Augmented Functional

The equilibrium conditions for a energy functional with a surface energy contribution are derived in this section restricted to coherent interfaces, where there is no slip along the interface. This derivation follows the derivation in [20, 21]. However,

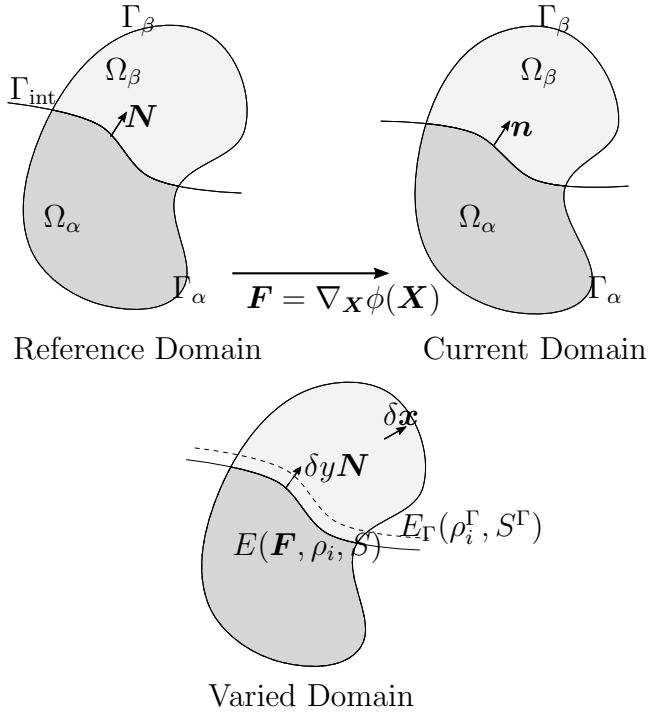

Figure 2.3. Variations involved in the Leo-Sekerka approach.

the effect of surface stresses is neglected. The energy functional that is considered is as follows,

$$E_{\text{tot}} = \underbrace{\sum_{\alpha,\beta} \int_{\Omega_{\alpha,\beta}} E_{\alpha,\beta}(\boldsymbol{F}, \rho_i, S) d\Omega_{\alpha,\beta}}_{I_\Omega} + \underbrace{\int_{\Gamma_{\text{int}}} E_\Gamma(\rho_i^\Gamma, S^\Gamma) d\Gamma_{\text{int}}}_{I_\Gamma}. \tag{2.44}$$

At equilibrium, Eq. (2.44) is minimized under the constraints of constant total ρ_i, S, which are enforced with Lagrange multipliers μ_i and T as in Eq. (2.30). These constraints are written as,

$$\underbrace{\sum_{k=\alpha,\beta} \int_{\Omega_k} \rho_i d\Omega_k + \int_{\Gamma_{\text{int}}} \rho_i^\Gamma d\Gamma_{\text{int}}}_{C^\rho} = \text{constant} \tag{2.45a}$$

$$\underbrace{\sum_{k=\alpha,\beta} \int_{\Omega_k} S d\Omega_k + \int_{\Gamma_{\text{int}}} S^\Gamma d\Gamma_{\text{int}}}_{C^S} = \text{constant}. \tag{2.45b}$$

In the above, the domains $\Omega_{\alpha,\beta}$ are the reference domains of the individual phases. The variations of the individual parts of Eqs. (2.44) and (2.45) are next written using Eqs. (A.38) and (2.43) as,

$$\delta I_\Omega = \sum_{k=\alpha,\beta} \int_{\Omega_k} \left(\frac{\partial E}{\partial \boldsymbol{F}} : \delta \boldsymbol{F} + \frac{\partial E}{\partial S} \delta S + \sum_{i=1}^{N} \frac{\partial E}{\partial \rho_i} \delta \rho_i \right) d\Omega_k + \int_{\Gamma_{\text{int}}} [\![E]\!]\, \delta y d\Gamma_{\text{int}}, \quad (2.46a)$$

$$\delta I_\Gamma = \int_{\Gamma_{\text{int}}} \left(\sum_{i=1}^{N} \frac{\partial E_\Gamma}{\partial \rho_i^\Gamma} \delta \rho_i^\Gamma + \frac{\partial E_\Gamma}{\partial S^\Gamma} \delta S^\Gamma - E_\Gamma \kappa \delta y \right) d\Gamma_{\text{int}}, \quad (2.46b)$$

$$\delta C^\rho = \sum_{k=\alpha,\beta} \int_{\Omega_k} \delta \rho_i d\Omega_k + \int_{\Gamma_{\text{int}}} [\![\rho_i]\!]\, \delta y d\Gamma_{\text{int}} + \int_{\Gamma_{\text{int}}} \left(\delta \rho_i^\Gamma - \kappa \rho_i^\Gamma \delta y \right) d\Gamma_{\text{int}}, \quad (2.46c)$$

$$\delta C^S = \sum_{k=\alpha,\beta} \int_{\Omega_k} \delta S d\Omega_k + \int_{\Gamma_{\text{int}}} [\![S]\!]\, \delta y d\Gamma_{\text{int}} + \int_{\Gamma_{\text{int}}} \left(\delta S^\Gamma - \kappa S^\Gamma \delta y \right) d\Gamma_{\text{int}}. \quad (2.46d)$$

In Eq. (2.46), the fact that

$$\delta \boldsymbol{y}.\boldsymbol{n}_\alpha = -\delta \boldsymbol{y}.\boldsymbol{n}_\beta \quad (2.47)$$

is used. This leads to,

$$g_\alpha \delta \boldsymbol{y}.\boldsymbol{n}_\alpha + g_\beta \delta \boldsymbol{y}.\boldsymbol{n}_\beta = g_\alpha \delta \boldsymbol{y}.\boldsymbol{n}_\alpha - g_\beta \delta \boldsymbol{y}.\boldsymbol{n}_\alpha \quad (2.48)$$

$$= [\![g]\!]\, \delta y. \quad (2.49)$$

Introducing the Lagrange multipliers μ_i for the constraints Eq. (2.45a), and the Lagrange multiplier T for the constraint Eq. (2.45b), the condition for equilibrium can be written as,

$$\delta I_\Omega + \delta I_\Gamma - \sum_{i=1}^{N} \mu_i \delta C_i^\rho - T \delta C^S = 0. \quad (2.50)$$

Substituting Eq. (2.46) into Eq. (2.50) and grouping terms,

$$\begin{aligned}\sum_{k=\alpha,\beta}\int_{\Omega_k}\left(\frac{\partial E}{\partial \boldsymbol{F}}:\delta\boldsymbol{F}+\left(\frac{\partial E}{\partial S}-T\right)\delta S+\sum_{i=1}^{N}\left(\frac{\partial E}{\partial \rho_i}-\mu_i\right)\delta\rho_i\right)d\Omega_k \\ +\int_{\Gamma_{\text{int}}}\left(\llbracket E\rrbracket-\sum_{i=1}^{N}\mu_i\llbracket\rho_i\rrbracket-T\llbracket S\rrbracket\right)\delta y d\Gamma_{\text{int}} \\ +\int_{\Gamma_{\text{int}}}\left(\sum_{i=1}^{N}\left(\frac{\partial E^{\Gamma}}{\partial \rho_i^{\Gamma}}-\mu_i\right)\delta\rho_i^{\Gamma}+\left(\frac{\partial E^{\Gamma}}{\partial S^{\Gamma}}-T\right)\delta S\right)d\Gamma_{\text{int}} \\ -\int_{\Gamma_{\text{int}}}\left(E_{\Gamma}-\sum_{i=1}^{N}\mu_i\rho_i^{\Gamma}-TS^{\Gamma}\right)\kappa\delta y d\Gamma_{\text{int}}=0.\end{aligned} \tag{2.51}$$

Using the arbitrariness of the variations $\delta\rho_i, \delta\rho_i^{\Gamma}, \delta S$ and δS^{Γ} the following conditions for equilibrium can be written,

$$\mu_i=\frac{\partial E}{\partial \rho_i}=\frac{\partial E_{\Gamma}}{\partial \rho_i^{\Gamma}} \tag{2.52a}$$

$$T=\frac{\partial E}{\partial S}=\frac{\partial E_{\Gamma}}{\partial S^{\Gamma}}. \tag{2.52b}$$

Introducing additional variables $\Psi=E-TS$ and $\Psi_{\Gamma}=E_{\Gamma}-TS^{\Gamma}$, identifying $\frac{\partial E}{\partial \boldsymbol{F}}$ with the first Piola-Kirchhoff stress, and using Eq. (2.52), Eq. (2.51) can be re-written as,

$$\begin{aligned}&\sum_{k=\alpha,\beta}\int_{\Omega_k}\left(\boldsymbol{\sigma}_{\text{PK}}^{I}:\delta\boldsymbol{F}\right)d\Omega_k+ \\ &\int_{\Gamma_{\text{int}}}\left(\llbracket\Psi\rrbracket-\sum_{i=1}^{N}\mu_i\llbracket\rho_i\rrbracket-\kappa\left(\Psi_{\Gamma}-\sum_{i=1}^{N}\mu_i\rho_i^{\Gamma}\right)\right)\delta y d\Gamma_{\text{int}}=0.\end{aligned} \tag{2.53}$$

Using Eq. (2.36), the above leads to

$$\begin{aligned}&\sum_{k=\alpha,\beta}\left(\int_{\Omega_k}-\nabla_{\boldsymbol{X}}.\boldsymbol{\sigma}_{\text{PK}}^{I}.\delta\boldsymbol{x}d\Omega_k+\int_{\Gamma_k}\boldsymbol{n}_k.\boldsymbol{\sigma}_{\text{PK}}^{I}.\delta\boldsymbol{x}d\Gamma_k\right)+ \\ &\int_{\Gamma_{\text{int}}}\left(\llbracket\Psi\rrbracket-\sum_{i=1}^{N}\mu_i\llbracket\rho_i\rrbracket-\kappa\left(\Psi_{\Gamma}-\sum_{i=1}^{N}\mu_i\rho_i^{\Gamma}\right)\right)\delta y d\Gamma_{\text{int}}=0.\end{aligned} \tag{2.54}$$

The arbitrariness of $\delta\boldsymbol{x}$ in the bulk leads to the standard momentum balance condition. Also, it is assumed that the outer boundary of the control volume is fixed. This allows Eq. (2.54) to be re-written as,

$$\begin{aligned}\int_{\Gamma_{\text{int}}} \left(\boldsymbol{N}_\alpha \boldsymbol{\sigma}_{\text{PK}}^{\alpha I}\delta\boldsymbol{x} + \boldsymbol{N}_\beta \boldsymbol{\sigma}_{\text{PK}}^{\beta I}\delta\boldsymbol{x}\right) d\Gamma_{\text{int}} \\ + \int_{\Gamma_{\text{int}}} \left(\left[\!\left[\Psi\right]\!\right] - \sum_{i=1}^{N}\mu_i \left[\!\left[\rho_i\right]\!\right] - \kappa\left(\Psi_\Gamma - \sum_{i=1}^{N}\mu_i\rho_i^\Gamma\right)\right)\delta y d\Gamma_{\text{int}} = 0.\end{aligned} \tag{2.55}$$

Rewriting $\delta\boldsymbol{x}$ as $\delta\boldsymbol{x}_{\text{tot}} - \boldsymbol{F}.\boldsymbol{N}\delta y$, and using $\boldsymbol{N}_\alpha = -\boldsymbol{N}_\beta$, Eq. (2.55) leads to,

$$\begin{aligned}&\int_{\Gamma_{\text{int}}} \boldsymbol{N}.\left[\!\left[\boldsymbol{\sigma}_{\text{PK}}^{I}\right]\!\right].\delta\boldsymbol{x}_{\text{tot}} d\Gamma_{\text{int}} + \\ &\int_{\Gamma_{\text{int}}} \left(\left(\left[\!\left[\Psi\right]\!\right] - \sum_{i=1}^{N}\mu_i \left[\!\left[\rho_i\right]\!\right] - \kappa\left(\Psi_\Gamma - \sum_{i=1}^{N}\mu_i\rho_i^\Gamma\right)\right)\delta y - \boldsymbol{N}.\boldsymbol{\sigma}_{\text{PK}}^{I}.\boldsymbol{F}\boldsymbol{N}\delta y\right) d\Gamma_{\text{int}} = 0.\end{aligned} \tag{2.56}$$

The arbitrariness of $\delta\boldsymbol{x}_{\text{tot}}$ leads to the condition for traction continuity at the interface. The arbitrariness of δy coupled with the arbitrariness of the area of integration, $d\Gamma_{\text{int}}$ on the other hand, leads to an additional condition for equilibrium which is stated as,

$$\left[\!\left[\Psi\right]\!\right] - \sum_{i=1}^{N}\mu_i \left[\!\left[\rho_i\right]\!\right] - \kappa\left(\Psi_\Gamma - \sum_{i=1}^{N}\mu_i\rho_i^\Gamma\right) - \boldsymbol{N}.\left[\!\left[\boldsymbol{\sigma}_{\text{PK}}^{I}\right]\!\right].\boldsymbol{F}\boldsymbol{N} = 0. \tag{2.57}$$

which can be re-arranged as

$$\boldsymbol{N}.\left(\underbrace{\left[\!\left[\Psi\right]\!\right]\boldsymbol{I} - \boldsymbol{F}^T\left[\!\left[\boldsymbol{\sigma}_{\text{PK}}^{I}\right]\!\right]}_{\text{Energy-momentum tensor}} - \sum_{i=1}^{N}\mu_i \left[\!\left[\rho_i\right]\!\right]\boldsymbol{I} - \kappa\left(\Psi_\Gamma - \sum_{i=1}^{N}\mu_i\rho_i^\Gamma\right)\boldsymbol{I}\right).\boldsymbol{N} = 0. \tag{2.58}$$

Other equilibrium conditions can be derived based on the terms that are significant in the above expression. The first case that we can consider is the one where there

are no diffusive phenomena. In this case all the terms involving ρ_i, ρ_i^{Γ} are set to zero. This leads to a simple interfacial equilibrium condition of the form,

$$[\![\Psi]\!]\, \boldsymbol{I} - \boldsymbol{F}^T . [\![\boldsymbol{\sigma}]\!]^I_{\mathrm{PK}} - \kappa \Psi_{\Gamma} \boldsymbol{I} = 0. \tag{2.59}$$

This is the equilibrium condition that is frequently used in studies of grain boundary motion. Another common approximation that is made is that the surface concentrations of the components are assumed to be negligible. This allows Eq. (2.58) to be written as,

$$[\![\Psi]\!]\, \boldsymbol{I} - \boldsymbol{F}^T . \left[\!\left[\boldsymbol{\sigma}^I_{\mathrm{PK}}\right]\!\right] - \sum_{i=1}^{N} \mu_i \, [\![\rho_i]\!]\, \boldsymbol{I} - \kappa \Psi_{\Gamma} \boldsymbol{I} = 0. \tag{2.60}$$

The above relation is frequently used as an interfacial condition in the study of interfacial diffusion processes. The condition above can be re-arranged and written as a condition on the chemical potential at an interface relating it to the curvature of the interface. Hence, Eq. (2.60) is also called a generalized form of the standard Gibb's Thomson relation [55], as it generalizes the idea to include more effects. Finally, in the case without any interfacial and diffusive effects, the condition for equilibrium is written simply as,

$$[\![\Psi]\!]\, \boldsymbol{I} - \boldsymbol{F}^T . [\![\boldsymbol{\sigma}]\!]^I_{\mathrm{PK}} = 0. \tag{2.61}$$

This condition was first derived in [90] as a condition for equilibrium in an elastic system with a moving interface.

2.4.3 Note: Variational Thermodynamics and Gradient Energies

A question with variational treatments of thermodynamics is the handling of energies with gradient energies of the form used in phase field methods. Considering the standard gradient energy (Eq. (1.8)),

$$\Psi(\phi, \nabla\phi) = \int_\Omega \left(\epsilon \|\nabla\phi\|^2 + \frac{1}{\epsilon} f(\phi) \right) d\Omega. \tag{2.62}$$

If the variable ϕ is an arbitrary quantity, the condition for equilibrium is simply the standard necessary condition for extrema. This can be written as,

$$\delta\Psi(\phi, \nabla\phi) = 0. \tag{2.63}$$

Or, assuming $\nabla\phi.\boldsymbol{n} = 0$, on the outer boundary of the control volume

$$\int_\Omega \left(-2\epsilon\nabla^2\phi + \frac{1}{\epsilon} f'(\phi) \right) \delta\phi = 0 d\Omega. \tag{2.64}$$

Assuming the arbitrariness of the control volume, or the arbitrariness of $\delta\phi$, the condition for equilibrium can be simply written as,

$$-2\epsilon\nabla^2\phi + \frac{1}{\epsilon} f'(\phi) = 0. \tag{2.65}$$

This is the condition at equilibrium. If $\Psi(\phi, \nabla\phi) > \Psi(\phi_{\text{eq}}, \nabla\phi_{\text{eq}})$, a descent condition can be proposed,

$$\frac{\partial\phi}{\partial t} = M \left(2\epsilon\nabla^2\phi - \frac{1}{\epsilon} f'(\phi) \right). \tag{2.66}$$

If the ϕ is now interpreted as a diffusing species, the necessary condition for extremalization is no longer the same, instead an augmented functional needs to be used, with a constraint on the total value of ϕ. The augmented functional can be written as,

$$\Psi_{\text{aug}} = \Psi + \mu \left(\int_{\Omega} \phi d\Omega - C \right). \tag{2.67}$$

The necessary conditions for extremalization are now writable as,

$$\delta\Psi_{\text{aug}} = \delta\Psi + \mu \int_{\Omega} \delta\phi d\Omega = 0 \tag{2.68a}$$

$$\int_{\Omega} \phi d\Omega = C. \tag{2.68b}$$

Making the same assumption that, $\nabla\phi.\boldsymbol{n} = 0$ on the boundary of the control volume and assuming that the control volume is arbitrary, the condition for equilibrium can be written as,

$$\mu = 2\epsilon\nabla^2\phi - \frac{1}{\epsilon} f'(\phi). \tag{2.69}$$

If it is assumed that this solution for the chemical potential is valid even when $\Psi(\phi, \nabla\phi) > \Psi(\phi_{\text{eq}}, \nabla\phi_{\text{eq}})$, and the system is allowed to equilibrate through a diffusive process, the governing equations lead to the Cahn-Hilliard equations. Though Eq. (2.69) is a local relation, it depends on making an assumption on $\nabla\phi$ on the boundary of the control volume. This constraint is the same as $\nabla^2\phi = 0$, or an assumption that no diffusion is occurring. This brings the discussion back to the issue of using variational *equilibrium* relations in a non-equilibrium sense. This is discussed in § 2.4.4.

2.4.4 Use in Non-Equilibrium Settings

The interfacial conditions Eqs. (2.57), (2.60) and (2.61) are used in a non-equilibrium setting in the same manner as in § 2.2. The equilibrium condition is assumed to hold

at every point on the interface. Spatial gradients in the quantities such as the chemical potential are then used to drive the non-equilibrium case. The other alternative approach is the gradient flow approach. The variation of the energy is kept in the variational form Eq. (2.56) and δy is treated as the normal velocity of the interface. This velocity is now specified so that the variation of the energy is minimized. This is an assumption that the interface evolves so that a global equilibrium is reached as fast as possible. Approaches based on this assumption are called gradient flow approaches [67,91,92]. The primary challenge with gradient flow approaches is handling external supplies and the inclusion of additional physics.

These approaches are valid mathematically and lead to physically reasonable models. However, there are a couple of issues with the variational approach with respect to their use in non-equilibrium simulations. The first is that the minimization principle is strictly only valid for the determination of equilibrium conditions. When a minimization approach is used for a non-equilibrium process, it implies an assumption of linear constitutive laws between the driving forces and the resultant non-equilibrium fluxes. The other important concern is that in variational approaches like the one described above, there is no separation between the constitutive laws, the balance laws and the equilibrium conditions. It is unclear whether the form of Eq. (2.58) is a result of a physical principle or of the constitutive laws assumed a priori. Owing to these issues, the variational approach to thermodynamics is problematic for the study of non-equilibrium effects.

The alternative to the variational approach is the approach of rational thermodynamics developed by Truesdell and Toupin [28]. The approach has been extended for the study of problems with interfacial effects by Gurtin and his co-authors in a series of papers [23,25,26,93]. This approach postulates the existence of an additional force system that acts in the same way with the velocity related to the interfacial motion as the standard force system relates to the deformation of the material. Considering the standard force system to be a *deformational* force system, the other force system is called the *configurational* force system. This is described in the following section.

2.5 Rational Thermodynamics Approach

In a rational thermodynamics approach, instead of using a variational approach and defining the intensive quantities as Lagrange multipliers at equilibrium, the intensive quantities are defined as specifying the energetic fluxes associated with fluxes of the extensive quantities. For example, instead of being defined as the Lagrange multiplier that enforces the constancy of the mass as in Eq. (2.7), the chemical potential is defined by defining the energetic fluxes associated with diffusive fluxes (either in mass terms or in number terms).

$$\frac{D}{Dt}\int_{\Omega} E_{\text{diff}} d\Omega = \int_{\Gamma} -\mu \boldsymbol{J}.\boldsymbol{n} d\Gamma. \tag{2.70}$$

This is similar to the way that the temperature is defined in rational thermodynamics through the Clausius-Clayperon inequality relating the change in the entropy over a control volume to the heat flux across the boundaries of the domain.

$$\frac{D}{Dt}\int_{\Omega} S d\Omega \geq -\int_{\Gamma} \frac{1}{T}\boldsymbol{q}.\boldsymbol{n} d\Gamma. \tag{2.71}$$

Equality is achieved at equilibrium, which leads to the standard definition of temperature. The standard force terms can also be defined so as to make sense in terms of energetic fluxes. The standard stress tensors relate the deformation at the boundary of a control volume to the energy supply to the control volume in the form of work. The first Piola-Kirchhoff stress in the derivation in § 2.3, for example can be considered to be defined as the tensorial quantity that relates the deformation and the normal at the boundary of the control volume to the work done on the control volume. This can be written as,

$$\frac{D}{Dt}\int_{\Omega} E d\Omega = \int_{\Gamma} \boldsymbol{N}.\boldsymbol{\sigma}^{I}_{\text{PK}}.\boldsymbol{v} d\Gamma. \tag{2.72}$$

In § 2.5.2, the above approach is used to define configurational forces that relate to *configurational* changes in the domain. These relations are first defined over the bulk of the material. Following this, relations at the interface are derived.

2.5.1 Bulk Relations

The balances over the bulk of the material are derived in this section. The free energy inequality in the bulk is used to derive the Maxwell relations in the bulk. These relations being unsuitable for analysis, a Legendre transform is used to derive the relation between the strain and the concentration, as well as a simple relation between the chemical potential and the stress.

Balance of Numbers

The Larché-Cahn approach with the species diffusion measured with respect to a hypothetical network is used, where the species balance is tracked over a control volume that deforms along with the lattice. This is in contrast to a more eulerian approach used in mixture theories [86], where the species are tracked over a control volume that is attached to a background frame. All the fluxes are measured with respect to this background frame. For each species that exists in the solid, a balance equation can be written over an arbitrary control volume Ω of the form,

$$\frac{D}{Dt}\int_{\Omega}\rho_i d\Omega = \int_{\Gamma} -\boldsymbol{J}_i.\boldsymbol{n}d\Gamma. \tag{2.73}$$

This relation can be localized using the divergence theorem,

$$\frac{D}{Dt}\rho_i = -\nabla.\boldsymbol{J}_i. \tag{2.74}$$

As the control volume in purely Lagrangian, there are no convective terms

$$\frac{\partial \rho_i}{\partial t} + \nabla . \boldsymbol{J}_i = 0. \tag{2.75}$$

A constraint on the total number of particles, such as Eq. (2.40) can also be written as a stronger constraint on the sum of the species,

$$\sum_{i=1}^{N} \nabla . \boldsymbol{J}_i = \boldsymbol{0}. \tag{2.76}$$

Balance of Momentum

While writing the momentum balance for the study of moving boundary problems with diffusion, the inertial terms are usually neglected. This is because the system reaches equilibrium with respect to stresses much faster than with respect to the diffusive terms. The momentum balance in the bulk can be written as,

$$\nabla . \boldsymbol{\sigma} + \sum_{i=1}^{N} \rho_i^{\text{mass}} \boldsymbol{b} = \boldsymbol{0}. \tag{2.77}$$

The above relation can also be written in terms of the first Piola-Kirchhoff stress as,

$$\nabla_{\boldsymbol{X}} . \boldsymbol{\sigma}_{PK}^{I} + \sum_{i=1}^{N} \rho_i^{\text{mass}} \boldsymbol{b} = \boldsymbol{0}. \tag{2.78}$$

Balance of Energy

The energy balance for an arbitrary control volume in the absence of kinetic energy and body forces can be written as,

$$\frac{D}{Dt} \int_{\Omega} E d\Omega = \int_{\Gamma} \boldsymbol{n} . \boldsymbol{\sigma} \boldsymbol{v} d\Gamma - \sum_{i=1}^{N} \int_{\Gamma} \mu_i \boldsymbol{J}_i . \boldsymbol{n} d\Gamma - \int_{\Gamma} \boldsymbol{q} . \boldsymbol{n} d\Gamma. \tag{2.79}$$

In the above, $\boldsymbol{q}$ is the heat flux into the domain. Localizing the above relation, and assuming a Lagrangian control volume,

$$\frac{\partial E}{\partial t} = \nabla.(\boldsymbol{\sigma}^T.\boldsymbol{v}) - \sum_{i=1}^{N} \nabla.\left(\mu_i \boldsymbol{J}_i\right). - \nabla.\boldsymbol{q}. \tag{2.80}$$

This can be expanded as

$$\frac{\partial E}{\partial t} = \nabla.\boldsymbol{\sigma}.\boldsymbol{v} + \boldsymbol{\sigma} : \nabla \boldsymbol{v} - \sum_{i=1}^{N} \left(\nabla \mu_i.\boldsymbol{J}_i + \mu_i \nabla.\boldsymbol{J}_i\right) - \nabla.\boldsymbol{q}. \tag{2.81}$$

From Eq. (2.77), in the absence of body forces, $\nabla.\boldsymbol{\sigma} = 0$, also, $\nabla.\boldsymbol{J}_i = -\frac{\partial \rho_i}{\partial t}$. With these, the energy balance can be written as,

$$\frac{\partial E}{\partial T} = \boldsymbol{\sigma} : \nabla \boldsymbol{v} - \sum_{i=1}^{N} \nabla \mu_i.\boldsymbol{J}_i + \sum_{i=1}^{N} \mu_i \frac{\partial \rho_i}{\partial t} - \nabla.\boldsymbol{q}. \tag{2.82}$$

Free Energy Inequality

To derive the free energy inequality, Eq. (2.71) is localized as,

$$\frac{\partial S}{\partial t} \geq -\frac{1}{T} \nabla.\boldsymbol{q} + \frac{1}{T^2} \boldsymbol{q}.\nabla T. \tag{2.83}$$

Multiplying Eq. (2.83) by T and subtracting it from Eq. (2.82),

$$\frac{\partial E}{\partial t} - T\frac{\partial S}{\partial t} \leq \boldsymbol{\sigma} : \nabla \boldsymbol{v} - \sum_{i=1}^{N} \nabla \mu_i.\boldsymbol{J}_i + \sum_{i=1}^{N} \mu_i \frac{\partial \rho_i}{\partial t} - \frac{1}{T^2} \nabla T.\boldsymbol{q}. \tag{2.84}$$

Adding and subtracting $\frac{\partial T}{\partial t} S$ and defining $\Psi = E - TS$, Eq. (2.84) can be written as,

$$\frac{\partial \Psi}{\partial t} + \frac{\partial T}{\partial t} S \leq \boldsymbol{\sigma} : \nabla \boldsymbol{v} - \sum_{i=1}^{N} \nabla \mu_i.\boldsymbol{J}_i + \sum_{i=1}^{N} \mu_i \frac{\partial \rho_i}{\partial t} - \frac{1}{T^2} \nabla T.\boldsymbol{q}. \tag{2.85}$$

The above equation can be simplified by splitting $\nabla \boldsymbol{v}$ into a symmetric and anti-symmetric part. Denoting the symmetric part as $\boldsymbol{D}$, and using the property that the product of a symmetric and anti-symmetric tensor is $\mathbf{0}$, the above can be simplified into

$$\frac{\partial \Psi}{\partial t} + \frac{\partial T}{\partial t} S \leq \boldsymbol{\sigma} : \boldsymbol{D} - \sum_{i=1}^{N} \nabla \mu_i . \boldsymbol{J}_i + \sum_{i=1}^{N} \mu_i \frac{\partial \rho_i}{\partial t} - \frac{1}{T^2} \nabla T . \boldsymbol{q}. \tag{2.86}$$

The above equation provides a simple way to test the validity of any constitutive laws that describe the evolution of the system. In contrast to the variational derivations, the equation above is valid without any assumptions of equilibrium or constitutive laws. In order to track the evolution of system, constitutive relations need to be introduced for the various quantities. In Eq. (2.86), the quantities that need constitutive laws are $\Psi, S, \boldsymbol{\sigma}, \mu_i, \boldsymbol{J}_i$ and $\boldsymbol{q}$. The arguments of this function are the rates and gradients of the other quantities in the expression. Equipresence implies that the arguments for each of the constitutive laws are the same. Here simple constitutive laws of the form,

$$\Psi = \Psi(T, \boldsymbol{\varepsilon}, \rho_i) \tag{2.87a}$$

$$\boldsymbol{\sigma} = \boldsymbol{\sigma}(T, \boldsymbol{\varepsilon}, \rho_i) \tag{2.87b}$$

$$\mu_i = \mu_i(T, \boldsymbol{\varepsilon}, \rho_i) \tag{2.87c}$$

$$\boldsymbol{q} = \boldsymbol{q}(T, \boldsymbol{\varepsilon}, \rho_i) \tag{2.87d}$$

$$\boldsymbol{J}_i = \boldsymbol{J}_i(T, \boldsymbol{\varepsilon}, \rho_i). \tag{2.87e}$$

are assumed. Substituting Eq. (2.87) into Eq. (2.86) and grouping terms,

$$\left(\frac{\partial \Psi}{\partial \boldsymbol{\varepsilon}} - \boldsymbol{\sigma}\right) : \boldsymbol{D} + \sum_{i=1}^{N} \left(\frac{\partial \Psi}{\partial \rho_i} - \mu_i\right) \dot{\rho} + \left(\frac{\partial \Psi}{\partial T} + S\right) \dot{T} \leq -\sum_{i=1}^{N} \boldsymbol{J}_i . \nabla \mu_i - \frac{1}{T^2} \boldsymbol{q} . \nabla T. \tag{2.88}$$

Eq. (2.88) must hold for arbitrary independent $\boldsymbol{D}, \dot{\rho}_i$ and $\dot{T}$. For this to hold,

$$\boldsymbol{\sigma} = \frac{\partial \Psi}{\partial \boldsymbol{\varepsilon}} \tag{2.89a}$$

$$\mu_i = \frac{\partial \Psi}{\partial \rho_i} \tag{2.89b}$$

$$S = -\frac{\partial \Psi}{\partial T}. \tag{2.89c}$$

The right hand side of Eq. (2.88) describes the dissipation associated with the non-equilibrium diffusion and heat transfer and needs to be positive. This allows the definition of simple constitutive laws for these processes. The heat transfer, for example can be described by a simple rule,

$$\boldsymbol{q} = -\boldsymbol{k}\nabla T. \tag{2.90}$$

where $\boldsymbol{k}$ is a symmetric positive semi-definite tensor. Similarly, in the absence of other restrictions on the diffusive processes, the diffusive fluxes can be written as,

$$\boldsymbol{J}_i = -\boldsymbol{M}\nabla \mu_i. \tag{2.91}$$

In the above $\boldsymbol{M}$ is a symmetric positive semi-definite matrix. Maxwell's relations can also be written based on Eq. (2.89a). These lead to relations of the form,

$$\frac{\partial \boldsymbol{\sigma}}{\partial \rho_i} = \frac{\partial \mu_i}{\partial \boldsymbol{\varepsilon}} \tag{2.92a}$$

$$\frac{\partial \boldsymbol{\sigma}}{\partial T} = -\frac{\partial S}{\partial \boldsymbol{\varepsilon}} \tag{2.92b}$$

$$\frac{\partial \mu_i}{\partial T} = -\frac{\partial S}{\partial \rho_i}. \tag{2.92c}$$

Eqs. (2.92a) and (2.92b) can be integrated to derive a form for Ψ, especially in cases where the system is assumed to behave in a simple linear form. However, Eqs. (2.92a) and (2.92b) lead to additional contributions to the stress in terms of the chemical potential and the entropy. It is difficult to directly apply an additional

stress in analysis schemes, especially as most numerical schemes are displacement based. Similarly, it is difficult to relate the chemical potential to the strain. Hence it is a common practice to use the enthalpy instead of the free energy to derive constitutive laws. This is done by taking a Legendre transform of Ψ with respect to the stress. The enthalpy is defined as,

$$\Phi(\boldsymbol{\sigma}, T, \rho_i) = \Psi - \boldsymbol{\sigma} : \boldsymbol{\varepsilon}. \tag{2.93}$$

The constitutive laws can now be defined in terms of the enthalpy as,

$$\frac{\partial \Phi}{\partial \boldsymbol{\sigma}} = -\boldsymbol{\varepsilon} \tag{2.94a}$$

$$\frac{\partial \Phi}{\partial \rho_i} = \mu_i \tag{2.94b}$$

$$\frac{\partial \Phi}{\partial T} = -S. \tag{2.94c}$$

These lead to Maxwell relations that can be written as,

$$\frac{\partial \boldsymbol{\varepsilon}}{\partial \rho_i} = -\frac{\partial \mu_i}{\partial \boldsymbol{\sigma}} \tag{2.95a}$$

$$\frac{\partial \boldsymbol{\varepsilon}}{\partial T} = \frac{\partial S}{\partial \boldsymbol{\sigma}} \tag{2.95b}$$

$$\frac{\partial \mu_i}{\partial T} = -\frac{\partial S}{\partial \rho_i}. \tag{2.95c}$$

For simple elastic systems which are invertible, it is possible to integrate the relations to get a form for the influence of the stress on the chemical potential and that of the concentration on the strain. The relationship between the stress and the chemical potential is derived first. For elastic solids, the stress can be written as,

$$\boldsymbol{\sigma} = \boldsymbol{C} : (\boldsymbol{\varepsilon} - \boldsymbol{\varepsilon}_0). \tag{2.96}$$

In the above, $\boldsymbol{\varepsilon}_0$ is the stress-free strain. Assuming $\boldsymbol{C}$ is invertible, a compliance matrix $\boldsymbol{K} = \boldsymbol{C}^{-1}$ is defined. Using this, the strain can be written as,

$$\boldsymbol{\varepsilon} - \boldsymbol{\varepsilon}_0 = \boldsymbol{K} : \boldsymbol{\sigma}. \tag{2.97}$$

Or with $\boldsymbol{\varepsilon} - \boldsymbol{\varepsilon}_0 \to \boldsymbol{\varepsilon}_{\text{elastic}}$

$$\boldsymbol{\varepsilon}_{\text{elastic}} = \boldsymbol{K} : \boldsymbol{\sigma}. \tag{2.98}$$

Eq. (2.95a) can be re-arranged as,

$$d\mu_i = -\frac{\partial \boldsymbol{\varepsilon}}{\partial \rho_i} d\boldsymbol{\sigma}. \tag{2.99}$$

This can be integrated from an initial stress to the current stress as,

$$\mu_i = \int_{\boldsymbol{\sigma}_0}^{\boldsymbol{\sigma}} -\frac{\partial \boldsymbol{\varepsilon}}{\partial \rho_i} d\boldsymbol{\sigma} + C(\rho_i). \tag{2.100}$$

In the above $C(\rho_i)$ only depends on ρ_i. Using Eq. (2.97),

$$\frac{\partial \boldsymbol{\varepsilon}}{\partial \rho_i} = \frac{\partial \boldsymbol{K}}{\partial \rho_i} : \boldsymbol{\sigma} + \frac{\partial \boldsymbol{\varepsilon}_0}{\partial \rho_i}. \tag{2.101}$$

This can be substituted back into Eq. (2.100) to get

$$\mu_i = \int_{\boldsymbol{\sigma}_0}^{\boldsymbol{\sigma}} \left(-\frac{\partial \boldsymbol{K}}{\partial \rho_i} : \boldsymbol{\sigma} - \frac{\partial \boldsymbol{\varepsilon}_0}{\partial \rho_i} \right) d\boldsymbol{\sigma} + C(\rho_i). \tag{2.102}$$

If the compliance is independent of the concentration, and

$$\frac{\partial \boldsymbol{\varepsilon}_0}{\partial \rho_i} = \beta_i. \tag{2.103}$$

is assumed,

$$\mu_i = -\beta_i \left(\boldsymbol{\sigma} - \boldsymbol{\sigma}_0\right) + C(\rho_i). \tag{2.104}$$

Eq. (2.104) needs to satisfy material symmetry requirements. In the case of cubic symmetry, it can be shown that an appropriate measure of the stress to be used is the hydrostatic pressure $p = -\frac{1}{3}\text{tr}(\boldsymbol{\sigma})$. In the case where the chemical potentials μ_i are independent of the concentration of other species and $\rho_{\text{total}} = \sum \rho_i$ is a constant, $C(\rho_i)$ is usually written as,

$$C(\rho_i) = RT \ln \frac{\rho_i}{\rho_{\text{total}}} + C_i^0. \tag{2.105}$$

Or

$$C(X_i) = RT \ln(X_i) + C_i^0. \tag{2.106}$$

The total chemical potential can therefore be written as,

$$\mu_i = RT \ln(X_i) + \beta_i p. \tag{2.107}$$

Similar material symmetry arguments are used to chose the strain measure for the concentration dependent strain. In the case of cubic symmetry, the concentration dependent strain should be volumetric. This allows the strain associated with the change in the concentration of the i^{th} speciesϵ_i, can be written using Eq. (2.103) as,

$$\boldsymbol{\varepsilon}_i = \int_{\rho_i^0}^{\rho} \beta_i d\rho_i \boldsymbol{I}, \tag{2.108}$$

which allows the strain to be written as

$$\boldsymbol{\varepsilon}_i = \beta_i \left(\rho_i - \rho_i^0\right) \boldsymbol{I}. \tag{2.109}$$

In terms of the mole fractions X_i, the above can be written as

$$\boldsymbol{\varepsilon}_i = \rho_{\text{total}} \beta_i \left(X_i - X_i^0 \right) \boldsymbol{I}. \tag{2.110}$$

β_i is called the concentration dependent volumetric strain and is related to the atomic volume of the i^{th} species. The total stress-free strain $\boldsymbol{\varepsilon}_0$ can then in this case be constructed by summing the individual contributions $\boldsymbol{\varepsilon}_i$. The expression for thermal strains can likewise be obtained by integrating Eq. (2.95b),

$$\boldsymbol{\varepsilon} = \alpha (T - T^0) \boldsymbol{I}. \tag{2.111}$$

where α is the co-efficient of thermal expansion. These additional strains are assumed to be stress-free in the absence of constraints on the displacement. When the method above is used to define the constitutive laws, standard stress-strain rules are used to determine the stresses.

2.5.2 Configurational Force Balance

Before introducing the interfacial balances for the numbers, momentum and energy, the configurational force balance is introduced. There are many different ways of introducing the configurational force systems into the thermodynamics of problems with evolving features. Maugin, in [94] treats the configurational force system purely as a consequence of invariance with respect to certain transformations of the velocity of evolution. The approach of Gurtin and Fried [23] is the one preferred here and is described in the following section. The authors in [23] postulate the existence of an additional stress system $\boldsymbol{c}$ that satisfies,

$$\nabla_{\boldsymbol{X}} . \boldsymbol{c} + \boldsymbol{g} = 0. \tag{2.112}$$

In the above $\boldsymbol{c}$ is a tensor quantity that is introduced through the energy supply over a control volume with accretion (Fig. A.4) while $\boldsymbol{g}$ is a configurational body force. In analogy to the introduction of the standard stresses as in Eq. (2.72), a configurational stress $\boldsymbol{c}$ is defined as the power involved in the accretive motion, as

$$\dot{W}_{\text{conf}} = \int_{\Gamma} \boldsymbol{n}.\boldsymbol{c}.\boldsymbol{u} d\Gamma. \tag{2.113}$$

In the above, $\boldsymbol{u}$ is the accretive velocity of the interface. The definition of the standard stress tensor is modified to account for the control volume with accretion,

$$\dot{W}_{\text{def}} = \int_{\Gamma} \boldsymbol{n}.\boldsymbol{\sigma}^{I}_{PK}.(\boldsymbol{v} + \boldsymbol{F}.\boldsymbol{u}) d\Gamma. \tag{2.114}$$

Using Eqs. (2.113) and (2.114), the free energy imbalance for the control volume in an isothermal case while neglecting body forces can be written as,

$$\frac{D}{Dt}\int_{\Omega} \Psi d\Omega \leq \int_{\Gamma} \left(\boldsymbol{n}.\boldsymbol{\sigma}^{I}_{PK}.(\boldsymbol{v} + \boldsymbol{F}.\boldsymbol{u}) + \boldsymbol{n}.\boldsymbol{c}.\boldsymbol{u}\right) d\Gamma - \sum_{i=1}^{N} \int_{\Gamma} \rho_i \mu_i \boldsymbol{J}_i.\boldsymbol{n} d\Gamma. \tag{2.115}$$

Using the transport theorem for control volumes with accretion Eq. (A.61), the above relation can be rewritten as,

$$\begin{aligned} \int_{\Omega} \dot{\Psi} d\Omega + \int_{\Gamma} \Psi \boldsymbol{u}.\boldsymbol{n} d\Gamma \leq & \int_{\Omega} \left((\nabla_{\boldsymbol{X}}.\boldsymbol{\sigma}^{I}_{PK}).\boldsymbol{v} + \boldsymbol{\sigma}^{I}_{PK}.\dot{\boldsymbol{F}}\right) d\Omega \\ & + \int_{\Gamma} \left(\boldsymbol{n}.\boldsymbol{c}.\boldsymbol{u} + \boldsymbol{n}.\boldsymbol{F}^{T}.\boldsymbol{\sigma}^{I}_{PK}.\boldsymbol{u}\right) d\Gamma \\ & + \int_{\Omega} \mu_i \dot{\rho}_i d\Omega - \int_{\Omega} \nabla \mu_i.\boldsymbol{J}_i d\Omega + \sum_{i=1}^{N} \int_{\Gamma} \rho_i \mu_i \boldsymbol{u}.\boldsymbol{n} d\Gamma. \end{aligned} \tag{2.116}$$

In the above, the fact that $\boldsymbol{u}$ is a velocity field that is defined to be uniformly $\mathbf{0}$ inside the domain. The terms in the above equation can be re-arranged as,

$$\begin{aligned}&\int_{\Omega}\left(\dot{\Psi}-\boldsymbol{\sigma}_{PK}^{I}:\dot{\boldsymbol{F}}-\sum_{i=1}^{N}\mu_{i}\dot{\rho}_{i}\right)d\Omega\\&+\int_{\Gamma}\left(\left(\Psi-\sum_{i=1}^{N}\rho_{i}\mu_{i}\right)\boldsymbol{u}.\boldsymbol{n}-\boldsymbol{n}.\boldsymbol{c}.\boldsymbol{u}+\boldsymbol{n}.\boldsymbol{F}^{T}.\boldsymbol{\sigma}_{PK}^{I}.\boldsymbol{u}\right)d\Gamma\leq-\int_{\Omega}\nabla\mu_{i}.\boldsymbol{J}_{i}d\Omega.\end{aligned}\tag{2.117}$$

Most of the terms in Eq. (2.117) lead to the same relations in § 2.5.1. However, there are additional term related to $\boldsymbol{u}$. At this point a constitutive assumption is made in [95] that the configurational power (Eq. (2.113)) is independent of the tangential component of $\boldsymbol{u}$. Substituting $\boldsymbol{u}=U\boldsymbol{n}+\boldsymbol{u}_{t}$. This is only possible for arbitrary $\boldsymbol{u}$ when,

$$\left(\Psi-\sum_{i=1}^{N}\rho_{i}\mu_{i}\right)\boldsymbol{I}-\boldsymbol{c}+\boldsymbol{F}^{T}.\boldsymbol{\sigma}_{PK}^{I}=0.\tag{2.118}$$

This can be re-written as

$$\boldsymbol{c}=\left(\Psi-\sum_{i=1}^{N}\rho_{i}\mu_{i}\right)\boldsymbol{I}+\boldsymbol{F}^{T}.\boldsymbol{\sigma}_{PK}^{I}.\tag{2.119}$$

The above relation recovers the Eshelby energy momentum tensor without a variational treatment, allowing its use in a more general non-equilibrium sense. Another consequence of the above treatment is that the configurational forces are not of importance in the bulk of the material as the velocity field $\boldsymbol{u}$ is assumed to be 0 in the interior. Hence they are only significant in the presence of interfaces. In the following section, the thermodynamics in the presence of an evolving interface is described.

2.5.3 Interfacial Relations

In the following section, relations are developed for the balances of number, momentum, configurational forces, free energy and momentum that are satisfied at mov-

ing interfaces. The starting point is the transport theorem for a control volume with accretion with an evolving interface described in § A.4.

Balance of Number

Using the local form for the interfacial transport theorem Eq. (A.62) with accretion, the balance of number at the interface for the species can be written as,

$$\frac{\partial \rho_i^\Gamma}{\partial t} - \kappa \rho_i^\Gamma V_\Gamma = - \left[\!\left[\boldsymbol{J}_i \right]\!\right] . \boldsymbol{n} + \left[\!\left[\rho_i \right]\!\right] V_\Gamma - \nabla_\Gamma . \boldsymbol{h}_i, \tag{2.120}$$

where $\boldsymbol{h}_i$ is the interfacial flux of the i^{th} species. In most cases, $\rho_i^\Gamma \to 0$ [96]. This allows the the relation to be written as,

$$\left[\!\left[\rho_i \right]\!\right] V_\Gamma = \left[\!\left[\boldsymbol{J}_i \right]\!\right] . \boldsymbol{n} + \nabla_\Gamma . \boldsymbol{h}_i. \tag{2.121}$$

This is the relation most commonly used in studies of interface motion due to diffusion. In some cases, it is necessary to account for the effects of interfacial supplies due to reactions or transformations. This requires modification of Eq. (2.121) as,

$$\left[\!\left[\rho_i \right]\!\right] V_\Gamma = \left[\!\left[\boldsymbol{J}_i \right]\!\right] . \boldsymbol{n} + \nabla_\Gamma . \boldsymbol{h}_i + r_i^\Gamma. \tag{2.122}$$

The above relation is used as a boundary condition in studies of diffusion in the presence of moving evolving interfaces, with the various terms excluded based on the specific conditions. For example, in the case of surface diffusion, the above relation can be reduced to,

$$V_\Gamma = \Omega \nabla_\Gamma . \boldsymbol{h}. \tag{2.123}$$

Where it is assumed that there is only one species, with no material on the one side with $\Omega = \frac{1}{\rho}$. Another commonly used statement in studies of growth of phases is [55],

$$V_\Gamma = \frac{[\![\boldsymbol{J}_i]\!].\boldsymbol{n}}{[\![\rho]\!]}. \tag{2.124}$$

Balance of Momentum

For the balance of momentum, the interfacial flux quantity in the interfacial transport theorem Eq. (A.62) is replaced by a surface stress. The surface stress is an interfacial tensor, $\boldsymbol{\sigma}_\Gamma$. This relates surface traction (defined in units of force per unit length) to the normal to an interfacial loop in the tangent loop.

$$\boldsymbol{\sigma}_\Gamma.\boldsymbol{m} = \boldsymbol{t}_\Gamma. \tag{2.125}$$

As any momentum terms are neglected, the accretive terms are not significant and the interfacial momentum balance can be written as,

$$\nabla_\Gamma.\boldsymbol{\sigma}_\Gamma + [\![\boldsymbol{\sigma}]\!].\boldsymbol{n} = 0. \tag{2.126}$$

This is a generalized form of the Laplace young equation. This can be seen by choosing, $\boldsymbol{\sigma}_\Gamma = \gamma \boldsymbol{P}$, where $\boldsymbol{P}$ is the interfacial projection tensor $\boldsymbol{I} - \boldsymbol{n} \otimes \boldsymbol{n}$. Substituting for $\boldsymbol{\sigma}_\Gamma$, Eq. (2.117) can be re-written using Eq. (A.7) as

$$\nabla_\Gamma.(\gamma \boldsymbol{P}) + [\![\boldsymbol{\sigma}]\!].\boldsymbol{n} = 0 \tag{2.127}$$

$$\nabla_\Gamma \gamma \boldsymbol{P} + \kappa \boldsymbol{n} + [\![\boldsymbol{\sigma}]\!].\boldsymbol{n} = 0. \tag{2.128}$$

Separating into tangential and normal components, the above can be reduced into two expressions

$$\nabla_\Gamma \gamma + \boldsymbol{t} \left[\!\left[\boldsymbol{\sigma} \right]\!\right] .\boldsymbol{n} = 0 \tag{2.129}$$

$$\kappa + \boldsymbol{n}. \left[\!\left[\boldsymbol{\sigma} \right]\!\right] .\boldsymbol{n} = 0. \tag{2.130}$$

Eq. (2.130) reduces to the standard Laplace-Young equation when $\boldsymbol{\sigma} = -p\boldsymbol{I}$. Equations of the form Eq. (2.129) are important in the study of Marangoni flows. While a general theory does exist for surface stresses and surface strains [97], the surface stresses are not very important at the length scales of most problems in solids. They are however more important in fluid flow problems at much longer length scales.

Interfacial Configurational Force Balance

Following Gurtin's approach [23], similar to the balance of momentum (or of deformational forces) at the interface, an interfacial configurational force balance can be written. In a manner similar to Eq. (2.117),

$$\nabla_\Gamma . \boldsymbol{c}_\Gamma + \left[\!\left[\boldsymbol{c} \right]\!\right] .\boldsymbol{n} = 0. \tag{2.131}$$

In the above $\boldsymbol{g}$ is an external configurational force. This is used to account for the forces that cause grain boundary migration. Usually it is only the normal component of the interfacial balance is important. This is due to the fact that tangential motions can't change the shape of the interface. This means that the tangential component of the interfacial configurational force balance is usually not significant and can be neglected. Using the form derived for $\boldsymbol{c}$ in Eq. (2.119), the normal component of the interfacial configurational force balance can be written as,

$$\boldsymbol{n}. \left(\nabla_\Gamma . \boldsymbol{c}_\Gamma + \boldsymbol{n}. \left[\!\left[\Psi \boldsymbol{I} - \sum_{i=1}^{N} \rho_i \mu_i \boldsymbol{I} - \boldsymbol{F}^T . \boldsymbol{\sigma}^I_{PK} \right]\!\right] \right) .\boldsymbol{n} = 0. \tag{2.132}$$

Again, if the interfacial configurational stress is assumed to be isotropic and equal to $\gamma_{\text{conf}}\boldsymbol{P}$, Eq. (2.132) can be written as,

$$\gamma\kappa + \boldsymbol{n}.\left[\!\!\left[\Psi\boldsymbol{I} - \sum_{i=1}^{N}\rho_i\mu_i\boldsymbol{I} - \boldsymbol{F}^T.\boldsymbol{\sigma}^I_{PK}\right]\!\!\right].\boldsymbol{n} = 0. \tag{2.133}$$

If the assumption is made that the chemical potential is continuous across the interface,

$$[\![\rho_i\mu_i]\!] = [\![\rho_i]\!]\,\mu_i. \tag{2.134}$$

With Eq. (2.134), Eq. (2.133) reduces to a boundary condition for the chemical potential of the species at the interface.

$$\sum_{i=1}^{N}[\![\rho_i]\!]\,\mu_i = \gamma\kappa + \boldsymbol{n}.\left[\!\!\left[\Psi\boldsymbol{I} - \boldsymbol{F}^T.\boldsymbol{\sigma}^I_{PK}\right]\!\!\right].\boldsymbol{n}. \tag{2.135}$$

Free Energy Inequality

To write an interfacial balance law for the energy, energy fluxes need to be specified for the interfacial fluxes. Very general derivations are possible for this and a more general derivation can be found in [23]. As interfacial deformational stresses for solids are neglected in this work, the power due to them is neglected in the derivation presented here. The total power on the interfacial control volume can be written as,

$$W^\Gamma = \oint_C \boldsymbol{m}.\boldsymbol{c}_\Gamma.\boldsymbol{u}_\Gamma dC + \int_\Gamma [\![\boldsymbol{n}.\boldsymbol{c}.\boldsymbol{u}]\!]\,d\Gamma + \int_\Gamma \left[\!\!\left[\boldsymbol{n}.\boldsymbol{\sigma}^I_{PK}.(\boldsymbol{v} + \boldsymbol{F}\boldsymbol{u})\right]\!\!\right] d\Gamma. \tag{2.136}$$

For convenience, the heat fluxes are neglected. The energy supplies due to mass fluxes can be written as,

$$E^{\Gamma} = \oint_C \sum_{i=1}^{N} \mu_i \boldsymbol{h}_i . \boldsymbol{m} dC + \int_{\Gamma} \left[\!\!\left[\sum_{i=1}^{N} \rho_i \mu_i V \right]\!\!\right] d\Gamma + \int_{\Gamma} \left[\!\!\left[\sum_{i=1}^{N} \mu_i \boldsymbol{J}_i . \boldsymbol{n} \right]\!\!\right] d\Gamma + \int_{\Gamma} \sum_{i=1}^{N} \mu_i^r r_i d\Gamma. \tag{2.137}$$

In the above μ_i^r is the energy added or removed from the system owing to the deposition or evaporation of the i^{th}species. This can be re-written in a localized form as,

$$E^{\Gamma} = \int_{\Gamma} \sum_{i=1}^{N} \left(\nabla_{\Gamma} \mu_i . \boldsymbol{h}_i + \mu_i \nabla_{\Gamma} . \boldsymbol{h} \right) d\Gamma + \int_{\Gamma} \left[\!\!\left[\sum_{i=1}^{N} \mu_i \boldsymbol{J}_i . \boldsymbol{n} \right]\!\!\right] d\Gamma + \int_{\Gamma} \sum_{i=1}^{N} \mu_i^r r_i d\Gamma. \tag{2.138}$$

Using Eqs. (2.137) and (2.138), the free energy inequality for the interfacial control volume can be written as,

$$\begin{aligned} \int_{\Gamma} \left(\frac{\partial \Psi_{\Gamma}}{\partial t} - \Psi_{\Gamma} \kappa V \right) d\Gamma + \oint_C \Psi_{\Gamma} \boldsymbol{u}_{\Gamma} . \boldsymbol{m} dC \leq \oint_C \boldsymbol{m} . \boldsymbol{c}_{\Gamma} . \boldsymbol{u}_{\Gamma} dC + \int_{\Gamma} \left[\!\!\left[\boldsymbol{n} . \boldsymbol{\sigma}_{PK}^{I} . \boldsymbol{v} \right]\!\!\right] d\Gamma \\ + \int_{\Gamma} \left[\!\!\left[\sum_{i=1}^{N} \rho_i \mu_i V + \mu_i \boldsymbol{J}_i . \boldsymbol{n} \right]\!\!\right] d\Gamma + \int_{\Gamma} \sum_{i=1}^{N} \mu_i r_i d\Gamma \\ - \int_{\Gamma} \sum_{i=1}^{N} \left(\mu_i \nabla_{\Gamma} . \boldsymbol{h}_i + \nabla_{\Gamma} \mu . \boldsymbol{h}_i \right) d\Gamma. \end{aligned} \tag{2.139}$$

The arbitrariness of C and the velocity $u_{\Gamma} . \boldsymbol{n}$ leads to the conclusion that $\Psi_{\Gamma} = c_{\Gamma}$. Eq. (2.139) can be further simplified by using the interfacial number balance (Eq. (2.122)), continuity of tractions at the interface (Eq. (2.126)) and the interfacial configurational force balance (Eq. (2.135)). This reduces the energy balance to,

$$\frac{\partial \Psi_{\Gamma}}{\partial t} \leq - \sum_{i=1}^{N} \nabla_{\Gamma} \mu_i . \boldsymbol{h}_i - \sum_{i=1}^{N} r_i \left(\mu_i - \mu_i^r \right). \tag{2.140}$$

The simplest constitutive laws for the interfacial quantities can therefore be specified simply as,

$$\boldsymbol{h}_i = -M_\Gamma \nabla_\Gamma \mu_i \tag{2.141a}$$

$$r_i = -k\left(\mu_i - \mu_i^r\right). \tag{2.141b}$$

The combined effect of the two parts of Eq. (2.141) are used in the Chapter 3 to define the vacancy accumulation rate at the interface as well as surface diffusion at the interface of voids. In the limited derivation in this section, the dissipation and the forces related to grain boundary migration by energy minimization are neglected. [23] has a full description of the physics, including the grain boundary migration.

2.6 Addition of Other Driving Forces

An important concern while developing the thermodynamics for evolution problems is the inclusion of additional driving forces, especially the electrical potential gradient. The inclusion of the electrical potential in the thermodynamics depends on whether the material is metallic or non-metallic. The charge density can not be used as a variable in metals, as any excess charge will move to the outer surface [98]. This implies that a relation of the form,

$$\phi_e = \frac{\partial \Psi}{\partial \rho_c}, \tag{2.142}$$

can not be written in the bulk of the material. This means that it is incorrect to use the electrical potential as a component of the chemical potential, as suggested by some authors [99]. Non-metals and other insulators are capable of holding an excess charge. In such a case, the electrical potential acts as a chemical potential for the charged species. This allows relations of the form Eq. (2.142) to be written and used. The free energy imbalance then allows a flow rule for the charge in terms of the electrical potential gradient. In metals, the interaction of the electrical effects

with the crystal lattice is through two effects. The first effect is the joule heating, which can be thought of as causing uncorrelated oscillations in the lattice leading to heating. The other effect is the electronic wind. At the quantum mechanical level of description, the electronic wind is the force that the atoms in the lattice feel when the electron wave is scattered [100]. In certain cases, this force is sufficient to knock the atoms out of their position in the lattice and to activate a diffusive mechanism. This is called electromigration. Owing to the particular, entirely dissipative nature of this mechanism, it is incorrect to have the electrical potential be a part of the free energy. Instead the electronic wind is introduced as an additional driving force, with an experimentally determined parameter Z^*, or one determined by theory [101]. The driving force for the diffusion is defined due to the electronic wind in metals is specified as,

$$f_{\text{elect}} = Z^* e \boldsymbol{J}_{\phi_e}. \tag{2.143}$$

In the above $\boldsymbol{J}_{\phi_e}$ is the electric current density, while e is the fundamental charge of the electron. This can be re-written in terms of the electrical potential gradient for Ohmic conductors as $\boldsymbol{J}_{\phi_e} = c\nabla\phi_e$, where c is the conductivity. This allows Eq. (2.143) to be re-written as,

$$f_{\text{elect}} = Z^* e c \nabla \phi_e. \tag{2.144}$$

This can then added to the driving force for diffusion ($\nabla\mu_i$). Further, it is assumed that the same mobility applies for both the electromigration driving force as well as for the standard driving force corresponding to the gradient of the chemical potential,

$$\boldsymbol{J} = -M\left(\nabla\mu + Z^* e \nabla\phi_e\right). \tag{2.145}$$

3. A PHASE FIELD MODEL FOR ELECTROMIGRATION: DEVELOPMENT

The decrease in the size of flip-chip solder joints has resulted in a corresponding increase in the current densities prevalent in the joints. This has led to an increase in the importance of failure due to electromigration in flip chip solder joints [102]. Electromigration is caused by the momentum exchange between electrons and ions that forces material diffusion in the direction of electron flow. This leads to the formation of voids near the cathode that might lead to an open failure. There is also the likelihood of the formation of hillocks at the anode that might cause a shorting failure. The formation and motion of the voids is also driven by the existence of stress and temperature gradients. A unique problem that occurs in solder joints is the failure due to current crowding. The current density in the signal trace leading up to the joint is significantly higher than the current density in the solder joint. At the interface between the two, there is a region of the solder joint, where the current density is an order of magnitude higher than the rest of the joint ($\approx 10^5 Acm^{-2}$ at the entrance versus $\approx 10^4 Acm^{-2}$ near the middle [102]). This causes the void formation to be very rapid near the current crowding region (see Fig. 3.1).

The computational simulation of the formation and propagation of voids in solder is a challenging problem. There are a multitude of interacting physical effects such as the electrical, thermal and stress fields that determine the void shape and its rate of evolution. A significant attempt at modeling electromigration in solder joints has been through use of damage mechanics to simulate the loss in load bearing capacity of the solder joints [103,104]. These models enable one to find locations of void formation and in modeling the motion of very small, diffuse, voids, whose boundaries are not explicitly captured. These methods do not explicitly model the geometry of the voids, but infer the effects of the formed voids through the damage to load-bearing capacity they cause. However, geometrically speaking, the removal of material from a region

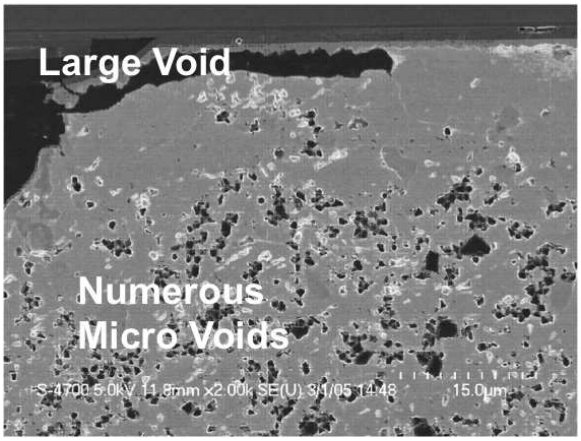

Figure 3.1. Formation of pancake voids in the current crowding region [108].

results in the formation of new surfaces. Further, energy-wise, every new surface formation has an associated surface energy cost [105] that needs to be accounted for in any complete simulation of the motion of voids.

An alternative approach to modeling electromigration is to capture the divergence of atomic flux directly within a finite element code [106, 107]. In these approaches, the modeling of motion and growth of larger voids, appears to rely mostly on element deletion schemes, which approximate the boundary of the voids accurately in the limit of mesh refinement [107]. Furthermore, these methods also ignore the surface energy associated with void boundaries or surface diffusion along the void boundary, and rely on the underlying physics of electromigration being captured entirely in the bulk through the divergence of flux.

The phase-field method has been used earlier to study electromigration in Al/Cu interconnects by various authors [66, 109], as it allows relatively easy handling of topological changes. In this chapter, a phase field model for simulating the motion and growth of pre-existing voids in flip-chip solder joints is developed. The presence of silver and copper in the solder is neglected as they form a very small fraction of the material in the solder joint. The only diffusion mechanism considered in the bulk of the solder joints is the self diffusion of Sn atoms due to a a vacancy mechanism. At

the interface of the voids, the voids evolve due to surface diffusion by motion of Sn atoms along the interface. In addition, the interface evolves by the accumulation and coalescence of vacancies at the void interface. In addition to the standard diffusion due to the gradients in the chemical potential in the bulk and at the interface, the diffusion is also driven by the electron wind (electromigration) as well as temperature gradients, (thermo-migration). Another effect that is considered in the model is the effect of stress. This comes into the picture both due to the back-stress developed on account of changes in the vacancy concentration in Sn, as well as external loads seen in the solder joint due to effects such as the mismatch in the co-efficient of thermal expansion. In § 3.1, a sharp interface model for the evolution of voids in solder joints is presented. Next, (§ 3.2) the phase field equations for the model are discussed coupled with a formal asymptotic analysis (§ 3.3) for the developed phase field equations.

A numerical method for the solution of the equations presented here is developed in Chapter 4. This numerical method is a staggered multi-physics code. Various numerical validation examples are presented there.

3.1 Sharp Interface Model

In this section, a sharp interface model for the electromigration growth and evolution of voids in solder is presented. The governing equations for the driving force systems are specified first, followed by the relations for the self-diffusion of tin, and the motion of the void by surface diffusion and void growth.

3.1.1 Distribution of the Electrical Potential Gradient

As solder is a conductor, there is no charge accumulation at any point in the bulk of the solder joint. Therefore, the electrical current or charge flux is divergence free, and the charge evolution is described as,

$$\nabla . \boldsymbol{J}_{\text{charge}} = 0. \tag{3.1}$$

The current is driven by gradients in the electrical potential. The current is related to the gradient in the electrical potential, ϕ_e through the conductivity,

$$\boldsymbol{J}_{\text{charge}} = -c\nabla\phi_e. \tag{3.2}$$

With Eq. (3.1)

$$-\nabla.c\nabla\phi_e = 0. \tag{3.3}$$

This is solved coupled with Dirichlet boundary conditions on the electrical potential,$\phi_e = \phi_e^0$ on Γ_{ϕ_e}, and Neumann boundary conditions as a condition on total electrical flux, $c\nabla\phi_e = \boldsymbol{J}_e$. On the internal void boundaries, the net charge flux into the void is zero, this leads to,

$$c\nabla\phi_e.\boldsymbol{n} = 0. \tag{3.4}$$

3.1.2 Temperature Distribution

The heat transfer equation is defined as follows,

$$\rho_{\text{mass}}C_p\frac{\partial T}{\partial t} = -\nabla.k\nabla T + s. \tag{3.5}$$

The heat generation s is due to many causes. Here, only the contributions due to Joule heating are considered as they are expected to be dominant. The heat generation due to Joule heating can be written as,

$$s = c|\nabla\phi_e|^2. \tag{3.6}$$

In addition, the boundary conditions that can be applied are Dirichlet boundary conditions of the form, $T = T_0$ on Γ_{T_0}, Neumann boundary conditions on the heat

flux, $k\nabla T = \boldsymbol{q}$ on $\Gamma_{\boldsymbol{q}}$. In addition, simple convection boundary conditions are applied of the form,

$$-k\nabla T.\boldsymbol{n} = h_c(T - T_{\text{amb}}). \tag{3.7}$$

At internal void boundaries, the net flux is assumed to be 0. This is defined through a boundary condition of the form,

$$k\nabla T.\boldsymbol{n} = 0. \tag{3.8}$$

The assumption here is that while there are some thermal storage terms involved, the thermal equilibrium is still faster than the pace at which diffusive equilibrium is attained.

3.1.3 Balance of Momentum

It is assumed that the stress equilibrium is reached much faster than diffusive equilibrium. Hence the time derivatives of displacement are neglected. The stress equilibrium condition is therefore simply,

$$\nabla.\boldsymbol{\sigma} = 0. \tag{3.9}$$

It is assumed that small-strain elasticity is sufficient for the purposes of this study and the constitutive law is written as,

$$\boldsymbol{\sigma} = \boldsymbol{C} : (\boldsymbol{\varepsilon} - \boldsymbol{\varepsilon}_{\text{thermal}} - \boldsymbol{\varepsilon}_{\text{diff}}). \tag{3.10}$$

In the above, $\boldsymbol{\varepsilon}$ is the standard small strain, defined as,

$$\boldsymbol{\varepsilon} = \frac{\nabla \boldsymbol{u} + \nabla \boldsymbol{u}^T}{2}. \tag{3.11}$$

$\boldsymbol{\varepsilon}_{\text{thermal}}$ is the standard thermal strain, defined as,

$$\boldsymbol{\varepsilon}_{\text{thermal}} = \alpha \left(T - T_0\right) \boldsymbol{I}. \tag{3.12}$$

In addition to the thermal strain, as the concentration of vacancies increases, a compressive stress-free strain develops in the solid. In the case, where there are constraints on the deformation, a stress develops with changes in the vacancy concentration. This additional stress also contributes to the diffusion of vacancies. This additional strain is written as,

$$\boldsymbol{\varepsilon}_{\text{diff}} = \beta \left(X - X_{\text{eq}}\right) \boldsymbol{I}. \tag{3.13}$$

β is a co-efficient for this additional strain, and is usually related to the atomic volume differences between the vacancies and the Sn atoms. $\beta < 0$ for vacancies usually. The reasoning for this form for the additional diffusive strain is provided in Eq. (2.108). This is because vacancies occupy less volume than the atoms, and if the concentration of the vacancies in the solid is greater than the equilibrium concentration, there is a compressive strain generated that tends to relax tensile strains in the solid.

The boundary conditions for the stress equilibrium problem are specified either as Dirichlet boundary conditions on the displacement, $\boldsymbol{u} = \boldsymbol{u}_o$ on $\Gamma_{\boldsymbol{u}}$. In addition, the standard Neumann boundary conditions can be applied, $\boldsymbol{\sigma}.\boldsymbol{n} = \boldsymbol{t}$ on $\Gamma_{\boldsymbol{t}}$, where $\boldsymbol{t}$ are the applied tractions. The void surfaces are assumed to be traction free, and the boundary conditions on the internal surfaces can be written as,

$$\boldsymbol{\sigma}.\boldsymbol{n} = \boldsymbol{0}. \tag{3.14}$$

3.1.4 Self Diffusion of Tin in the Bulk

The only bulk diffusion mechanism that is assumed to be operational is the self-diffusion of Sn atoms. This is modeled by a substitutional diffusion mechanism, with

vacancies assumed to be a hypothetical species, that lie at unoccupied lattice sites. This is necessary as the concentration of tin over the domain changes very marginally over the domain. The balance equations for the vacancies are written as,

$$\frac{\partial \rho_{\text{vac}}}{\partial t} = -\nabla . \boldsymbol{J}_{\text{vac}}. \tag{3.15}$$

$\boldsymbol{J}_{\text{vac}}$ is the vacancy flux. Owing to the substitutional flux constraint, this can be related to the flux of the tin through,

$$-\boldsymbol{J}_{\text{vac}} + \boldsymbol{J}_{\text{Sn}} = \boldsymbol{0}. \tag{3.16}$$

For substitutional diffusion, it is known that the driving force for diffusion is the difference in the chemical potentials instead of the chemical potential of the individual species. The diffusive flux can therefore be written as,

$$\boldsymbol{J}_{\text{vac}} = -\boldsymbol{M}_{\text{vac}} \nabla \left(\mu_{\text{vac}} - \mu_{\text{Sn}} \right). \tag{3.17}$$

. The mobility matrix is defined as a function of the concentration, and other variables. Rewriting the vacancy balance equation in terms of the number concentrations, and introducing the mobility diffusivity equation, the equation can be re-written as,

$$\frac{\partial \rho_{\text{vac}}}{\partial t} = -\nabla . \boldsymbol{J}_{\text{vac}} = -\nabla . \frac{-\boldsymbol{D}}{RT} \rho_{\text{vac}} \nabla \left(\mu_{\text{vac}} - \mu_{\text{Sn}} \right). \tag{3.18}$$

It is easier to solve the above in terms of the mole fraction instead of the concentration. This is due to the fact that constitutive laws for the chemical potential are usually formulated in terms of the mole fraction. Also, numerically quantities in terms of the mole fractions are better scaled. In terms of mole fractions, the balance equation for vacancies can be written as,

$$\frac{\partial X_{\text{vac}}}{\partial t} = -\nabla . \boldsymbol{M}_{\text{vac}} \nabla \left(\mu_{\text{vac}} - \mu_{\text{Sn}} \right). \tag{3.19}$$

The chemical potential for vacancies is assumed to have the form,

$$\mu_{\text{vac}} = RT \ln \frac{X_{\text{vac}}}{X_{\text{vac}}^{\text{eq}}} - \Omega_{\text{vac}} p. \tag{3.20}$$

In the above Ω_{vac} is the atomic volume of the vacancies and p is the hydrostatic pressure. With this definition of chemical potential a greater vacancy concentration is favorable at points where the stress is tensile. The chemical potential for the tin atoms is specified as,

$$\mu_{\text{Sn}} = RT \ln \frac{X_{\text{Sn}}}{X_{\text{Sn}}^{\text{eq}}} - \Omega_{\text{Sn}} p. \tag{3.21}$$

In most of the domain, $X_{\text{Sn}} \approx X_{\text{Sn}}^{\text{eq}}$. This implies that the first part of the chemical potential of tin is approximately $RT \ln 1 = 0$. This means that while this is strictly a substitutional diffusion problem, it can be treated as a simple interstitial diffusion problem for all practical purposes. Hence, the chemical potential of the vacancies is directly assumed to be,

$$\mu_{\text{vac}} = RT \ln \frac{X_{\text{vac}}}{X_{\text{vac}}^{\text{eq}}} + \beta p. \tag{3.22}$$

In the above $\beta = \Omega_{\text{Sn}} - \Omega_{\text{vac}}$ is a parameter that measures the relative atomic volumes of the tin and the vacancies. This is constructed so that, for positive β, the vacancies move towards regions of higher tensile stress. The vacancies release this stress by generating a compressive strain. This behavior of the vacancies is the reasoning behind many models of diffusion creep [110].

The chemical potential gradient is not the only cause for the diffusive flux. In addition, there is a diffusive flux due to the applied electric current. The electromigration driving force is written as,

$$\boldsymbol{f}_{\text{elec}} = Z^* e \rho \boldsymbol{J}_{\text{charge}}. \tag{3.23}$$

The above can be re-written as

$$\boldsymbol{f}_{\text{elec}} = Z^* e \nabla \phi_e. \tag{3.24}$$

Z^* is an experimentally determined parameter that is determined through electromigration experiments that relates the diffusive flux to the applied electrical current. It has to be noted that this is a parameter that is meaningless outside of the context of electromigration. The sign of the Z^* parameter can be either positive or negative based on the material, and it determines whether the material accumulates at the cathode or the anode.

In addition, while the temperature of the geometry under consideration is expected to be more or less constant throughout the domain, for the purposes of evaluating material properties. Owing to the very small length scales under consideration, even small changes in the temperature can lead to temperature gradients large enough to cause mass fluxes. This is specified in a manner similar to the electromigration flux and the driving force for diffusion due to thermomigration as,

$$\boldsymbol{f}_{\text{therm}} = Q^* \nabla T. \tag{3.25}$$

The thermo-migration is expected to cause the motion of atoms from zones of higher temperature to zones of lower temperature. The vacancy flux is expected to be equal and opposite to this flux. Hence the vacancy flux due to thermo-migration will be the same as the flux of Sn atoms, however, the direction will be reversed. The total driving force for diffusion is written as,

$$\boldsymbol{f}_{\text{tot}} = RT \frac{\nabla X_{\text{vac}}}{X_{\text{vac}}} + \beta \nabla p + Z^* e \nabla \phi_e + Q^* \nabla T. \tag{3.26}$$

To relate the driving force for diffusion with the total flux for diffusion, through the mobility diffusivity relation. This leads to the total flux of vacancies being defined as,

$$\boldsymbol{J}_{\text{vac}} = \frac{\boldsymbol{D}}{RT} X_{\text{vac}} \left(RT \frac{\nabla X_{\text{vac}}}{X_{\text{vac}}} + \beta \nabla p + Z^* e \nabla \phi_e + Q^* \nabla T \right). \tag{3.27}$$

The total diffusion equation in the bulk can be written as,

$$\frac{\partial X_{\text{vac}}}{\partial t} = \nabla . \frac{\boldsymbol{D}}{RT} X_{\text{vac}} \left(\nabla RT \ln \frac{X_{\text{vac}}}{X_{\text{vac}}^{\text{eq}}} + \beta \nabla p + Z^* e \nabla \phi_e + Q^* \nabla T \right). \tag{3.28}$$

Boundary conditions

The boundary conditions for the bulk diffusion are specified as either dirichlet boundary conditions on the mole fraction. $X_{\text{vac}} = X_{\text{vac}}^0$ on $\Gamma_{X_{\text{vac}}^0}$. The external boundaries of the domain are otherwise assumed to be flux-free boundaries. $\boldsymbol{J}_{\text{vac}}.\boldsymbol{n} = 0$. At the moving void boundaries, the boundary conditions are specified differently. Balancing the number of vacancies over an interfacial control volume,

$$X_{\text{vac}} V = \boldsymbol{J}_{\text{vac}}.\boldsymbol{n} + \lambda X_{\text{vac}} \left(\mu_{\text{vac}}^{\Gamma} - \mu_{\text{Sn}}^{\Gamma} \right). \tag{3.29}$$

The final term in the above equation is due to the absorption of vacancies at the interface. The form of Eq. (3.29) can be reasoned as follows. The vacancies are at equilibrium at the boundary when the difference between the chemical potential of the vacancies and the chemical potential of the tin is 0. Vacancies are either absorbed or created at the interface, based on the current concentration of vacancies at the interface X_{vac}, a rate constant λ and the difference between the chemical potential of the tin and the chemical potential of the vacancies. A boundary condition very similar to Eq. (3.29) is used in [66]. However, the dimensions of the additional applied flux in that work are incorrect, and the accretive term $X_{\text{vac}} V$ is neglected while deriving the boundary condition. In the absence of any vacancy coalescence at the interface,

if the interface evolves due to other effects, such as surface diffusion, the vacancies will pile up in front of a moving void while there will be a deficit of voids at least temporarily behind the interface Fig. 3.2.

The final term can be understood as a type of evaporation-condensation relation on the interface. This term will cause the void to grow. Boundary conditions of this type have a long history in the simulation of void growth in diffusion creep [111–113]. The justification for the form of the vacancy coalescence is through Eq. (2.141) as this process is very similar to the condensation or evaporation at an interface. If the chemical potential of the vacancies in the bulk is greater than the chemical potential of the tin, the vacancies will *condense* on the interface, causing the void to grow, and causing a consumption of vacancies in the bulk. On the other hand, if the chemical potential of the vacancies at the interface is less than that in the bulk, the vacancies will *evaporate* and the void will shrink, and the concentration of vacancies in the bulk will increase. It should be noted that in Eq. (3.29), any contribution due to the diffusion of vacancies on the void boundaries is neglected.

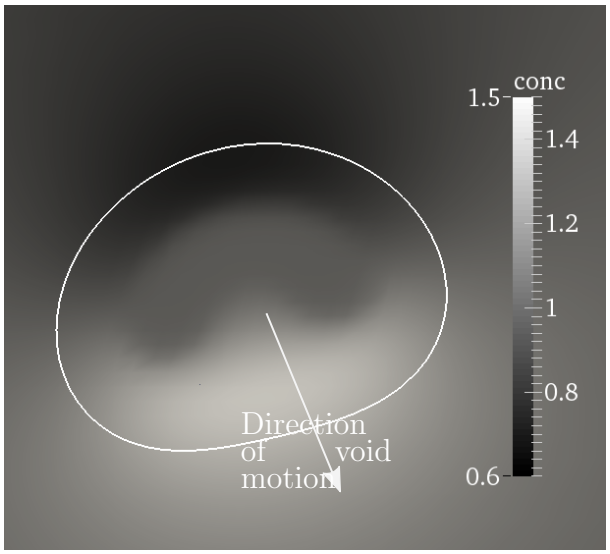

Figure 3.2. Vacancy pile up ahead of a moving interface.

Diffusivity for Vacancies

Self-diffusion of tin is an example of substitutional diffusion. In the case of substitutional diffusion the mobility matrices for vacancy diffusion and tin diffusion are not independent but are instead linked by a constraint of the form.

$$\boldsymbol{M}_{\mathrm{vac}} - \boldsymbol{M}_{\mathrm{Sn}} = 0. \tag{3.30}$$

Rewriting the above in terms of the concentration of the vacancies and the diffusivities of the tin and the vacancies,

$$\boldsymbol{D}_{\mathrm{vac}}\rho_{\mathrm{vac}} = \boldsymbol{D}_{\mathrm{Sn}}\rho_{\mathrm{Sn}}. \tag{3.31}$$

Dividing throughout by ρ_{Sn}, the equation above can be written in terms of mole fractions.

$$\boldsymbol{D}_{\mathrm{vac}}X_{\mathrm{vac}} = \boldsymbol{D}_{\mathrm{Sn}}X_{\mathrm{Sn}}. \tag{3.32}$$

Using the fact that $X_{\mathrm{Sn}} \approx 1$, Eq. (3.32) leads to,

$$\boldsymbol{D}_{\mathrm{vac}} = \frac{\boldsymbol{D}_{\mathrm{Sn}}}{X_{\mathrm{vac}}}. \tag{3.33}$$

This relation is necessary as most experimental results state the self diffusivity of tin, which can't be directly used with the vacancy diffusion equation. In the process of simulation it is assumed that the vacancy mole fraction does not change too significantly from the equilibrium vacancy concentration of tin, and the diffusivity for vacancies is assumed to be constant and equal to,

$$\boldsymbol{D}_{\mathrm{vac}} = \frac{\boldsymbol{D}_{\mathrm{Sn}}}{X^{\mathrm{eq}}_{\mathrm{vac}}}. \tag{3.34}$$

3.1.5 Void Motion

Finally, the relations that hold at the void interface are described in this subsection. The void is assumed to evolve by two mechanisms. The first is through the diffusion of Sn atoms on the void interface due to the flux of Sn atoms on the interface. This is described by the surface diffusion equation. In addition, the void can grow or sink based on the accumulation and coalescence of vacancies at the interface. The balance of number at the interface is written as,

$$\rho_{\mathrm{Sn}} V = \boldsymbol{J}_{\mathrm{Sn}}.\boldsymbol{n} + \nabla_{\Gamma}.\boldsymbol{h}_{\Gamma} + \lambda\rho_{\mathrm{vac}}\left(\mu^{\Gamma}_{\mathrm{vac}} - \mu^{\Gamma}_{\mathrm{Sn}}\right). \tag{3.35}$$

In the above, $\boldsymbol{J}_{\mathrm{Sn}}.\boldsymbol{n}$ is the contribution of the flux of Sn atoms into the interface. This is negligible compared to the other contributions, and is neglected. $\nabla_{\Gamma}.\boldsymbol{h}_{\Gamma}$ is the contribution due to the diffusive motion on the interface. If the ρ_{Sn} stays reasonably constant through the evolution and $\Omega_{\mathrm{Sn}} = \frac{1}{\rho_{\mathrm{Sn}}}$. This allows Eq. (3.35) to be written as,

$$V = \Omega_{\mathrm{Sn}}\left(\nabla_{\Gamma}.\boldsymbol{h}_{\Gamma} - \lambda\rho_{\mathrm{vac}}\left(\mu^{\Gamma}_{\mathrm{vac}} - \mu^{\Gamma}_{\mathrm{Sn}}\right)\right). \tag{3.36}$$

The final terms in the above are the growth in the void due to vacancy coalescence at the interface that was specified in Eq. (3.29). The flux for the surface diffusion needs to be specified now. As shown in Eq. (2.135) The configurational force balance at the interface leads to,

$$\rho_{\mathrm{Sn}}\mu^{\Gamma}_{\mathrm{Sn}} = \Psi - \gamma\kappa. \tag{3.37}$$

Using the same arguments used to write Eq. (3.36),

$$\mu^{\Gamma}_{\mathrm{Sn}} = \Omega_{\mathrm{Sn}}\left(\Psi - \gamma\kappa\right). \tag{3.38}$$

All contributions to Ψ other than the strain energy density at the interface are usually neglected, and

$$\mu_{\mathrm{Sn}}^{\Gamma} = \Omega_{\mathrm{Sn}} \left(W - \gamma \kappa \right). \tag{3.39}$$

With this definition of the chemical potential at the interface, the standard surface diffusion flux is specified as,

$$\boldsymbol{h} = -M \nabla \mu_{\mathrm{Sn}}. \tag{3.40}$$

In addition, by the same arguments used to introduce the electromigration and thermal driving force to the bulk vacancy flux, the total surface flux is written as,

$$\boldsymbol{h} = -M \left(\nabla_{\Gamma} \mu_{\mathrm{Sn}} + Z_{\Gamma}^{*} e \nabla_{\Gamma} \phi_e + Q_{\Gamma}^{\star} \nabla T \right). \tag{3.41}$$

The surface mobility can now be related to the surface diffusivity using a mobility-diffusivity relation, assuming a constant volumetric concentration of atoms at the interface as,

$$M = \frac{D_{\Gamma} h}{RT}. \tag{3.42}$$

In the above, h is the interfacial thickness, which is usually taken to be one atomic layer [55]. A more detailed reasoning for this form of the equation can be found in [55]. The final equations for the motion of the interface can therefore be summarized as,

$$V = \Omega \left(\nabla_{\Gamma} . M_{\Gamma} \left(\nabla_{\Gamma} \mu_{\mathrm{Sn}}^{\Gamma} + Z^{*} e \nabla_{\Gamma} \phi_e + Q_{\Gamma}^{*} \nabla T \right) + \lambda \rho_{\mathrm{vac}} \left(\mu_{\mathrm{vac}}^{\Gamma} - \mu_{\mathrm{Sn}}^{\Gamma} \right) \right) \tag{3.43}$$

$$\mu_{\mathrm{Sn}}^{\Gamma} = \Omega \left(W - \gamma \kappa \right). \tag{3.44}$$

These equations are difficult to solve owing to the existence of moving boundaries. These equations are solved in this thesis using a phase field method. In the diffuse interface method used in this thesis, the phase field equations have no physical mean-

ing. The only interpretation that can be attached to them is through the asymptotic analysis in § 3.3.

3.2 Phase Field Equations

The equations derived in the previous section are solved using a phase field approach. The phase field or diffuse interface versions of the equations in § 3.1 are derived by using smoothed approximations for the Heaviside step function and the Dirac δ function. In this study, the version of the Heaviside step function that is used is,

$$H(\boldsymbol{x}) = \frac{1 + \tanh \frac{r}{\sqrt{2}\epsilon}}{2}. \tag{3.45}$$

In the above r is the distance from the interface. This function is chosen so that it tends to 0 in the interior of the void and 1 in the bulk of the material. As $\epsilon \to 0$, the function tends to a sharp Heaviside step function. It should be noted that the Heaviside step function used reaches 1 or 0 only asymptotically. However, the function is reasonably close to the values of 1, 0 for most practical purposes when $r \ll \epsilon$. The Dirac δ function corresponding to this that is used is,

$$\delta(\boldsymbol{x}) = (1 - \tanh^2 \frac{r}{\sqrt{2}\epsilon})^2. \tag{3.46}$$

This function usually appears in a normalized form in the phase field equations. This normalization is omitted here, as the value of the normalization constant depends on the context and is different for the diffuse interface version of the surface motion equation, and for the vacancy diffusion equation. Using this, the equations for the driving force systems are described first. The diffuse interface versions of the driving force systems are described first. This is followed by the diffuse interface equations for the motion of the interface and the diffuse interface equations for the diffusion equation. The vacancy diffusion equation is described last as they are more closely

related to the phase-field equations for the evolution of the voids, than the other equations here are.

3.2.1 Electric Potential, Heat Transfer and Momentum Balance

The diffuse interface versions of these three equations are described together as the bulk equations and the boundary conditions at the interface can be described in a similar fashion. The sole boundary condition at the moving interface for all three of these, is a relation of the form,

$$\boldsymbol{J}.\boldsymbol{n} = 0. \tag{3.47}$$

The equation for the electrical potential is written by modifying the conductivity as,

$$c = H(\boldsymbol{x})c_0. \tag{3.48}$$

This allows the equation to be written as

$$-\nabla.H(\boldsymbol{x})c_0\nabla\phi_e = 0. \tag{3.49}$$

In finite element solutions of the above, as $H(\boldsymbol{x}) \to 0$, the system matrix will become singular. To counter this, the conductivity of the material actually used in simulations is,

$$c_{\text{diff}} = c_{\text{diff}}(H(\boldsymbol{x}) + \eta). \tag{3.50}$$

Where η is a small number, typically $\approx 1 \times 10^{-6}$. Similarly, the equation for the stress equilibrium in the bulk is written for the diffuse interface solution by modifying $\boldsymbol{C}$ to $(H(\boldsymbol{x}) + \eta)\boldsymbol{C}_0$. This can be written as,

$$\nabla.(H(\boldsymbol{x}) + \eta)\boldsymbol{C}_0\left(\boldsymbol{\varepsilon} - \boldsymbol{\varepsilon}_{\text{thermal}} - \boldsymbol{\varepsilon}_{\text{diff}}\right) = 0. \tag{3.51}$$

The heat transfer equation is similarly modified by modifying all the bulk quantities by multiplying them by the Heaviside function. The heat transfer equation is therefore written in the diffuse interface form as,

$$\rho c_p \frac{\partial T}{\partial dt} - \nabla . H(\boldsymbol{x}) k \nabla T = c|\nabla \phi_e|^2. \tag{3.52}$$

3.2.2 The Modified Cahn-Hilliard Equation

From [68], it is known that the Cahn-Hilliard equation with a degenerate mobility approximates surface motion by the surface diffusion equation. Hence to track the motion of the interface, a modified form of the Cahn- Hilliard equation is used with terms added to account for the other driving forces for interface motion. While the language used for the description of the Cahn-Hilliard model is similar to the language used in other models. It has to be noted that the Cahn-Hilliard equation here has no physical meaning. It is solely to be considered as a numerical construct, to recover the geometric evolution laws in the limit of $\epsilon \to 0$. The modified Cahn-Hilliard equation for the evolution of the interface is written as,

$$\frac{\partial \phi}{\partial t} = \frac{3}{2\sqrt{2}} \left(\Omega_{\mathrm{Sn}} \nabla . \frac{M_\Gamma \delta(\phi)}{\epsilon} \left(\nabla \mu_\Gamma + Z_\Gamma^* e \nabla \phi_e + Q_\Gamma^* \nabla T \right) + \frac{\delta}{\epsilon} \lambda X \left(\mu_\Gamma + \mu_{\mathrm{vac}} \right) \right) \tag{3.53a}$$

$$\mu_\Gamma = -\frac{3}{\sqrt{2}} \gamma \Omega_{\mathrm{Sn}} \left(\epsilon \nabla^2 \phi + \frac{1}{\epsilon} f'(\phi) \right) - \frac{15}{8} \Omega_{\mathrm{Sn}} \delta(\phi) W. \tag{3.53b}$$

The reasoning behind the constants in Eq. (3.53) will described in the next section § 3.3.

3.2.3 Vacancy Diffusion Equation

For the vacancy diffusion equation, the diffuse interface equations are developed following the method of [114]. The equation can be written as,

$$\frac{\partial HX}{\partial t} = \nabla.H\boldsymbol{D}\left(\nabla X + X\left(\beta\frac{\nabla p}{RT} + Z^*e\nabla\phi_e + Q^*\nabla T\right)\right) - \frac{3\delta}{4\sqrt{2}\epsilon}\lambda X_{\text{vac}}\left(\mu_{\text{vac}} + \mu_\Gamma\right). \tag{3.54}$$

Again, the reasoning for the constants in the above can be seen in the next section.

3.3 Formal Asymptotic Analysis

In the approach used in this work, the phase field equations by themselves don't have any physical meaning. It is necessary to show that the diffuse interface equations can be shown to be the same as the sharp interface equations described in § 3.1. This is done using the method of matched formal asymptotic analysis. This is done in two parts. First, the diffuse interface versions of the stress, electric current and heat transfer equations are analysed to show equivalence to their sharp interface forms. Then the diffusion equations for the bulk and the interface are analysed. A more detailed discussion of the technique of formal asymptotic analysis can be found in Appendices B to D. In the section that follows, ρ is the scaled distance from the interface, defined as,

$$\rho = \frac{r}{\epsilon}. \tag{3.55}$$

Throughout this section, $\bullet_\rho$, is defined as $\frac{\partial \bullet}{\partial \rho}$, while $\bullet_{\rho\rho}$ is defined as $\frac{\partial^2 \bullet}{\partial \rho^2}$. The domain for the asymptotic analysis can be seen in Fig. 3.3.

The following statements regarding the Heaviside step function H and the Dirac δ function, are necessary before starting the asymptotic analysis. In the outer region I, $H = 1$ and $H = 0$ in region II. In both region I and II, $\delta = 0$.

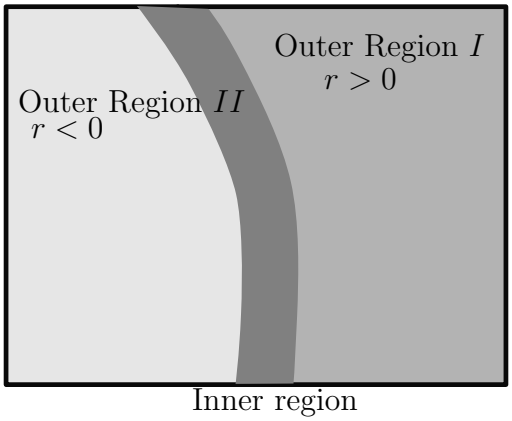

Figure 3.3. Domain for the formal asymptotic analysis.

3.3.1 Asymptotic Analysis of the Driving Force Systems

First the equations related to the driving forces, Eqs. (3.50) to (3.52), are analysed.

Electrical Potential Field

Expanding the electrical potential in the outer region as $\phi_e(\boldsymbol{x}) = \phi_e^0(\boldsymbol{x}) + \epsilon\phi_e^I(\boldsymbol{x}) + \ldots$. As $H^0 = 1$ in the outer region, Eq. (3.50) reduces to the standard charge balance equation in the outer region. In the inner region, neglecting all tangential components, the inner equation can be written using Eq. (B.34),

$$\frac{cH}{\epsilon^2}\Phi_{e\rho\rho} - \frac{cH}{\epsilon}\kappa\Phi_{e\rho} + \frac{c}{\epsilon^2}H_\rho\Phi_{e\rho\rho}. \tag{3.56}$$

Substituting the inner expansion, $\Phi_e(\rho) = \Phi_e^0(\rho) + \epsilon\Phi_e^1(\rho) + \ldots$ into Eq. (3.56) and grouping terms together, the following equations can be written at different orders. At the ϵ^{-2} order,

$$\left(cH\Phi_{e\rho}^0\right)_\rho = 0. \tag{3.57}$$

The above equation can integrated with respect to ρ to get,

$$\Phi_e^0 = \text{constant}. \tag{3.58}$$

Using the matching condition, $\lim_{\rho\to\infty} \Phi_e^0 = \lim_{r\to 0} \phi_e^0$, it can be concluded that the $\lim_{r\to 0} \phi_e^0 = \text{constant}$. The inner solution is continuous with the outer solution at the leading order. At the ϵ^{-1} order,

$$cH\Phi^1_{e\rho\rho} = 0. \tag{3.59}$$

Integrating the above equation, and using the fact that $\lim_{r\to 0^-} c\nabla\phi_e^0.\boldsymbol{n} = 0$ (inside the void)

$$cH\Phi^1_{e\rho} = 0 \implies \lim_{r\to 0^+} c\nabla\phi_e^0 = 0. \tag{3.60}$$

The above shows that the diffuse interface version of the charge balance correctly and the no -flux boundary condition at the void interface is correctly captured as $\epsilon \to 0$.

Momentum Balance Field

Writing the temperature in the outer region as $T(r) = T_0(r) + \epsilon T_1(r) + \ldots$, as $H \to 1$ in the outer region I, the standard heat transfer equation is recovered. In the inner region, the heat generation is 0, as $\Phi_{e\rho} = 0$ in the inner region. The rest of the analysis is similar to the analysis for the charge balance system.

Stress equilibrium

For the stress equilibrium equation in the outer region I, the standard stress equilibrium equation is recovered as $H = 1$. For the analysis in the inner region, using Eq. (B.19),

$$\boldsymbol{\sigma}.\boldsymbol{n} = 0. \tag{3.61}$$

This recovers the traction free boundary condition on the void interfaces. It has to be noted that in the analysis for the mechanical equilibrium conditions, no mention is made of the variation of the stress and strain invariants in the interfacial region. These quantities are not constants over the interfacial region and can cause problems while calculating the diffusion due to gradients in the stress (pressure gradient), if gradients in the pressure are not suppressed over the interfacial region. This is ameliorated to a certain extent by the averaging scheme described by Eqs. (4.3) and (4.4).

3.3.2 Asymptotic Analysis of the Phase Field Equations

The asymptotic analysis for the Eq. (3.53) is based on the analysis in [68]. The solutions ϕ, μ to Eq. (3.53) can be expanded in the outer regions as,

$$\mu = \mu^0 + \epsilon\mu^1 + \epsilon^2\mu^2 + \dots \tag{3.62a}$$

$$\phi = \phi^0 + \epsilon\phi^1 + \epsilon^2\phi^2 + \dots . \tag{3.62b}$$

The solution in the inner region can be written as,

$$\mu_{\text{in}} = \mu^0_{\text{in}} + \epsilon\mu^1_{\text{in}} + \epsilon^2\mu^2_{\text{in}} + \dots , \tag{3.63a}$$

$$\Phi = \Phi^0 + \epsilon\Phi^1 + \epsilon^2\Phi^2 + \dots . \tag{3.63b}$$

The outer analysis is performed first. Substituting Eq. (3.62) into Eq. (3.53b), the leading order in the outer expansion is the ϵ^{-1} term. This leads to,

$$f'(\phi^0) = 0. \tag{3.64}$$

From Fig. 4.5, it can be seen that $f'(\phi^0)$ has two roots at ± 1. Hence, the solution to ϕ in the outer regions tends to either ± 1. This allows the phases to be discriminated, with 1 indicating the presence of material and -1 the void. This also leads to $\mu^0 = 0$ in the outer region, as the only other term in the ϵ^0 order for Eq. (3.53b) is $-\frac{15}{8}\Omega_{\mathrm{Sn}}\delta W$, which is 0 in the outer region. Therefore, in the outer region, Eq. (3.53a) can be reduced to $0 = 0$ in all orders.

For the inner-expansion, Eq. (3.53) needs to be transformed into a co-ordinate system that is attached to the interface. Using Eq. (B.34), the modified Cahn-Hilliard equation can be written as,

$$\begin{aligned}\Phi_t - \frac{1}{\epsilon}V\Phi_\rho =& \frac{3}{2\sqrt{2}}\frac{M\delta'(\Phi)}{\epsilon}\left(\frac{\Phi_\rho}{\epsilon}\hat{\boldsymbol{e}}_\rho + \nabla_\Gamma\Phi\right).\left(\frac{G_\rho}{\epsilon}\hat{\boldsymbol{e}}_\rho + \nabla_\Gamma G\right) \\ &+ \frac{3}{2\sqrt{2}}\frac{M\delta(\Phi)}{\epsilon}\left(\frac{1}{\epsilon^2}G_{\rho\rho} - \frac{1}{\epsilon}\kappa G_\rho + \nabla_\Gamma^2\left(G\right)\right) \\ &+ \frac{3}{2\sqrt{2}}\frac{\delta(\Phi)}{\epsilon}\lambda\rho_{\mathrm{vac}}\left(\mu_{\mathrm{in}} + \mu_{\mathrm{vac}}\right).\end{aligned} \tag{3.65a}$$

In the above, $G = \mu_{\mathrm{in}} + Z^* e\Phi_e + Q^* T$.

$$\mu_{\mathrm{in}} = -\frac{3}{\sqrt{2}}\gamma\left(\frac{1}{\epsilon}\Phi_{\rho\rho} - \kappa\Phi_\rho + \frac{1}{\epsilon}f'(\Phi) + \epsilon\nabla_\Gamma^2\Phi\right) - \frac{15}{8}\delta(\Phi)W. \tag{3.65b}$$

Substituting Eq. (3.63) into Eq. (3.65), the leading order terms in Eq. (3.65b) are at the ϵ^{-1} order and can be written as,

$$-{\Phi^0}_{\rho\rho} + f'(\Phi^0) = 0. \tag{3.66}$$

The boundary conditions that Eq. (3.66) needs to satisfy the matching conditions with the outer regions I and II are, $\lim_{\rho\to-\infty}\Phi^0 \to -1$ and $\lim_{\rho\to\infty}\Phi^0 \to 1$. With these boundary conditions, the solution to Eq. (3.66) is found to be,

$$\Phi^0 = \tanh\frac{\rho}{\sqrt{2}}. \tag{3.67}$$

This implies that the equilibrium profile of Φ is a hyperbolic tangent. Eq. (3.67) also explains the choice of the approximation to the Heaviside step function in Eq. (3.45), as that can be computed quite simply as $H(\boldsymbol{x}) = \frac{1+\Phi(\boldsymbol{x})}{2}$. At the ϵ^0 order in Eq. (3.65b), the terms that remain are,

$$\mu^0_{\text{in}} = \frac{3}{\sqrt{2}}\gamma\kappa{\Phi^0}_\rho - \frac{15}{8}\delta(\Phi^0)W. \tag{3.68}$$

To make the left hand side of Eq. (3.68) integrable, both sides are multiplied by Φ_ρ. Integrating w.r.t ρ over $-\infty, \infty$, Eq. (3.68) can be shown to be,

$$2\mu^0_{\text{in}} = \Omega_{\text{Sn}}\left(\frac{3}{\sqrt{2}}\frac{2\sqrt{2}}{3}\gamma\kappa - \frac{15}{8}\frac{16}{15}\delta(\Phi)W\right). \tag{3.69}$$

The above relation implies

$$\mu^0_{\text{in}} = \Omega_{\text{Sn}}\left(\gamma\kappa - W\right). \tag{3.70}$$

In the above, the following integrals are used,

$$\int_{-\infty}^{\infty}\tanh\frac{\rho}{\sqrt{2}}_\rho\, d\rho = 2, \tag{3.71}$$

$$\int_{-\infty}^{\infty}\tanh\frac{\rho}{\sqrt{2}}_\rho^{\,2} d\rho = \frac{2\sqrt{2}}{3}, \tag{3.72}$$

and

$$\int_{-\infty}^{\infty} \tanh \frac{\rho}{\sqrt{2}}{}_{\rho} \left(1-\Phi^2\right)^2 d\rho = \frac{16}{15}. \tag{3.73}$$

Eq. (3.70) shows that the phase field equation actually computes the negative of the chemical potential of the solder interface. An important assumption made in the above derivation is that the computed value of the strain energy is more or less constant over the interfacial region. The result Eqs. (3.67) and (3.70) can be used along with results from the inner solution of the driving force systems in § 3.3.1 to analyse the solutions to Eq. (3.65a). From the results in § 3.3.1, the following can be stated,

$$T^0{}_{\rho} = \Phi^0_{e\rho} = 0. \tag{3.74}$$

Additionally, Eq. (3.70) also leads to $\mu_{\text{in}_\rho} = 0$. The leading orders Eq. (3.65a) are $\epsilon^{-2}, \epsilon^{-3}$. Terms of order ϵ^{-3} lead to,

$$\left(M\delta(\Phi)G^0{}_{\rho}\right)_{\rho} = 0. \tag{3.75}$$

Coupled with boundary conditions from the matching conditions,(Eq. (C.12)), the above leads again to $\mu^0_{\text{in}\rho} = 0$. The next order that is considered is terms of order ϵ^{-2}. Grouping these terms leads to,

$$M\delta'(\Phi^0)\left(\Phi^0{}_{\rho}\hat{\boldsymbol{e}}_{\rho}.\nabla_\Gamma G^0 + \nabla_\Gamma\Phi.G^0{}_{\rho}\hat{\boldsymbol{e}}_{\rho}\right) - \kappa G^0{}_{\rho} = 0. \tag{3.76}$$

Using the orthogonality of the surface gradient to $\hat{\boldsymbol{e}}_\rho$ as well as the fact that $G^0{}_{\rho} = 0$. The above relation reduces to $0 = 0$. Considering terms of order ϵ^{-1}, the following can be written,

$$-V\Phi^0{}_{\rho} = \frac{3}{2\sqrt{2}}M\delta(\Phi^0)\nabla^2_\Gamma G + \frac{3}{2\sqrt{2}}\rho_{\text{vac}}\delta(\Phi^0)\lambda(\mu^0_{\text{in}} + \mu^0_{\text{vac}}). \tag{3.77}$$

Substituting the terms of G, and using the fact that $\mu^0_{\text{in}} = -\mu^{\Gamma}_{\text{Sn}}$ (Eq. (3.70)), Eq. (3.77) can be written as,

$$-V{\Phi^0}_{\rho} = \frac{3}{2\sqrt{2}} M\delta(\Phi^0)\nabla^2_{\Gamma}\left(-\mu^{\Gamma}_{\text{Sn}} + Z^* e\Phi^0_e + Q^* T^0\right) + \frac{3}{2\sqrt{2}}\rho_{\text{vac}}\delta(\Phi^0)(\mu_{\Gamma} + \mu^0_{\text{vac}}). \tag{3.78}$$

Integrating the above from $-\infty$ to ∞ with respect to ρ, the expression reduces to,

$$-2V = \frac{3}{2\sqrt{2}}\frac{4\sqrt{2}}{3} M\nabla^2_{\Gamma}\left(-\mu_{\Gamma} + Z^* e\Phi^0 + Q^* T^0\right) + \frac{3}{2\sqrt{2}}\frac{4\sqrt{2}}{3}\rho_{\text{vac}}(-\mu^{\Gamma}_{\text{Sn}} + \mu^0_{\text{vac}}). \tag{3.79}$$

On simplification, Eq. (3.78) therefore recovers the relation for the motion of the interface (Eq. (3.43)).

Vacancy Diffusion Equation

Finally, the phase field version of the vacancy diffusion equation is studied. A result from this section is used to derive Eq. (3.79). This is the fact that $\mu_{\text{vac}_\rho} = 0$ in the inner region. A crucial assumption made in this derivation, here is that the pressure variation in the interfacial region is negligible. This is not strictly true, as only the displacements are constant over the interfacial region. However, in this thesis, the value of the pressure and other stress/ strain related quantities is averaged over the interfacial region Fig. 4.2 and hence $p_{\text{in}_\rho} = 0$ is reasonable.

In the outer domain, the interfacial terms drop out as $\delta(\phi) = 0$, and the standard bulk diffusion equation (Eq. (3.28)) is recovered. In the inner region, expanding the chemical potential as

$$X_{\text{vac}} = X^0_{\text{vac}} + \epsilon X^1_{\text{vac}} + \dots \tag{3.80}$$

This lets the chemical potential to be expanded as,

$$\mu_{\text{in vac}} = \mu_{\text{in vac}} + \epsilon\mu^1_{\text{in vac}} + \ldots = RT \ln X^0_{\text{vac}} X^{\text{eq}}_{\text{vac}} + \epsilon \frac{RTX^1_{\text{vac}}}{X^0_{\text{vac}}} + \beta(p^0 + \epsilon p^1 + \ldots) \tag{3.81}$$

In the leading order

$$\mu^0_{\text{in vac}} = RT \ln \frac{X^0_{\text{vac}}}{X^{\text{eq}}_{\text{vac}}} + \beta p^0. \tag{3.82}$$

Transforming Eq. (3.54) into the inner co-ordinate system, the diffusion equation in the inner region can be written using Eq. (B.20) as,

$$\frac{\partial H X_{\text{vac}}}{\partial t} - \frac{V}{\epsilon}(H X_{\text{vac}})_\rho = \frac{1}{\epsilon}\boldsymbol{n}.\boldsymbol{J}_\rho + \frac{3}{4\sqrt{2}}\frac{\delta}{\epsilon} X_{\text{vac}} \lambda \left(\mu_{\text{in vac}} - \mu^\Gamma_{\text{Sn}}\right). \tag{3.83}$$

In the above, $\boldsymbol{J}$ can be written as,

$$\boldsymbol{J} = H D_{\text{vac}} X_{\text{vac}} \left(\nabla \mu_{\text{in vac}} + Z^* e \nabla \Phi_e + Q^* \nabla T\right). \tag{3.84}$$

Expanding the above in the inner region, terms of order ϵ^{-1} can be grouped to get,

$$H D_{\text{vac}} X_{\text{vac}} \mu^0_{\text{in vac}\rho} = 0. \tag{3.85}$$

As $H D_{\text{vac}} X_{\text{vac}} \geq 0$ in the inner region, the above relation implies, $\mu^0_{\text{in vac}} = \text{constant}$ in the inner region. The implications for the mole fraction are that,

$$X^0_{\text{vac}\rho} = -\frac{X^{\text{eq}}_{\text{vac}}}{RT} \beta {p^0}_\rho. \tag{3.86}$$

With the stress/strain quantities smoothed over the interfacial region (Eq. (4.4)), ${p^0}_\rho \approx 0$ and this leads to,

$$X^0_{\text{vac}\rho} = 0. \tag{3.87}$$

Terms of order ϵ^{-1} in Eq. (3.83) can now be grouped to get,

$$-VH_\rho X_{\text{vac}} - VHX_{\text{vac}\rho} = \boldsymbol{n}.\boldsymbol{J}_\rho + X_{\text{vac}}\frac{3}{4\sqrt{2}}\delta\lambda\left(\mu_{\text{in vac}} - \mu_{\text{Sn}}^{\Gamma}\right). \tag{3.88}$$

Integrating the above equation from $-\infty$ to ∞, the relation can be re-written as,

$$-VX_{\text{vac}} = n.\boldsymbol{J} + X_{\text{vac}}\lambda\left(\mu_{\text{in vac}} - \mu_{\text{Sn}}^{\Gamma}\right). \tag{3.89}$$

This recovers the boundary condition for the vacancies on the moving interface Eq. (3.29).

3.4 Summary

The phase field model developed in this chapter is solved using a finite element method, that is described in the next chapter (Chapter 4). The diffuse interface model developed in this chapter is summarized in Table 3.1. A numerical implementation of the diffuse interface model described and analyzed here is described in Chapter 4. Further details of the implementation, in terms of the code can be found in Appendix E.

Table 3.1. Summary of the phase field model. The boundary conditions specified for the sharp interface model are the boundary conditions on the moving internal interface.

Physics	**Sharp Interface Model**	**Phase Field Model**
Electrical Potential Distribution	$-\nabla.c\nabla\phi_e = 0$ in Ω $c\nabla.\phi_e.\boldsymbol{n} = 0$on Γ	$-\nabla.cH\nabla\phi_e = 0$ in Ω
Temperature Distribution	$\rho_{\text{mass}}C_p\dfrac{\partial T}{\partial t} = -\nabla.k\nabla T + s$ in Ω $k.\nabla T = 0$ in Γ	$\rho c_p\dfrac{\partial HT}{\partial dt} - \nabla.Hk\nabla T = cH\lvert\nabla\phi_e\rvert^2$ on Ω
Momentum Balance	$\nabla.\boldsymbol{C}.(\boldsymbol{\varepsilon} - \boldsymbol{\varepsilon}_{\text{thermal}} - \boldsymbol{\varepsilon}_{\text{vac}}) = 0$ in Ω $\boldsymbol{\sigma}.\boldsymbol{n} = 0$ on Γ	$\nabla.H\boldsymbol{C}(\boldsymbol{\varepsilon} - \boldsymbol{\varepsilon}_{\text{thermal}} - \boldsymbol{\varepsilon}_{\text{vac}}) = 0$ in Ω
Vacancy Diffusion	$\dfrac{\partial X_{\text{vac}}}{\partial t} = \nabla.\dfrac{\boldsymbol{D}}{RT}X_{\text{vac}}\left(\nabla RT\ln\dfrac{X_{\text{vac}}}{X_{\text{vac}}^{\text{eq}}}\right.$ in Ω $\left.+\beta\nabla p + Z^*e\nabla\phi_e + Q^*\nabla T\right)$ $X_{\text{vac}}V = \boldsymbol{J}_{\text{vac}}.\boldsymbol{n} + \lambda X_{\text{vac}}\left(\mu_{\text{vac}}^{\Gamma} - \mu_{\text{Sn}}^{\Gamma}\right)$ on Γ	$\dfrac{\partial HX}{\partial t} = \nabla.H\boldsymbol{D}\left(\nabla X + X\left(\beta\dfrac{\nabla p}{RT}\right.\right.$ $\left.\left.+\dfrac{Z^*e}{RT}\nabla\phi_e + \dfrac{Q^*\nabla T}{RT}\right)\right) + \dfrac{3\delta}{4\sqrt{2}\epsilon}\lambda X_{\text{vac}}\left(\mu_{\text{vac}} + \mu_\Gamma\right)$ in Ω
Void Evolution Equation	$V = \Omega_{\text{Sn}}\left(\nabla_\Gamma.M_\Gamma\left(\nabla_\Gamma\mu_{\text{Sn}}^{\Gamma} + Z^*e\nabla_\Gamma\phi_e + Q_\Gamma^*\nabla T\right)\right.$ $\left.+\lambda\rho_{\text{vac}}\left(\mu_{\text{vac}}^{\Gamma} - \mu_{\text{Sn}}^{\Gamma}\right)\right)$ $\mu_{\text{Sn}}^{\Gamma} = \Omega\left(W - \gamma\kappa\right)$ on Γ	$\dfrac{\partial\phi}{\partial t} = \dfrac{3}{2\sqrt{2}}\Omega_{\text{Sn}}\left(\nabla.\dfrac{M_\Gamma\delta(\phi)}{\epsilon}\left(\nabla\mu_\Gamma + Z_\Gamma^*e\nabla\phi_e + Q_\Gamma^*\nabla T\right)\right.$ $\left.+\dfrac{\delta}{\epsilon}\lambda\rho_{\text{vac}}\left(\mu_\Gamma + \mu_{\text{vac}}\right)\right)$ $\mu_\Gamma = -\dfrac{3}{\sqrt{2}}\gamma\Omega_{\text{Sn}}\left(\epsilon\nabla^2\phi + \dfrac{1}{\epsilon}f'(\phi)\right) - \dfrac{15}{8}\Omega_{\text{Sn}}\delta(\phi)W$

4. A PHASE FIELD MODEL FOR ELECTROMIGRATION: NUMERICAL IMPLEMENTATION

In this chapter, the numerical solution to the system of equations derived in Chapter 3 is described. The model developed in Chapter 3 is a system of coupled differential equations. Ideally, they should be solved simultaneously. However, the coupling between the different systems is sufficiently weak, and solution by a staggered multi-physics approach is usually accurate enough. The approach used in this thesis is shown in Fig. 4.1. A more complete description of the code developed as part of this thesis can be found in Appendix E. Following the description of the numerical approach, the use of the code on several examples is demonstrated.

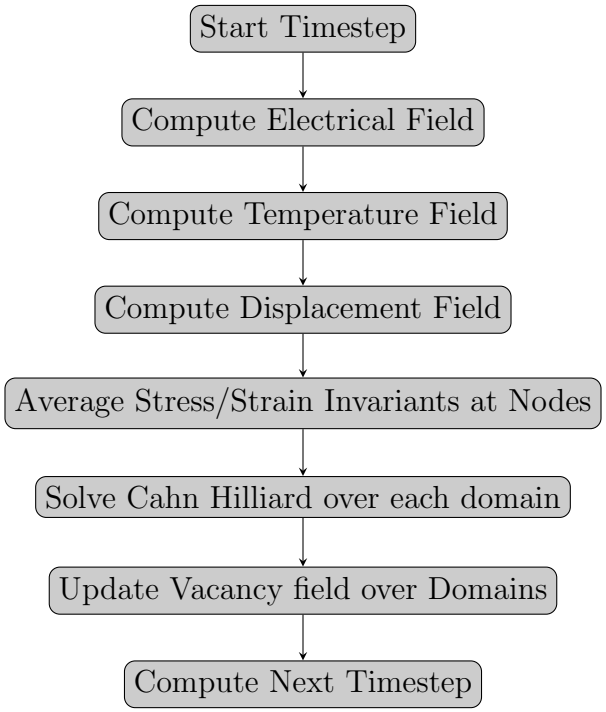

Figure 4.1. Staggered multi-physics simulation of the electromigration model.

4.1 Finite Element Implementation

The different driving force terms are solved for first, followed by the solution of the Cahn Hilliard equation to update the interface. This is then followed by the solution of the vacancy diffusion equation. The solution for the thermal, electrical and stress problems are computed by the standard finite element method. The stress problem is solved with a standard displacement based finite element method. The model for the diffusion of vacancies in the bulk (Eq. (3.28)) require the computation of the gradient of pressure. Most numerical methods for elasticity and other stress problems are based on using the displacements as the primary variable. Quantities related to stress are computed in a post-processing phase after the displacements have been found out. These values are found at the Gauss points, as the stress quantities depend on the gradients of the primary displacement variables, the level of continuity and differentiability is reduced. For example, with linear C^0 elements, the displacements are continuous at the nodes, while the gradients of the displacement are discontinuous across element boundaries. This makes the computing the gradients of stres quantities difficult. The stress quantities are therefore computed at the Gauss points and then extrapolated to the nodes by means of a global least squares solution.

Consider a quantity $\tilde{q}$ defined over the elements. Let $q(\boldsymbol{x})$ be an approximation of $\tilde{q}$ at the nodes. $q(\boldsymbol{x})$ can be found by minimizing the functional,

$$I(q(\boldsymbol{x}))\int_{\Omega}\|q(\boldsymbol{x})-\tilde{q}\|^2 d\Omega. \tag{4.1}$$

Eq. (4.1) can be minimized by a Galerkin finite element method by letting $q=\sum N_i q_i$. This leads to the solution of a linear system of equations of the form,

$$\int_{\Omega}\sum_j\sum_i N_j N_i q_i d\Omega=\int_{\Omega}\sum_j \tilde{q} d\Omega. \tag{4.2}$$

This approach works very well for regular meshes, and meshes without dangling edges. However, it does not result in a sufficiently smooth approximation of the stress

over the domain (Fig. 4.2a). Another consideration in this work is to eliminate the effect of the sharp gradients in the stress quantities at the void interface and the value of the void. Both these can be solved by adding a small diffusive component to the solution. The functional Eq. (4.1) is modified by adding a small diffusive contribution. Further smoothing over the void interface is obtained by only averaging the stress values over the material regions. This can be written as

$$I\left(q(\boldsymbol{x}), \nabla q(\boldsymbol{x})\right) = \int_{\Omega} \left(\|q(\boldsymbol{x}) - \tilde{q}\|^2 + \left(d_{\text{smoothing}}\Omega_{\text{el}}\right) \|\nabla q(\boldsymbol{x})\|^2 \right) d\Omega. \tag{4.3}$$

In the above, $d_{\text{smoothing}}\Omega_{\text{el}}$ is an additional diffusivity like quantity. $d_{\text{smoothing}}$ is a small dimensionless parameter, while Ω_{el} is the volume of the element. This lets the smoothing goes to zero as the element size goes to zero. The Euler-Lagrange equations for Eq. (4.3) can be written as,

$$-\nabla.\left(d_{\text{smoothing}}\Omega_{\text{el}}\right) \nabla q(\boldsymbol{x}) + h(\boldsymbol{x}) \left(\left(\ q(\boldsymbol{x}) - \tilde{q}\right) = 0. \tag{4.4}$$

The effect of this smoothing can be seen in Fig. 4.2. On the left, Fig. 4.2a the pressure and the strain energy as computed by Eq. (4.2) are shown on an adapted mesh. As the mesh becomes coarser, the approximations for the pressure and the strain energy develop oscillations. These can be troublesome while solving the diffusion equations, where the gradient of the pressure is needed. The addition of the diffusive term of Eq. (4.4) allows the features of the stress solution to be captured, while eliminating the oscillations that develop in the solution § 4.1.

4.1.1 Phase Field Solution

The Cahn Hilliard equation is a non-linear 4^{th} order partial differential equation. Solving a 4^{th} order partial differential equation using the finite element method directly requires the use of a C^1 discretization [115]. The standard way to solve the Cahn Hilliard equations using the finite element method is by splitting the equation

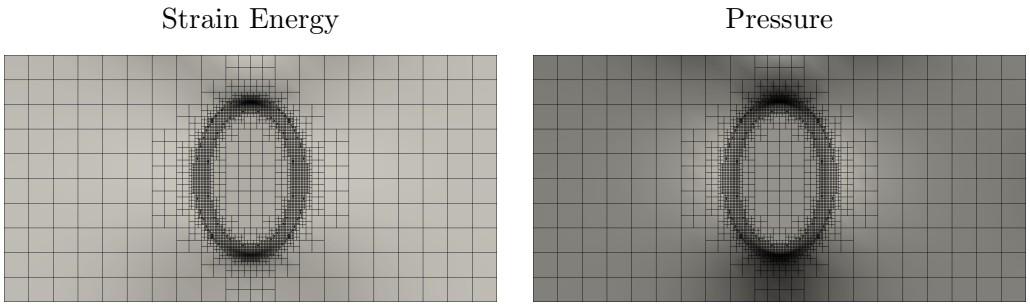

(a) Unsmoothed strain energy and pressure.

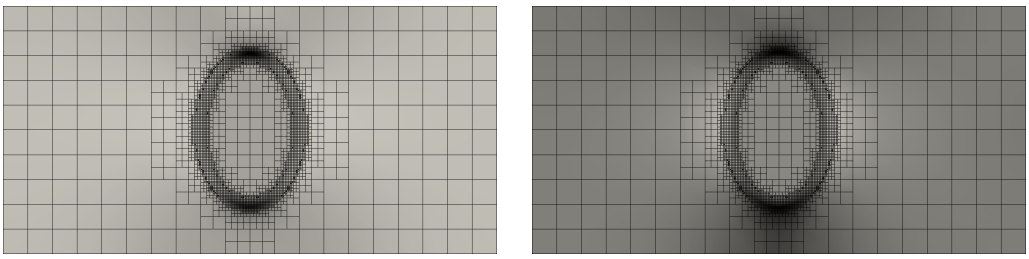

(b) Smoothed strain energy and pressure with $d_{\text{smoothing}} = 1.0$.

Figure 4.2. Smoothing of Gauss-point quantities by introducing a diffusive parameter. The strain energy and pressure distribution for an elliptical void in a rectangle under uniaxial tension.

into a system of two equations [116]. The system of equations that needs to be solved is however still a non-linear system of equations. A further complication is presented by the nature of the $f'(\phi)$ term in the Cahn-Hilliard equation. This term makes the system of equations non-convex. As a result, the numerical solution scheme fails for larger time-step values [72]. In [72], the author proposes a method based on the splitting the phase field potential function into the difference of two convex functions (Fig. 4.4),

$$f(\phi) = f_{\text{convex}}(\phi) - f_{\text{concave}}(\phi). \tag{4.5}$$

$$\tag{4.6}$$

During the time integration of the equations, the convex part of the equation is treated implicitly, while the concave part is treated explicitly from the previous time step. This leads to,

$$f'(\phi) = f_{\text{convex}}(\phi^t) - f_{\text{concave}}(\phi^{t-1}). \tag{4.7}$$

This split can be performed in a way to allow the implicit part of the problem to be completely linear. Here, $f(\phi) = \frac{1}{4}(1-\phi^2)^2$ is used. A split for the potential function that allows the solution to be computed in an easier fashion is the split,

$$f(\phi) = \underbrace{\phi^2}_{\text{convex}} \underbrace{- \frac{1}{4}\left(1 - 6\phi^2 + \phi^4\right)}_{\text{concave}}. \tag{4.8}$$

In Fig. 4.4, the convex and concave parts of the phase field functions are indicated by the solid black and red lines. It can be seen that the negative of the concave part of the function is not purely convex. This leads to numerical problems, when the

time-steps are large, and hence a modified form of the phase field function shown by the red line in Fig. 4.3 is used. This can be written as,

$$f(\phi) = \begin{cases} (\phi+1)^2 & \text{if } \phi < -1 \\ \frac{1}{4}(1-\phi^2)^2 & \text{if } \|\phi\| \leq 1 \\ (\phi-1)^2 & \text{if } \phi > 1 \end{cases} \tag{4.9}$$

This can be split into a convex and concave function as,

$$f(\phi) = \underbrace{\phi^2}_{\text{convex}} - \underbrace{\begin{cases} 1+2\phi & \text{if } \phi < -1 \\ \frac{1}{4}\left(1-6\phi^2+\phi^4\right) & \text{if } \|\phi\| \leq 1 \\ 1-2\phi & \text{if } \phi > 1 \end{cases}}_{\text{concave}} . \tag{4.10}$$

As can be seen in the dashed red line in Fig. 4.4, the concave part of the split in Eq. (4.10) is fully concave. As the convex part of $f(\phi)$ is quadratic, $f'_{\text{convex}}(\phi)$ is linear and treating it implicitly leads to a linear system of equations at every time step.

In this study, the second order stabilized solution scheme of [73] is modified and used. In this instead of using a simple concave-convex split, a more involved split, based on the backward extrapolation of f'_{convex} and the forward extrapolation of f'_{concave}. This can be written as,

$$f'(\phi) = f'_{\text{convex}}(\phi^t) - \frac{f''(\phi^t)}{2}\left(\phi^t - \phi^{t-1}\right) - f'_{\text{concave}}(\phi^{t-1}) - \frac{f''(\phi^{t-1})}{2}\left(\phi^t - \phi^{t-1}\right). \tag{4.11}$$

The method of [73], similar to the method of [117] also adds a stabilization term to the solution. [117] adds a simple penalty stabilization, while [73] adds a small diffusional stabilization. Here, the diffusional smoothing of [73] is used. This helps removes some small oscillations that appear in the solutions to the phase field equa-

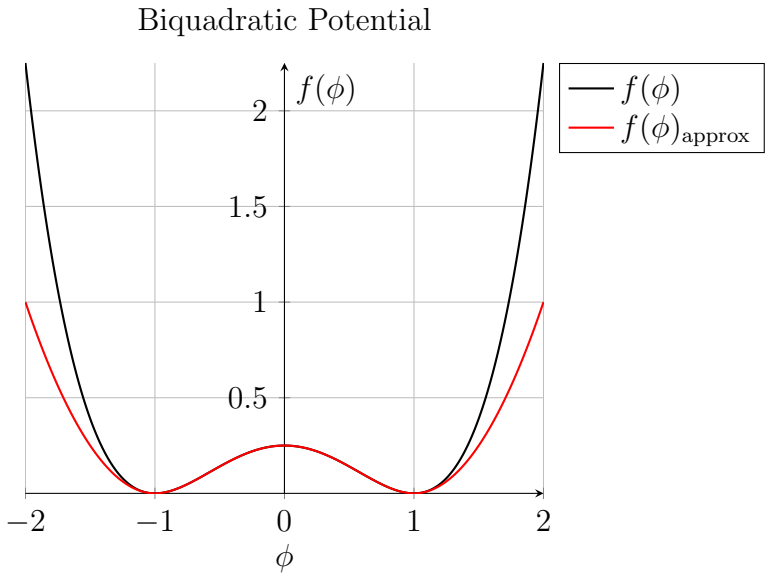

Figure 4.3. Biquadratic energy function used for enforcing the phase separation. Also shown is the relaxed version of the phase field energy.

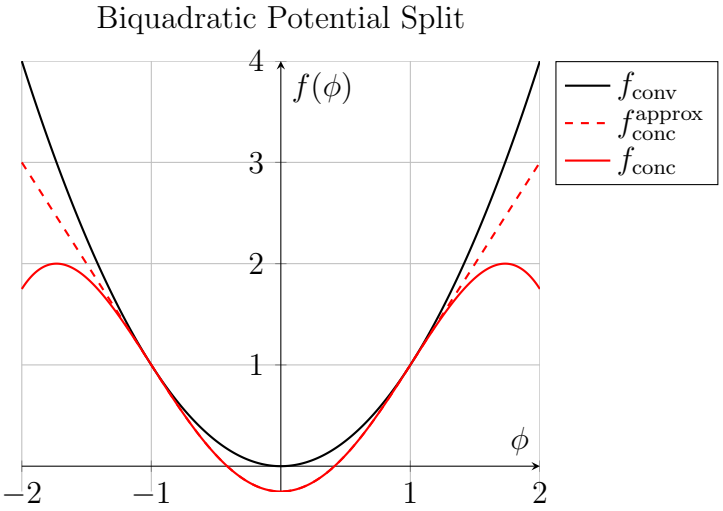

Figure 4.4. Convex and concave parts of the phase field energy used in the numerical algorithm.

tions. This is essentially the same as adding a term of the form to the semi-discrete form of the equation for the surface chemical potential,

$$\eta_{\text{stab}} \nabla^2 \left(\phi^t - \phi^{t-1} \right). \tag{4.12}$$

As $\phi^t \rightarrow \phi^{t-1}$, it does not change the solutions too much. However, it does add a small amount of error to the solution. This has been analyzed in detail in [73,117]. In all our simulations, a value of $\eta_{\text{stab}} = 10$ is used. This value meets the requirements for η_{stab} derived in [73].

The final terms that needs to be accounted for in the solution scheme for the phase field equation is the terms that are related to the coalescence of the vacancies at void interface. These are handled in a semi implicit manner as,

$$\text{vac. acc} = \delta(\phi)\left(\mu_\Gamma^t + RT\ln\frac{X^{t-1}}{X_0} + \beta p^t\right). \tag{4.13}$$

Finally, using Eqs. (4.11) to (4.13), the matrix that needs to be solved at every time-step for the solution of the phase evolution problem can be written as follows,

$$\begin{bmatrix} A_{\mu\mu} & A_{\mu\phi} \\ A_{\phi\mu} & A_{\phi\phi} \end{bmatrix} \begin{bmatrix} \mu^t \\ \phi^t \end{bmatrix} = \begin{bmatrix} F_\mu \\ F_\phi \end{bmatrix}. \tag{4.14}$$

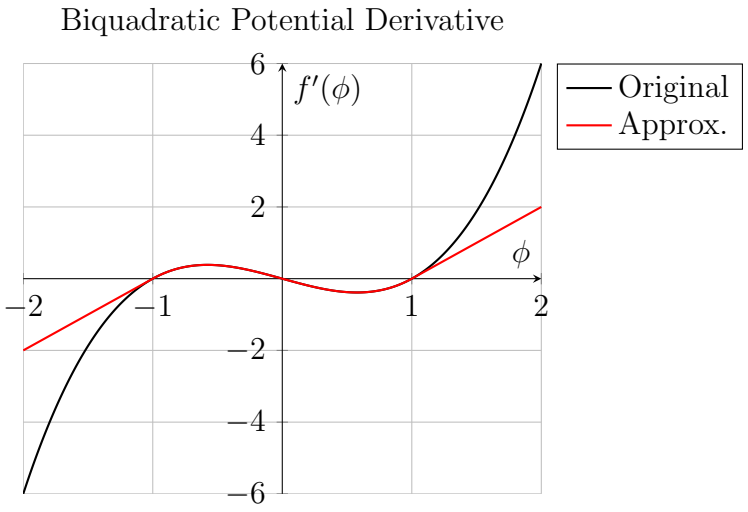

Figure 4.5. Derivative of the phase field energy functions, used in this study.

In the above, the individual submatrices can be written as,

$$(A_{\mu\mu})_{lm} = \int_{\Omega_{\text{el}}} dt \left(\frac{M(\phi^{\text{extrap}})}{\epsilon} \nabla N_l \nabla N_m - 2\frac{\delta(\phi^{\text{extrap}})}{\epsilon} \lambda X^{t-1} N_l N_m \right) d\Omega_{\text{el}} \tag{4.15a}$$

$$(A_{\mu\phi})_{lm} = \int_{\Omega_{\text{el}}} N_l N_m d\Omega_{\text{el}} \tag{4.15b}$$

$$(A_{\phi\mu})_{lm} = -\int_{\Omega_{\text{el}}} N_l N_m d\Omega_{\text{el}} \tag{4.15c}$$

$$(A_{\phi\phi})_{lm} = \int_{\Omega_{\text{el}}} \left(\frac{\gamma}{\epsilon} \left(\frac{\epsilon^2}{2} + \eta_{\text{stab}} dt \right) \nabla N_l . \nabla N_m + \frac{\gamma}{\epsilon} \left(1 - \frac{1}{2} f''_{\text{concave}}(\phi^{t-1}) \right) N_l N_m \right) d\Omega_{\text{el}}. \tag{4.15d}$$

The elements of the right hand side solution vectors can be shown to be the following,

$$(F_\mu)_l = \int_{\Omega_{\text{el}}} (N_l N_m + dt \frac{M(\phi^{\text{extrap}})}{\epsilon} \nabla N_l \left(Z_\Gamma \nabla \phi_e + Q_\Gamma \nabla T \right) + dt N_l 2\lambda \frac{\delta(\phi^{\text{extrap}})}{\epsilon} \mu_{\text{vac}}^{t-1} X_{\text{vac}}^{t-1} \Bigg) d\Omega_{\text{el}}. \tag{4.16a}$$

$$(F_\phi)_l = \int_{\Omega_{\text{el}}} \left(N_l \frac{\gamma}{\epsilon} \left(f'_{\text{concave}}(\phi^{t-1}) \phi^{t-1} + \frac{1}{2} f''_{\text{concave}}(\phi^{t-1}) \phi^{t-1} \right) - \frac{\delta(\phi)}{\epsilon} N_l W + \nabla N_l . \nabla \phi^{t-1} \frac{\gamma}{\epsilon} \left(-\frac{1}{2}\epsilon^2 + \eta_{\text{stab}} dt \right) \right) d\Omega_{\text{el}}. \tag{4.16b}$$

4.1.2 Vacancy Diffusion Equation

The vacancy diffusion equation is challenging to solve with the finite element method for a few reasons. The first is that the equations lead to an asymmetric system of equations. The second is the presence of the advective terms due to the electromigration flux, thermomigration flux as well as due to the presence of the pressure gradient driven flux. Finally, the application of the vacancy coalescence boundary condition on the void interface. With the parameter values commonly seen in practice however, the concentration gradient terms are significant to eliminate the

need for stabilization. The interfacial vacancy coalescence terms are non-linear, and are treated in a semi-implicit fashion. The surface vacancy coalescence relation terms are written as,

$$\text{vac. coal.} = \frac{\delta}{\epsilon}\lambda X\left(RT\ln\frac{X}{X_0}+\beta p+\mu_\Gamma\right). \tag{4.17}$$

While computing this, the vacancy coalescence term is expanded in a Taylor series around X^t. This can be written as,

$$\begin{aligned}\text{vac. coal.}^t = & \quad X^{t-1}(RT\ln X^{t-1})+X^t(\beta p^t+\mu_\Gamma^t)\\ & +\left(RT\ln X^{t-1}+X^{t-1}\frac{RT}{X^{t-1}}\right)\left(X^t-X^{t-1}\right)\\ = & \quad X^t(\beta p^t+\mu_\Gamma^t+RT\ln X^{t-1}+RT)\\ & -RTX^{t-1}.\end{aligned} \tag{4.18}$$

The other term that needs to be handled in the solution of the vacancy diffusion equation is the term related to the time derivative of the vacancies. In order to handle the accretive terms, the derivative used here is $\frac{\partial HX}{\partial t}$ instead of $\frac{\partial X}{\partial t}$. This is expanded as,

$$\frac{\partial HX}{\partial t}=\frac{\partial H}{\partial t}X+H\frac{\partial X}{\partial t}. \tag{4.19}$$

In the numerical solution, this is approximated as,

$$\frac{\partial HX}{\partial t}\approx\left(\frac{H^t-H^{t-1}}{dt}\right)X^t+H^t\left(\frac{X^t-X^{t-1}}{dt}\right). \tag{4.20}$$

With the above, the system of equations that needs to be solved is

$$[A][X]=[F]. \tag{4.21}$$

Where, the elements of the matrix A can be written as,

$$\begin{aligned}(A)_{lm} = \int_{\Omega_{\text{el}}} \Bigg(& N_l N_m \left(2H^t - H^{t-1} + dt\lambda \frac{\delta^t}{\epsilon} \left(RT \ln X^{t-1} + \mu_\Gamma^t + 1 \right) \right) \\ & + dt \nabla N_l . \boldsymbol{D} H^t . \nabla N_m \\ & + dt \nabla N_l . \boldsymbol{D} H^t . \left(Ze \nabla \phi_e + \beta \nabla p + Q^* \nabla T \right) \Bigg) \, d\Omega_{\text{el}}.\end{aligned} \tag{4.22}$$

Similarly, the elements of the force vector can be written as,

$$(F)_l = \int_{\Omega_{\text{el}}} N_l \left(H^t X^{t-1} + dt\lambda \frac{\delta}{\epsilon} X^{t-1} \right) d\Omega_{\text{el}}. \tag{4.23}$$

4.1.3 Linear Solvers

The numerical solution to the electrical and thermal stress are solved using the conjugate gradient method (provided by `PETSc`) and preconditioned using an algebraic multigrid method, (provided by the `HYPRE` libraries (also accessible through `PETSc`). The stress system, the Cahn Hilliard system and the vacancy diffusion systems are solved using the GMRES (**G**eneralized **M**inimum **Res**idual) method preconditioned by a Jacobi preconditioner. While the `HYPRE` preconditioner is suitable for the solution of the stress problem, it is not used owing to the excessive memory demands of the preconditioner. This also necessitates the use of GMRES instead of conjugate gradient for the stress solution, as the Jacobi-conjugate gradient combination fails occasionally. The vacancy diffusion and the Cahn Hilliard system are solved using the Jacobi -GMRES combination as the matrices are not symmetric. The matrix system obtained in the solution of the Cahn Hilliard system is suitable for preconditioning with block-preconditioners but this has not been explored in this dissertation.

4.1.4 Adaptivity

In order to reduce the computational cost of the phase field method, the problem is solved over an $h-$adaptive mesh. The adaptivity features in this code are provided

by `libMesh`. In this study, the mesh is adapted solely on the basis of the phase field value. Elements are marked for adaptivity based on the average value of the phase field parameter over the element. This is computed as,

$$\phi_{\mathrm{el}}^{\mathrm{av}} = \frac{1}{n_{\mathrm{qp}}} \left(\sum_{i=1}^{n_{\mathrm{qp}}\phi_{\mathrm{qp}^i}} \right). \tag{4.24}$$

If the value of $\phi_{\mathrm{el}}^{\mathrm{av}}$ is between -0.97 and 0.97, the element is marked for refinement, otherwise, the element is marked to be coarsened. This method has been preferred to the alternative of using an error estimator as numerical examples have shown the solution to be more reliable with time stepping. More details about the implementation, including the setting up of initial conditions can be found in Appendix E.

4.1.5 Validation

The primary validation example for models of electromigration by surface diffusion is the reproduction of the analytical solution [118]. This provides a relation for the velocity of the center of area of the void as

$$\boldsymbol{v}_{com} \propto \frac{Z^* \nabla \phi_e}{r}. \tag{4.25}$$

In the above, r is the radius of the prexisting void. It is easy to see from the form of the phase field equations that for a void of constant radius, the relation $\boldsymbol{v} \propto Z^* \nabla \phi_e$ is automatically satisfied. This is a simple linear relation and is easily verified. The relation at constant electrical potential gradient, however needs to be verified. The local value of the electrical potential gradient gets elevated around the void, speeding up the larger voids. The analytical relation in [118], on the other hand assumes that the solution is To avoid this, a very large domain, (5×2) is used, one side of which is maintained at constant electrical potential, while a unit electrical potential gradient

is applied on the other side (Fig. 4.6). The other material properties used in the validation simulation are listed in Table 4.1.

Table 4.1. Properties for validation.

ϵ	5×10^{-3}
$Z^*_\Gamma e$	-10
$\frac{3}{2\sqrt{2}} M\Omega_{\mathrm{Sn}}$	1×10^{-3}
$\frac{3}{\sqrt{2}} \gamma\Omega_{\mathrm{Sn}}$	.05
Δt	5×10^{-5}

The simulations are run from $t = 0$ to $t = 1.5$. The center of area of the void is computed as,

$$\boldsymbol{x}_{\mathrm{c.o.a}} = \frac{\sum_{el} \sum_{qp} |J_{qp}| w_{qp} \frac{1-\phi_{qp}}{2} \boldsymbol{x}_{qp}}{\sum_{el} \sum_{qp} |J_{qp}| w_{qp} \frac{1-\phi_{qp}}{2}}. \tag{4.26}$$

The velocity of the void is now computed as,

$$\boldsymbol{v}_{\mathrm{c.o.a}} = \frac{\boldsymbol{x}^{1.5}_{\mathrm{c.o.a}} - \boldsymbol{x}^{0}_{\mathrm{c.o.a}}}{1.5}. \tag{4.27}$$

The code is run for four values of the radius of the void, $0.1, 0.15, 0.2$ and 0.25. These values are chosen as they don't perturb the value of the electrical potential gradient around the void significantly. The results are plotted in Fig. 4.7b. The initial and final location of the voids are shown in Fig. 4.7a. Using a power-law fit, the relation for the velocity with respect to the radius was found to be,

$$\boldsymbol{v}_{\mathrm{c.o.a}} = 0.194 r^{-0.993}. \tag{4.28}$$

This value is extremely close to the analytical result of -1, showing the ability of the code to capture these effects to a high level of accuracy.

The next test for the validation of the code, is to evaluate the surface diffusion in the void under the combined effect of surface diffusion with an applied strain energy.

Figure 4.6. Boundary conditions for the validation examples.

The initial condition for this numerical experiment is shown in Fig. 4.8. The size of the domain used is 2.5×1 and an initial elliptical void with semi-major axis 0.3 and semi-minor axis 0.2 is placed in the center of the domain. The domain is placed under uni-axial tension by encastring the left side and applying a displacement of 0.001 on the right size. The elastic modulus of the material is set to 1×10^{-3}, and $\gamma\Omega_{\mathrm{Sn}}$ is varied between,$\frac{2\sqrt{2}}{3}$, $\frac{2\sqrt{2}}{30}$ and $\frac{2\sqrt{2}}{300}$. The modulus of elasticity is kept constant at $\frac{8}{15\Omega_{\mathrm{Sn}}} \times 10^6$ and a 0 poisson's ratio is used. In the first case, Fig. 4.9a, the surface energy dominates the surface strain energy density, and the elliptical void evolves into a circular void. In Figs 4.9b and 4.9c, the surface energy is progressively reduced. As the surface energy is reduced, the void tends to elongate and align itself along the direction of the loading. This is because the lowest energy state now is a state where the strain energy rather than the surface energy that is minimum. This is achieved when the void transforms into a slit. The solution shown here initially transforms into a rectangular void instead of an elliptical void owing to a small compressing stress that is generated along the tips of ellipse along the axis of loading.

4.2 Examples

In the section a few examples of the use of the code under various circumstances is demonstrated. The first two cases that are demonstrated are reproducing the standard instabilities that are observed tfor a circular void under electromigration by surface diffusion. The existence of these instabilities can be determined through a linear stability analysis, [119]. In [119], perturbations on the circle at 0° and 180°

$t = 0.0$ $t = 1.5$

(a) Initial and final location of voids of various sizes, under constant electrical potential gradient.

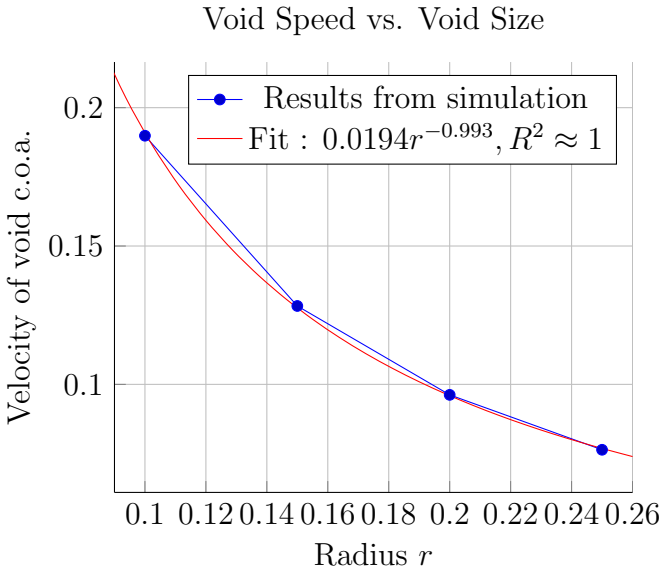

(b) Power law fit of velocities to size. The $\boldsymbol{v} \propto \frac{1}{r}$ [118] is recovered to very good accuracy.

Figure 4.7. Validation examples for velocity of voids of different sizes under a constant electrical potential gradient.

to the direction of the current density are found to be unstable. When the surface energy is high, it stabilizes the void and it trends to translate without shape change. On the other hand when the electrical current density is much larger than the surface energy effect, the solution displays actually displays the instabilities. Two types of solutions are observed, one where the void evolves into a kidney shape [37] while in

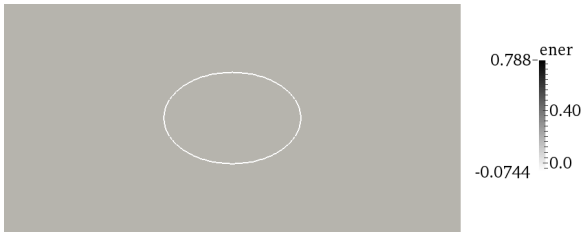

Figure 4.8. Initial condition for comparison of the relative effect of strain energy and surface energy.

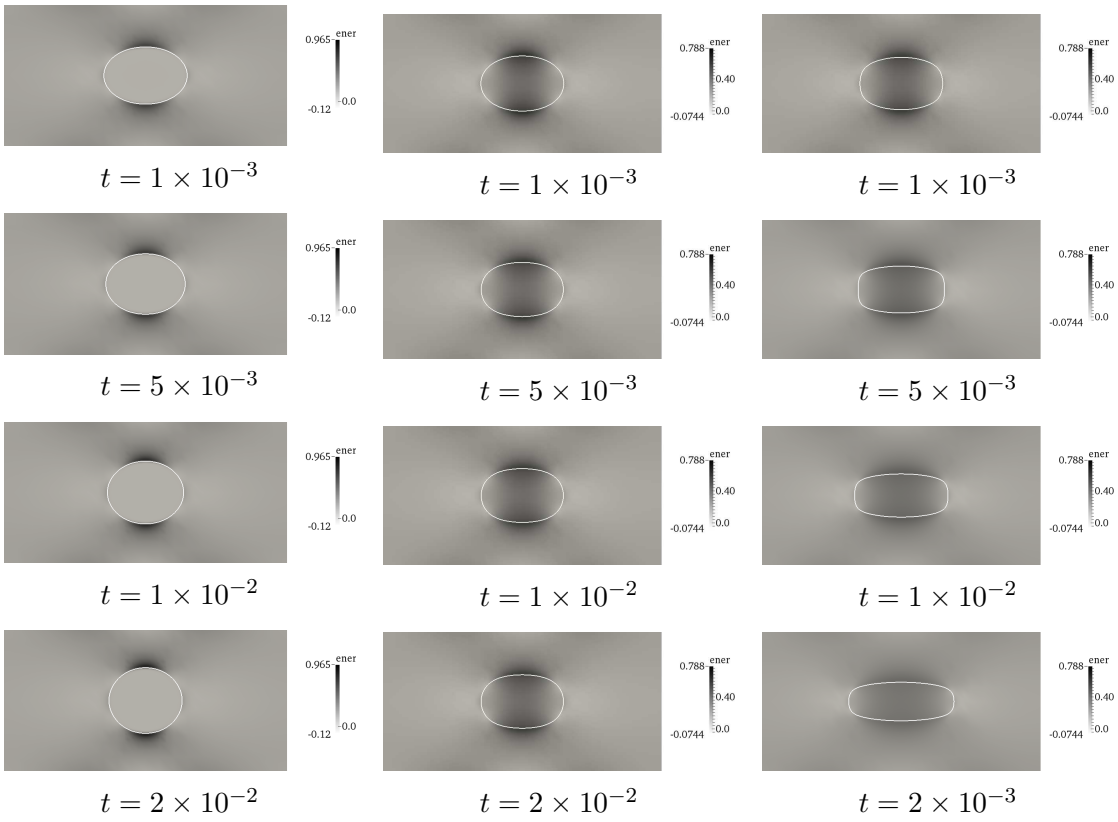

(a) High Surface Energy, $\gamma\Omega_{\mathrm{Sn}} = \frac{2\sqrt{2}}{3}$. (b) Medium Surface Energy, $\gamma\Omega_{\mathrm{Sn}} = \frac{2\sqrt{2}}{30}$. (c) Low Surface Energy, $\gamma\Omega_{\mathrm{Sn}} = \frac{2\sqrt{2}}{300}$.

Figure 4.9. Evolution of an elliptic void due to surface diffusion in a solid under uni-axial loading. The competing effect of the strain energy density and the surface energy.

the other one, the void splits into two separate voids [120]. Both these solutions are simulated here with the properties as shown in Table 4.2. The loading for both the

cases is shown in Fig. 4.10. To simulate the case where the void transforms into a kidney shape Fig. 4.11, the initial void is an ellipse with the major axis orthogonal to the direction of the electrical potential gradient. In the second case Fig. 4.12, the initial void is an ellipse with the major axis aligned with the direction of the electrical potential gradient. Both these case reproduce the phenomena observed by earlier sharp and diffuse interface method solutions of the surface electromigration equations. In Fig. 4.12, after the ellipse splits into two voids, the size relation from Fig. 4.7 is seen again, and the smaller void moves much faster than the larger void under the effect of the same electrical potential gradient.

Table 4.2. Material properties and simulation paramters for the simulation of the demonstration of kidney formation (Fig. 4.11) and the splitting of an ellipse (Fig. 4.12).

$\frac{3}{2\sqrt{2}}\gamma\Omega_{\mathrm{Sn}}$	0.01
$\frac{3}{\sqrt{2}}M\Omega_{\mathrm{Sn}}$	0.001
$Z^*_\Gamma e$	-20
Δt	1×10^{-5}
ϵ	5×10^{-3}

Figure 4.10. Loading conditions for the kidney formation (Fig. 4.11) and void splitting examples (Fig. 4.12).

4.2.1 Void Growth Due to Vacancy Coalescence

Vacancy coalescence at the interface is a commonly proposed model for the growth of voids [110, 112, 121]. As shown in Eq. (3.13), vacancies cause a compressive strain,

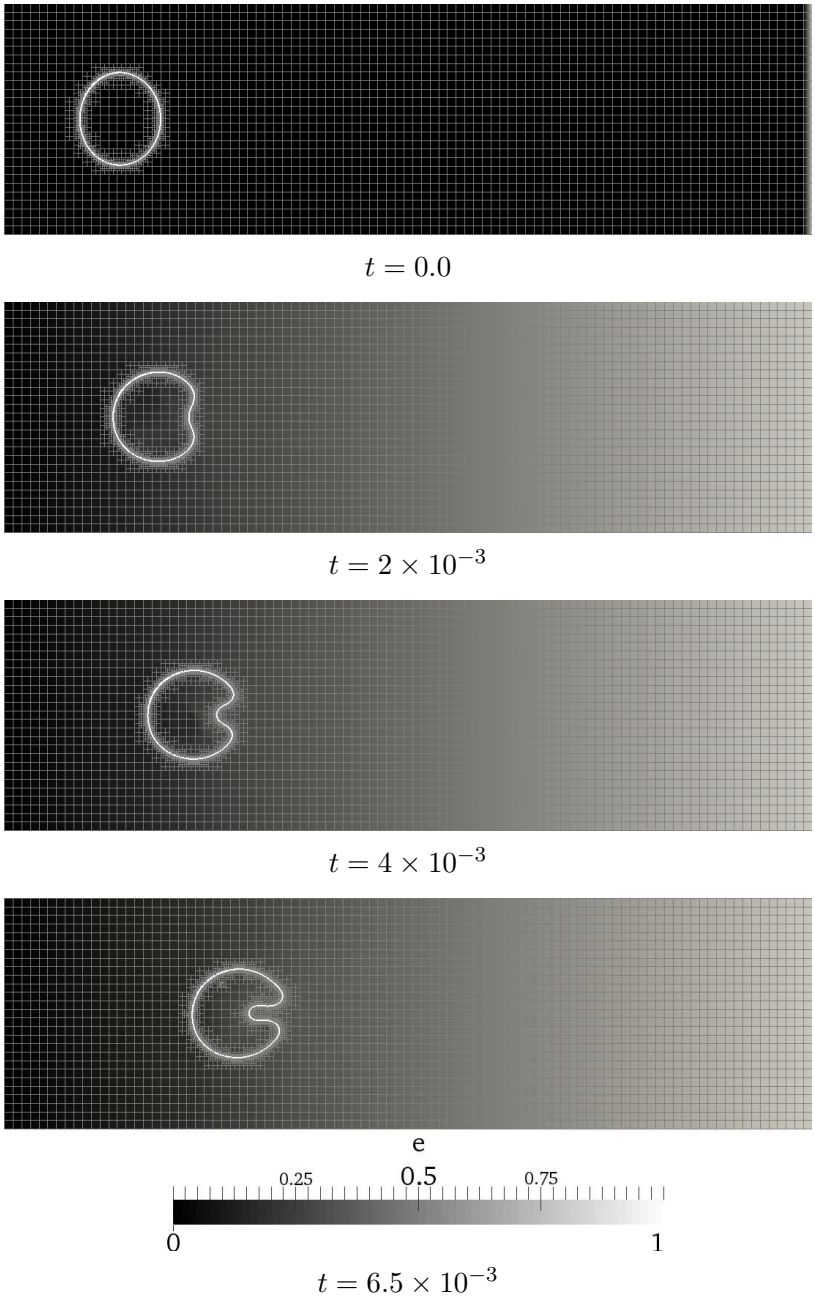

Figure 4.11. Instability at low surface energies.

as the crystal deforms around the site of the vacancy. This also has the effect of leading to a reduction in the tensile stress. Vacancies therefore, tend to accumulate in regions of high tensile stress, or where p is most negative. In the case of an elliptical void loaded as in Fig. 4.13, the regions of highest tensile stress are the regions around

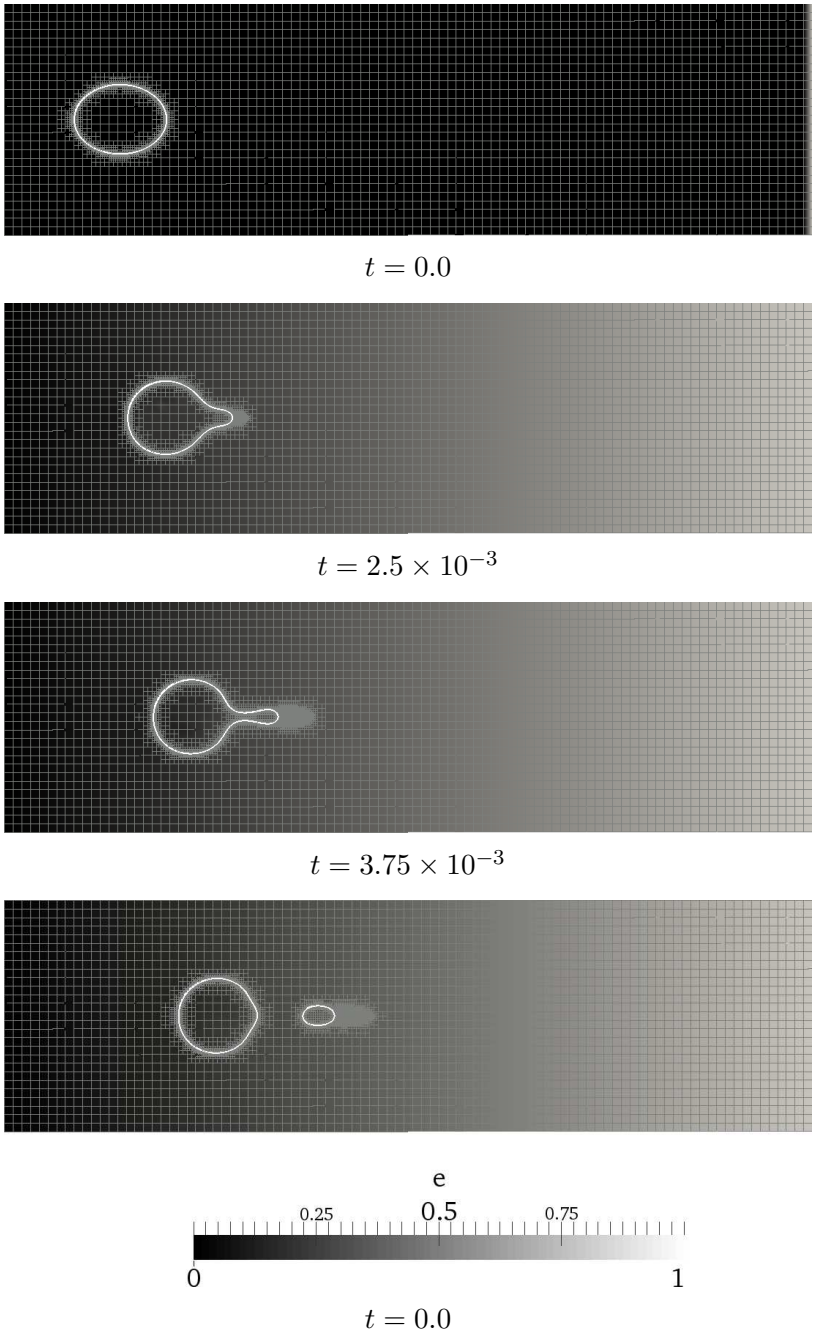

Figure 4.12. Instability in an elliptical void with the major axis aligned with the direction of the electrical current.

the major axis of the void. The vacancies tend to accumulate in these regions. As the vacancy concentration increases, it becomes more likely (Eq. (3.29)) that the

vacancies will coalesce into the void and cause the void to grow. For some loads, the system will reach a new equilibrium and the void growth will stabilize, however for some values of the applied load, the void growth will continue unabated and the void will grow into a crack. This is demonstrated in Fig. 4.14. The material and other simulation properties used are listed in Table 4.3. There is no electromigration in this example and hence the parameters related to electromigration are set to 0.

Table 4.3. Simulation parameters used for the simulations of void growth in Fig. 4.14

Δt	1×10^{-5}
ϵ	5×10^{-3}
E	1000
ν	0.33
$\frac{3}{2\sqrt{2}}\gamma\Omega_{\mathrm{Sn}}$	0.01
$\frac{3}{\sqrt{2}}M\Omega_{\mathrm{Sn}}$	0.01
β	1.0
RT	3.0
D	1.0
$\frac{3}{\sqrt{2}}\lambda\Omega_{\mathrm{Sn}}$	10

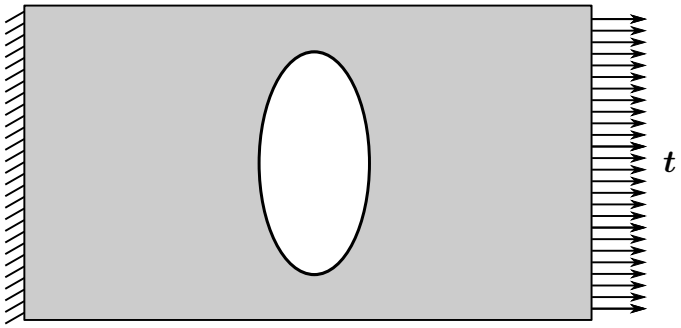

Figure 4.13. Loading for the simulations shown in Fig. 4.14.

As the load on the system is increased from $\boldsymbol{t} = \{0, 0\}$ (Fig. 4.14a) to $\boldsymbol{t} = \{2, 0\}$ (Fig. 4.14c), the void tends to grow into the region of the highest negative pressure, as the vacancy concentration in that region increases, in order to release that pressure. At the intermediate loading (Fig. 4.14b), it is seen that the void grows a bit, however, the system reaches a new equilibrium, and the system doesn't reach failure.

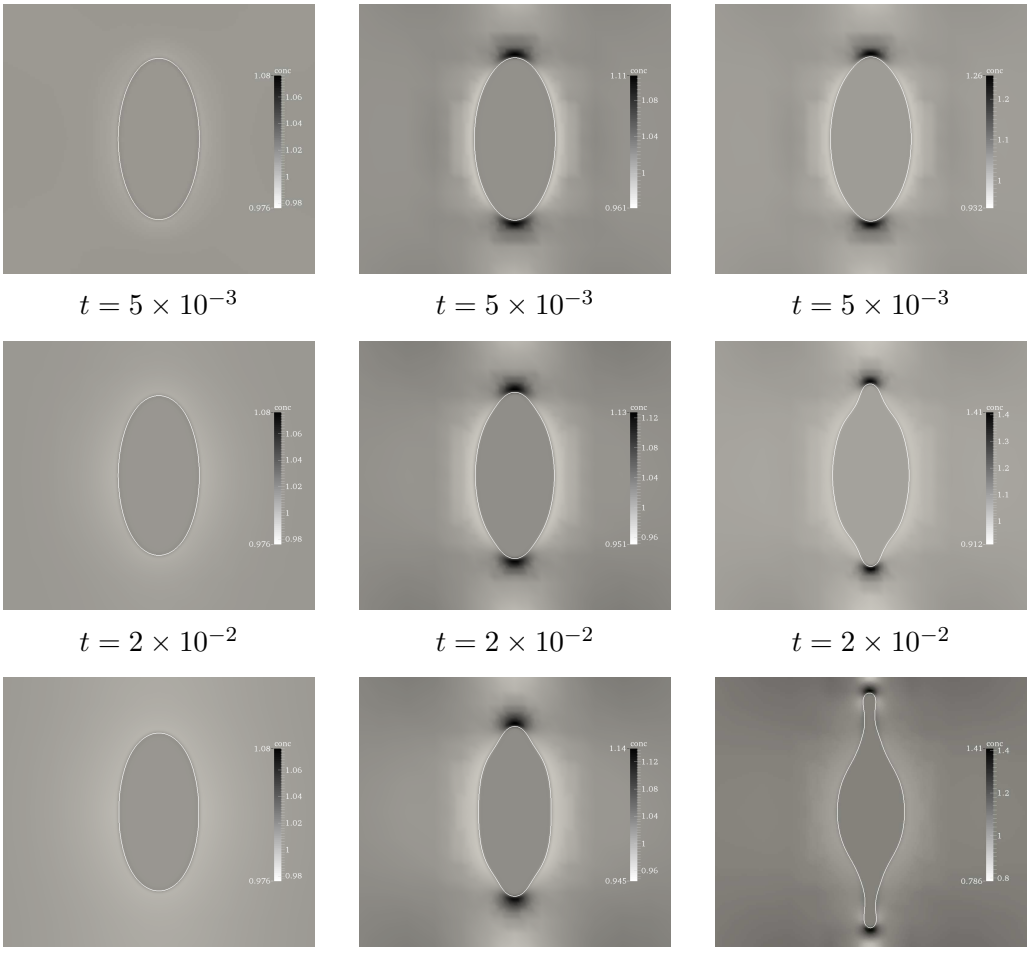

(a) 0 applied traction (b) Applied traction, $\boldsymbol{t} = \{1, 0\}$ (c) Applied traction, $\boldsymbol{t} = \{2, 0\}$

Figure 4.14. Growth of an elliptical void due to vacancy coalescence at the tip. (a) is a reference case with no applied tractions. (b) has a unit traction applied, while (c) has a traction of 2 units applied.

This suggests that there is a value of the applied traction, beyond which the system transitions from having stable solutions to a state where the system fails by void growth.

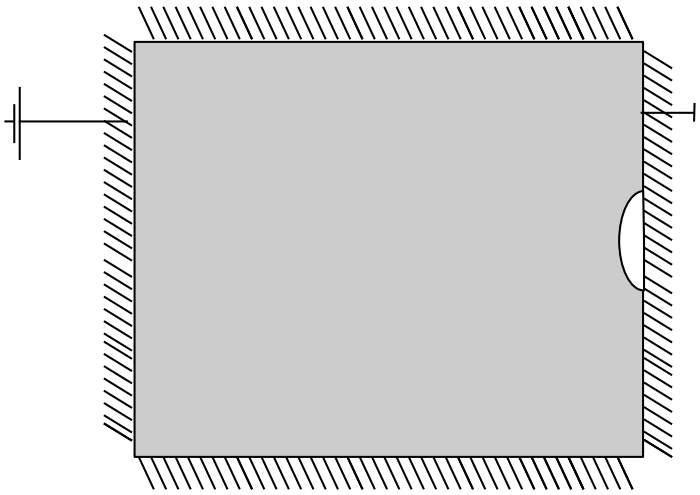

Figure 4.15. Loading conditions for simulations of effect of interconnect size on electromigration void growth.

4.2.2 Dependence of Void Growth on Size of Interconnect Structure: Blech Length

The next case that is studied is the effect of the size of the interconnect structure on the growth rate of voids. This is an important effect in the study of failure behavior, as the size is an important design parameter. More importantly, the relation of the size of the joint to the applied current density can be used to determine the maximum electrical current that can be carried by the joint. In this study, the growth of a void at the interface in structures of various sizes is tracked. The joint sizes used are, 0.4×1, 0.6×1, 0.8×1 and 1.2×1. A constant unit electrical potential gradient is applied in each of the cases ($\nabla \phi_e . \boldsymbol{n} = 1$). All the boundaries are completely constrained with respect to deformation. For the vacancy diffusion equation, it is assumed that the outer boundaries are closed, material neither enters nor exists the interconnect structure. A constant initial vacancy is applied over the entire domain. An initial semi-circular void of radius 0.06 is placed at the center of the further corner. The other simulation parameters used in this study are listed in Table 4.4.

The results of the simulations are shown in Fig. 4.16. As is clearly seen, the void growth is greatest in the longest void. Also, as the size of the interconnect increases,

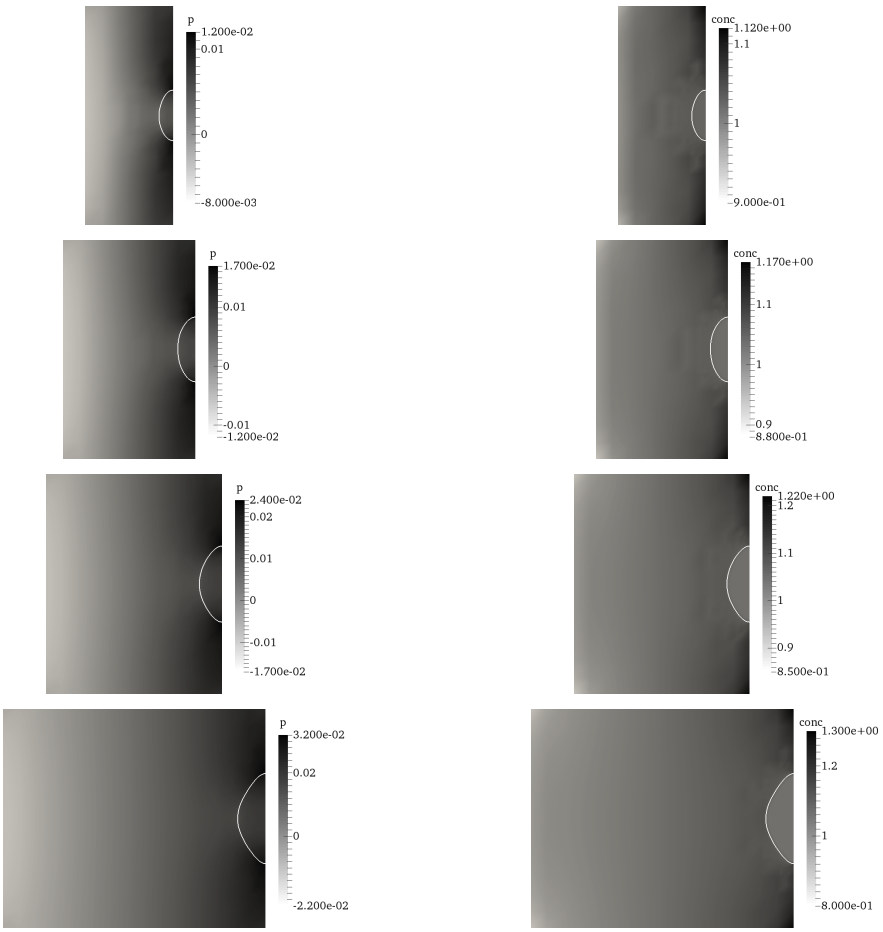

(a) Pressure (b) Concentration

Figure 4.16. Effect of the length of the domain on electromigration void growth. As the length of the joint is reduced, the back pressure gradient generated due to the vacancy concentration increases. This reduces the concentration of vacancies available for void growth, consequently reducing the void growth. The pressures at time $t = .54$ are shown in (a) while the concentration of vacancies is shown in (b). In (b), darker regions correspond to regions of greater vacancy concentration. On the other hand, in (a) darker, regions correspond to regions of greater pressure.

Table 4.4. Simulation parameters for the study of size effects in interconnect structures (Fig. 4.16).

Δt	1×10^{-5}
ϵ	5×10^{-3}
c	1.0
E	1000
ν	0.33
$\frac{Z^* e}{RT}$	-1.0
$\frac{\beta}{RT}$	20
$\frac{3}{2\sqrt{2}}\gamma\Omega_{\mathrm{Sn}}$	0.01
$\frac{3}{\sqrt{2}}M\Omega_{\mathrm{Sn}}$	0.01
ρ_0	1×10^{-5}

the void growth in the same timespan is greater. The relationship between the size of the joint/line and electromigration has long been observed experimentally [122]. The reasoning for the dependence is that as the electromigration progresses, a chemical potential gradient develops on account of the concentration gradient developed due to the vacancy accumulation, as well as the stress developed owing to the increase in the vacancy concentration (Eq. (3.13)).

4.2.3 Simulations on Assemblies of Solder Joints

Finally the effect of these various effects on the failure of an assembly of solder joints is studied. The geometry used is shown in Fig. 4.17. The geometry in Fig. 4.17 is chosen to be representative of the cases commonly seen in practice. 4 voids are placed in various regions that are likely to be locations of failure. The opening of the solder joint is 1 unit. A potential difference of 2 units is applied across the entire assembly. This is so that each joint has a unit potential difference across it. In terms of mechanical loading, tractions $\boldsymbol{t} = \{-0.1, 0\}$ on the left hand side connector and $\boldsymbol{t} = \{0.1, 0\}$ on the right had side connector is applied. In this simulation, it is assumed that the system is closed, and the only way for the number of vacancies in the joint to change is through absorption at the void interface.

The material properties used in the simulation are listed in Table 4.5. The material properties are not physical, but are only indicative of the relative properties of tin and copper. The value of ϵ used in the dissertation is 5×10^{-3}, and $\Delta t = 1 \times 10^{-4}$.

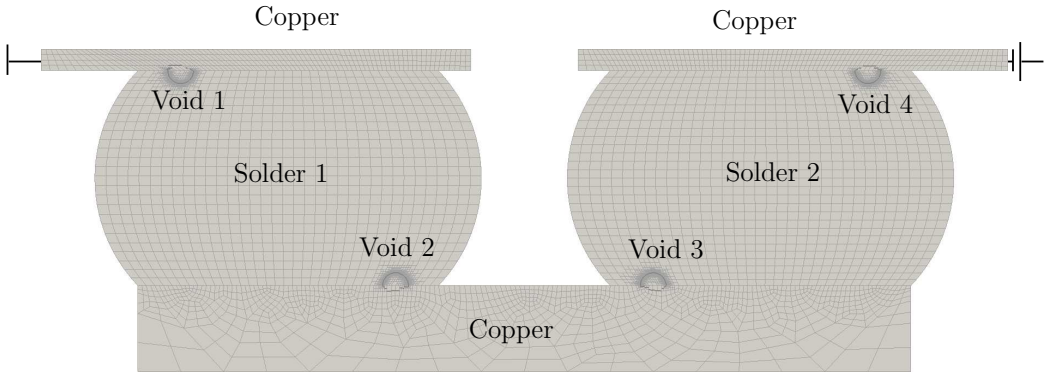

Figure 4.17. Geometry of assembly of solder joints used in simulations of electromigration damage.

Table 4.5. Material properties for simulations on assemblies of solder joints.

c_{solder}	1.0
c_{copper}	7.0
C_{solder}	1.0
C_{copper}	10.0
ν	0.33
$\frac{3}{2\sqrt{2}}\gamma\Omega_{\text{Sn}}$	0.001
$\frac{3}{\sqrt{2}}M\Omega_{\text{Sn}}$	0.001
D_{vac}	1.0
$\frac{Z^*e}{RT}$	1.0
$Z^*_\Gamma e$	1.0
$\frac{3}{\sqrt{2}}\lambda\Omega_{\text{Sn}}$	1.0
$\frac{\beta}{RT}$	10.0
$\frac{\rho\beta}{RT}$	1.0×10^{-4}

The results of the simulations are shown in Fig. 4.18. As can be seen, void 1 and void 3 grow, while void 2 and void 4 reduce in size and eventually disappear. Void 1 grows and evolves into a *pancake* void, a form of void that has been commonly observed in the literature (Fig. 3.1, [108]). Another important feature is the difference

in the growth rates of void 1 and void 3, in spite of both of them having the same initial size and location from the edge of the joint. The primary difference is the value of the electrical potential gradient in the vicinity of void 1 and void 3 (Fig. 4.20). As $|\nabla\phi_e|$ is greater in the vicinity of the void 1, the mass-flux divergence and vacancy concentration is higher in that region. This causes void 1 to grow at a significantly higher rate than void 3. This feature of electromigration failure in assemblies of solder joints has been frequently observed in experimental studies on daisy chains of solder joints [102], where depending on the direction of the applied electric current, only every other solder joint shows electromigration related void growth (Fig. 4.19).

4.3 Extension to 3-Dimensions

The code developed as part of this thesis Appendix E is capable of solving the electromigration void evolution problem in both 2 and 3 dimensions, as the code itself is programmed in a dimension agnostic fashion. However, owing to the expense of 3-dimensional simulations using a phase field method, only limited examples are presented here. The first example Fig. 4.21. Shows the evolution of a void in a 3-dimensional line of dimensions $2.5 \times 1 \times 1$. An initial spherical void of radius 0.1 is placed in the line and a constant electrical potential difference of 5 is applied across the ends of the line. The value of $Z^*_\Gamma e$ used is -1, while $\frac{3}{2\sqrt{2}} M\Omega_{\mathrm{Sn}} = 0.1$, and $\frac{3}{\sqrt{2}}\gamma\Omega_{\mathrm{Sn}} = 1 \times 10^{-2}$. The timestep used is $\Delta t = 5 \times 10^{-5}$.

As expected and observed in Fig. 4.7a, The void moves into the region of high electrical potential. This example was run on an AMD Opteron computer with 96GB of memory using 24 2.0GHz processors. The code is discretized so that there are 4 elements between ± 0.97. On average the code takes a minute per time step. The results in the simulation took approximately 20 hours to simulate. The solution to the stress problem was turned off in order to reduce the time required for solution.

A large void was also simulated in order to replicate the instability seen in Fig. 4.11. This was done by putting an initial oblate spheroid void of size $(0.3, 0.3, 0.2)$ with the

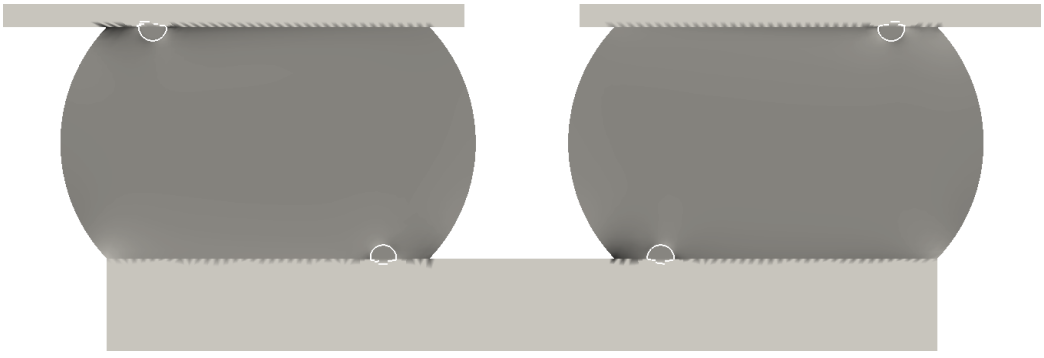

$t = .1$

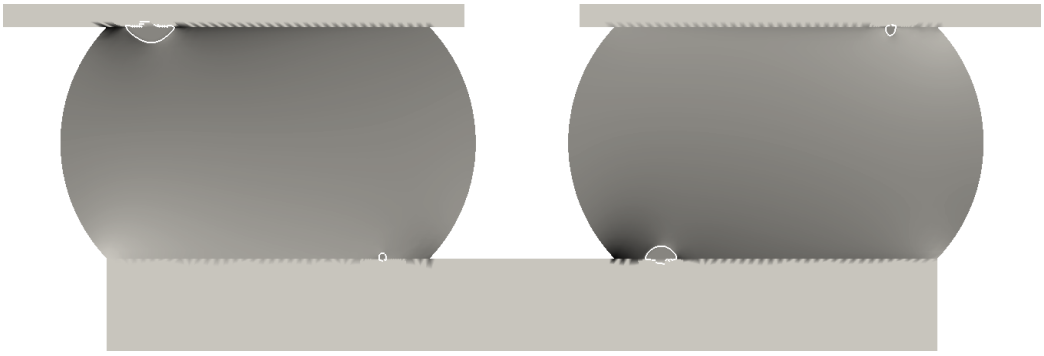

$t = 1.3$

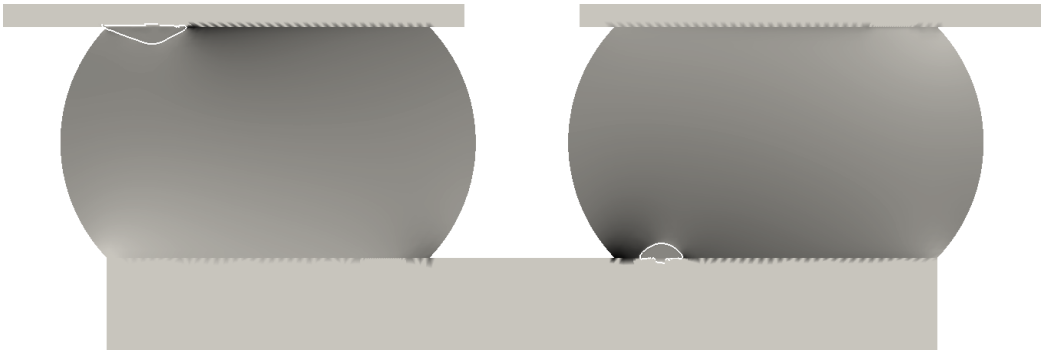

$t = 2.6$

Figure 4.18. Evolution of voids in Fig. 4.17. As time progresses, material is removed from the regions of void 1 and void 3 and deposited in the regions of void 2 and void 4. The deposition of material in the regions of void 2 and void 4, causes the voids to disappear. Meanwhile, void 1 and void 3 continue to grow. Darker regions represent regions with higher.

axis aligned with the direction of the electrical potential gradient. These can be seen in Fig. 4.22.

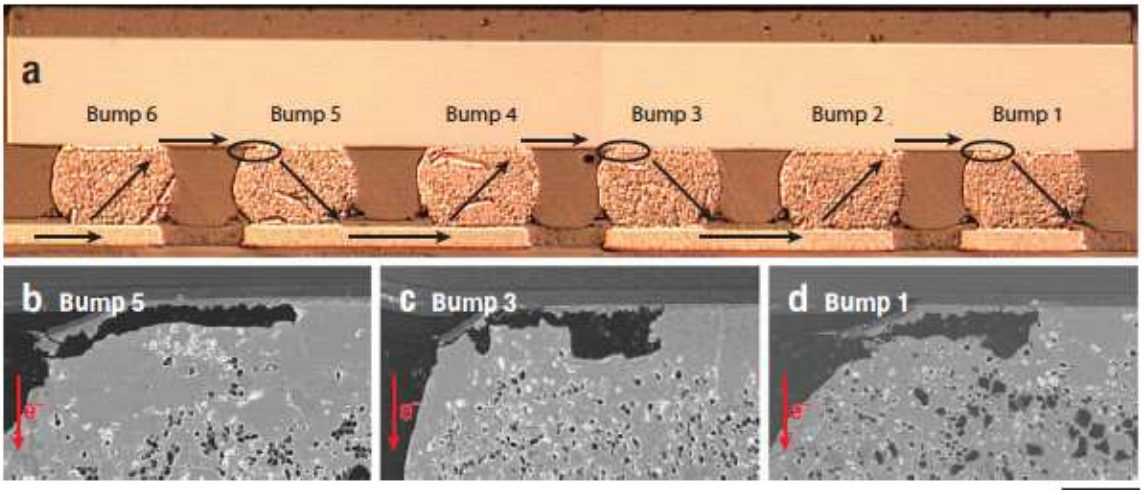

Figure 4.19. Electromigration damage in every alternate joint [102].

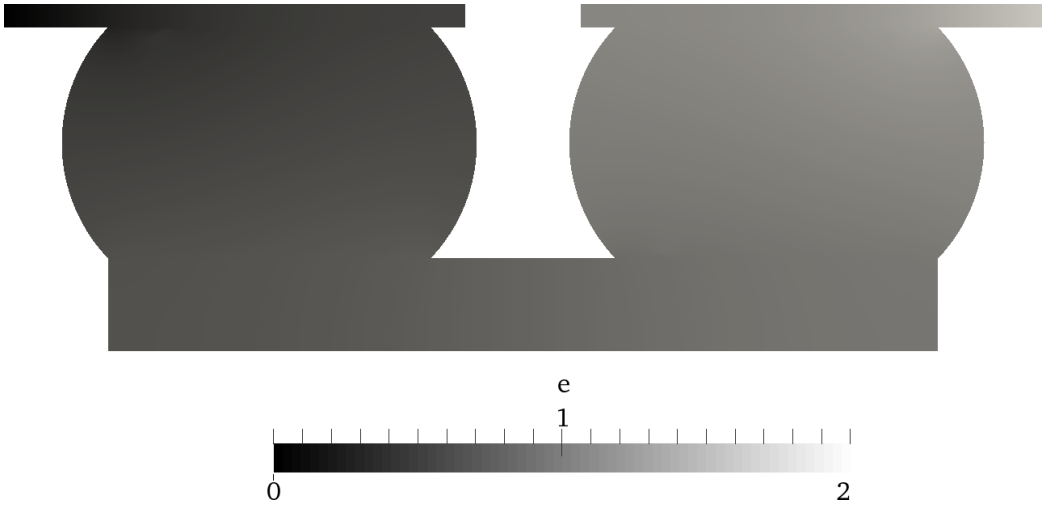

Figure 4.20. Electrical potential throughout the domain of the solder joints at time $t = 1.3$ in Fig. 4.18.

4.4 Summary

In this chapter and the previous one (Chapter 3), a phase field model for the simulation of electromigration related damage in solder and other interconnect structures is developed and demonstrated. Various known features of the physics of void evolution, such as the motion of voids due to surface electromigration § 4.1.5. The evolution of elliptical voids under the competing effects of strain energy and surface

energy are demonstrated. Further, the code is demonstrated for simulating the growth of an elliptical void due to the effect of vacancy coalescence at the tips of the ellipse. Also demonstrated is the effect of the size of the joint on the growth rate of voids at the interface. Finally, in § 4.2.3, electromigration is simulated over an assembly of joints.

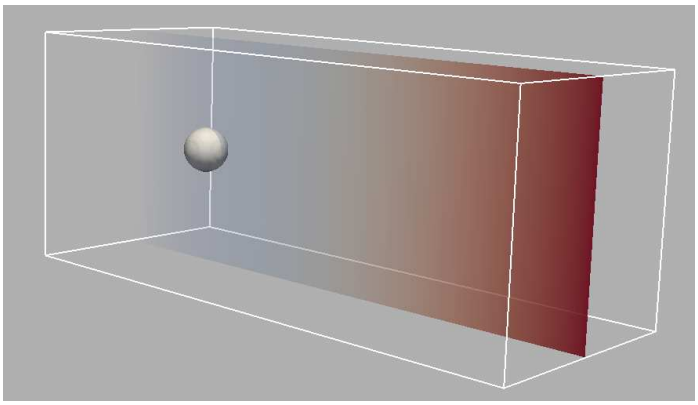

$t = 1 \times 10^{-4}$

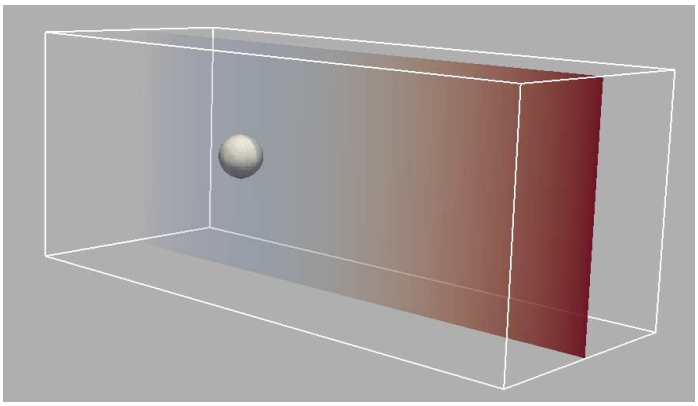

$t = 0.04$

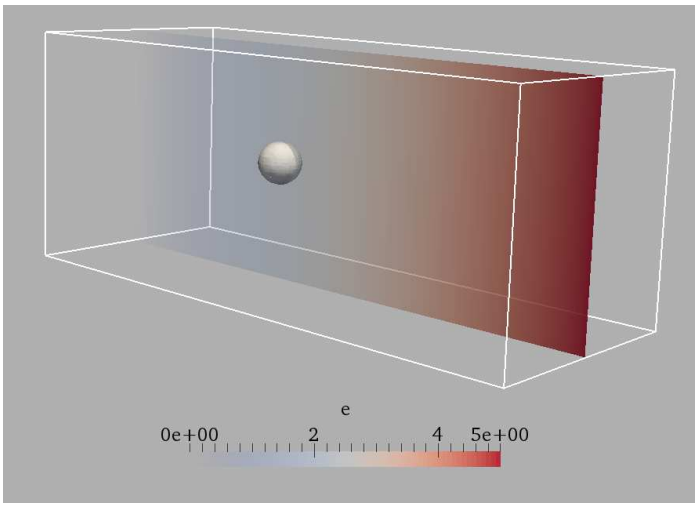

$t = 0.08$

Figure 4.21. 3D void evolution: A single void evolving under electromigration in a 3-dimensional void.

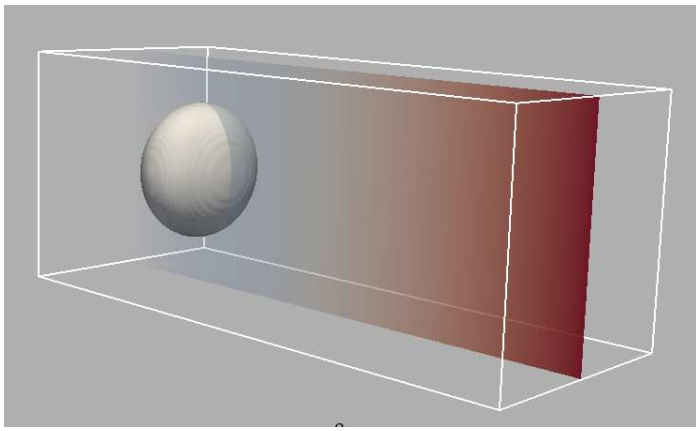

$t = 1 \times 10^{-4}$

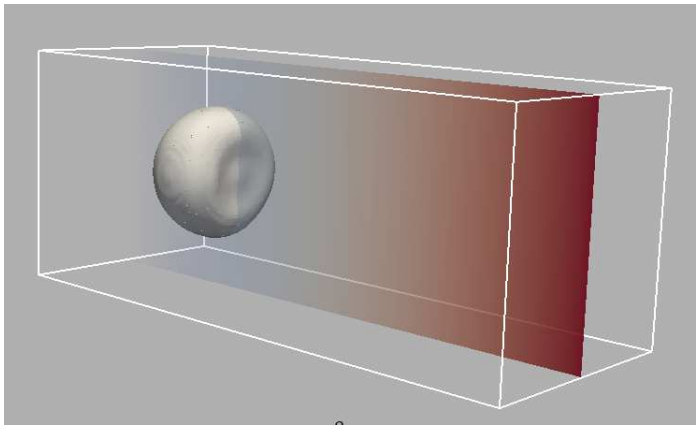

$t = 3.4 \times 10^{-3}$

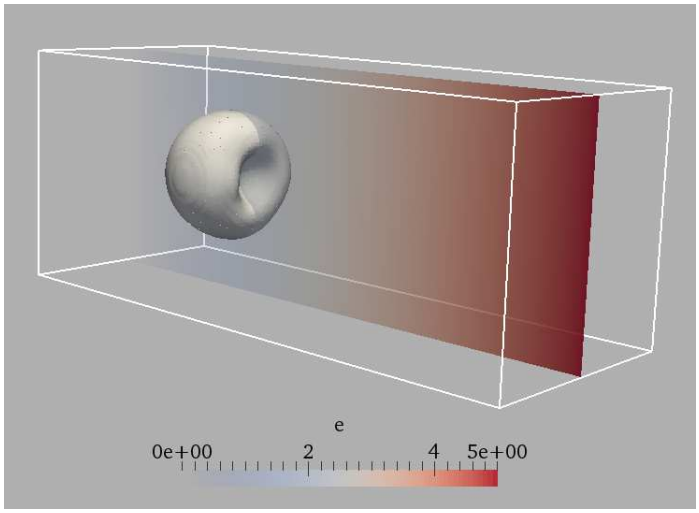

$t = 6.8 \times 10^{-3}$

Figure 4.22. 3D void evolution: Evolution of a large oblate spheroid into a rotated kidney shape, under surface electromigration.

5. SIMULATION OF EFFECT OF CONTACT ANGLE AND DIFFUSION ANISOTROPY ON ELECTROMIGRATION FAILURE

5.1 Introduction

Sn displays a significant anisotropy in its self diffusivity, with $\frac{D_a}{D_b} \approx 2$ at $T = 180°C$ and ≈ 3 at $T = 223°C$ [123]. With large joints, the anisotropy effect is ameliorated by the polycrystalline nature of the material. In solder joints with a limited number of grains, the electromigration failure is observed to depend strongly on the orientation of the grains with respect to the direction of the electromigration [124]. The anisotropy is also observed to influence the failure behavior under creep, in the absence of electromigration [125].

This anisotropy is a serious concern as the length scales of interconnects become smaller and the material can no longer be considered isotropic for modeling purpose. The mechanics of the growth and evolution of voids is complicated due to surface energy effects. Additionally the angle of adhesion between the interconnect and the surrounding is known to affect the electromigration failure of the interconnect [126].

In this chapter, the electromigration model developed in Chapter 3, is extended to account for the effects of contact energy at the interface between the solder and the die. Phase field equations are usually solved using a zero Neumann boundary conditions. This leads to the interface interacting with the outer interface at a 90° angle. Energetically, this is the case where the contact is neither favorable or unfavorable. It is known that as the wetting between the solder and the die becomes favorable, the contact angle between the void and the interface becomes more acute, Fig. 5.2a. Conversely, when the wetting between the solder and the die is unfavorable the contact angle between the void and the die becomes less acute Fig. 5.2b.

5.2 Modeling Contact Angles

In terms of the model for the electromigration, this can be modeled as a condition on the configurational force at a triple point Fig. 5.1 where the die, the solder and the void meet. This can be written as,

$$\gamma_{12}\boldsymbol{t}_{12} + \gamma_{23}\boldsymbol{t}_{23} + \gamma_{31}\boldsymbol{t}_{31} = 0. \tag{5.1}$$

Separating Eq. (5.1) into x and y co-ordinates. As the triple point is fixed in the y directions, the forces in the y direction is indeterminate. In the x direction, the balance can be written as,

$$\gamma_{12} - \gamma_{23} = -\gamma_{13}\cos\theta_c. \tag{5.2}$$

Where, θ_c is the contact angle. Simplifying the relation, the contact angle can be written as,

$$\theta_c = \arccos\frac{\gamma_{23} - \gamma_{12}}{\gamma_{13}}. \tag{5.3}$$

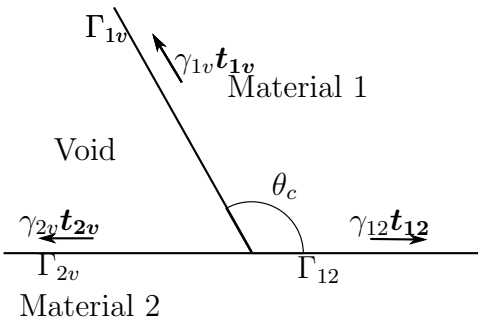

Figure 5.1. Balance of forces at a triple point.

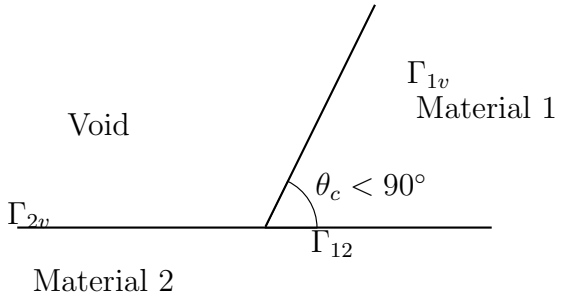

(a)

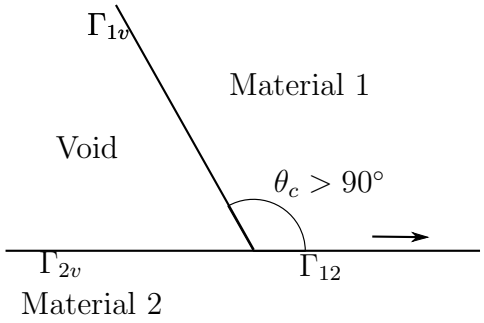

(b)

Figure 5.2. Favorable (a) and unfavorable (b) conditions for solder wetting the die.

In terms of the numerical model developed in § 3.2, the equation Eq. (5.3) is realized as an neumann boundary condition on Eq. (3.53b). This follows the approach of [127] for the simulation of contact lines in fluids, and can be written as

$$\frac{3}{2\sqrt{2}}\epsilon\gamma\nabla\phi.\boldsymbol{n} = -\frac{3\gamma}{4}(1-\phi^2)\cos\theta_c. \tag{5.4}$$

where $\cos\theta$ is the cosine of the contact angle. This can be reasoned as follows. $\nabla\phi$ is a vector field that indicates the normal to the interface. In the standard Cahn-Hilliard equation, the Neumann boundary condition can be written as,

$$\nabla\phi.\boldsymbol{n} = 0. \tag{5.5}$$

The above relation indicates that the interface is always orthogonal to the outer interface. In terms of Eq. (5.4), this is the case, when $\theta_c = \frac{\pi}{2}$. When $\theta_c \neq 0$, the right hand side of Eq. (5.4) is non-zero only when $(1 - \phi^2) \neq 0$, and when integrated in an inner co-ordinate system from $-\infty$ to $+\infty$ over the outer boundary of the system, it can be shown that,

$$\boldsymbol{n}_\Gamma^\phi . \boldsymbol{n} = -\cos\theta_c. \tag{5.6}$$

The negative sign in Eq. (5.6) arises because the normal to the interface is pointing outwards as shown in Fig. 5.3, while the opposite sense is used while defining the contact angles in Fig. 5.1.

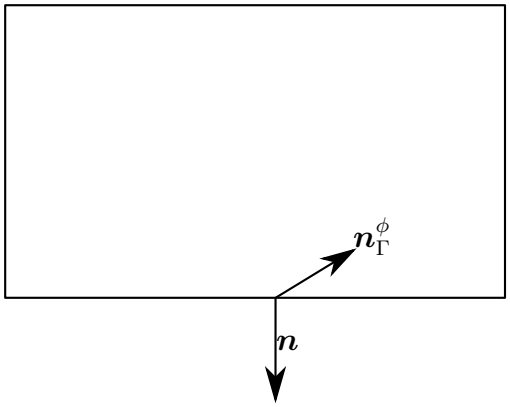

Figure 5.3. Definition of the contact angle at the outer interface for a phase field.

5.3 Numerical Implementation

The numerical formulation of the equations for the bulk of the domain is the same as in § 4.1. The boundary condition Eq. (5.4) is a non-linear boundary condition, and can be treated in either a fully explicit, fully implicit or a semi-explicit fashion. Here the approximation used for numerical solution is purely explicit, based on an

extrapolated value of ϕ. This lets the contributions to the F_ϕ in, Eq. (4.14) due to the application of Eq. (5.4) be written as

$$(F_\phi)_i = \int_{\Gamma_{\text{el}}} N_i \gamma \frac{3\gamma}{4} (1 - \phi^{\text{extrap.}})^2 \cos\theta_c d\Gamma_{\text{el}}. \tag{5.7}$$

In the above, $\phi^{\text{extrap.}} = \frac{3}{2}\phi^{t-1} - \frac{1}{2}\phi^{t-2}$.

This method of applying contact boundary conditions works well for intermediate values of the θ_c. At very low (≈ 0), or very high $\approx \pi$) contact angles, the method fails to apply the boundary conditions with very good accuracy. A simple verification is presented in Fig. 5.4. The initial condition is set as a circle of radius 0.5 centered at $(0.1, 0.1)$. A value of $\epsilon = 6 \times 10^{-3}$ is chosen. In Fig. 5.4a, a contact angle of 30° is specified. As time progresses, the system reaches the equilibrium value of approximately 30°. In Fig. 5.4b, a contact angle of 150° is specified. In this case, the initial condition is significantly different than the initial condition. However, the system evolves throughout to try and maintain a 150° contact angle.

5.4 Numerical Examples

In this section, some numerical examples are demonstrated that study the effect of anisotropy and the interfacial contact angle at the interface on the growth rate of voids at the interface. The geometry used for these simulations is shown in Fig. 5.5. The dimensions for these simulations are in arbitrary units at present, and the various material parameters are dimensionless. However, the relative numerical values for the conductivity are chosen to mimic the relative properties of copper and tin. The properties for the other material properties are similarly indicative. The value of the surface diffusion properties are chosen to minimize them so that the bulk diffusion processes dominate the dynamics. These are found in Tables 5.1 and 5.2.

A constant unit electric potential is applied between the top pad and the base of the copper pillar. Two sets of anisotropic diffusivities are used. In the first, the diffusivity is dominant along the x axis (roughly orthogonal to the direction of the

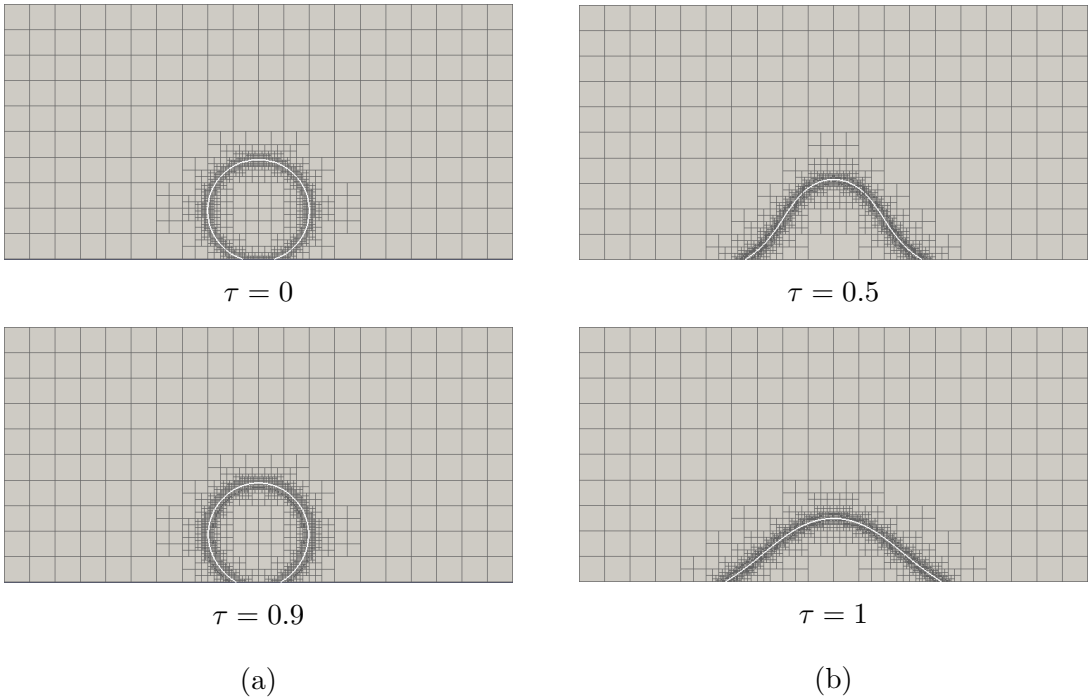

Figure 5.4. Validation of contact angle boundary condition application. In (a) A contact angle of 30° is applied on the interface, while in (b) a contact angle of 150° is applied on the interface.

Table 5.1. Conductivity properties for the materials.

Material property	Copper	Solder
Conductivity	10	1

applied potential gradient). In the second the diffusivity is dominant along the y axis, in the direction of the potential gradient. A small semi-ellipsoidal void with major axis 0.04 and minor axis 0.03 is placed close to the current crowding region of the solder joint. The growth of this void with time is tracked using the code. For the vacancy concentration, the bottom copper-solder interface is assumed to be a source of vacancies at $X_{\text{vac}} = 1.0$. The initial condition is set so that the vacancies are at equilibrium with the surface of the void at the end of the first time step. A time-step of $\Delta t = 5 \times 10^{-5}$ is used. Note that this time step is in arbitrary units. The contact angle at the interface is set to 160° in the first set of examples, and to 80° in the

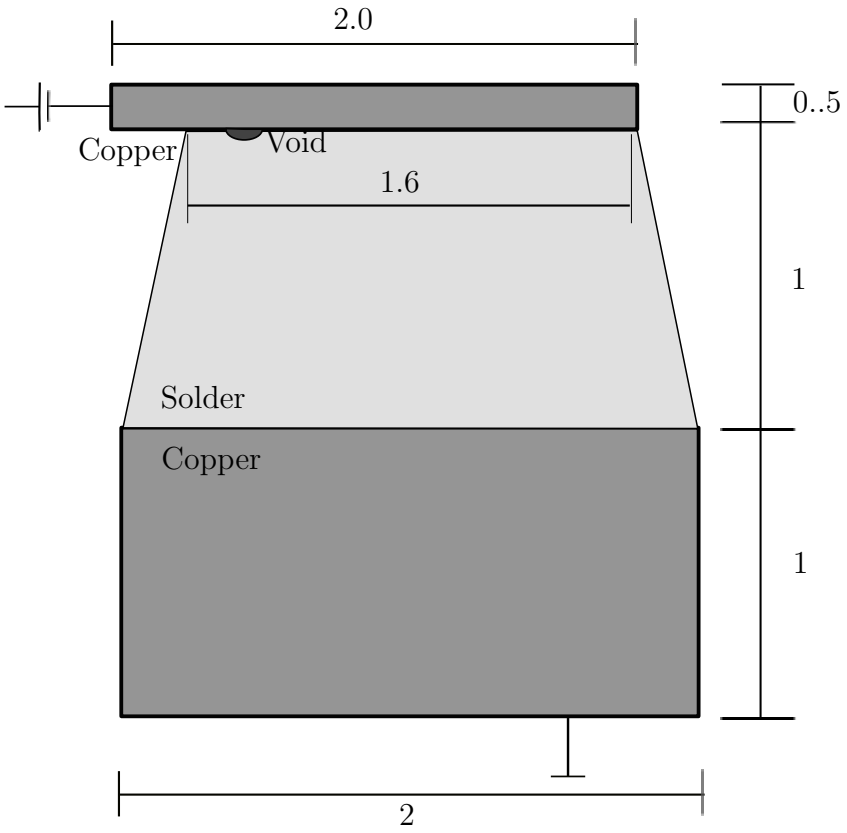

Figure 5.5. Geometry used for simulations.

Table 5.2. Diffusion and phase motion related properties for the solder.

Material property	Solder
$\gamma\Omega$	4.7×10^{-4}
$\frac{D_\Gamma h}{RT}$	1.17×10^{-8}
D_a	0.25
D_b	0.05
Ze_Γ	0.0
$\frac{Ze_\Omega}{RT}$	1.0
α	0.94
RT	1

second set. A contact angle of 80° implies that the adhesion between the copper and the solder is greater than the adhesion between the copper and the void, while the contact angle of 160° implies that the adhesion between the copper and the solder

Table 5.3. Parameters used in the simulations.

Δt	5×10^{-5}
ϵ	5×10^{-3}

is poor and it is easy to remove material from the interface. The stress effects are neglected in the simulations below.

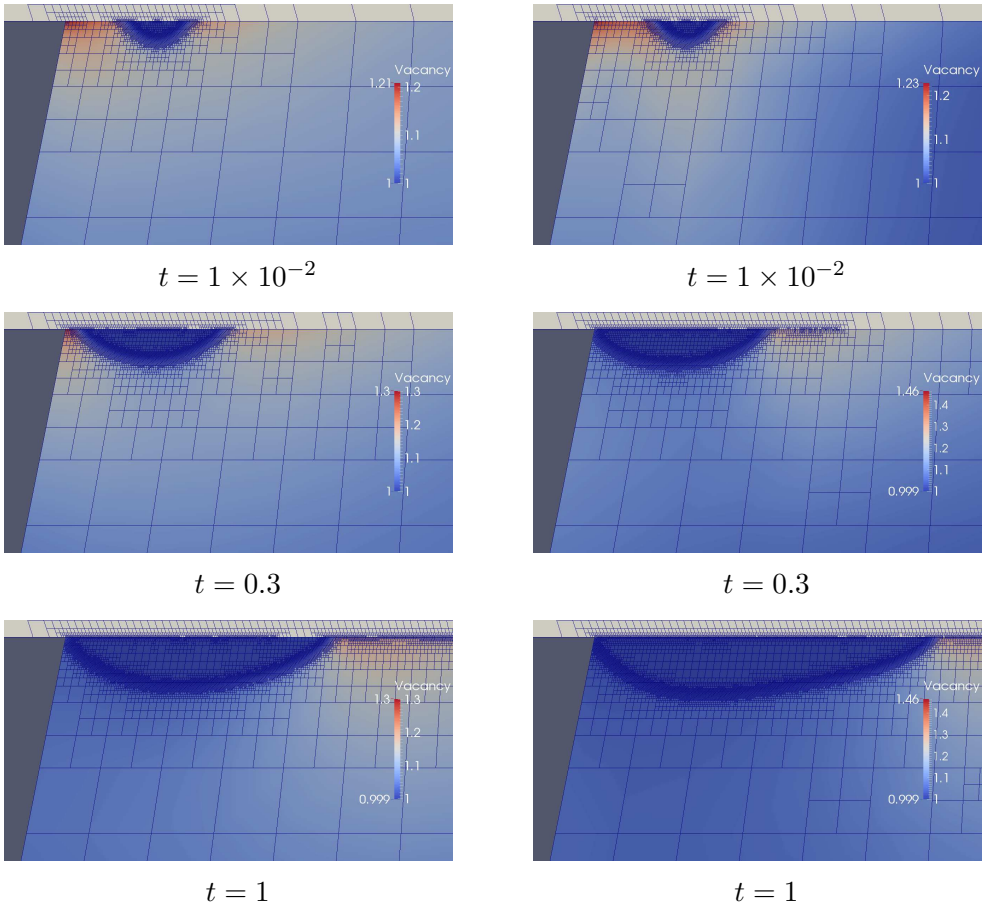

$t = 1 \times 10^{-2}$ $t = 1 \times 10^{-2}$

$t = 0.3$ $t = 0.3$

$t = 1$ $t = 1$

(a) Diffusivity dominant along the $x-$axis.

(b) Diffusivity dominant along the $y-$axis.

Figure 5.6. Evolution of void at interface due to vacancy accumulation under different anisotropic diffusivities and a contact angle of 160°.

From Figs. 5.6 and 5.7, It can be seen that the growth of the interfacial void is most rapid when the principal diffusivity is along the same direction where the

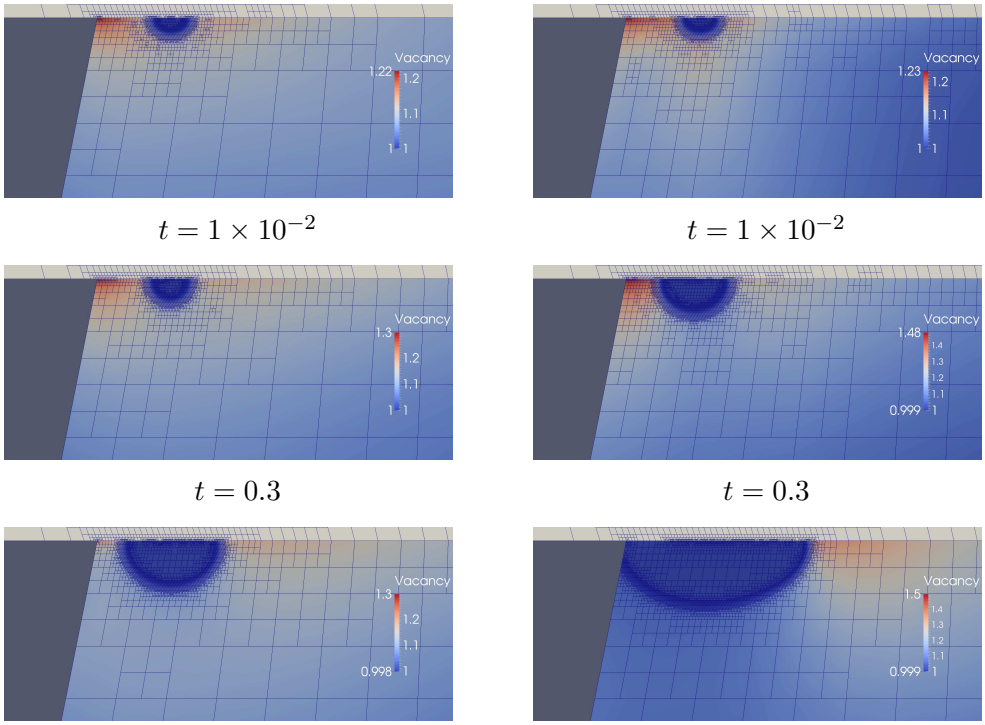

$t = 1 \times 10^{-2}$ $t = 1 \times 10^{-2}$

$t = 0.3$ $t = 0.3$

$t = 1$ $t = 1$

(a) Diffusivity dominant along the $x-$axis.

(b) Diffusivity dominant along the $y-$axis.

Figure 5.7. Evolution of void at interface due to vacancy accumulation under different anisotropic diffusivities and a contact angle of 80°.

electrical potential gradient is maximum, and when the spreading of the void along the interface is energetically favorable. This appears to agree with the experimental observations in the literature [124, 126]. On the other hand, when the spreading of the void is not energetically favorable, the spreading of the void along the interface is minimal. Furthermore, as the supply of vacancies to allow the growth of the void is limited, the void does not extend significantly into the interfacial region. On the other hand, when the diffusivity is parallel to the direction of the electrical potential gradient and the spreading of the void is unfavorable, the void can grow to a large size simply because of the large supply of vacancies into the region of the void.

5.5 Summary

The effect of anisotropy and contact angle on the growth of voids at a copper solder interface are studied using a newly developed phase field code. It is found that the contact line conditions at the interface between the solder and copper plays an important part in the evolution of the voids. It is suspected on the basis of these simulations that the anisotropy of the solder is more likely to dominate the failure effects. The effect of the concentration related stress is not included in these simulations, and the interaction of the diffusion driven stress on the void growth rates remains to be studied. The behavior at the interface Eq. (5.3) is likely to be a more general adhesive law, and the effect of this on the growth needs to be studied.

6. PHASE EVOLUTION IN MULTIPHASE SOLIDS: DEVELOPMENT

Real material systems often consist of many phases, whose evolution frequently has engineering significance. For example, void evolution in solder joints is actually a multiphase problem, with the void evolution usually occurring at regions such as grain boundaries, junctions, and at the copper/solder interface. The evolution of the void is governed by the properties of all the phases adjoining the void. An example of the complicated mechanics of void evolution in anisotropic joints with multiple phases can be seen in Fig. 6.1, where the growth of the void at the junction of the grains due to electromigration is affected by the anisotropic diffusivity of the different grains.

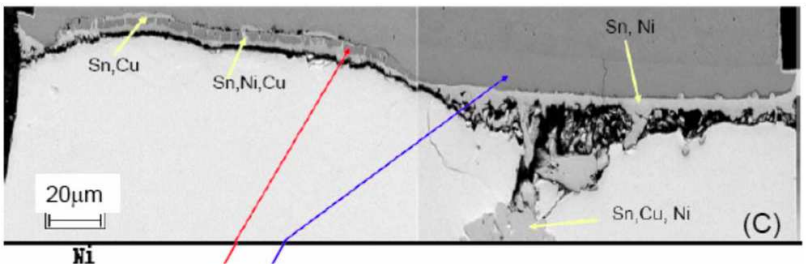

Figure 6.1. Growth of a void at the junction of two solder grains and the copper pillar. The anisotropy of the diffusivity of copper in the solder leads to the selective growth of the void in one grain [124].

The primary challenges in constructing numerical models to simulate the evolution of multi-phase systems are separating the domain into the different phases and assigning material properties. The other challenge is the assigning of interface properties to the different possible combinations of interfaces. This is especially challenging in cases where there are greater than 3 phases.

In this chapter and in Chapter 7, a phase field model is developed for the study of systems with multiple phases based on a micro-force balance [45, 46]. This model is

very similar to the one developed in [128]. Here, the model is also extended to allow for the simulation of intergranular void evolution by surface electromigration.

In the first part of this chapter, the reasons why the standard methods of derivation used for the study of multi-phase evolution are insufficient are discussed and the concept of a micro-force balance is introduced. This motivates the concept of a micro-force balance. These micro-force balances are coupled with the idea of the Larché-Cahn derivatives, [19] to derive a phase field model that is usable for an $n-$phase energy function with gradient terms. This model is studied with both constant and degenerate concentration dependent mobilities. A preliminary analysis is done to show the existence of solutions that separate into phases. Further, the model is studied at locations where only two of the phases are non-zero to determine the actual geometric evolution law being solved at the point and to find the constants that relate the diffuse interface model to the sharp interface equations determined from continuum mechanics. A more thorough analysis for the triple (in 2-D) and quadruple (in 3-D) points can be found in [129, 130].

In Chapter 7, a numerical implementation based on an Implicit-Explicit solution, where the phase field energy is split into the difference of a convex function and a concave function, with the convex part being treated implicitly is demonstrated. Finally, a few examples of the use of the implementation, such as phase separation in an $n-$phase system with degenerate and non-degenerate mobilities, the evolution of three phase systems to equilibrium, and electromigration in three phase systems is demonstrated.

6.1 Derivation of Phase Field Equations Based on Continuum Mechanics

It is challenging to derive equations of the phase field type as the free energy function driving the evolution of the system depends on the gradient of the phase

field variable. The traditional derivation defines the chemical potential through the variational derivative of the free energy functional $\int_\Omega \Psi(\phi, \nabla\phi) d\Omega$.

$$\mu = \frac{\delta \Psi(\phi, \nabla\phi, \boldsymbol{\varepsilon})}{\delta \phi}. \tag{6.1}$$

For the Cahn-Hilliard evolution of the phase field is then governed through a Fick's diffusion law

$$\frac{D}{Dt}\phi = \nabla . M(\phi) . \nabla \mu. \tag{6.2}$$

The variational derivative in Eq. (6.1) for a general functional $\int_\Omega F(\phi, \nabla\phi, \ldots) d\Omega$ is defined through the following,

$$\delta \int_\Omega F(\phi, \nabla\phi, \ldots) d\Omega = \int_\Omega \frac{\delta F(\phi, \nabla\phi, \ldots)}{\delta \phi} \delta\phi d\Omega. \tag{6.3}$$

For the related Allen-Cahn equation, the evolution is defined as a steepest descent rule as,

$$\frac{D}{Dt}\phi = -M \frac{\delta \int_\Omega \Psi(\phi, \nabla\phi, \boldsymbol{\varepsilon}) d\Omega}{\delta \phi}. \tag{6.4}$$

The function $\Psi(\phi, \nabla\phi, \varepsilon)$ most commonly used for the Cahn-Hilliard equation is a gradient energy of the form,

$$\Psi(\phi, \nabla\phi) = \int_\Omega \left(\gamma \left\| \nabla\phi \right\|^2 + f(\phi) \right) d\Omega. \tag{6.5}$$

with $f(\phi)$ a non-negative function with two roots at ϕ_1, ϕ_2 and reaching ∞ as $\phi \to \pm\infty$. The above derivations are physically reasonable and intuitive. However, the mathematical form makes it inconvenient to add additional features to the evolution. An alternative way to derive and define the above relations is by considering the evolution equations as gradient flows. Gradient flows [131] for functionals are defined

as follows. Consider a functional $I = \int_\Omega F(\phi, \nabla\phi) d\Omega$. The variation of the functional can be written as follows,

$$\delta I = \left\langle \frac{\delta F(\phi, \nabla\phi)}{\delta\phi}, \delta\phi \right\rangle. \tag{6.6}$$

The above equation is a gradient for the functional I. The right hand side of Eq. (6.6) is an inner product in a particular norm and can be written as,

$$\delta I = \left\langle \frac{\delta F(\phi, \nabla\phi)}{\delta\phi}, \mathcal{L}\delta\phi \right\rangle, \tag{6.7}$$

where $\mathcal{L}$ is a linear positive-semi definite operator that defines the inner product and the norm. Assuming that the system evolves so that the energy rate is minimized, the system evolves according to

$$\frac{D}{Dt}\phi = -\mathcal{L}^{-1}\delta F(\phi, \nabla\phi). \tag{6.8}$$

This is a steepest descent argument similar to the one used in Eq. (6.4). The Allen-Cahn equation itself can be described as a gradient flow in an L_2 norm. The Cahn-Hilliard equation on the other hand can be described and derived as a gradient flow in the H_{-1} [67, 132] norm, which is defined as follows,

$$\langle u, v \rangle_{H^{-1}} \equiv \langle \nabla\psi_u, \nabla\psi_v \rangle_{L^2}. \tag{6.9a}$$

where

$$\nabla^2\psi_{u,v} = u, v \quad \text{on } \Omega \tag{6.9b}$$

$$\nabla\psi_{u,v}.\boldsymbol{n} = 0 \quad \text{on } \Gamma \tag{6.9c}$$

and

$$\int_{\Omega} \psi_u d\Omega = 0. \tag{6.9d}$$

Eq. (6.9d) ensures that a gradient flow in the H^{-1} inner product conserves the value of the evolving quantity over the domain. To get the Cahn-Hilliard equation from the definition of the gradient energy) the first variation of Eq. (6.5) is taken and written as follows,

$$\delta\Psi(\phi, \nabla\phi) = \int_{\Omega} \left(-\gamma\nabla^2\phi + f'(\phi)\right) \delta\phi d\Omega. \tag{6.10}$$

Replacing the $\delta\phi$ in the right hand side with $\delta\phi = \nabla^2\psi_{\delta\phi}$, integrating by parts once and using $\nabla\psi_{\delta\phi}.\boldsymbol{n} = 0$,

$$\delta\Psi(\phi, \nabla\phi) = \int_{\Omega} \nabla\left(-\gamma\nabla^2\phi + f'(\phi)\right).\nabla\psi_{\delta\phi} d\Omega. \tag{6.11}$$

Comparing this to the right hand side of Eq. (6.9a),

$$\delta\Psi(\phi, \nabla\phi) = \left\langle \nabla\left(-\gamma\nabla^2\phi + f'(\phi)\right), \nabla\psi_{\delta\phi} \right\rangle_{L^2}. \tag{6.12}$$

From Eq. (6.9a),

$$\left\langle \frac{\delta\Psi}{\delta\phi}, \delta\phi \right\rangle = \left\langle \nabla^2\left(-\gamma\nabla^2\phi + f'(\phi)\right), \delta\phi \right\rangle_{H^{-1}}. \tag{6.13}$$

Using the definition of the gradient flow, the evolution rule can now be written as

$$\frac{\partial\phi}{\partial t} = -M\nabla^2\left(-\gamma\nabla^2\phi + f'(\phi)\right). \tag{6.14}$$

The approaches above (other than the gradient flow approach) have the advantage that they are simple, intuitive and physically reasonable. The gradient flow derivations have a convenient interpretation in terms of constrained optimization by

projected steepest descent [133]. However, they have serious deficiencies in terms of including additional physics such as stress and deformation, electrically driven fluxes etc. It is also difficult to modify these relationships to account for external fluxes. A serious limitation is that the kinetics for the evolution is limited a priori to linear laws. It is difficult to ascribe physical meaning to the various inner products and their related gradient flows. The methods of rational thermodynamics and continuum mechanics allow the definition and derivation of equations of motion for continuous systems in the most general form with the minimum of assumptions and limitations on the form of the free energy function and the resulting evolution models.

6.2 Limitations of Continuum Mechanics for Systems with Gradient Based Energies

Consider a system with a free energy density function,

$$\psi = \psi(\phi, \nabla\phi, \boldsymbol{\varepsilon}). \tag{6.15}$$

ϕ is an arbitrary conserved quantity that evolves by diffusion. Hence it can be assumed to follow the following conservation rule,

$$\frac{D}{Dt}\phi = -\nabla.\boldsymbol{J}_{\phi}. \tag{6.16}$$

In addition, it is assumed that the system is in mechanical equilibrium and hence, the stress is divergence-free,

$$\nabla.\boldsymbol{\sigma} = \mathbf{0}. \tag{6.17}$$

For the above system, the free energy change for an arbitrary control volume, neglecting any thermal flows can be written as,

$$\frac{D}{Dt}\int_{\Omega}\psi d\Omega \leq \int_{\Gamma}\left(\boldsymbol{v}.(\boldsymbol{\sigma}.\boldsymbol{n}) - \mu \boldsymbol{J}_{\phi}\right) d\Gamma. \tag{6.18}$$

Localizing this relation and using Eq. (6.16) gives,

$$\dot{\psi} \leq \boldsymbol{\sigma} : \dot{\boldsymbol{\varepsilon}} + \dot{\phi}\mu - \boldsymbol{J}_{\phi}.\nabla\mu. \tag{6.19}$$

Or

$$\dot{\psi} - \boldsymbol{\sigma} : \dot{\boldsymbol{\varepsilon}} - \dot{\phi}\mu \leq -\boldsymbol{J}_{\phi}.\nabla\mu. \tag{6.20}$$

The relation Eq. (6.20) should hold for *all* possible physical processes of the type under consideration. In addition to the constitutive law Eq. (6.15), the following constitutive laws are introduced for the quantities, $\boldsymbol{\sigma}, \mu, \boldsymbol{J}_{\phi}$ as,

$$\boldsymbol{\sigma} = \boldsymbol{\sigma}(\phi, \nabla\phi, \boldsymbol{\varepsilon}) \tag{6.21}$$

$$\mu = \mu(\phi, \nabla\phi, \boldsymbol{\varepsilon}) \tag{6.22}$$

$$\boldsymbol{J} = \mu(\phi, \nabla\phi, \boldsymbol{\varepsilon}. \tag{6.23}$$

Substituting the constitutive laws Eq. (6.15) into Eq. (6.20), neglecting any explicit time dependence in ψ and grouping terms,

$$\left(\frac{\partial\psi}{\partial\phi} - \mu\right)\dot{\phi} + \left(\frac{\partial\psi}{\partial\epsilon} - \sigma\right)\dot{\epsilon} + \frac{\partial\psi}{\partial\nabla\phi}\dot{\nabla\phi} \leq -\nabla\mu.\boldsymbol{J}_{\phi}. \tag{6.24}$$

Imposing that the above should be valid for arbitrary variations of the arguments ($\dot{\phi}$, $\dot{\boldsymbol{\varepsilon}}$ and $\dot{\nabla}\phi$). This is only possible if the following conditions hold,

$$-\nabla\mu.\boldsymbol{J}_{\phi} \geq 0 \tag{6.25a}$$

$$\frac{\partial\psi}{\partial\phi} = \mu \tag{6.25b}$$

$$\frac{\partial\psi}{\partial\boldsymbol{\varepsilon}} = \boldsymbol{\sigma} \tag{6.25c}$$

$$\frac{\partial\psi}{\partial\nabla\phi} = 0. \tag{6.25d}$$

. Eq. (6.25d) implies that there can be no dependence of the free energy function on the gradient of the order parameter variable ϕ. Thus the conventional theory is incomplete for use in developing models for phase field and other similar models.

6.3 Definition of Microforces

To allow the process of continuum mechanics to be used for models with gradient energies, the concept of interstitial working or microforces was introduced in [45, 46]. Changes in the total energy of a control volume are related to the power supplied by the change in $\dot{\phi}$ across the boundary of a control volume by defining a *microstress* denoted by $\boldsymbol{xi}$. This is defined as,

$$\dot{W} = \int_{\Gamma} \boldsymbol{\xi}.\boldsymbol{n}\dot{\phi}d\Gamma. \tag{6.26a}$$

Localizing, this can be written as,

$$\dot{W}_{local} = \nabla.\boldsymbol{\xi}\dot{\phi} - \dot{\nabla}\phi.\boldsymbol{\xi}. \tag{6.26b}$$

The functioning of these forces can be observed by adding Eq. (6.26a) to the right hand side of Eq. (6.18).

$$\frac{D}{Dt}\int_{\Omega}\psi d\Omega \leq \int_{\Gamma}\left(\boldsymbol{v}.(\boldsymbol{\sigma}.\boldsymbol{n}) - \mu\boldsymbol{J}_{\phi} + (\boldsymbol{\xi}.\boldsymbol{n})\dot{\phi}\right)d\Gamma. \tag{6.27}$$

Localizing Eq. (6.27),

$$\dot{\psi} - \boldsymbol{\sigma} : \dot{\boldsymbol{\varepsilon}} - \dot{\phi}\mu + \nabla.\boldsymbol{\xi}\dot{\phi} - \dot{\nabla}\phi.\boldsymbol{\xi} \leq -\boldsymbol{J}_{\phi}.\nabla\mu. \tag{6.28}$$

Introducing the constitutive law Eq. (6.15) and grouping terms, Eq. (6.28) can be re-written as,

$$\left(\frac{\partial\psi}{\partial\phi} - \mu + \nabla.\boldsymbol{\xi}\right)\dot{\phi} + \left(\frac{\partial\psi}{\partial\boldsymbol{\varepsilon}} - \boldsymbol{\sigma}\right)\dot{\boldsymbol{\varepsilon}} + \left(\frac{\partial\psi}{\partial\nabla\phi} - \boldsymbol{\xi}\right)\dot{\nabla}\phi \leq -\nabla\mu.\boldsymbol{J}_{\phi}. \tag{6.29}$$

For the above to be true for any arbitrary processes, the following conditions need to be satisfied,

$$\boldsymbol{\sigma} = \frac{\partial\Psi}{\partial\boldsymbol{\varepsilon}}, \tag{6.30a}$$

$$\mu = \frac{\partial\Psi}{\partial\phi} - \nabla.\boldsymbol{\xi}, \tag{6.30b}$$

$$\boldsymbol{\xi} = \frac{\partial\Psi}{\partial\nabla\phi} \tag{6.30c}$$

along with the condition

$$-\nabla\mu.\boldsymbol{J}_{\phi} \geq 0. \tag{6.30d}$$

Equations of the type Eq. (6.30c) are called microforce balances in [46].

6.3.1 Derivation of the Cahn-Hilliard Equation through Micro-forces

To get a better understanding of the mechanics of the process, consider the following specialized form for the for the free energy function,

$$\Psi(\phi, \nabla\phi) = \frac{\gamma}{2\epsilon}(1-\phi^2)^2 + \frac{\gamma\epsilon}{2}\|\nabla\phi\|^2 . \tag{6.31}$$

Applying the process of Eq. (6.30) to Eq. (6.31), the equations of motion can be written as,

$$\boldsymbol{\xi} = \frac{\partial\Psi}{\partial\nabla\phi} = \gamma\epsilon\nabla\phi \tag{6.32a}$$

$$\mu = -\frac{\gamma}{\epsilon}(1-\phi^2)\phi - \nabla.\boldsymbol{\xi}. \tag{6.32b}$$

In addition to the above two relations, a form needs to be specified for $\boldsymbol{J}_\phi$ such that $-\boldsymbol{J}_\phi.\nabla\mu \geq 0$. The simplest law that satisfies a relation of this form is,

$$\boldsymbol{J}_\phi = -M\nabla\mu. \tag{6.33}$$

Substituting the relation Eq. (6.33) into Eq. (6.16), the following evolution equation is obtained

$$\frac{\partial\phi}{\partial t} = \nabla.M\nabla\mu. \tag{6.34}$$

Eq. (6.34) along with Eq. (6.32) define the classical Cahn-Hilliard equation. In the following section, the above process will be generalized to a system with n phases evolving via a diffusion equation.

6.4 n-Phase Cahn-Hilliard system

The n phase system of Cahn-Hilliard equations is a non-linear n component diffusion equation with the general form,

$$\frac{\partial \phi_i}{\partial t} = \nabla.(\boldsymbol{J}_i) \tag{6.35a}$$

subject to the constraint,

$$\sum_{i=1}^{n} \phi_i = 1. \tag{6.35b}$$

This is usually derived from an augmented n-Phase gradient energy functional of the form,

$$\Psi_{\text{aug}}(\phi_{i=1,\ldots n}, \lambda) = \int_{\Omega} \sum_{i=1}^{n} \gamma_i \left\|\nabla \phi_i\right\|^2 + f(\phi_{i=1,\ldots n}) + \lambda(\sum_{i=1}^{n} \phi_i - 1) d\Omega. \tag{6.36}$$

In the above λ is a field of Lagrange multipliers that enforces Eq. (6.35b) everywhere in the domain. $f(\phi_{i,\ldots n})$ is a function such that $f(\ldots, \phi_i = 0, 1, \ldots) = 0$. Also, $f(\phi_{i\ldots n}) \geq 0 \forall \phi_i \in \mathbf{R}^n$. The n-Phase Cahn-Hilliard equation can then be derived by defining the chemical potentials as,

$$\begin{aligned} \mu_i &= \frac{\delta \Psi}{\delta \phi_i} \\ &= -\gamma_i \nabla^2 \phi_i + \frac{\partial f(\phi_{1,\ldots n})}{\partial \phi_i} + \lambda. \end{aligned} \tag{6.37}$$

This is then used to define the flux in the standard form as,

$$\frac{\partial \phi_i}{\partial t} = \nabla . M_i \nabla \mu_i. \tag{6.38}$$

The pointwise Lagrange multiplier λ can be eliminated (for constant equal M_i, and γ_i) by adding Eq. (6.37) for each of the phases, giving,

$$\sum_{i=1}^{n} \mu_i = -\gamma \sum_{i=1}^{n} \nabla^2 \phi_i + \sum_{i=1}^{n} \left(\frac{\partial f(\phi_{1,\ldots n}}{\partial \phi_i} + \lambda \right). \tag{6.39}$$

As $\sum_{i=1}^{n} \nabla^2 \phi_i = \nabla^2 \sum_{i=1}^{n} \phi_i = \nabla^2 1 = 0$,

$$\sum_{i=1}^{n} \mu_i = \sum_{i=1}^{n} \frac{\partial f(\phi_{1,\ldots n)}}{\partial \phi_i} + n\lambda. \tag{6.40}$$

Adding Eq. (6.38) for each of the phases, and using $\frac{\partial \sum_{i=1}^{n} \phi_i}{\partial t} = 0$

$$0 = \nabla . \sum_{i=1}^{n} M_i \nabla \mu_i. \tag{6.41}$$

One of the solutions to this, with the boundary conditions $\nabla \mu_i . \boldsymbol{n} = 0$ leads to

$$\nabla \left(\sum_{i=1}^{n} \mu_i \right) = 0, \tag{6.42}$$

which implies that $\sum_{i=1}^{n} \mu_i =$ constant which can be set as

$$\sum_{i=1}^{n} \mu_i = 0. \tag{6.43}$$

Using this in Eq. (6.40)

$$0 = \sum_{i=1}^{n} \frac{\partial f(\phi_{1\ldots n})}{\partial \phi_i} + n\lambda \tag{6.44}$$

$$\lambda = -\frac{1}{n} \sum_{i=1}^{n} \frac{\partial f(\phi_{1\ldots n})}{\partial \phi_i}. \tag{6.45}$$

The above equations can also be derived as a gradient flow in the H^{-1} space. Following Eq. (6.13), for each of the phase variables

$$\left\langle \frac{\delta \Psi}{\delta \phi_i}, \delta \phi_i \right\rangle = \left\langle \nabla^2 \left(-\gamma \nabla^2 \phi_i + \frac{\partial f(\phi_{1\ldots n})}{\partial \phi_i} + \lambda \right), \delta \phi_i \right\rangle_{H^{-1}}. \tag{6.46}$$

This can then be used to define an evolution law of the same form as Eq. (6.38). The Lagrange multiplier can now be eliminated in the same way. The above derivations have the same benefits of being mathematically and physically reasonable. However, the method of this derivation imposes certain very onerous restrictions on the form of the evolution equation, and on the method of solution. The first is the use of the Lagrange multiplier to enforce the constraint that the phase variables add up to one. As shown above, in order to eliminate this constraint it is necessary to assume that the mobilities are constant and equal. There are attempts in the literature to eliminate the Lagrange multiplier in the absence of this constraint [63,64] but this comes at the cost of tying the energetic quantities γ_i into the mobilities M_i. Ideally these should be independent. This also means that it is difficult to assign independent mobility properties to each pair of phases, restricting options in terms of modeling the interface evolution between pairs of phases. In the following section, the microforce approach is extended to a system with n phases evolving via a diffusion equation. Owing to the use of continuum mechanics, the model will allow independent definition of the mobilities without using a Lagrange multiplier to enforce the constraint.

6.4.1 Microforce Balance Derivation of the n-Phase Cahn-Hilliard Equations

Owing to the limitations listed above, a derivation of the n-phase Cahn-Hilliard equations is presented below. This is done by extending the idea of the microforces to more than one phase variable. Hence the microforces for each of the phases is defined through the work done towards the change of $\dot{\phi}_i$ over the boundaries of a

control volume by forces external to the control volume. A very similar derivation is presented in [128]

$$W_i = \int_\Gamma \dot{\phi}_i \boldsymbol{\xi}_i . \boldsymbol{n} d\Gamma. \tag{6.47}$$

In addition to the micro-forces, the chemical potentials μ_i are defined as

$$E_i = \int_\Gamma \mu_i \boldsymbol{J} . \boldsymbol{n} d\Gamma. \tag{6.48}$$

This relates the chemical potential of each of the phases with the total energy supply by diffusive fluxes of that phase through the boundary of the control volume. In contrast to the earlier derivation in § 6.3.1, the difference in the derivation for the n-phase case is the existence of the contraint, $\sum_{i=1}^{n} \phi_i = 1$. This has certain implications for the phase balance and the postulation of constitutive laws.

Balance of Phases

The phase-variable balance for each phase can be written as,

$$\frac{D}{Dt}\phi_i = -\nabla . \boldsymbol{J}_i. \tag{6.49}$$

Adding the species balance equations together, this leads to

$$\frac{D}{Dt}\sum_{i=1}^{n}\phi_i = -\sum_{i=1}^{n}\nabla . \boldsymbol{J}_i. \tag{6.50}$$

As, $\sum_{i=1}^{n}\phi_i = 1$, the above can be written as

$$\sum_{i=1}^{n}\nabla . \boldsymbol{J}_i = 0 \tag{6.51}$$

or, a stronger condition, which is

$$\sum_{i=1}^{n} \boldsymbol{J}_i = 0. \tag{6.52}$$

Balance of Energy

Before writing the balance of energy, the consequences of the constraint on the phase field variables on the net energy fluxes on the domain need to be examined. As the chemical potentials are energetic quantities, the total energy flux into a control volume due to diffusive fluxes should be invariant under a transformation of the type [23]

$$\mu_i \to \mu_i + \lambda. \tag{6.53}$$

In the above the λ is an arbitrary scalar. The net energy flux into the domain due to diffusion can therefore be written as

$$E_{diff} = \int_\Gamma \sum_{i=1}^{n} \mu_i \boldsymbol{J}_i.\boldsymbol{n} d\Gamma = \int_\Gamma \sum_{i=1}^{n} (\mu_i + \lambda) \boldsymbol{J}_i.\boldsymbol{n} d\Gamma = \int_\Gamma \sum_{i=1}^{n} \mu_i \boldsymbol{J}.\boldsymbol{n} d\Gamma + \int_\Gamma \lambda \sum_{i=1}^{n} \boldsymbol{J}_i.\boldsymbol{n} d\Gamma. \tag{6.54}$$

Using Eq. (6.52)

$$E_{diff} = \sum_{i=1}^{n} \int_\Gamma \mu_i \boldsymbol{J}_i.\boldsymbol{n} d\Gamma = \int_\Gamma \sum_{i=1}^{n} (\mu_i + \lambda) \boldsymbol{J}_i.\boldsymbol{n} d\Gamma. \tag{6.55}$$

As λ is an arbitrary constant, it can now be set equal to μ_j, where j is a chosen *reference* phase. This is written concisely as,

$$E_{diff} = \int_\Gamma \sum_{i=1}^{n} \mu_{ij} \boldsymbol{J}_i.\boldsymbol{n} d\Gamma. \tag{6.56}$$

In the above $\mu_{ij} \equiv \mu_i - \mu_j$ For the microstresses, the same argument can't quite be made. However relative microstresses will be introduced with the following argument. Say phase ϕ_j is evolving at a rate $\dot{\phi}_j$. The net power due to this change is defined through the micro-force $\boldsymbol{\xi}_j$. However the evolution of ϕ_j is not independent. It necessarily means that the other species are evolving such that $\sum_{i=1,i\neq j}^{n} \dot{\phi}_i = -\dot{\phi}_j$. Choosing a species (say ϕ_j) as a reference species, the net power supplied due to the change in the value of any species can be written as,

$$\dot{W} = \int_\Gamma \sum_{i=1,i\neq j}^{n} \dot{\phi}_i \left(\boldsymbol{\xi}_i - \boldsymbol{\xi}_j\right) .\boldsymbol{n} d\Gamma. \tag{6.57a}$$

Expanding this out, the above can be written as

$$\dot{W} = \int_\Gamma \sum_{i=1,i\neq j}^{n} \dot{\phi}_i \boldsymbol{\xi}_i .\boldsymbol{n} d\Gamma - \int_\Gamma \sum_{i=1,i\neq j}^{n} \dot{\phi}_i \boldsymbol{\xi}_j .\boldsymbol{n} d\Gamma \tag{6.57b}$$

$$\implies \dot{W} = \int_\Gamma \sum_{i=1}^{n} \dot{\phi}_i \boldsymbol{\xi}_i .\boldsymbol{n} d\Gamma. \tag{6.57c}$$

From the above discussion, it is possible to define a relative microstress of the form,

$$\boldsymbol{\xi}_{ij} = \boldsymbol{\xi}_i - \boldsymbol{\xi}_j. \tag{6.58}$$

It is clear from Eq. (6.57) that no information is lost by the definition of this relative quantity.

Neglecting thermal energy fluxes, the free energy inequality for the control volume Ω can now be written as follows,

$$\frac{D}{Dt}\int_\Omega \Psi d\Omega \leq \int_\Gamma (\boldsymbol{n}.\boldsymbol{\sigma}).\boldsymbol{v} d\Gamma - \int_\Gamma \sum_{i=1}^{n} \mu_{ij} \boldsymbol{J}_i .\boldsymbol{n} d\Gamma + \int_\Gamma \sum_{i=1}^{n} \dot{\phi}_i \boldsymbol{\xi}_{ij} .\boldsymbol{n} d\Gamma. \tag{6.59}$$

As stress equilibrium is set up much quicker than diffusion and phase evolution processes, the momentum balance can be assumed,

$$\nabla.\boldsymbol{\sigma} = 0. \tag{6.60}$$

Localizing Eq. (6.59) using the divergence theorem, with the phase balance equations (Eq. (6.49)) and the stress equilibrium condition, the free energy inequality at an arbitrary point can be written as,

$$\dot{\Psi} \leq \boldsymbol{\sigma} : \boldsymbol{\varepsilon} + \sum_{i=1}^{n} \left(\mu_{ij}\dot{\phi}_i - \nabla\mu_{ij}.\boldsymbol{J}_i \right) + \sum_{i=1}^{n} \left(\boldsymbol{\xi}_{ij}\nabla\dot{\phi} - \nabla.\boldsymbol{\xi}_{ij}\dot{\phi} \right) \tag{6.61}$$

$$\implies \dot{\Psi} - \boldsymbol{\sigma} : \boldsymbol{\varepsilon} - \sum_{i=1}^{n} \mu_{ij}\dot{\phi}_i - \sum_{i=1}^{n} \boldsymbol{\xi}_{ij}\nabla\dot{\phi} - \sum_{i=1}^{n} \nabla.\boldsymbol{\xi}_{ij}\dot{\phi} \leq -\sum_{i=1}^{n} \nabla\mu_{ij}.\nabla\boldsymbol{J}_i. \tag{6.62}$$

Constitutive relations are now introduced of the form,

$$\Psi = \Psi(\phi_{1\ldots n}, \nabla\phi_{1\ldots n}, \boldsymbol{\varepsilon}) \tag{6.63a}$$

$$\boldsymbol{\sigma} = \boldsymbol{\sigma}(\phi_{1\ldots n}, \nabla\phi_{1\ldots n}, \boldsymbol{\varepsilon}) \tag{6.63b}$$

$$\mu_i = \mu_i(\phi_{1\ldots n}, \nabla\phi_{1\ldots n}, \boldsymbol{\varepsilon}) \tag{6.63c}$$

$$\boldsymbol{\xi}_i = \boldsymbol{\xi}_i(\phi_{1\ldots n}, \nabla\phi_{1\ldots n}, \boldsymbol{\varepsilon}) \tag{6.63d}$$

$$\boldsymbol{J}_i = \boldsymbol{J}_i(\phi_{1\ldots n}, \nabla\phi_{1\ldots n}, \boldsymbol{\varepsilon}). \tag{6.63e}$$

The standard treatment does not apply here as the partial derivatives of Ψ with respect to each of the phase field variables are not independent. This problem is solved through the use of the Larché Cahn derivatives introduced in [18] for the development of the thermodynamics of systems undergoing substitutional diffusion. Consider a function $g(\phi_{1,\ldots n})$, with a constraint on the variables $\sum_{i=1}^{n} \phi_i = c$, where c is a positive constant. Choosing $\phi_j = c - \sum_{i=1, i\neq j}^{n} \phi_i$ is chosen as a reference, and the function $g(\phi_{1,\ldots n})$ is redefined as follows,

$$g^{(j)}(\phi_{i=1\ldots j-1,j+1\ldots}) = g(\phi_{i=1\ldots j-1,j+1\ldots n}). \tag{6.64}$$

The Larché Cahn derivatives of the function are then defined as,

$$\frac{\partial g^{(j)}}{\partial \phi^{(i)}} \text{ and } \frac{\partial^2 g^{(j)}}{\partial \phi_i \partial \phi_k}. \tag{6.65}$$

This also implies that,

$$\frac{\partial g^{(j)}}{\partial \phi_j} = 0. \tag{6.66}$$

The derivatives can also be defined as follows,

$$\frac{\partial g^{(j)}}{\partial \phi_i} = \frac{d}{d\epsilon} g(\phi_1, \ldots, \phi_i + \epsilon, \ldots, \phi_j - \epsilon, \ldots, \phi_n)|_{\epsilon=0}. \tag{6.67}$$

In the above, the change in one quantity is compensated by a change in the reference species. In a similar fashion the second Larché Cahn can be defined as

$$\begin{aligned} \frac{\partial^{2(j)} g}{\partial \phi_i \partial \phi_k} = \frac{d^2}{d\epsilon d\lambda} g(\phi_1, \ldots, \phi_i + \epsilon, \ldots, \\ \phi_j - \epsilon - \gamma, \ldots, \phi_k + \gamma \ldots, \phi_n)|_{\epsilon=0,\lambda=0}. \end{aligned} \tag{6.68}$$

The two definitions can be shown to be equivalent. Some important properties of the Larché Cahn derivatives are as follows. The first is,

$$\frac{\partial^{(j)} g}{\partial \phi_i} = -\frac{\partial^{(i)} g}{\partial \phi_j}. \tag{6.69}$$

This can be seen easily from Eq. (6.67). Similarly, the chain rule for a function $g(\phi_{1\ldots n}(t))$ is given as

$$\dot{g(\phi_{1\ldots n}(t))} = \sum_{i=1, i\neq j}^{n} \frac{\partial f^{(j)}}{\partial \phi_i} \dot{\phi_i}. \tag{6.70}$$

Definition of Constitutive Laws

The material derivative of the free energy, with the arguments can be written by substituting Eq. (6.63) into Eq. (6.62) and grouping terms,

$$\sum_{i=1}^{n}\left(\frac{\partial\Psi^{(j)}}{\partial\phi_i}-\mu_{ij}+\nabla.\boldsymbol{\xi}_{ij}\right)\dot{\phi}_i+\sum_{i=1}^{n}\left(\frac{\partial\Psi^{(j)}}{\partial\nabla\phi_i}-\boldsymbol{\xi_{ij}}\right)\dot{\nabla\phi}_i + \left(\frac{\partial\Psi}{\partial\boldsymbol{\varepsilon}}-\boldsymbol{\sigma}\right)\dot{\boldsymbol{\varepsilon}}\leq-\sum_{i=1}^{n}\nabla\mu_{ij}.\boldsymbol{J}_i. \tag{6.71}$$

In the above, instead of partial derivatives with respect to ϕ_i and $\nabla\phi_i$, the Larché Cahn derivatives are used. This allows the variation of all terms $i\neq j$ to be treated as arbitrary and independent, while for the case where $i=j$, the Larché Cahn derivatives are 0. In essence, the process of taking Larché-Cahn derivatives reduces the number of free variables by one. For Eq. (6.71) to be true for any variations of $\phi_{i\neq j}$ and $\boldsymbol{\varepsilon}$, the following relations need to hold for all allowed processes.

$$\frac{\partial\Psi^{(j)}}{\partial\phi_i}=\mu_{ij}-\nabla.\boldsymbol{\xi}_{ij} \tag{6.72a}$$

$$\frac{\partial\Psi^{(j)}}{\partial\nabla\phi_i}=\boldsymbol{\xi}_{ij} \tag{6.72b}$$

$$\frac{\partial\Psi}{\partial\boldsymbol{\varepsilon}}=\boldsymbol{\sigma}. \tag{6.72c}$$

Additionally, for Eq. (6.71) to be valid for arbitrary diffusive processes, the simplest flux rule is given as,

$$\boldsymbol{J}_i=-\sum_{k=1}^{n}M(\phi_{i=1,\ldots n},\boldsymbol{\sigma})_{ik}\nabla\mu_{kj}. \tag{6.73}$$

where, M is a positive semi-definite matrix. The elements of the matrix M_{ij} are not independent owing to the existence of the constraint on all the phases, this needs to satisfy two conditions [23]

- The flux should be invariant with respect to the choice of the reference species.

- The fluxes should sum to 0 Eq. (6.52)

The consequences of the first limitation can be seen by changing the reference species from j to p.

$$\boldsymbol{J}_i = -\sum_{k=1}^{n} M(\phi_{i=1,\dots n}, \boldsymbol{\sigma})_{ik} \nabla \mu_{kj} = -\sum_{k=1}^{n} M(\phi_{i=1,\dots n}, \boldsymbol{\sigma})_{ik} \nabla \mu_{kp} \tag{6.74}$$

$$\implies \sum_{k=1}^{n} M(\phi_{i=1,\dots n}, \boldsymbol{\sigma})_{ik} \nabla \mu_{kj} = \sum_{k=1}^{n} M(\phi_{i=1,\dots n}, \boldsymbol{\sigma})_{ik} \nabla (\mu_{kj} - \mu_{pj}) \tag{6.75}$$

$$\implies \left(\sum_{k=1}^{n} M(\phi_{i=1,\dots n}, \boldsymbol{\sigma})_{ik} \right) \nabla \mu_{pj} = 0 \tag{6.76}$$

$$\implies \left(\sum_{k=1}^{n} M(\phi_{i=1,\dots n}, \boldsymbol{\sigma})_{ik} \right) = 0. \tag{6.77}$$

Hence, the invariance with respect to the choice of the reference species leads to a constraint that each row of M sums to zero. The strong flux constraint, Eq. (6.52) with Eq. (6.73), leads to

$$-\sum_{i=1}^{n} \sum_{k=1}^{n} M(\phi_{i=1,\dots n}, \boldsymbol{\sigma})_{ik} \nabla \mu_{kj} = 0. \tag{6.78}$$

The above must hold irrespective for arbitrary choice of j, this can be shown to be

$$\sum_{i=1}^{n} M(\phi_{i=1,\dots n}, \boldsymbol{\sigma})_{ik} = 0. \tag{6.79}$$

The section above allows us to construct a system of equations given an energy function that depends on the gradients of an arbitrary number of phase-field like parameters, as long as the relations Eqs. (6.52), (6.77) and (6.79) are satisfied. This allows phase field equations to be easily constructed in a systematic fashion, based either on a simple extension of the binary gradient energy or the more involved anti-symmetric Steinbach-Pezzola type energy [134].

To make this clearer, in the following equation, particular equations will be derived from a given energy function. In this dissertation, the standard multiphase energy which can be written as the sum of n gradient terms is used [63, 131].

6.5 Specialization of Equations

In this section, the results of the section above are applied to a given free energy function that depends on n order parameter values as well as their gradients. As the interest is in developing a phase field model that can be used for the simulation of arbitrary geometric evolution laws, a standard multi-phase energy of the form considered in [63] is considered.

$$\Psi(\phi_{i,\dots n}) = \sum_{i=1}^{n} \gamma_i \left(\frac{\epsilon}{2} |\nabla \phi_i|^2 + \frac{1}{\epsilon} f(\phi_i) \right) \tag{6.80}$$

where

$$f(\phi) = \phi^2 (1 - \phi)^2. \tag{6.81}$$

For convenience, the following function is also defined,

$$F(\phi_{i=1,\dots n}) = \sum_{i=1}^{n} \gamma_i f(\phi_i). \tag{6.82}$$

The functional above has the property that the minimizers to $\int_\Omega \Psi d\Omega$ tend to either 1 or 0 in most of the domain. Coupled with the fact that the evolution equations restrict the values to the Gibbs simplex Fig. 7.2, this allows the evolution of n phases

to be tracked. Applying the conclusions of Eq. (6.72) to Eq. (6.80) and choosing ϕ_n to be the reference species,

$$\begin{aligned}\mu_{in} &= \frac{\partial F^{(n)}}{\partial \phi_i} + \nabla.\boldsymbol{\xi}_{in} \\ &= \frac{\partial F}{\partial \phi_i} - \frac{\partial F}{\partial \phi_n} + \nabla.\boldsymbol{\xi_{in}}\end{aligned} \tag{6.83a}$$

$$\boldsymbol{\xi}_{in} = \gamma_i \nabla\phi_i - \gamma_n \nabla\phi_n \tag{6.83b}$$

$$\frac{\partial \phi_i}{\partial t} = -\nabla.\sum_{j=1}^{n} M_{ij} \nabla\mu_{jn}. \tag{6.83c}$$

This is a valid n phase system of Cahn-Hilliard equations, which satisfies the constraint $\sum_{i=1}^{n}\phi_i = 1$ as long as Eqs. (6.77) and (6.79) are satisfied by M. The properties of this system of equation will be considered in § 6.6.

For numerical implementations, the elimination of the n^{th} phase is useful as it reduces the number of equations to be solved significantly. Using the substitution, $\phi_n = 1 - \sum_{i=1}^{n-1}\phi_i$, the derivatives in terms of ϕ_n can be re-written using the chain-rule as

$$\frac{\partial F}{\partial \phi_n} = \sum_{i=1}^{n-1} \frac{\partial F}{\partial \phi_i}\frac{\partial \phi_i}{\partial \phi_n} \tag{6.84}$$

$$\implies \frac{\partial F}{\partial \phi_n} = -\sum_{i=1}^{n-1} \frac{\partial F}{\partial \phi_i}. \tag{6.85}$$

As

$$\frac{\partial \phi_j}{\partial \phi_k} = -1 \tag{6.86}$$

for arbitrary $j \neq k$. The constraint also allows in a simpler fashion

$$\nabla\phi_n = -\sum_{i=1}^{n-1} \nabla\phi_i. \tag{6.87}$$

Using Eqs. (6.85) and (6.87) in Eq. (6.83), it can now be written as,

$$\mu_{in} = \frac{\partial F}{\partial \phi_i} + \sum_{j=1}^{n-1} \frac{\partial F}{\partial \phi_j} + \nabla . \boldsymbol{\xi}_{in} \tag{6.88}$$

$$\boldsymbol{\xi}_{in} = \gamma_i \nabla \phi_i + \gamma_n \sum_{i=1}^{n-1} \nabla \phi_j. \tag{6.89}$$

While it may seem that the species ϕ_n is being treated differently from the other species in order to eliminate it, it must be noted that invariance in terms of the choice of ϕ_n is built into the choice of the mobility matrix M. A simple form for the matrix M can be defined as

$$M_{ij,i\neq j} = M_{ji} = M_{ij}^0 \text{and } M_{ij}^0 < 0 \tag{6.90a}$$

$$M_{ii} = \sum_{j=1, j\neq i}^{n} - M_{ij}. \tag{6.90b}$$

As the rows and columns add up to 0, the matrix M is singular and hence indefinite. Also, it can be shown that the non-zero eigenvalues of this matrix are positive, hence satisfying the condition for allowable mobilities. This satisfies the restriction on diffusive processes causing an increase of the free energy. A more useful form from the perspective of modeling phase evolution problems is the degenerate mobility. This is a mobility function that is non-zero only in the interfacial region, and hence restricts the phase evolution to the interface. The simple form that is considered in this work is,

$$M_{ij,i\neq j} = M_{ji} = M_{ij}^0 \phi_i^2 \phi_j^2, \text{and } M_{ij}^0 < 0 \tag{6.91a}$$

$$M_{ii} = \sum_{j=1, j\neq i}^{n} - M_{ij}^0 \phi_i^2 \phi_j^2. \tag{6.91b}$$

As in Eq. (6.90), the rows and columns of the matrix M add up to 0 and hence satisfy both Eqs. (6.77) and (6.79) as well as the requirement that the energy of the system not increase.

A significant advantage of the model developed in the above section (Eqs. (6.83), (6.88), (6.90) and (6.91) is that for a 3-phase system, it allows the definition of the mobilities and the surface tensions in a pairwise fashion without linking the two quantities together (as done in [63]) and this is done without the use of a Lagrange multiplier to enforce the constraint on the phase field variables. These two properties together make it easy to use this model to simulate more complex phenomena with driven diffusion and other evolution phenomena added to the interfaces.

6.5.1 Adding Electromigration Terms

The simplest extension to the model presented here is to add electromigration at the interfaces. This is done through a simple addition to the flux term of the form,

$$\boldsymbol{J}_i^{\text{elec}} = \sum_{i=1}^{i\neq j,n} M_{ij} Z_{ij} \nabla \phi_e. \tag{6.92}$$

To maintain the constraint on the sum of the phases, Z_{ij} is not free, but has the following constraint on it

$$Z_{ij} = -Z_{ji}. \tag{6.93}$$

In the simplest case, where there no other phases,

$$\boldsymbol{J}_i^{\text{elec}} + \boldsymbol{J}_j^{\text{elec}} = M_{ij}(Z_{ij} + Z_{ji})\nabla \phi_e \tag{6.94}$$

$$\implies \boldsymbol{J}_i^{\text{elec}} + \boldsymbol{J}_j^{\text{elec}} = 0. \tag{6.95}$$

6.6 Analysis of the $n-$ Phase System of Cahn-Hilliard Equations

In this section, the $n-$ phase system of Cahn-Hilliard equations described in the section above is analysed using a simplified formal analysis. The first part is to study the outer solution to show that the solutions to the phase field equations lead to phase

separation. The next step is to study the equations when only two of the phases are present. It will be seen in this section that the 2-phase equations don't correspond to a physical process in the case of constant mobilities. However, with degenerate mobility functions, the equations reduce to motion of each pair of interfaces by surface diffusion. In the multi-phase field case, further analysis is needed where more than one phase is non-zero. This analysis is not part of this dissertation and can be found in [129, 130]. The primary result from the analysis at points where more than two phases are non-zero for the multi-phase field equations is that the interfaces satisfy Young's rule for contact at triple points,

$$\frac{\sin\theta_{12}}{\gamma_{12}} = \frac{\sin\theta_{23}}{\gamma_{23}} = \frac{\sin\theta_{13}}{\gamma_{13}}. \tag{6.96}$$

The angles used here can be seen in Fig. 6.2.

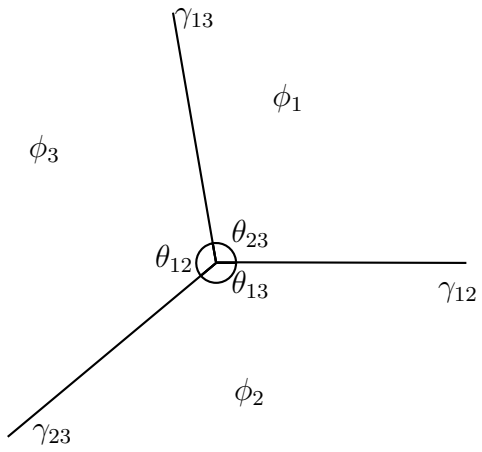

Figure 6.2. Young's rule at triple points.

The analysis in this section is performed on the following scaled version of the $n-$ phase Cahn-Hilliard equation,

$$\frac{\partial \phi_i}{\partial t} = \nabla . \sum_{i=1}^{n} \frac{M_{ij}}{\epsilon} \left(\nabla \mu_{jn} + Z_{ij} \nabla \phi_e \right) \tag{6.97a}$$

$$\mu_{in} = -\nabla . \epsilon \left(\gamma_i \nabla \phi_i - \gamma_n \nabla \phi_n \right) + \frac{1}{\epsilon} \left(\gamma_i f'(\phi_i) - \gamma_n f'(\phi_n) \right). \tag{6.97b}$$

To perform the asymptotic analysis, the solution is split into inner and outer solutions (Appendix B). The outer solution is studied first. The term of the highest order in the outer region for Eq. (6.97) are the terms of order ϵ^{-1} related to the derivatives of the phase field potential function. These can be written as,

$$f'(\phi_i) - f'(\phi_n) = 0. \tag{6.98}$$

The above is true for all ϕ_i. This allows us to state more generally that, $f'(\phi_i) = 0$ for all i. $f'(\phi_i)$ has two roots at $\phi = 0, 1$ (Fig. 7.4. This implies that in the solutions to the $n-$phase Cahn-Hilliard equations tend to $\phi_i = 1, 0$, over the outer regions. As, $\sum_{i=1}^{n} \phi_i = 1$, this implies that solutions to the $n-$Phase Cahn-Hilliard equations separate the domain into regions where,

$$\phi_i = 1, \quad \phi_{j \neq i} = 0. \tag{6.99}$$

This relation holds for both the degenerate as well as the constant mobility cases, and it clearly shows that Eq. (6.97) leads to phase separation.

6.6.1 Constant Mobility

The constant mobility is case is now analyzed for the case where there are only two phases present. The electromigration is neglected for the case of constant mobility. As the choice of the reference phase is arbitrary, the phases chosen are ϕ_1 and ϕ_2 with

ϕ_2 as the reference phase. Also, as there are only 2 phases present, $\phi_2 = 1 - \phi_1$. This transforms Eq. (6.97), into

$$\frac{\partial \phi_1}{\partial t} = \nabla . \left(\frac{M}{\epsilon} \right) \nabla \mu_{12} \tag{6.100a}$$

$$\mu_{12} = -\epsilon \left(\gamma_1 + \gamma_2 \right) \nabla . \nabla \phi_1 + \frac{1}{\epsilon} \left(\gamma_1 + \gamma_2 \right) f'(\phi_i). \tag{6.100b}$$

Here, two facts have been used, the first that $\nabla \phi_1 = -\nabla \phi_2$, and the second is $f'(\phi_1) = -f'(\phi_2)$. The $n-$phase Cahn-Hilliard equation therefore reduces to a standard binary Cahn-Hilliard equation in the case of the absence of the other phases. An important thing to note here is that constant-equal mobilities are considered for all the phases here. The reason for this is that the mobilities are not separable in terms of pairs of phases in the binary case with constant mobilities.

6.6.2 Degenerate Mobility

In the case of a degenerate mobility, with the mobility function of the form Eq. (6.91), Eq. (6.97) reduces to,

$$\frac{\partial \phi_1}{\partial t} = \nabla . \frac{M_{12} \phi_1^2 (1 - \phi_1)^2}{\epsilon} \left(\nabla \mu_{12} + Z_{12} \nabla \phi_e \right) \tag{6.101a}$$

$$\mu_{12} = -\epsilon \left(\gamma_1 + \gamma_2 \right) + \frac{1}{\epsilon} \left(\gamma_1 + \gamma_2 \right) f'(\phi_i). \tag{6.101b}$$

In contrast to the Eq. (6.100), the mobility in the degenerate case can be completely separated as the mobilities are zero in the absence of the other phases when both the phases corresponding to the particular interface are not present. Eq. (6.101) is a standard degenerate Cahn-Hilliard equation. This can be shown to be equivalent to the surface diffusion equation. (In this case the surface diffusion equation with an electromigration term.) The scaling parameters for this equation can be easily determined through a classical 2-phase asymptotic analysis. The coordinate system used for this is shown in Fig. 6.3. The inner expansion to Eq. (6.101), can be written

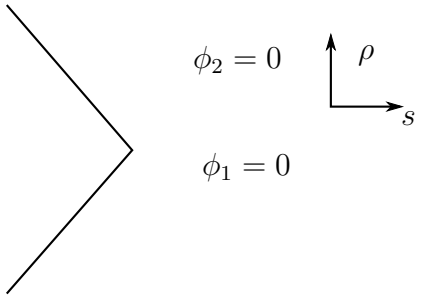

Figure 6.3. Co-ordinate system used in the asymptotic analysis

in the (ρ, s) co-ordinate system as,

$$\Phi_1(\rho, s; \epsilon) = \Phi_1^0(\rho, s; \epsilon) + \epsilon\Phi_1^1(\rho, s; \epsilon) + \epsilon^2\Phi_1^2(\rho, s; \epsilon) + \dots \tag{6.102a}$$

$$\mu_{12}(\rho, s; \epsilon) = \mu_{12}^0(\rho, s; \epsilon) + \epsilon\mu_{12}^1(\rho, s; \epsilon) + \epsilon^2\mu_{12}^2(\rho, s; \epsilon). \tag{6.102b}$$

Substituting these into an appropriately scaled version of Eq. (6.101). The leading order term of Eq. (6.101b) (ϵ^{-1}) leads to,

$$\frac{\partial^2\Phi_1^0}{\partial\rho^2} + f'(\Phi_1^0) = 0. \tag{6.103}$$

The solution to the above with the boundary conditions $\lim_{\rho\to-\infty}\Phi_1^0 = 0, \lim_{\rho\to\infty}\Phi_1^0 = 1$ leads to,

$$\Phi_1^0(\rho) = \frac{1 + \tanh\frac{\rho}{\sqrt{2}}}{2}. \tag{6.104}$$

Hence the $n-$ phase system of Cahn-Hilliard equations as formulated here leads to a hyperbolic tangent approximation of the Heaviside step function between any two phases. As $\phi_1 + \phi_2 = 1$, the value of ϕ_2 in the interfacial region can be written as,

$$\Phi_2^0(\rho) = \frac{1 - \tanh\frac{\rho}{\sqrt{2}}}{2}. \tag{6.105}$$

Terms of ϵ^0 order in Eq. (6.101b) leads to,

$$\mu_{12}^0 = (\gamma_1 + \gamma_2)\,\kappa_{12}\Phi_{1\rho}^0. \tag{6.106}$$

κ_{12} is the curvature of the interface between phase 1 and phase 2. Integrating Eq. (6.106) from $-\infty$ to ∞ after multiplying both sides by $\Phi_{1\rho}^0$,

$$\int_{-\infty}^{\infty} \mu_{12}^0 \Phi_{1\rho}^0 d\rho = (\gamma_1 + \gamma_2)\,\kappa_{12} \int_{-\infty}^{\infty} \Phi_{1\rho}^{0\,2} d\rho \tag{6.107}$$

This leads to

$$\mu_{12}^0 = \frac{1}{3\sqrt{2}}\,(\gamma_1 + \gamma_2)\,\kappa_{12}. \tag{6.108}$$

The ϵ^{-1} order terms of Eq. (6.101a) now lead to,

$$-V_{12}\Phi_{0\rho}^1 = M_{12}(\Phi_1^0)^2(1-\Phi_1^0)^2\nabla_\Gamma^2.\left(\mu_{12}^0 + Z_{12}\Phi_e\right). \tag{6.109}$$

Integrating both sides from $-\infty$ to ∞,

$$-V_{12} = \nabla_\Gamma^2\left(\frac{1}{3\sqrt{2}}\,(\gamma_1+\gamma_2)\,\kappa + Z_{12}\Phi_e\right)\int_{-\infty}^{\infty}(\Phi_1^0)^2(1-\Phi_1^0)^2 d\rho. \tag{6.110}$$

The final integral is equal to $\frac{1}{6\sqrt{2}}$, and hence

$$V_{12} = -\frac{1}{36}.\nabla_\Gamma^2\left((\gamma_1+\gamma_2)\,\kappa + Z_{12}\Phi_e\right). \tag{6.111}$$

Hence, the model in Eq. (6.97), leads to a surface electromigration equation between any two phases. The relation of the simulation parameters γ_i to the actual physical surface energies γ_{ij} are specified in the next section. An important case that is not mentioned in the analysis here is the analysis at the triple point. A detailed derivation of such cases can be found in [129, 130]. The approach is to integrate terms of type Eq. (6.108) for each pair of phases over a triangular region containing the triple point.

6.6.3 Construction of Surface Energies

From Eqs. (6.100) and (6.101) it is clear that the surface energy term that appears in the reduced 2-phase components of the Cahn Hilliard system are $\gamma_i + \gamma_j$ where i and j are the two phases that are non-zero, and are separated by the interface. Considering a system with n phase field variables, the surface energy contributions for each interface can be written as,

$$\gamma_{ij} = \gamma_i + \gamma_j. \tag{6.112}$$

This system of equations possesses a unique non-trivial solution, only in the case where there are less than 3 phases, or if all the surface energies are equal. For the simple 3 phase case, the solution can be written as,

$$\gamma_1 = \frac{1}{2}\left(\gamma_{12} + \gamma_{13} - \gamma_{23}\right) \tag{6.113a}$$

$$\gamma_2 = \frac{1}{2}\left(\gamma_{12} + \gamma_{23} - \gamma_{13}\right) \tag{6.113b}$$

$$\gamma_3 = \frac{1}{2}\left(\gamma_{23} + \gamma_{13} - \gamma_{12}\right). \tag{6.113c}$$

For systems with more than 3 phases, the Steinbach-Pezzola multiphase energy is more appropriate [134]. As it is formulated directly in terms of the surface energies between the different phases, a solution of the type shown here in Eq. (6.113) is unnecessary. As much of the derivation in this chapter was independent of the form of $\Psi(\phi_i, \nabla\phi_i)$, the same equations can be used for the Steinbach-Pezzola energy without significant modification.

However, the form of the final partial differential equations obtained is more complex, and the model developed here is sufficient for several practical problems. In Chapter 7, a numerical implementation of the phase field model derived and analysed here is described, and some simulation examples are presented.

7. PHASE EVOLUTION IN MULTIPHASE SOLIDS: NUMERICAL FORMULATION AND IMPLEMENTATION

The system of partial differential equations derived in Chapter 6, are coupled non-linear partial differential equations. Numerical solution to these equations are expensive owing to the multiple degrees of freedom at every node (A system with 4 phases will have 6 degrees of freedom at every node). Similar to the numerical algorithm described in Chapter 4, a convex-concave implicit splitting is used to solve the differential equations Eq. (6.97). This numerical approach is described in § 7.1. Following this numerical examples are presented. In § 7.2, examples of phase separation from initially random input are presented. The effect of degenerate and constant mobilities are shown. This is followed by specific examples of phase evolution in a 3-phase case, with the lens formation (§ 7.3) and double bubble (§ 7.4). Finally, a few examples of multi-phase evolution with electromigration are presented in § 7.5.

7.1 Numerical Implementation of the $n-$Phase System Cahn-Hilliard Equations

The approach used in this work is similar to the approach described in [64]. However, while the authors in [64] use a Lagrange multiplier to enforce the constraint of the sum of the phases being unity, the derivation in Chapter 6 based on continuum mechanics eliminates the necessity of the Lagrange multiplier. The constraint is automatically enforced. The convex-concave splitting [72] is used in these simulations to reduce the cost of the solution of non-linear problems. All the simulations in this dissertation use a biquadratic potential. The combined effect of the potential over the Gibbs simplex can be seen in Fig. 7.2. For different combinations of the γ_i, the free energy contours, possess different shapes. In this formulation of the $n-$phase

Cahn-Hilliard equations, it is possible for the combination of γ_i to cause a loss of convexity and consequent failure of the solution algorithm.

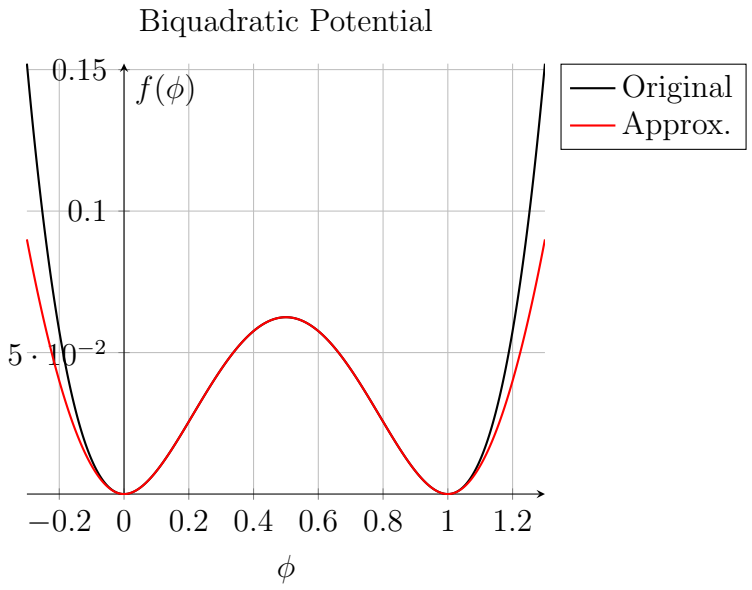

Figure 7.1. Biquadratic and modified phase field energy form used in the simulations.

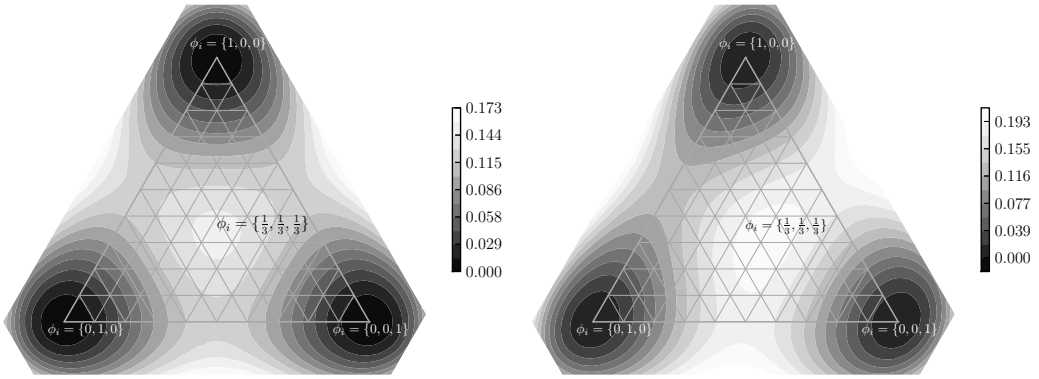

(a) $\gamma_i = 1.0$. (b) $\gamma_1 = \gamma_2 = 1, \gamma_3 = 2$.

Figure 7.2. Biquadratic potentials over the Gibbs simplex for a 3 phase case.

Instead of the standard biquadratic potential function, $\sum_{i=1}^{N}\gamma\phi_i^2(1-\phi_i)^2$, a modified form based on the form used in [73], is used. This can be written as $f(\phi_{i=1,\dots n}) = \sum_{i=1}^{N}\gamma_i f_i(\phi_i)$. $f(\phi_i)$ is a function that is defined piecewise as,

$$f(\phi_i) = \begin{cases} \phi_i^2 & \text{if } \phi_i \leq 0 \\ \phi_i^2(1-\phi_i)^2 & \text{if } 0 < \phi_i < 1 \\ (\phi_i - 1)^2 & \text{if } \phi_i \geq 1 \end{cases}. \tag{7.1}$$

This is shown by the red line in Fig. 7.1. The numerical simulations are simplified when the potential functions are treated as the difference of two convex functions. A split for the standard phase field function is written as,

$$f_i(\phi_i) = \underbrace{\phi_i^2 - \phi_i}_{\text{convex}} \underbrace{- \left(\phi_i - 2\phi_i^3 + \phi^4\right)}_{\text{concave}}. \tag{7.2}$$

This is shown by the black line and the solid red line in Fig. 7.3. As can be seen the concave part of the function is not entirely convex. This causes problems with the numerical solution. For the modified phase field potential function, Eq. (7.1), the split is written as,

$$f_i^m(\phi_i) = \underbrace{\phi_i^2 - \phi_i}_{\text{convex}} \underbrace{- \begin{cases} \phi_i, & \text{if } \phi_i \leq 0 \\ \phi_i^4 - 2\phi_i^3 + \phi_i, & \text{if } 0 < \phi_i < 1 \\ 1 - \phi_i, & \text{if } \phi_i \geq 1 \end{cases}}_{\text{concave}}. \tag{7.3}$$

This split is shown by the black line and the dashed red line in Fig. 7.3. As can be seen, the two functions are the same in the domain $0 < \phi_i < 1$, and are monotonically increasing and decreasing in the rest of the domain, in contrast with the standard split. This reduces the possibility of instabilities in the numerical solution schemes. The nature of the convex and concave functions over the Gibbs' simplex can be seen in Fig. 7.5.

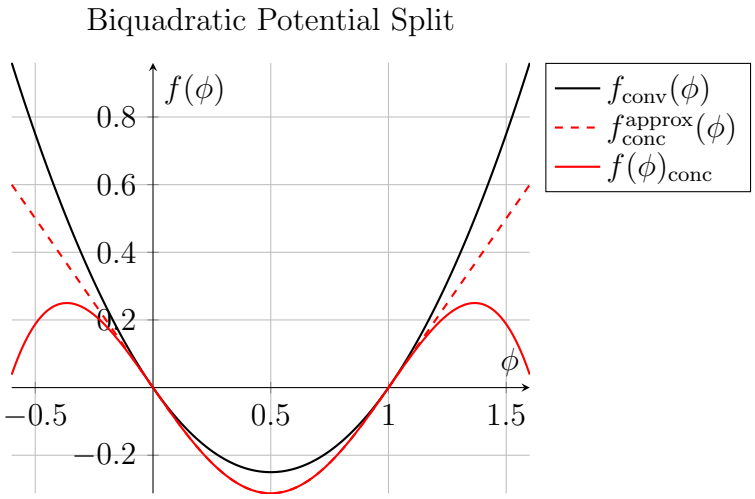

Figure 7.3. Bi-quadratic and modified phase field energy form used in the simulations.

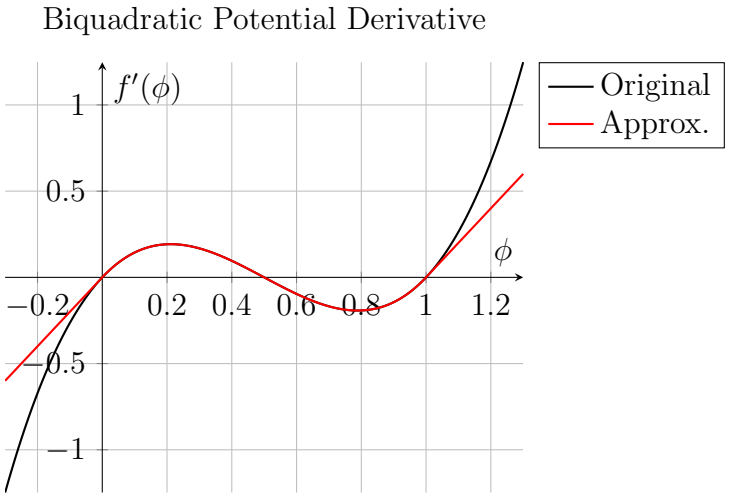

Figure 7.4. Derivative of the biquadratic and the modified phase field function.

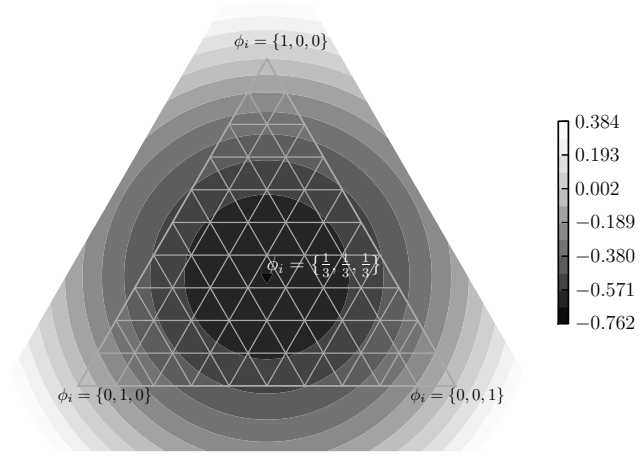

Convex part

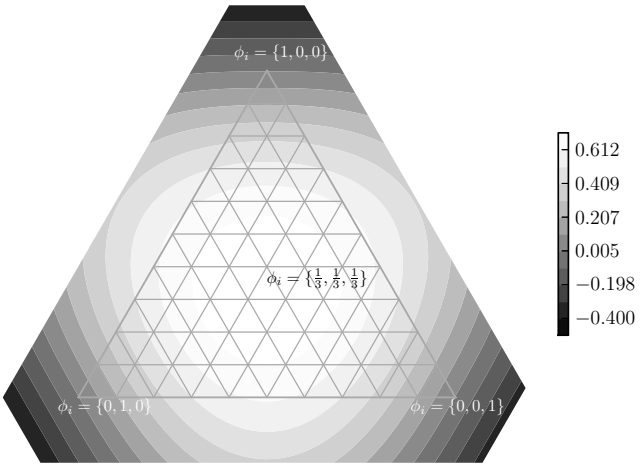

Concave part

Figure 7.5. The convex and concave parts of the phase field functions over the Gibbs triangle for equal surface energies.

Using the split in Eq. (7.3), the finite element solutions for Eq. (6.97) can be written as follows for the

$$\begin{bmatrix} A^{\phi\phi}_{i=j} & A^{\phi\phi}_{i\neq j} & A^{\phi\mu}_{i=j} & A^{\phi\mu}_{i\neq j} \\ A^{\phi\phi}_{i\neq j} & A^{\phi\phi}_{i=j} & A^{\phi\mu}_{i\neq j} & A^{\phi\mu}_{i=j} \\ A^{\mu\phi}_{i=j} & A^{\mu\phi}_{i\neq j} & A^{\phi\mu}_{i=j} & A^{\phi\mu}_{i\neq j} \\ A^{\mu\phi}_{i\neq j} & A^{\mu\phi}_{i=j} & A^{\mu\mu}_{i\neq j} & A^{\mu\mu}_{i=j} \end{bmatrix} \begin{bmatrix} \phi^t_i \\ \phi^t_j \\ \mu^t_{in} \\ \mu^t_{jn} \end{bmatrix} = \begin{bmatrix} F^{\phi}_i \\ F^{\phi}_j \\ F^{\mu}_{in} \\ F^{\mu}_{jn} \end{bmatrix}. \tag{7.4}$$

In Eq. (7.4), the elements of the system matrix can be written as follows,

$$(A^{\phi\phi}_{i=j})_{lm} = \int_{\Omega_{\text{el}}} [(\gamma_i + \gamma_n)\epsilon \nabla N_l \nabla N_m + \frac{(\gamma_i f''_{\text{convex}}(\phi^t_i) + \gamma_n f''_{\text{convex}}(\phi^t_n))}{\epsilon} N_l N_m \Big] d\Omega_{\text{el}} \tag{7.5a}$$

$$(A^{\phi\phi}_{i\neq j})_{lm} = \int_{\Omega_{\text{el}}} \left[\gamma_n \left(\epsilon \nabla N_l \nabla N_m + \frac{f''_{\text{convex}}(\phi^t_n)}{\epsilon} N_l N_m\right)\right] d\Omega_{\text{el}} \tag{7.5b}$$

$$(A^{\phi\mu}_{i=j})_{lm} = -A^{\mu\phi}_{i=j} = \int_{\Omega_{\text{el}}} -N_l N_m d\Omega_{\text{el}} \tag{7.5c}$$

$$(A^{\phi\mu}_{i\neq j})_{lm} = A^{\mu\phi}_{i\neq j} = 0 \tag{7.5d}$$

$$(A^{\mu\mu}_{i=j})_{lm} = \int_{\Omega_{\text{el}}} dt \sum_{j=1}^{N} \frac{M_{ij}(\phi^{\text{extrap}}_{i,\ldots n})}{\epsilon} \nabla N_l \nabla N_m d\Omega_{\text{el}} \tag{7.5e}$$

$$(A^{\mu\mu}_{i\neq j})_{lm} = -\int_{\Omega_{\text{el}}} dt \frac{M_{ij}(\phi^{\text{extrap}}_{i,\ldots n})}{\epsilon} \nabla N_l \nabla N_m d\Omega_{\text{el}}. \tag{7.5f}$$

The mobilities can be computed in either a fully implicit fashion, a fully explicit fashion. Here the mobility is computed based on extrapolated values for the phase field variables. Specifically,

$$\phi^{\text{extrap}}_i = \frac{3}{2}\phi^{t-1}_i - \frac{1}{2}\phi^{t-2}_i. \tag{7.6}$$

This acts as an estimate for the current value on the phase field based on past values. The elements of the the right hand can be written as,

$$(F_i^{\phi})_m = \int_{\Omega_{\text{el}}} \left[N_m \left(\frac{\gamma_i}{\epsilon} f'_{\text{concave}}(\phi_i^{t-1}) - \frac{\gamma_n}{\epsilon} f'_{\text{concave}}(\phi_n^{t-1}) \right) \right] d\Omega_{\text{el}} \tag{7.7a}$$

$$(F_i^{\mu})_m = \int_{\Omega_{\text{el}}} \left[N_m \phi_i^{t-1} + dt \sum_{j=1}^{n,i\neq j} \frac{M_{ij}(\phi_{i,\ldots n}^{\text{extrap}})}{\epsilon} Z_{ij} \nabla N_m \nabla \phi_e \right] d\Omega_{\text{el}}. \tag{7.7b}$$

It should be noted in the terms of the form $\gamma_i f'_{\text{convex}}(\phi_i) - \gamma_n f'_{\text{convex}}(\phi_n)$ appear in the matrix. The retention of the convexity of the entire matrix can be seen by noting that these terms are constrained derivatives over paths on the Gibb's triangle. Fig. 7.5 show that the functions are convex/concave over any path on the Gibb's triangle, and hence their constrained derivatives have properties similar to the derivatives of convex/concave functions. This can be shown more rigorously, but this is skipped here.

7.2 Phase Separation

The approach is first tested with an example of phase separation. The numerical method is implemented in a manner such that the phase separation of any number of phases can be studied. In the example presented below, phase separation for 4 phases presented. A random initial condition is set over a square with 150×150 unit mesh of linear quadrilateral elements. This is set using the `C++ std::rand()` function as `std::rand()`%10/30. This leads to a random value of between 0 and 0.333 for phases $\phi_{1..3}$. ϕ_4 is set as $1 - \sum_{i=1}^{N} \phi_i$. γ_{12}, γ_{23}, and γ_{31} are set equal to 1. The mobility functions for all the phases are set as $M_{il} = 1$ in the non-degenerate case. For the degenerate case, the mobility function is set as, $M_{ik} = M_0 \delta(\phi_1, \phi_2)$, where $\delta(\phi_1, \phi_2) = \frac{3}{2\sqrt{2}} \phi_1^2 \phi_2^2$. The system is solved with $\epsilon = 5 \times 10^{-3}$. and a timestep, $\Delta\tau = 1 \times 10^{-3}$.

The results of the simulation for constant mobility are shown in Fig. 7.6a. Initially, the phases precipitate out. Where the system, precipitates into 1 phase completely en-

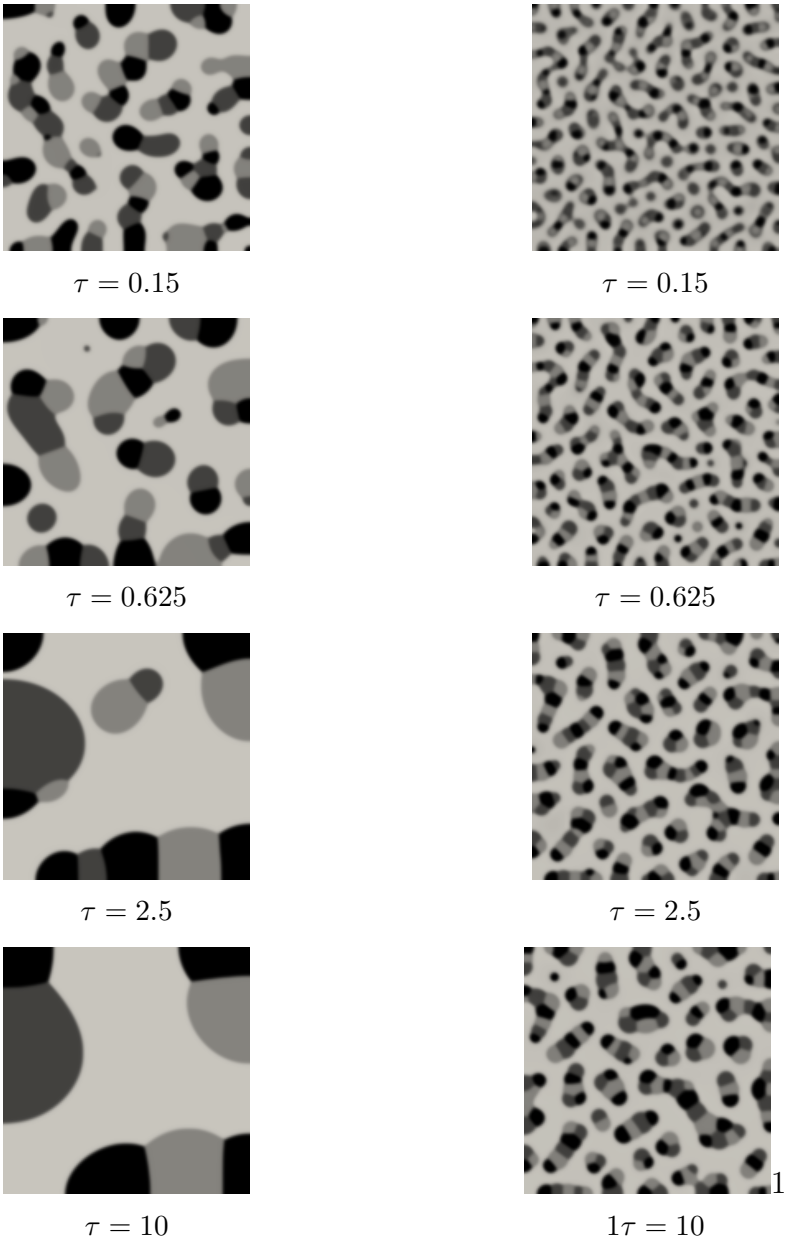

(a) Constant mobility.

(b) Degenerate mobility.

Figure 7.6. Phase separation examples with constant and degenerate mobilities. The examples start with random noise with 4 phases. The figures on the left (a) are with a constant mobility M_0, and the examples on the right (b) are solved with a degenerate mobility $M_0\delta(\phi_i, \phi_j)$.

capsulated by another phase, the precipitates are circular, as required by the isotropy of the surface energy. At locations where the system evolves into multiple adjacent phases, the system evolves while satisfying the conditions on the contact angle at triple points. As the mobility is constant, the system continues to evolve to minimize the total surface energy of the system, over all the combinations of interface. On the other hand, with the degenerate mobility Fig. 7.6b, Initially, as the values of the phase field variables ϕ_i are not close to $0, 1$. The evolution of the system is similar to the case with the constant mobility. However, once the phases separate, the mobility function is restricted only to the interfacial regions. The system still evolves to minimize the total surface energy of the system. However, this is no longer possible by the coarsening of the phases. Phases only coarsen when two phases come into contact. Following this, the precipitates evolve by surface diffusion at the boundaries.

An important measure for the success of numerical algorithms for the Cahn-Hilliard and related equations is the accuracy with which the volume of the phases is conserved with time. In numerical experiments it is observed that the volume conservation evaluated as $\int_\Omega \phi_i(\boldsymbol{x}, t) d\Omega$ is satisfied to $O(10^{-5})$ over time.

7.3 Lens Formation

The other important example that is commonly studied in multiphase system is the formation of lenses at interfaces. For this, the code is used with the adaptivity turned on. The mesh is adapted based on the Kelly error adaptor. This tends to add more elements in regions where the gradient in the solution is highest. The error measure in this case is computed by weighting the Kelly error for ϕ_1 and ϕ_2. 70% of the elements are marked for refinement, based on the value of the error. The rest of the elements are marked to be coarsened. The initial condition (Fig. 7.7) is set in the following manner. The lens is created as the product of two Heaviside functions. One for the parting line between phase 1 and phase 2. the second is the semi-circle

between the phase 1 phase 3. This is repeated for phase s2. The equation of the Heaviside function for the line is written as,

$$\phi_1^l(\boldsymbol{x}) = \frac{1 + \tanh \frac{y-0.5}{\sqrt{2}\epsilon}}{2}. \tag{7.8}$$

The Heaviside function for the semi-circle between ϕ_1 and ϕ_3 is written as,

$$\phi_1^c(\boldsymbol{x}) = \frac{1 + \tanh \frac{r-r_0}{\sqrt{2}\epsilon}}{2}. \tag{7.9}$$

In the above, r is the distance of the point $\boldsymbol{x}$from the center of the phase 3 precipitate $\{0.5, 0.5\}$. r_0 is the radius of the precipitate. The combined Heaviside function for phase 1, which is used for the initial condition is then set as,

$$\phi_1(\boldsymbol{x}) = \phi_1^c(\boldsymbol{x})\phi_1^l(\boldsymbol{x}). \tag{7.10}$$

The initial condition for ϕ_2 is set in a similar manner, except,

$$\phi_2^l(\boldsymbol{x}) = \frac{1 - \tanh \frac{y-0.5}{\sqrt{2}\epsilon}}{2}. \tag{7.11}$$

In the results shown below, $r_0 = 0.13, \epsilon = 5 \times 10^{-3}$. The initial mesh is a unit square, with 10 linear quadrilateral elements to each side, which is refined 4 times, to better approximate the initial conditions. All the results for the lens formation, as well as for the evolution of the double bubble use a degenerate mobility, with the evolution restricted to the interfacial region.

The first test that is performed is the case when the surface energies are the same for all three of the interfaces. i.e $\gamma_{12} = \gamma_{23} = \gamma_{31} = 0.1$. In this case (Fig. 7.8a), the system evolves to minimize the total surface energy. The minimum energy state for a 3 phase system needs to satisfy the condition for included angles between the phase boundaries at the triple points. For equal surface energies. It can be shown that the included angles are all $\frac{2\pi}{3}$. This can be seen in Fig. 7.8a where the interfaces evolve

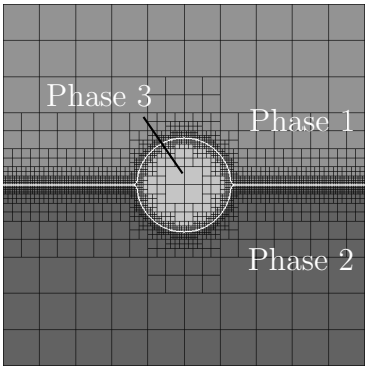

Figure 7.7. Initial configuration for lens formation examples.

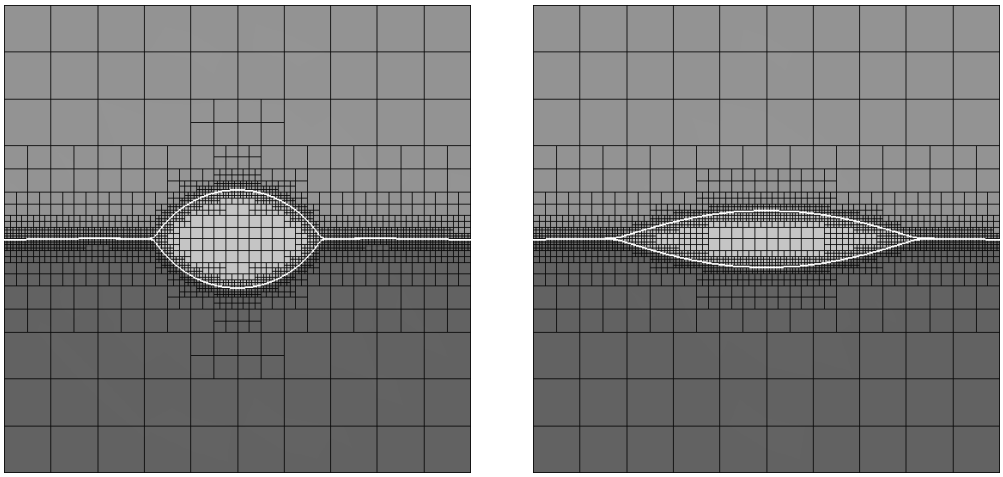

(a) $\gamma_{12} = \gamma_{23} = \gamma_{31} = 0.1$ (b) $\gamma_{12} = .19$,$\gamma_{23} = \gamma_{31} = 0.1$

Figure 7.8. Lens formation in a 3-phase system for different combinations of γ_{12}, γ_{23}, and γ_{13} at $\tau = 5$, starting from the initial condition Fig. 7.7.

so that the angle between the interfaces is maintained at $\frac{2\pi}{3}$. In Fig. 7.8b, the 1-2 interface is penalized and its length reduces as the system evolves. As the volume is conserved, the lens flattens and spreads at the interface. The included angles still match the conditions at the interface governed by the condition Eq. (6.96).

7.4 Double Bubble

The next case that is studied is the case of the double bubble. In the case of the double bubble, the phases 1 and 2 are adjacent to each other as shown in Fig. 7.9. The initial conditions are set in a manner similar to the way in § 7.3. The only difference is that the signs are flipped. Hence,

$$\phi_1^l(\boldsymbol{x}) = \frac{1 - \tanh \frac{y-0.5}{\sqrt{2}\epsilon}}{2}. \tag{7.12}$$

$$\phi_{1,2}^c(\boldsymbol{x}) = \frac{1 - \tanh \frac{r-r_0}{\sqrt{2}\epsilon}}{2}. \tag{7.13}$$

For the examples in this section, $r_0 = 0.18$. The mesh used is the same as the mesh used in § 7.3

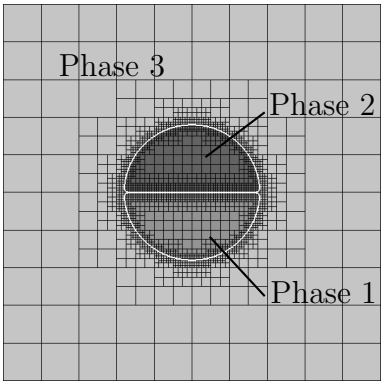

Figure 7.9. Initial condition for the double-bubble examples.

Similar to the examples in § 7.3, the first example is the case with equal surface energies for all the phases. In this case, (Fig. 7.10a) the system evolves so that the included angles reach the $\frac{2\pi}{3}$ value. The 1-3 and 2-3 phase boundaries then evolve to circular sectors to minimize their surface energy. In Fig. 7.10b, the energy of the 1-2 phase interface is very high compared to the energy of the 1-3 and the 2-3 interfaces. As the system evolves, it is energetically favorable for the 1-2 interface to shrink. This causes the double bubble to separate into two circles. Another example of the same effect is seen in Fig. 7.10c. In this case, the 2-3 interface is penalized by it's high

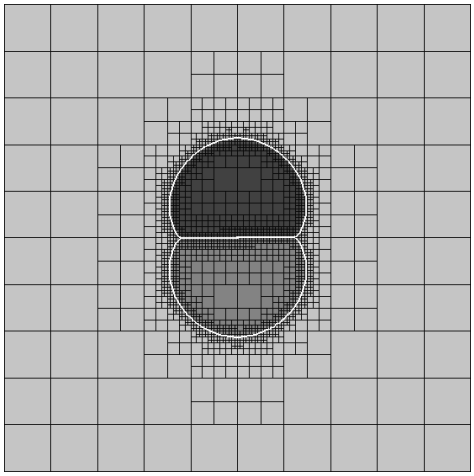

(a) $\gamma_{12} = \gamma_{23} = \gamma_{31} = 0.1$

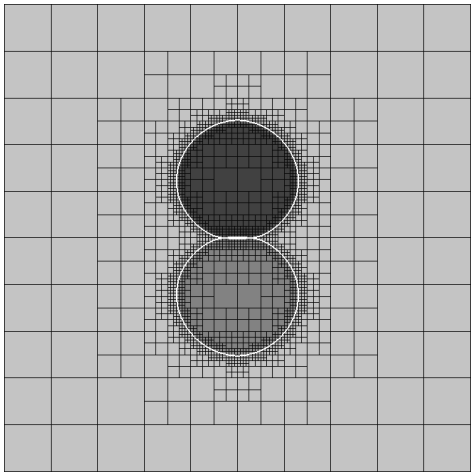

(b) $\gamma_{12} = 5$ and $\gamma_{31} = \gamma_{23} = .1$

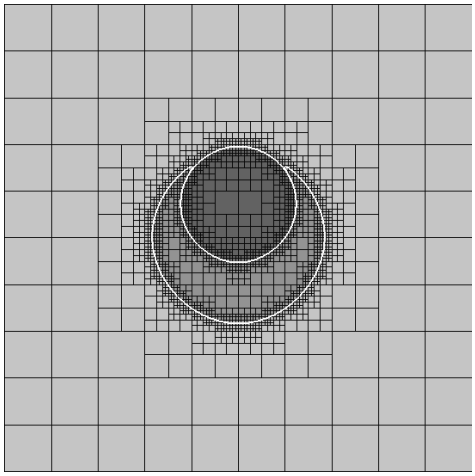

(c) $\gamma_{12} = \gamma_{31} = 0.1$, and $\gamma_{23} = 10$

Figure 7.10. Solutions to the double-bubble problem for different combinations of γ_{12}, γ_{23} and γ_{13}.

energy. As the system evolves, this interface shortens. As the volume is conserved, this causes phase 1 to spread around phase 2, as this reduces the length of the 2-3 phase.

7.5 Electromigration

The final examples in the chapter are those of void electromigration in a multi-phase system. The construction of the initial conditions is similar to the cases described in § 7.3. In addition, there is a constant unit potential difference applied between two opposite sides of the mesh. The conductivity of the material is written as

$$\eta = \sum_{i=1}^{3} \eta_i \phi_i \tag{7.14}$$

In the simulation results that follow, it is assumed that $\eta_{1,2} = 1.0$ and $\eta_3 = 0.0$. The electromigration parameters at each interface are also assumed to have unit magnitude or $|Z_{ij}| = 1$.

The first case considered is the motion of a void along a phase interface. An initially circular void is placed with the center coinciding with the phase boundary. In the first example, (Fig. 7.12a), it is assumed that the phase boundary itself is not affected by the electrical potential gradient ($Z_{12} = 0$). In this case, it is observed that the void initially evolves to take a lens like shape. Following this, the void propagates along the interface, while maintaining the same lens-like profile. In the second example of void motion along the interface Fig. 7.12b, $Z_{12} = 1.0$, allowing the 1-2 interface to evolve in response to the applied electrical potential gradient. It has to be noted that though, evolution of the 1-2 interface is allowed, the steady motion seen in Fig. 7.12a is still a possible solution for this case. This is due to the fact that the surface divergence of the surface gradient of the electrical potential, is initially 0, and hence the normal velocity of the phase interface due to electromigration is zero. However, when the void propagates, it sets up small perturbations in the 1-2 interface. These perturbations grow to to cause the motion of the 1-2 interface seen in Fig. 7.12b. The instability of a flat surface which can evolve under electromigration is a known fact, and has been analyzed using linear stability analysis in [135].

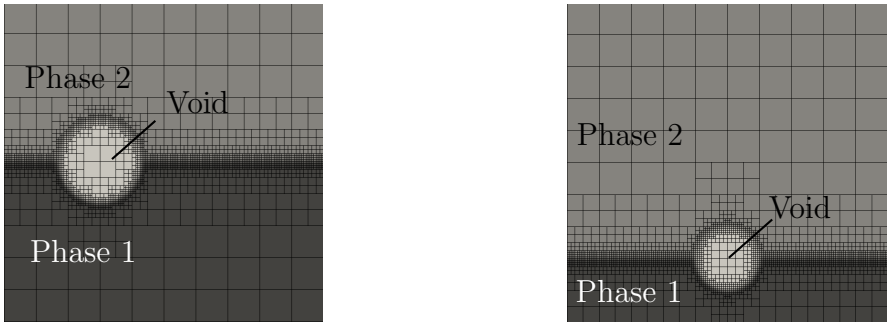

(a) Initial condition for simulations of void electromigration along the interface

(b) Initial condition for the electromigration - void pinch-off examples.

Figure 7.11. Initial condition for the electromigration examples.

Next the motion of a void that is separating from an interface is simulated. In this case a unit potential difference is applied between the top and the bottom of a unit square and a circular void (phase 3) is placed at the 1-2 interface Fig. 7.11b. $\epsilon = 5 \times 10^{-3}$ is used, as in the other examples. In the first set of examples, Fig. 7.13, the mobility for all three interfaces is a unit degenerate mobility. However, while the 1-3 and 2-3 interfaces are allowed to evolve by electromigration. The 1-2 interface only evolves as a reaction to the evolution to the evolution of the 1-3 and 2-3 interfaces. The three columns in Fig. 7.13 correspond to three different combinations of the the relative surface energies between the phases. In Fig. 7.13a, γ_{23}, and γ_{13} are set equal to each other at 1×10^{-3}, while γ_{12} is set to 1×10^{-2}. In this case, the void initial starts spreading across the 1-2 interface. However, the electromigration prevents this from happening and causes the void to pinch off from the interface. It should be noted that the angle condition at the triple point is still maintained to a fair extent. In the example in Fig. 7.13b, $\gamma_{12}, \gamma_{23} = 1 \times 10^{-2}$, while $\gamma_{13} = 1 \times 10^{-3}$. In this case the 1-3 interface is energetically favorable compared to the 2-3 and 1-2 interface. This causes the neck at $\tau = 1.5$ is much narrower. In the final example in Fig. 7.13, it is γ_{23} that is reduced to 1×10^{-3}. Hence it is energetically favorable for the void to maintain contact with the interface for as long as possible. Hence, at $\tau = 3.0$, it is the

only case where the void is still in contact with the interface. Following pinch-off, the voids behave normally and move in the direction of the electrical potential gradient.

In the final group of electromigration examples, the 1-2 interface is also allowed to evolve through electromigration. The motion of the 1-2 interface is usually not significant as the surface gradient of the electrical potential is usually not significant along the 1-2 interface. In Fig. 7.14a, $\gamma_{ij} = 1 \times 10^{-2}$. Similar to the case in Fig. 7.13a. The void tends to initially spread along the interface and then the electromigration tends to cause the void to pinch-off. In contrast to Fig. 7.13a, though, the 1-2 interface also evolves and develops a waviness that persists and grows owing to the electromigration. In Fig. 7.14b, $\gamma_{12} = \gamma_{23} = 1 \times 10^{-1}$, while $\gamma_{13} = 1 \times 10^{-2}$. In this case the pinch-off progresses faster as the void possesses lower surface energy in the 1 phase than at the interface. Finally in Fig. 7.14c, it is γ_{23} that is the lowest at 1×10^{-3}. As the system evolves, the void tends to maintain contact with the 1-2 interface. As the 1-2 interface also evolves in this case, it rises along with the void.

7.6 Summary

The $n-$Phase and 3 phase simulations demonstrated in this thesis, serve mostly as a validation of the numerical approach developed in this thesis. The idea of *numerical* phase field approaches such as the one developed in this thesis, is to augment the phase field equation with additional physics, in order to simulate different physical velocity laws. As shown in Eq. (6.109), the velocity for the evolution of the different interfaces is applied at the $\frac{1}{\epsilon}$. This allows a fairly simple extension to applying arbitrary velocity profiles over the interface at the $\frac{1}{\epsilon}$ level. This can be exploited for the simulation of various physical phenomena, a simple and obvious one being the simulation of intergranular void growth during diffusional creep [136]. Other phenomena that need to be explored are a more thorough investigation of intergranular void evolution during electromigration.

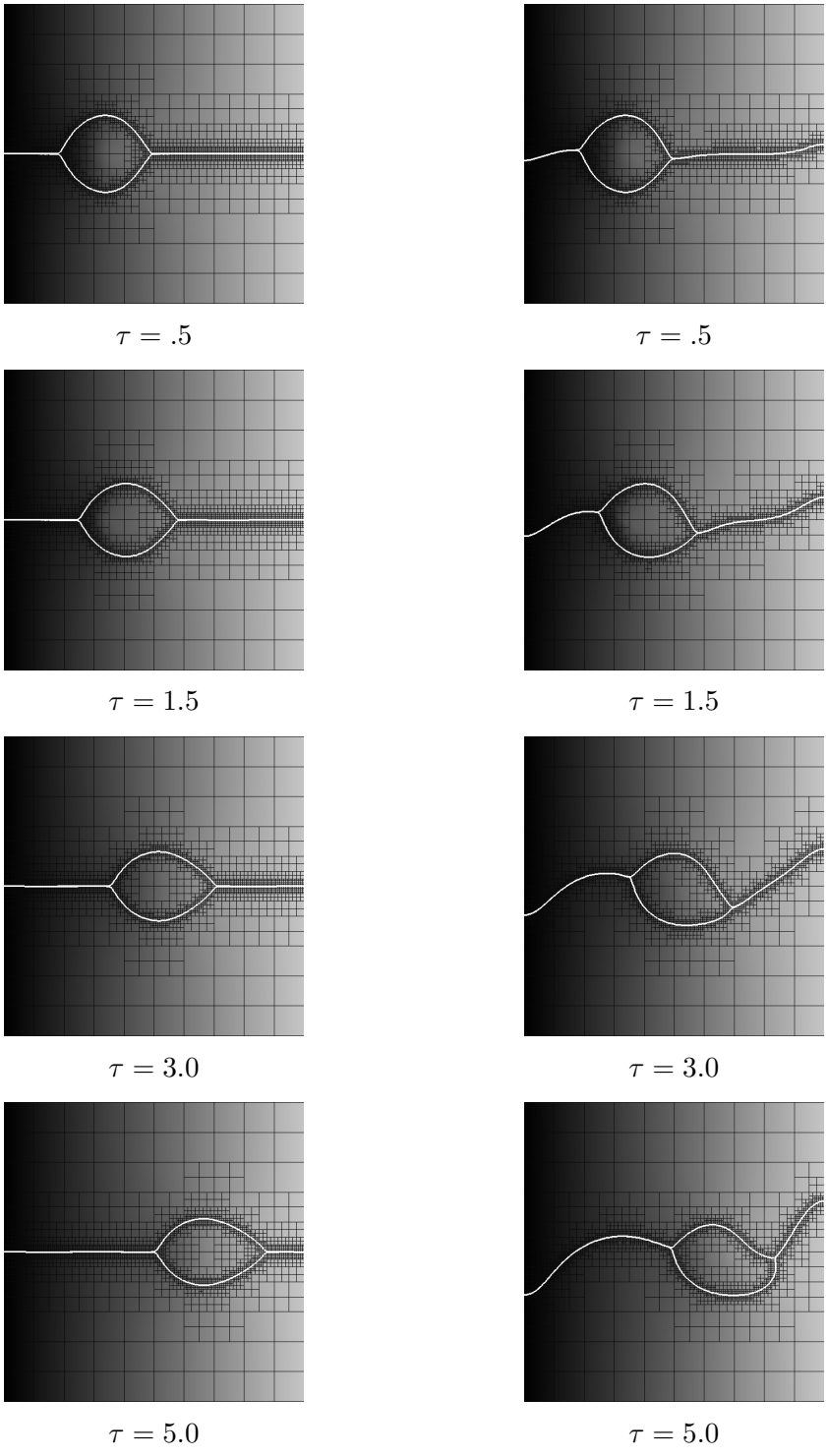

(a) No electromigration evolution of 1-2 interface

(b) Electromigration evolution of 1-2 interface

Figure 7.12. Evolution of void at interface with an electrical potential gradient aligned with the interface. $Z_{12} = 0$ in a and $Z_{12} = -1$ in b. In both, $Z_{23} = Z31 = -1$.

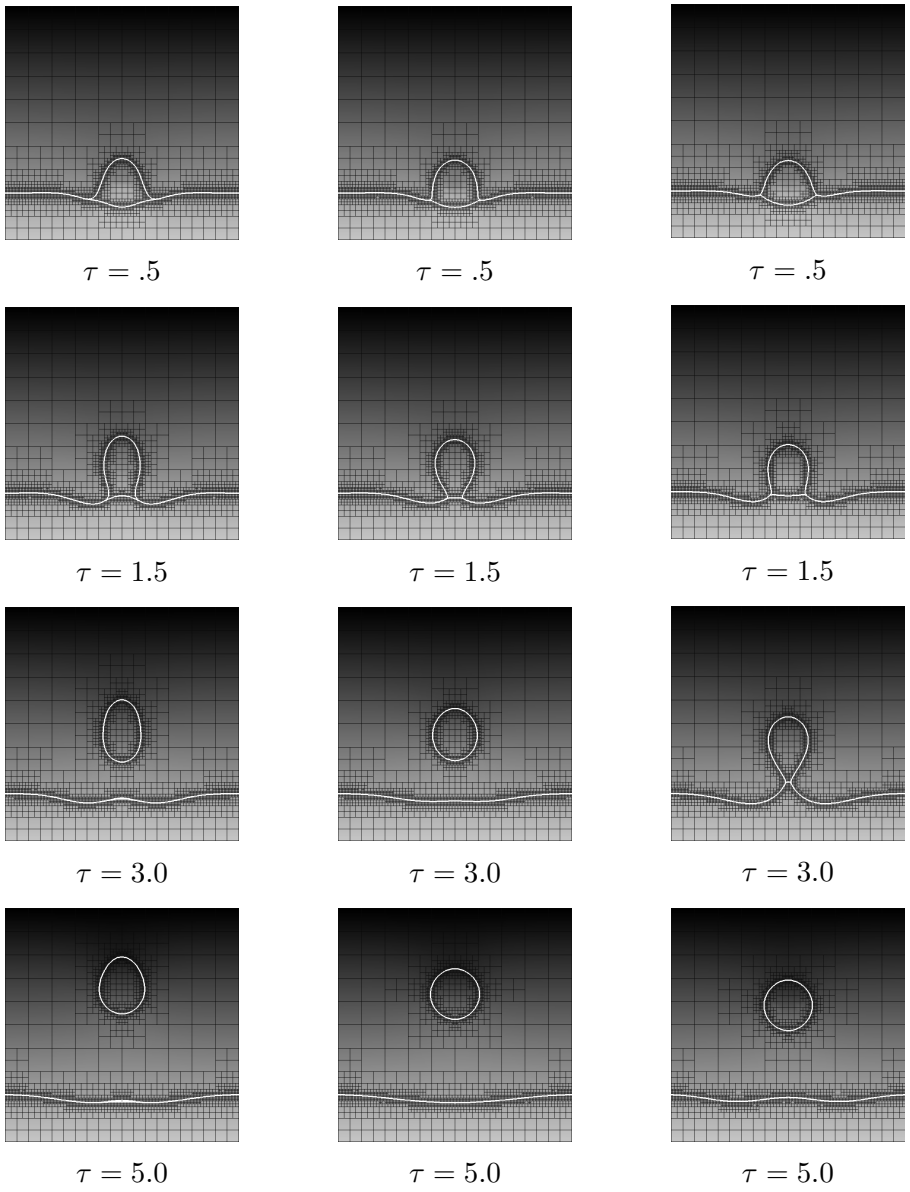

(a) $\gamma_{23} = \gamma_{13} = 1 \times 10^{-3}, \gamma_{12} = 0.1$

(b) $\gamma_{12} = \gamma_{23} = 0.1, \gamma_{13} = 1 \times 10^{-1}$

(c) $\gamma_{12} = \gamma_{13} = 0.1, \gamma_{23} = 1 \times 10^{-3}$

Figure 7.13. Void electromigration in a 3-phase system. The void is initially attached to the 1-2 phase interface. The electric potential then drives the void upwards via surface diffusion. In this case the 1-2 interface is not allowed to evolve via electromigration.

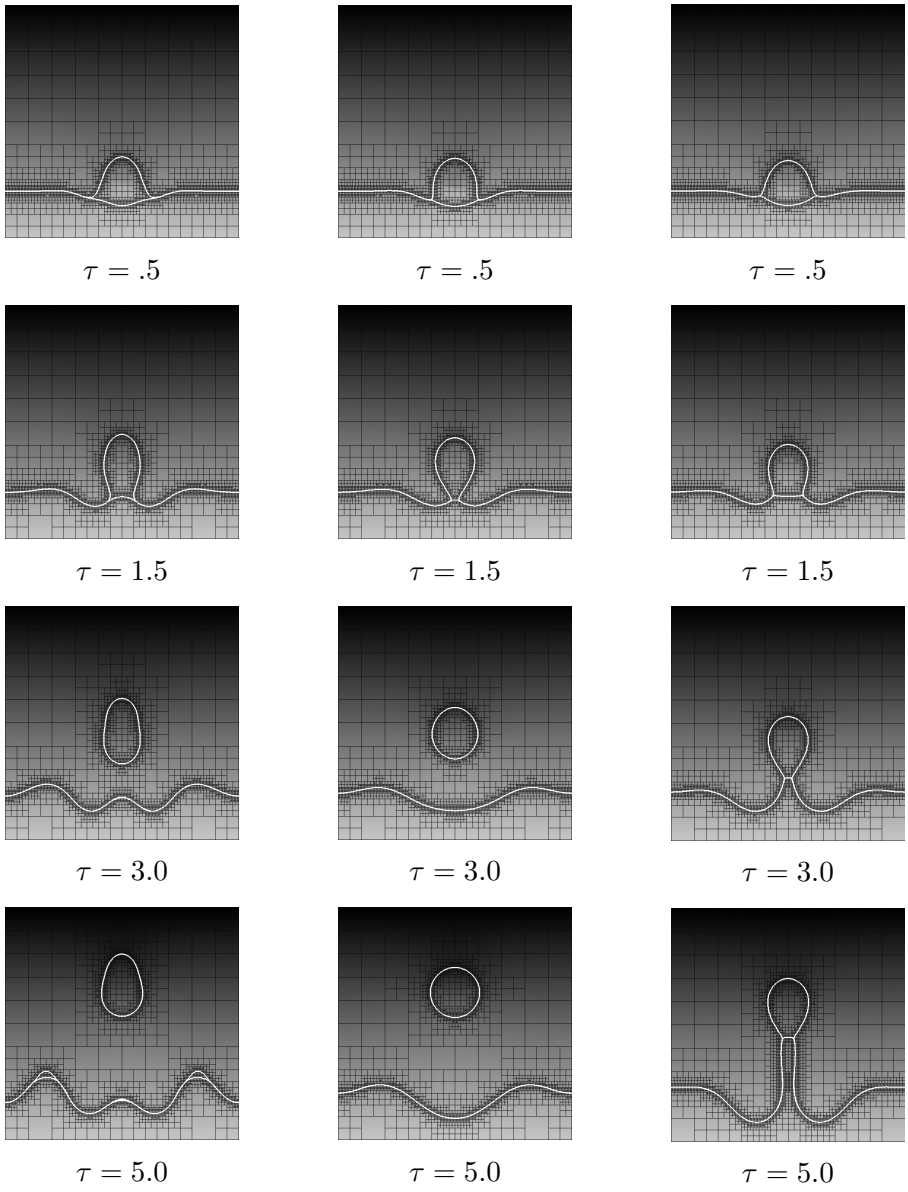

(a) $\gamma_{ij} = 1 \times 10^{-2}$ (b) $\gamma_{12} = \gamma_{23} = 0.1, \gamma_{13} = 1 \times 10^{-3}$ (c) $\gamma_{12} = \gamma_{13} = 0.1, \gamma_{23} = 1 \times 10^{-3}$

Figure 7.14. Void electromigration in a 3-phase system. The void is initially attached to the 1-2 phase interface. The electric potential then drives the void upwards via surface diffusion. In this case all three interfaces are allowed to evolve by electromigration.

8. SUMMARY AND RECOMMENDATIONS

This dissertation describes the formulation, diffuse interface approximation and numerical implementation of a model for the growth and evolution of voids in solids. The continuum thermodynamics and mechanics for the growth and evolution of interfaces in solids was studied. This was used in Chapter 3 to demonstrate a phase field model for the evolution of voids in solder joints and other interconnect structures. Both the evolution of voids due to surface diffusion, as well as their growth due to vacancy accumulation was considered. The phase field model has been implemented in a `C++` code using `libMesh` for the finite element framework. This code was also extended to include the effects of the contact angle at the interface of the solder copper joint, and the effect of various phenomenon on the failure of the joint are studied. In Chapters 6 and 7, a multi-phase Cahn-Hilliard model was derived for simulation of cases where more than two distinct phases are to be tracked. This was used then to construct a phase field model for the motion of interfaces in multiphase solids due to surface electromigration. In this chapter, some thoughts on the advantages and disadvantages of phase field schemes for the modeling of moving boundary problems are presented based on experience. This is followed by a few recommendations for future research.

8.1 Advantages of Phase Field Schemes

The primary advantage of phase field schemes is the ease of implementation. In contrast to various other methods, phase–field methods give rise to a series of standard diffusion equations. This makes it very easy and time efficient from the point of view of implementation, if a robust framework for solution of PDEs based on finite elements, finite volume or finite differences is available. Recently, a variety of open

source projects [137–142] for this purpose have become available for general use. These software libraries make it relatively easy to implement solution schemes for phase field and other equations. These can be easily used on computers of all speeds (from desktops to supercomputers), with the limit on the size of the simulations only being dictated by the availability of computational resources. Improvements in linear and non-linear solver technology [138, 143, 144] have also improved the time and memory efficiency of the simulations. The computational expense argument against the use of phase field methods has been eliminated to a certain extent. The time and computational cost of 3-Dimensional simulations of problems with moving boundaries is expected to be significant for any computational method, and hence phase field methods are a reasonable tool. The other important advantage of phase field type schemes is the automatic separation of scales that they provide. In cases, where the boundary conditions are simple, this separation allows for application of boundary conditions through simple modifications of the governing equations [114]. However, this is not without limitations and boundary conditions involving multiple field variables and non-linearities are difficult to analyse, while implementation is not expected to present significant additional difficulty.

8.2 Disadvantages of Phase Field Schemes

While solutions using phase field methods have become more reasonable, the numerical challenges are still the most significant stumbling block. The first major challenge is the value the notional interface thickness ϵ. To capture some of the features of physical systems at the smallest length scales, this must be much smaller than the smallest radius of curvature present in the system. As for successful solutions the discretization size $h \ll \epsilon \ll \frac{1}{\kappa_{\max}}$. These two facts together, severely limit the utility of phase field methods for the study of actual physical problems, involving very sharp anisotropies or fractal phenomena such as dendrite formation. However, numerical solution for such problems is very likely to be prohibitive irrespective of the

choice of the numerical method used. Adaptive mesh codes [137, 139, 141, 142] have ameliorated this to a certain extent, however some of the benefits accrued from the usage of adaptive meshing techniques is lost due to the necessity of reconstructing the mesh data structures frequently. These costs can be significant, and this must be considered while making a choice about numerical methods.

The most significant point with developing phase field models, where the phase field is only used as a numerical approximation, is that boundary conditions are always applied in a weak averaged sense. This is often insufficient for more complex boundary conditions. The author is unaware of attempts to handle cases such as sliding interfaces using the phase field method.

8.3 Recommendations for Future Research

This section lists some suggestions for further research in moving boundary problems. Phase field methods are suited to the solution of the problems suggested here, though it is also possible to use other methods for solution such as the standard level-set scheme with interface reconstruction [36], or NURBS based compositional iso-geometric approaches [145].

8.3.1 Computational Improvements

Phase field methods are computationally intensive, and even small improvements in computational efficiency can make a significant improvement in the ability to solve problems. Over the course of this research project, first a method based on fixed point iterations were used for solution of the phase field equations. Following this, a method based on the obstacle potential, solved using the method of Douglas and Rachford was tried [146]. This method had the advantage of reducing the region over which the problem needs to be solved. The phase field equations with an obstacle potential can also be solved using an optimization based methods such as a semi-smooth Newton solver [147]. These methods have the advantage of generating very

accurate solutions while having sharply defined interfacial regions. However, there are difficulties with handling degenerate mobilities, as the solution for the chemical potential loses quality at the boundary of the interfacial region. The splitting schemes used in this dissertation have been found to been the most computationally tractable for the solution of small to medium problems on 10-20 processors. In the case of multiphase simulations, the problem with solutions based on an obstacle potential is that one of the constraints, $\sum_{i=1}^{n-1}\phi_i < 1$ is not writable in the form of a bounds constraint. Optimization algorithms for constraints of this type are developed in terms of very few variables and are not suitable for the millions of degrees of freedom usually seen in phase field problems [133]. A common tool that is used in solutions of large non-linear coupled multiphysics problems is the Jacobian Free Newton Krylov method [143], which has been exploited to allow much larger fully coupled solutions by eliminating the construction of the full Jacobian and thereby reducing memory requirements. The use of this method in both phase field and also the compositional approaches needs to be evaluated.

Mesh Improvements

A significant cost in phase field solutions is the necessity of using very dense meshes. The current approach is based on using an $h-$adaptive mesh, where the mesh is subdivided in the interfacial region. However, this approach imposes two additional costs on the computational process. The first is the cost of constructing the sparsity patterns at the end of each time step. The second is the cost of applying constraints on the degrees of freedom at the hanging nodes. In $r-$adaptive or moving mesh schemes [148], the positions of the nodes themselves are treated as variable and are moved in order to better approximate sharp gradients (Fig. 8.1). The governing partial differential equations are usually recast into an arbitrary Lagrange-Eulerian (ALE) framework and an additional PDE is solved for the node locations. While this moving mesh PDE is usually highly non-linear, this can be ameliorated to a certain

extent by using semi-implicit schemes, and treating terms of order greater than 2 explicitly. The approach has been used for the solution of the Cahn-Hilliard Navier-Stokes equations [117]. Its utility for other variants of the Cahn-Hilliard equation, as well as other variants of the phase field equations needs to be evaluated.

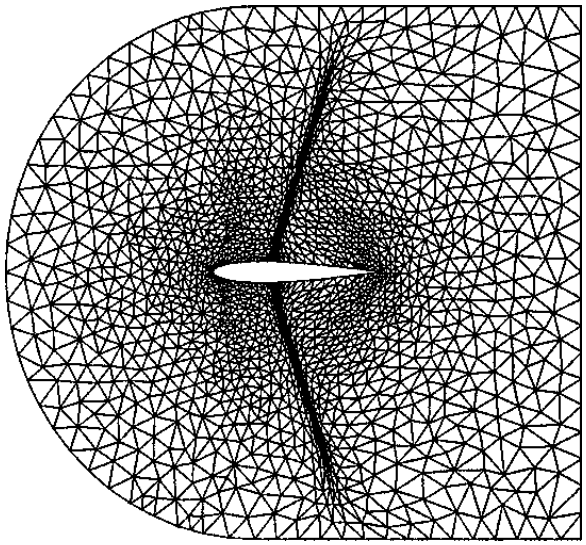

Figure 8.1. An example of an $r-$adaptive mesh. The mesh is evolved by moving the nodes into locations where the solution shows sharper gradients. The connectivity of the mesh is kept constant [149].

Time-stepping improvements

Purely explicit and implicit timesteps face severe restrictions while using the phase field method. The splitting schemes used here provide a compromise between the two. However, they are still limited to fairly small time-steps. It is therefore essential to evaluate time-stepping schemes for the phase field problem that ameliorate this problem to an extent. An approach that is likely to help are error based adaptive time-stepping schemes [150]. In these schemes, the value of the next time step is decided based on the value of the error in the solution (computed using the Kelly error estimator [151], say), and updated, to keep the error within acceptable bounds.

8.3.2 Multiphase Multicomponent Systems

There are many problems in the study of multiphase- multicomponent systems that have not been studied in great detail. This is due to the extremely non-linear nature of the problem and the difficulty in experimentally verifying model results. A few of these problems are described below. These are amenable to solution using both phase field as well as sharp interface methods.

Coarsening in Multicomponent Systems

The Gibbs-Thomson condition is simple to analyse in binary systems [152]. This is because at equilibrium, the interfacial concentration of the species is solely dependent on the curvature of the interface. This simplifies the analysis of Ostwald ripening in binary systems. In addition to the interface concentration, the only additional relation required is a kinetic relation that relates the velocity of the interface to the interfacial concentration.

In mixtures with 3 or more components, the interfacial concentration can't be written only in terms of the curvature [153, 154]. In addition to the curvature of the interface, the relative concentrations of the components also play a part as can be seen by the form of the Gibbs-Thomson relation at the interface,

$$\sum_{i=1}^{N} [\![\rho_i]\!] \, \mu_i = \gamma\kappa. \tag{8.1}$$

This needs to be taken into account when the interface evolves. To the best of the author's knowledge, there haven't been numerical studies of these systems for arbitrary geometries [121]. However, owing to the complicated nature of these boundary conditions, it is likely that sharp interface methods are more suited to their solution.

Intermetallic Growth Kinetics

As electronics components reduce in size, the solder joints reduce in size. In some of the designs that are being proposed/evaluated, the solder joint is composed almost entirely of intermetallic compounds (Fig. 8.2a). Intermetallic compounds are stiff and brittle materials. As a result they are at cross-purposes with the role of solder joints in providing compliance in electronics packages. The growth of the intermetallics is known to be accelerated or retarded by electromigration depending on the direction of the electric field . Models of the electromigration accelerated growth of the intermetallics have hitherto been restricted to 1-dimensional models [155] or to complex *physical* phase field models [156]. These models are useful for the study of early stage coarsening. For late stage coarsening, there is value to developing numerical models based on continuum mechanics, assuming sharp interfaces. These features are expected to have an effect on the fracture behavior of the joint, especially under delamination fracture. This is owing to the fact that the crack is forced to travel a longer distance on a scalloped interface as opposed to a smooth interface [12]. The models developed in this dissertation for the solution of void growth due to vacancy accumulation can be modified to study this effect, and this problem constitutes a relatively easy extension to the abilities of the code developed here (Fig. 8.2b).

Another applied problem that exists in next generation electronics packages is the formation of voids in through silicon vias (TSV) during thermal annealing. The preliminary studies [158] suggest, that the void growth mechanism is controlled by a vacancy diffusion mechanism. The numerical tools developed in this dissertation are a good method to verify the models suggested for void growth in TSVs during annealing.

8.3.3 Phase Field Simulations of Diffusion Driven Fracture

The phase field method has been used successfully for the study of brittle fracture in the past few years by many authors, using both finite elements [61, 62] as well

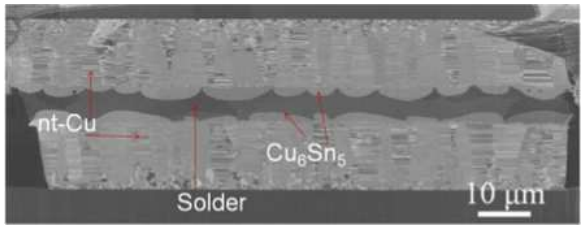

(a) Formation of intermetallic scallops in SnPb/Cu solder joints [157]. As can be seen, a significant part of the solder joint is composed of the intermetallic

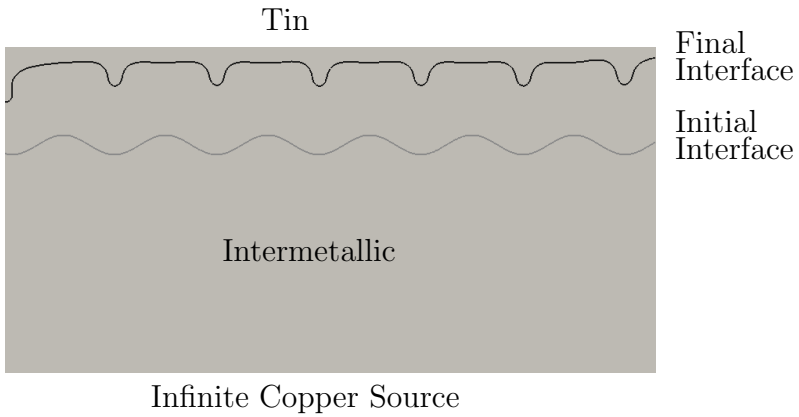

(b) Initial simulation results using `DiffCode`showing the formation of scallops due to diffusion driven growth. In the figure above, the grey line shows the initial profile of the intermetallic. The bottom surface is kept at a constant concentration of copper. The copper diffuses through the intermetallic and reacts with the tin above the interface to form the scallops. This process is controlled by a curvature dependent boundary condition on the copper concentration at the intermetallic/tin interface.

Figure 8.2. Intermetallic formation in solder joints.

as using *isogeometric* methods [159]. The phase field method is uniquely suited for fracture methods, owing to the relative simplicity of the boundary conditions in the absence of contact and sliding, and the easy interpretation of the phase field parameter ϕ as a damage parameter. When there is species diffusion in a brittle matrix, the strains due to the change in the species concentration can be significant enough to cause fracture. This is a serious concern in lithium ion batteries [160], where the existence of finite strains complicates the problem. A related issue is the fracture of intermetallics (Fig. 8.3). As the growth of the intermetallics is coupled with its fracture, this can be thought to be an example of diffusion coupled with fracture.

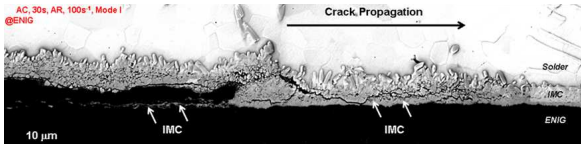

Figure 8.3. Fracture in intermetallics [12]

A comparison of the phase field fracture approach to the iso-geometric and XFEM type approaches for problems of this nature, should be instructive. Grain boundary diffusion and surface diffusion causing the evolution and intergranular voids is a common model for creep in metals [136, 161–163]. The multi-phase field model developed in Chapters 6 and 7 can be extended to study the mechanisms of creep due to intergranular diffusion and creep.

LIST OF REFERENCES

LIST OF REFERENCES

[1] J. B. S. Haldane. On Being the Right Size. *A Treasury of Science*, page 321, 1928.

[2] V. Cristini, J. Lowengrub, and Q. Nie. Nonlinear Simulation of Tumor Growth. *Journal of Mathematical Biology*, 46(3):191–224, 2003.

[3] J. E. Nör, J. Christensen, J. Liu, M. Peters, D. J. Mooney, R. M. Strieter, and P. J. Polverini. Up-regulation of bcl-2 in Microvascular Endothelial Cells Enhances Intratumoral Angiogenesis and Accelerates Tumor Growth. *Cancer Research*, 61(5):2183–2188, 2001.

[4] R. W. Balluffi and J. W. Cahn. Mechanism for Diffusion Induced Grain Boundary Migration. *Acta Metallurgica*, 29(3):493–500, 1981.

[5] C. Günster, D. A. Molodov, and G. Gottstein. Magnetically Driven Migration of Specific Planar Grain Boundaries in Zn Bicrystals. *Scripta Materialia*, 63(3):300–303, 2010.

[6] F. Renken and G. Subbarayan. NURBS-based Solutions to Inverse Boundary Problems in Droplet Shape Prediction. *Computer Methods in Applied Mechanics and Engineering*, 190(11):1391–1406, 2000.

[7] R. L. Panton, J. W. Lee, L. Goenka, and A. Achari. Simulation of Void Growth in Molten Solder Bumps. *Journal of Electronic Packaging*, 125(3):329, 2003.

[8] E. Ou, F. Ren, A. Huang, A. Wu, J. O. Suh, and K. N. Tu. Electromigration of Solder Joints in Flip–Chip Technology. *Materials Science*, 2004.

[9] K. N. Tu. Recent Advances on Electromigration in very Large-scale Integration of Interconnects. *Journal of Applied Physics*, 94(9), 2003.

[10] K. N. Tu. Physics and Materials Challenges for Lead-free Solders. *Journal of Applied Physics*, 93(3), 2003.

[11] Y. C. Hu, Y. H. Lin, C. R. Kao, and K. N. Tu. Electromigration Failure in Flip Chip Solder Joints due to Rapid Dissolution of Copper. *Journal of Materials Research*, 18(11):2544–2548, 2003.

[12] Z. Huang, P. Kumar, I. Dutta, R. Sidhu, M. Renavikar, and R. Mahajan. Incorporation of Interfacial Intermetallic Morphology in Fracture Mechanism Map for Sn-Ag-Cu Solder Joints. *Journal of Electronic Materials*, 43(1):88–95, 2014.

[13] J. W. Gibbs. *On the Equilibrium of Heterogeneous Substances*. The Academy, 1877.

[14] C. Eckart. The Thermodynamics of Irreversible Processes. I. The Simple Fluid. *Physical Review*, 58:267–269, 1940.

[15] C. Eckart. The Thermodynamics of Irreversible Processes. II. Fluid Mixtures. *Physical Review*, 58(3):269, 1940.

[16] S. R. de Groot and P. O. Mazur. *Non - Equilibrium Thermodynamics*. Dover Books on Physics Series. Dover Publications, Incorporated, 1962.

[17] W. Heidug and F. Lehner. Thermodynamics of Coherent Phase Transformations in Nonhydrostatically Stressed Solids. *Pure and Applied Geophysics*, 123(1):91–98, 1985.

[18] F. C. Larché and J. W. Cahn. A Linear Theory of Thermochemical Equilibrium of Solids Under Stress. *Acta Metallurgica*, 21(8):1051–1063, 1973.

[19] F. C. Larché and J. W. Cahn. Overview no. 41 : The Interactions of Composition and Stress in Crystalline Solids. *Acta Metallurgica*, 33(3):331–357, 1985.

[20] P. H. Leo and R. F. Sekerka. Overview no. 86: The Effect of Surface Stress on Crystal-Melt and Crystal-Crystal Equilibrium. *Acta Metallurgica*, 37(12):3119–3138, 1989.

[21] W. C. Johnson and J. I. D. Alexander. Interfacial Conditions for Thermomechanical Equilibrium in Two-phase Crystals. *Journal of Applied Physics*, 59(8):2735–2746, 1986.

[22] E. Fried and M. E. Gurtin. The Role of the Configurational Force Balance in the Nonequilibrium Epitaxy of Films. *Journal of the Mechanics and Physics of Solids*, 51(3):487–517, 2003.

[23] E. Fried and M. E. Gurtin. A Unified Treatment of Evolving Interfaces Accounting for Small Deformations and Atomic Transport with Emphasis on Grain-boundaries and Epitaxy. *Advances in Applied Mechanics*, 40:1–177, 2004.

[24] M. E. Gurtin, E. Fried, and L. Anand. *The Mechanics and Thermodynamics of Continua*. The Mechanics and Thermodynamics of Continua. Cambridge University Press, 2010.

[25] S. Angenent and M. E. Gurtin. Multiphase Thermomechanics with Interfacial Structure 2. Evolution of an Isothermal Interface. *Archive for Rational Mechanics and Analysis*, 108(3):323–391, 1989.

[26] M. E. Gurtin. *Thermomechanics of Evolving Phase Boundaries in the Plane*. Oxford Mathematical Monographs. Clarendon Press, 1993.

[27] F. Davi and M. E. Gurtin. On the Motion of a Phase Interface by Surface Diffusion. *Zeitschrift für Angewandte Mathematik und Physik (ZAMP)*, 41(6):782–811, 1990.

[28] C. Truesdell and R. A. Toupin. The Classical Field Theories. In S. Flügge, editor, *Principles of Classical Mechanics and Field Theory / Prinzipien der Klassischen Mechanik und Feldtheorie*, volume 2 / 3 / 1 of *Encyclopedia of Physics / Handbuch der Physik*, pages 226–858. Springer Berlin Heidelberg, 1960.

[29] I. S. Liu. *Continuum Mechanics*. Advanced Texts in Physics. Springer, 2002.

[30] J. W. Cahn and J. E. Taylor. Surface Motion by Surface Diffusion. *Acta Metallurgica et Materialia*, 42(4):1045–1063, 1994.

[31] O. Penrose and P. C. Fife. On the Relation between the Standard Phase-Field Model and a "Thermodynamically Consistent" Phase-Field Model. *Physica D: Nonlinear Phenomena*, 69(1):107–113, 1993.

[32] H. Emmerich. *The Diffuse Interface Approach in Materials Science: Thermodynamic Concepts and Applications of Phase-Field Models*, volume 73. Springer, 2003.

[33] J. Donea, A. Huerta, J.-P. Ponthot, and A. Rodríguez-Ferran. Arbitrary Lagrangian–Eulerian Methods. *Encyclopedia of Computational Mechanics*, 2004.

[34] L. Xia, A. F. Bower, Z. Suo, and C. F. Shih. A Finite Element Analysis of the Motion and Evolution of Voids due to Strain and Electromigration induced Surface Diffusion. *Journal of the Mechanics and Physics of Solids*, 45(9):1473–1493, 1997.

[35] T. Ogurtani and O. Akyildiz. Morphological Evolution of Voids by Surface Drift Diffusion Driven by Capillary, Electromigration, and Thermal-stress Gradients Induced by Steady-State Heat Flow in Passivated Metallic Thin Films and Flip Chip Solder joints. I. Theory. *Journal of Applied Physics*, 104(2):023521, 2009.

[36] S. Osher and J. A. Sethian. Fronts Propagating with Curvature Dependent Speed: Algorithms Based on Hamilton-Jacobi Formulations. *Journal of Computational Physics*, 79(1):12–49, 1988.

[37] Z. Li, H. Zhao, and H. Gao. A Numerical Study of Electro-migration Voiding by Evolving Level Set Functions on a Fixed Cartesian Grid. *Journal of Computational Physics*, 152(1):281–304, 1999.

[38] J. E. Pilliod Jr and E. G. Puckett. Second-Order Accurate Volume-of-Fluid Algorithms for Tracking Material Interfaces. *Journal of Computational Physics*, 199(2):465–502, 2004.

[39] C. W. Hirt and B. D. Nichols. Volume of Fluid (VOF) Method for the Dynamics of Free Boundaries. *Journal of computational physics*, 39(1):201–225, 1981.

[40] J. D. van der Waals. The Thermodynamic Theory of Capillarity under the Hypothesis of a Continuous Variation of Density. *Verhandel. Konink. Akad. Weten. Amsterdam*, 8:197–244, 1893.

[41] D. Korteweg. Sur la forme qui prennent les equations du mouvement des fluids si l'on tient compte des forces capillaires par des variations de densité considérables mais continues et sur la théorie de la capillarité dans l'hypothèse d'une variation continue de la densité. *Archives Néerlandaises des Sciences Exactes et Naturelles*, 6(2):1–24, 1901.

[42] P. C. Hohenberg and B. I. Halperin. Theory of Dynamic Critical Phenomena. *Reviews of Modern Physics*, 49(3):435, 1977.

[43] D. Danilov and B. Nestler. Phase-field Modeling of Solidification in Multicomponent and Multi-phase Alloys. *Phase Transformations in Multicomponent Melts*, 2009.

[44] D. A. Cogswell. *A Phase-Field Study of Ternary Multiphase Microstructures*. PhD thesis, Massachusetts Institute of Technology, 2010.

[45] J. E. Dunn and J. Serrin. On the Thermomechanics of Interstitial Working. In *The Breadth and Depth of Continuum Mechanics*, pages 705–743. Springer, 1986.

[46] M. E. Gurtin. Generalized Ginzburg-Landau and Cahn-Hilliard Equations Based on a Microforce Balance. *Physica D: Nonlinear Phenomena*, 92(3):178–192, 1996.

[47] J. W. Cahn and J. E. Hilliard. Free Energy of a Nonuniform System. I. Interfacial Free Energy. *The Journal of Chemical Physics*, 28(2):258–267, 1958.

[48] S. M. Allen and J. W. Cahn. A Microscopic Theory for Antiphase Boundary Motion and its Application to Antiphase Domain Coarsening. *Acta Metallurgica*, 27(6):1085–1095, 1979.

[49] G. Caginalp. Solidification Problems as Systems of Nonlinear Differential Equations. *Lectures in Applied Mathematics*, 23:347–369, 1986.

[50] S.-L. Wang, R. F. Sekerka, A. A. Wheeler, B. T. Murray, S. R. Coriell, R. J. Braun, and G. B. McFadden. Thermodynamically Consistent Phase-Field Models for Solidification. *Physica D: Nonlinear Phenomena*, 69(1):189–200, 1993.

[51] J. E. Guyer, W. J. Boettinger, J. A. Warren, and G. B. McFadden. Phase Field Modeling of Electrochemistry. I. Equilibrium. *Physical Review E*, 69(2):021603, 2004.

[52] J. E. Guyer, W. J. Boettinger, J. A. Warren, and G. B. McFadden. Phase Field Modeling of Electrochemistry. II. Kinetics. *Physical Review E*, 69(2):021604, 2004.

[53] W. Villanueva, W. J. Boettinger, G. B. McFadden, and J. A. Warren. A diffuse-interface model of reactive wetting with intermetallic formation. *Acta Materialia*, 60(9):3799–3814, 2012.

[54] M. S. Park, S. L. Gibbons, and R. Arróyave. Prediction of Processing Maps for Transient Liquid Phase Diffusion Bonding of Cu/Sn/Cu Joints in Microelectronics Packaging. *Microelectronics Reliability*, 54(6):1401–1411, 2014.

[55] R. W. Balluffi, S. Allen, and W. C. Carter. *Kinetics of Materials*. Wiley, 2005.

[56] R. L. Pego. Front Migration in the Nonlinear Cahn-Hilliard Equation. *Proceedings of the Royal Society of London. A. Mathematical and Physical Sciences*, 422(1863):261–278, 1989.

[57] L. Ambrosio and V. M. Tortorelli. Approximation of Functional Depending on Jumps by Elliptic Functional via Γ-convergence. *Communications on Pure and Applied Mathematics*, 43(8):999–1036, 1990.

[58] D. Mumford and J. Shah. Optimal Approximations by Piecewise Smooth Functions and Associated Variational Problems. *Communications on Pure and Applied Mathematics*, 42(5):577–685, 1989.

[59] P. C. Fife. *Dynamics of Internal Layers and Diffusive Interfaces*. CBMS-NSF Regional Conference Series in Applied Mathematics. Society for Industrial and Applied Mathematics, 1988.

[60] A. Braides. *Gamma-convergence for Beginners*. Oxford Lecture Series in Mathematics and its Applications. Oxford University Press, 2002.

[61] B. Bourdin, G. A. Francfort, and J.-J. Marigo. Numerical Experiments in Revisited Brittle Fracture. *Journal of the Mechanics and Physics of Solids*, 48(4):797–826, 2000.

[62] C. Miehe, F. Welschinger, and M. Hofacker. Thermodynamically Consistent Phase Field Models of Fracture: Variational Principles and Multi-field FE Implementations. *International Journal for Numerical Methods in Engineering*, 83(10):1273–1311, 2010.

[63] F. Boyer, C. Lapuerta, S. Minjeaud, B. Piar, and M. Quintard. Cahn–Hilliard/Navier–Stokes Model for the Simulation of Three-phase Flows. *Transport in Porous Media*, 82(3):463–483, 2010.

[64] F. Boyer and S. Minjeaud. Numerical Schemes for a Three Component Cahn-Hilliard Model. *ESAIM: Mathematical Modelling and Numerical Analysis*, 45(04):697–738, 2011.

[65] J. W. Barrett, R. Nürnberg, and V. Styles. Finite Element Approximation of a Phase Field Model for Void Electromigration. *SIAM Journal on Numerical Analysis*, 42(2):738–772, 2004.

[66] D. Bhate, A. F. Bower, and A. Kumar. A Phase Field Model for Failure in Interconnect Lines due to Coupled Diffusion Mechanisms. *Journal of the Mechanics and Physics of Solids*, 50(10):2057–2083, October 2002.

[67] J. E. Taylor and J. W. Cahn. Linking Anisotropic Sharp and Diffuse Surface Motion Laws via Gradient Flows. *Journal of Statistical Physics*, 77(1-2):183–197, 1994.

[68] J. W. Cahn, C. M. Elliott, and A. Novick-Cohen. The Cahn-Hilliard Equation with a Concentration Dependent Mobility: Motion by Minus the Laplacian of the Mean Curvature. *European Journal of Applied Mathematics*, 7(3):287–302, 1996.

[69] N. Saunders and A. P. Miodownik. *CALPHAD (Calculation of Phase Diagrams): A Comprehensive Guide: A Comprehensive Guide*, volume 1. Elsevier, 1998.

[70] S. Puri and Y. Oono. Effect of Noise on Spinodal Decomposition. *Journal of Physics A: Mathematical and General*, 21(15):L755, 1988.

[71] F. Liu and J. Shen. Stabilized Semi-implicit Spectral Deferred correction methods for Allen–Cahn and Cahn–Hilliard equations. *Mathematical Methods in the Applied Sciences*, 2013.

[72] D. J. Eyre. An Unconditionally Stable One-step Scheme for Gradient Systems. *Unpublished article*, 1998.

[73] X. Wu, G. J. Zwieten, and K. G. Zee. Stabilized Second-order Convex Splitting Schemes for Cahn–Hilliard Models with Application to Diffuse-Interface Tumor-Growth Models. *International Journal for Numerical Methods in Biomedical Engineering*, 30(2):180–203, 2014.

[74] J. W. Barrett, J. F. Blowey, and H. Garcke. Finite Element Approximation of the Cahn–Hilliard Equation with Degenerate Mobility. *SIAM Journal on Numerical Analysis*, 37(1):286, 1999.

[75] S. J. Benson and T. S. Munson. Flexible complementarity solvers for large-scale applications. *Optimization Methods and Software*, 21(1):155–168, 2006.

[76] L. Blank, H. Garcke, L. Sarbu, and V. Styles. Nonlocal Allen–Cahn Systems: Analysis and a Primal–Dual Active Set Method. *IMA Journal of Numerical Analysis*, page drs039, 2013.

[77] L. Blank, M. Butz, H. Garcke, L. Sarbu, and V. Styles. Allen-Cahn and Cahn-Hilliard variational inequalities solved with optimization techniques. In *Constrained Optimization and Optimal Control for Partial Differential Equations*, pages 21–35. Springer, 2012.

[78] R. H. Stogner, G. F. Carey, and B. T. Murray. Approximation of Cahn–Hilliard Diffuse Interface Models using Parallel Adaptive Mesh Refinement and Coarsening with C_1 Elements. *International Journal for Numerical Methods in Engineering*, 76(5):636–661, 2008.

[79] H. Gómez, V. M. Calo, Y. Bazilevs, and T. J. R. Hughes. Isogeometric Analysis of the Cahn–Hilliard Phase-field Model. *Computer Methods in Applied Mechanics and Engineering*, 197(49):4333–4352, 2008.

[80] C. M. Elliott, D. A. French, and F. A. Milner. A Second Order Splitting Method for the Cahn–Hilliard Equation. *Numerische Mathematik*, 54(5):575–590, 1989.

[81] L. Zhang, M. R. Tonks, D. Gaston, J. W. Peterson, D. Andrs, P. C. Millett, and B. S. Biner. A Quantitative Comparison between C_0 and C_1 Elements for Solving the Cahn–Hilliard Equation. *Journal of Computational Physics*, 236:74–80, 2013.

[82] M. E. Gurtin and M. E. Jabbour. Interface Evolution in Three Dimensions with Curvature-Dependent Energy and Surface Diffusion: Interface-Controlled Evolution, Phase Transitions, Epitaxial Growth of Elastic Films. *Archive for Rational Mechanics and Analysis*, 163(3):171–208, 2002.

[83] M. E. Gurtin. *Configurational Forces as Basic Concepts of Continuum Physics*, volume 137. Springer, 1999.

[84] R. K. P. Zia, E. F. Redish, and S. R. McKay. Making Sense of the Legendre Transform. *American Journal of Physics*, 77(7):614–622, 2009.

[85] H. B. Callen. *Thermodynamics & an Introduction to Thermostatistics*. John Wiley & Sons, 2006.

[86] R. M. Bowen. Toward a Thermodynamics and Mechanics of Mixtures. *Archive for Rational Mechanics and Analysis*, 24(5):370–403, 1967.

[87] J. T. Oden, A. Hawkins, and S. Prudhomme. General Diffuse-Interface Theories and an Approach to Predictive Tumor Growth Modeling. *Mathematical Models and Methods in Applied Sciences*, 20(03):477–517, 2010.

[88] A. G. McLellan. The Chemical Potential in Thermodynamic Systems under Non-hydrostatic Stresses. *Proceedings of the Royal Society of London. Series A. Mathematical and Physical Sciences*, 307(1488):1–13, 1968.

[89] J. W. Cahn and F. Larché. A Simple Model for Coherent Equilibrium. *Acta Metallurgica*, 32(11):1915–1923, 1984.

[90] J. D. Eshelby. The Elastic Energy-Momentum Tensor. *Journal of Elasticity*, 5(3-4):321–335, 1975.

[91] I. Vardoulakis and E. C. Aifantis. A Gradient Flow Theory of Plasticity for Granular Materials. *Acta Mechanica*, 87(3-4):197–217, 1991.

[92] J. W. Cahn and J. E. Taylor. Overview no. 113 Surface motion by surface Diffusion. *Acta Metallurgica et Materialia*, 42(4):1045–1063, 1994.

[93] M. E. Gurtin. The Dynamics of Solid-Solid Phase Transitions 1. Coherent interfaces. *Archive for Rational Mechanics and Analysis*, 123(4):305–335, 1993.

[94] G. A. Maugin. *Configurational Forces: Thermomechanics, Physics, Mathematics, and Numerics*. CRC Press, 2010.

[95] M. E. Gurtin. *The Nature of Configurational Forces*. Springer, 1999.

[96] H. Ibach. *Physics of Surfaces and Interfaces*. Springer, 2006.

[97] M. E. Gurtin and A. I. Murdoch. A Continuum Theory of Elastic Material Surfaces. *Archive for Rational Mechanics and Analysis*, 57(4):291–323, 1975.

[98] D. J. Griffiths. *Introduction to Electrodynamics*. Pearson, 2013.

[99] K. Tu. Electromigration in Stressed Thin Films. *Physical Review B*, 45(3):1409, 1992.

[100] P. Rimbey and R. Sorbello. Strong-Coupling Theory for the Driving Force in Electromigration. *Physical Review B*, 21(6):2150, 1980.

[101] W. Schaich. Driving Forces for Electromigration by Linear Response. *Physical Review B*, 13(8):3360, 1976.

[102] C. Chen, H. M. Tong, and K. N. Tu. Electromigration and Thermomigration in Pb-Free Flip-Chip Solder Joints. *Annual Review of Materials Research*, 40(1):531–555, June 2010.

[103] C. Basaran, M. Lin, and H. Ye. A Thermodynamic Model for Electrical Current Induced Damage. *International Journal of Solids and Structures*, 40:7315–7327, 2003.

[104] C. Basaran and M. Lin. Damage Mechanics of Electromigration Induced Failure. *Mechanics of Materials*, 40:66–79, 2008.

[105] J. R. Rice and D. C. Drucker. Energy C in Stressed Bodies due to Void and Crack growth. *International Journal of Fracture*, 3(1):19–27, 1967.

[106] M. Lin and C. Basaran. Electromigration Induced Stress Analysis using Fully Coupled Mechanical – Diffusion Equations with Nonlinear Material Properties. *Computational Materials Science*, 34:82–98, 2005.

[107] Y. Liu, Y. Zhang, and L. Liang. Prediction of Electromigration Induced Voids and Time to Failure for Solder Joint of a Wafer Level Chip Scale Package. *IEEE Transactions on Components and Packaging Technologies*, 33(3):544–552, September 2010.

[108] L. Zhang, S. Ou, J. Huang, K. N. Tu, S. Gee, and L. Nguyen. Effect of Current Crowding on Void Propagation at the Interface between Intermetallic Compound and Solder in Flip Chip Solder joints. *Applied Physics Letters*, 88(1):012106, 2006.

[109] M. Mahadevan and R. M. Bradley. Simulations and Theory of Electromigration-Induced Slit Formation in Unpassivated Single-Crystal Metal Lines. *Physical Review B*, 59(16):11037, 1999.

[110] R. W. Balluffi and L. L. Seigle. Growth of Voids in Metals during Diffusion and Creep. *Acta Metallurgica*, 5(8):449–454, 1957.

[111] F. Fischer and J. Svoboda. Void Growth due to Vacancy Supersaturation–A Non-equilibrium Thermodynamics Study. *Scripta Materialia*, 58(2):93–95, 2008.

[112] A. Cuitiño and M. Ortiz. Ductile Fracture by Vacancy Condensation in F.C.C. Single Crystals. *Acta Materialia*, 44(2):427 – 436, 1996.

[113] D. Hull and D. E. Rimmer. The Growth of Grain-Boundary Voids under Stress. *Philosophical Magazine*, 4(42):673–687, 1959.

[114] X. Li, J. Lowengrub, A. Rätz, and A. Voigt. Solving PDEs in Complex Geometries: a Diffuse Domain Approach. *Communications in Mathematical Sciences*, 7(1):81–107, 2009.

[115] O. C. Zienkiewicz, R. L. Taylor, P. Nithiarasu, and J. Z. Zhu. *The Finite Element Method*. Butterworth-Heinemann, 2005.

[116] C. M. Elliott, D. A. French, and F. A. Milner. A Second Order Splitting Method for the Cahn–Hilliard Equation. *Numerische Mathematik*, 54(5):575–590, 1989.

[117] J. Shen and X. Yang. An Efficient Moving Mesh Spectral Method for the Phase Field Model of Two-phase Flows. *Journal of Computational Physics*, 228(8):2978–2992, 2009.

[118] P. S. Ho. Motion of Inclusion Induced by a Direct Current and a Temperature Gradient. *Journal of Applied Physics*, 41(1):64–68, 1970.

[119] M. Mahadevan and R. M. Bradley. Stability of a Circular Void in a Passivated, Current-Carrying Metal Film. *Journal of Applied Physics*, 79(9):6840–6847, 1996.

[120] R. Nürnberg and A. Sacconi. An Unfitted Finite Element Method for the Numerical Approximation of Void Electromigration. *Journal of Computational and Applied Mathematics*, 270:531–544, 2014.

[121] J. Svoboda, F. D. Fischer, P. Fratzl, and E. Kozeschnik. Modelling of Kinetics in Multi-component Multi-phase Systems with Spherical Precipitates: I: Theory. *Materials Science and Engineering: A*, 385(1):166–174, 2004.

[122] I. Blech. Electromigration in Thin Aluminum Films on Titanium Nitride. *Journal of Applied Physics*, 47(4):1203–1208, 1976.

[123] P. J. Fensham. Self-Diffusion in Tin Crystals. *Australian Journal of Chemistry*, 3(1):91–104, 1950.

[124] M. Lu, D.-Y. Shih, P. Lauro, C. Goldsmith, and D. W. Henderson. Effect of Sn Grain Orientation on Electromigration Degradation Mechanism in High Sn-based Pb-free Solders. *Applied Physics Letters*, 92(21):211909, 2008.

[125] A. U. Telang and T. R. Bieler. The Orientation Imaging Microscopy of Lead-free Sn-Ag Solder Joints. *JOM*, 57(6):44–49, 2005.

[126] J. R. Lloyd, M. W. Lane, and E. G. Liniger. Relationship between Interfacial Adhesion and Electromigration in Cu Metallization. In *Integrated Reliability Workshop Final Report, 2002. IEEE International*, pages 32–35. IEEE, 2002.

[127] D. Jacqmin. Contact-line Dynamics of a Diffuse Fluid Interface. *Journal of Fluid Mechanics*, 402:57–88, 2000.

[128] C. M. Elliott and S. Luckhaus. A Generalised Diffusion Equation for Phase Separation of a Multi-component Mixture with Interfacial Free Energy. *Unpublished article*, 1991.

[129] H. Garcke and A. Novick-Cohen. A Singular Limit for a System of Degenerate Cahn-Hilliard Equations. *Advances in Differential Equations*, 5(4-6):401–434, 2000.

[130] L. Bronsard and F. Reitich. On Three-phase Boundary Motion and the Singular Limit of a Vector-valued Ginzburg-Landau Equation. *Archive for Rational Mechanics and Analysis*, 124(4):355–379, 1993.

[131] J. Kim. Phase-Field Models for Multi-Component Fluid Flows. *Communications in Computational Physics*, 12(3):613–661, 2012.

[132] J. E. Taylor. Diffuse Interfaces with Sharp Corners and Facets: Phase Field Models with Strongly Anisotropic Surfaces. *Physica D: Nonlinear Phenomena*, 112(3-4):381–411, February 1998.

[133] J. Nocedal and S. Wright. *Numerical Optimization*. Springer Series in Operations Research and Financial Engineering. Springer, 2006.

[134] I. Steinbach, F. Pezzolla, B. Nestler, M. Seeßelberg, R. Prieler, G. J. Schmitz, and J. L. L. Rezende. A Phase Field Concept for Multiphase Systems. *Physica D: Nonlinear Phenomena*, 94(3):135–147, 1996.

[135] M. Schimschak and J. Krug. Surface Electromigration as a Moving Boundary Value Problem. *Physical Review Letters*, 78(2):278, 1997.

[136] C. Tâe-Jer and J. R. Rice. The Shape of Intergranular Creep Cracks Growing by Surface Diffusion. *Acta Metallurgica*, 21(12):1625 – 1628, 1973.

[137] B. S. Kirk, J. W. Peterson, R. H. Stogner, and G. F. Carey. `libMesh`: A C++ Library for Parallel Adaptive Mesh Refinement/Coarsening Simulations. *Engineering with Computers*, 22(3–4):237–254, 2006. `http://dx.doi.org/10.1007/s00366-006-0049-3`.

[138] S. Balay, W. D. Gropp, L. C. McInnes, and B. F. Smith. Efficient Management of Parallelism in Object Oriented Numerical Software Libraries. In E. Arge, A. M. Bruaset, and H. P. Langtangen, editors, *Modern Software Tools in Scientific Computing*, pages 163–202. Birkhäuser Press, 1997.

[139] W. Bangerth, T. Heister, L. Heltai, G. Kanschat, M. Kronbichler, M. Maier, B. Turcksin, and T. D. Young. The `deal.ii` Library, Version 8.1. *arXiv preprint,* *http://arxiv.org/abs/1312.2266v4*, 2013.

[140] J. E. Guyer, D. Wheeler, and J. A. Warren. FiPy: Partial Differential Equations with Python. *Computing in Science & Engineering*, 11(3):6–15, 2009.

[141] A. Schmidt and K. G. Siebert. *Design of Adaptive Finite Element Software: The Finite Element Toolbox ALBERTA*. Lecture Notes in Computational Science and Engineering. Springer, 2006.

[142] S. Vey and A. Voigt. AMDiS: Adaptive Multidimensional Simulations. *Computing and Visualization in Science*, 10(1):57–67, 2007.

[143] D. A. Knoll and D. E. Keyes. Jacobian-free Newton–Krylov Methods: A Survey of Approaches and Applications. *Journal of Computational Physics*, 193(2):357–397, 2004.

[144] M. Heroux, R. Bartlett, V. H. R. Hoekstra, J. Hu, T. Kolda, R. Lehoucq, K. Long, R. Pawlowski, E. Phipps, A. Salinger, H. Thornquist, R. Tuminaro, J. Willenbring, and A. Williams. An Overview of Trilinos. Technical Report SAND2003-2927, Sandia National Laboratories, 2003.

[145] A. Tambat. *Explicit Geometry Based Enriched Field Approximations*. PhD thesis, PURDUE UNIVERSITY, 2013.

[146] P. Lions and B. Mercier. Splitting Algorithms for the Sum of Two Nonlinear Operators. *SIAM Journal on Numerical Analysis*, 16(6):964–979, 1979.

[147] L. Wang, J. Lee, M. Anitescu, A. Azab, L. C. McInnes, T. Munson, and B. Smith. A Differential Variational Inequality Approach for the Simulation of Heterogeneous Materials. In *Proceedings of SciDAC 2011 Conference*, 2011.

[148] W. Huang and R. D. Russell. A High Dimensional Moving Mesh Strategy. *Applied Numerical Mathematics*, 26(1):63–76, 1998.

[149] W. Cao, W. Huang, and R. D. Russell. An r-Adaptive Finite Element Method Based upon Moving Mesh PDEs. *Journal of Computational Physics*, 149(2):221 – 244, 1999.

[150] G. Söderlind. Automatic Control and Adaptive Time-stepping. *Numerical Algorithms*, 31(1-4):281–310, 2002.

[151] D. W. Kelly, D. S. R. Gago, O. C. Zienkiewicz, and I. Babuska. A Posteriori Error Analysis and Adaptive Processes in the Finite Element Method: Part I–Error Analysis. *International Journal for Numerical Methods in Engineering*, 19(11):1593–1619, 1983.

[152] P. W. Voorhees. The Theory of Ostwald Ripening. *Journal of Statistical Physics*, 38(1-2):231–252, 1985.

[153] A. Umantsev and G. Olson. Ostwald Ripening in Multicomponent Alloys. *Scripta Metallurgica et Materialia*, 29(8):1135–1140, 1993.

[154] C. J. Kuehmann and P. W. Voorhees. Ostwald Ripening in Ternary Alloys. *Metallurgical and Materials Transactions A*, 27(4):937–943, 1996.

[155] B. Chao, S.-H. Chae, X. Zhang, K.-H. Lu, J. Im, and P. S. Ho. Investigation of Diffusion and Electromigration Parameters for Cu–Sn Intermetallic Compounds in Pb-Free Solders using Simulated Annealing. *Acta Materialia*, 55(8):2805–2814, 2007.

[156] M. S. Park and R. Arróyave. Early Stages of Intermetallic Compound Formation and Growth during Pb-free Soldering. *Acta Materialia*, 58(14):4900–4910, 2010.

[157] K. N. Tu, H.-Y. Hsiao, and C. Chen. Transition from Flip Chip Solder Joint to 3D IC Microbump: Its Effect on Microstructure Anisotropy. *Microelectronics Reliability*, 53(1):2–6, 2013.

[158] L. W. Kong, J. R. Lloyd, A. C. Rudack, and A. C. Diebold. Thermally Induced Void Growth in Through-Silicon Vias. *Journal of Micro/Nanolithography, MEMS, and MOEMS*, 12(2):023010–023010, 2013.

[159] M. J. Borden, C. V. Verhoosel, M. A. Scott, T. J. Hughes, and C. M. Landis. A Phase Field Description of Dynamic Brittle Fracture. *Computer Methods in Applied Mechanics and Engineering*, 217:77–95, 2012.

[160] W. H. Woodford, Y.-M. Chiang, and W. C. Carter. Electrochemical Shock of Intercalation Electrodes: A Fracture Mechanics Analysis. *Journal of The Electrochemical Society*, 157(10):A1052–A1059, 2010.

[161] S. H. Goods and T. G. Nieh. Mechanisms of Intergranular Cavity Nucleation and Growth During creep. *Scripta Metallurgica*, 17(1):23 – 30, 1983.

[162] S. H. Goods and W. D. Nix. The Kinetics of Cavity Growth and Creep Fracture in Silver Containing Implanted Grain Boundary Cavities. *Acta Metallurgica*, 26(5):739 – 752, 1978.

[163] E. van der Giessen, M. van der Burg, A. Needleman, and V. Tvergaard. Void Growth due to Creep and Grain Boundary Diffusion at High Triaxialities. *Journal of the Mechanics and Physics of Solids*, 43(1):123 – 165, 1995.

[164] A. J. McConnell. *Application of Tensor Analysis*. Courier Dover Publications, 1957.

[165] M. E. Gurtin. *An Introduction to Continuum Mechanics*. Academic Press, 1982.

[166] L. E. Malvern. *Introduction to the Mechanics of a Continuous Medium*. Prentice-Hall, Englewood Cliffs, NJ, 1969.

[167] P. Cermelli, E. Fried, and M. E. Gurtin. Transport Relations for Surface Integrals Arising in the Formulation of Balance Laws for Evolving Fluid Interfaces. *Journal of Fluid Mechanics*, 544:339–351, 2005.

[168] P. C. Fife and O. Penrose. Interfacial Dynamics for Thermodynamically Consistent Phase Field Models with Nonconserved Order Parameter. *Electronic Journal of Differential Equations*, 16:1–49, 1995.

[169] S. Balay, J. Brown, K. Buschelman, W. D. Gropp, D. Kaushik, M. G. Knepley, L. C. McInnes, B. F. Smith, and H. Zhang. PETSc Web Page, 2012.

[170] S. Balay and J. Brown. PETSc Users Manual. Technical Report ANL-95/11 - Revision 3.3, Argonne National Laboratory, 2012.

[171] D. Gaston, C. Newman, G. Hansen, and D. Lebrun-Grandié. MOOSE: A Parallel Computational Framework for Coupled Systems of Nonlinear Equations. *Nuclear Engineering and Design*, 239(10):1768–1778, 2009.

[172] V. Rvachev. Theory of R-functions and Some Applications. *Naukova Dumka, Kiev*, 1982.

[173] F. R. Schaefer. GetPot Command Line Parser / Configuration Parser Library. `http://getpot.sourceforge.net`. Accessed: 2014-09-30.

[174] S. Sadasiva, G. Subbarayan, L. Jiang, and D. Pantuso. Numerical simulations of electromigration and stressmigration Driven void evolution in Solder interconnects. *Journal of Electronic Packaging*, 134(2):020907, 2012.

[175] S. Sadasiva, G. Subbarayan, L. Jiang, and D. Pantuso. Numerical simulations of electromigration and stress migration Driven void propagation in pb free Solder interconnects. In *ASME 2011 Pacific Rim Technical Conference and Exhibition on Packaging and Integration of Electronic and Photonic Systems*, pages 585–590. American Society of Mechanical Engineers, 2011.

[176] A. Udupa, S. Sadasiva, and G. Subbarayan. Numerical simulations of late stage growth of intermetallics in pb free Solder microbumps. *in preparation for submission to Modelling and Simulations in Materials Science*, 2015.

[177] S. Sadasiva and G. Subbarayan. Multiphase field simulations of electromigration Driven intergranular void growth and evolution. *in preparation for submission to Modelling and Simulations in Materials Science*, 2015.

[178] S. Sadasiva and G. Subbarayan. Numerical simulations of the effect of anisotropic diffusivity in tin on electromigration failure in Solder interconnects. *in preparation for submission to Journal of Electronics Packaging*, 2015.

[179] S. Sadasiva, G. Subbarayan, and D. Pantuso. 3 dimensional simulations of electromigration Driven void growth and failure in Solder joints. *in preparation for submission to Modeling and Simulations in Material Science*, 2015.

APPENDICES

A. DERIVATION OF A TRANSPORT THEOREM FOR INTERFACIAL QUANTITIES

In this appendix, the balance laws that are needed for the formulation of the thermodynamics of problems with moving interfaces are derived. The approach used in [82] is used where interfacial vector and tensor fields as well as differential operators on the surface are defined through the projection of the corresponding bulk operators on the interface. This is done by defining the interfacial projection operator $\boldsymbol{P}$ defined as,

$$\boldsymbol{P} = \boldsymbol{I} - \boldsymbol{n} \otimes \boldsymbol{n}. \tag{A.1}$$

The surface differential operators (gradient and divergence) are then defined in terms of the gradient and divergence of a smooth extension of the surface field into the bulk. This approach allows the usage of standard continuum mechanics to derive transport theorems and balance laws on the interface without necessitating the use of differential geometry and Christoffel symbols [164].

A.1 Definition of Surface Differential Operators

The surface gradient of an interfacial scalar field is defined as the projection of the gradient of the smooth extension of the interfacial field in 3-Dimensional space onto the interface.

$$\nabla_\Gamma \phi = \boldsymbol{P}.\nabla \phi_\Omega. \tag{A.2}$$

In the above ϕ_Ω is an extension of the interfacial field into the bulk. This can be done, for example by maintaining a constant value along the normals. Similarly the surface gradient of an interfacial vector field is defined as follows,

$$\nabla_\Gamma \boldsymbol{v} = \nabla \boldsymbol{v}.\boldsymbol{P}. \tag{A.3}$$

This allows the surface divergence of an interfacial vector field to be defined, in a manner similar to the bulk divergence [165] as

$$\nabla_\Gamma.\boldsymbol{v} = \mathrm{tr}(\nabla_\Gamma \boldsymbol{v}) = \nabla \boldsymbol{v} : \boldsymbol{P}. \tag{A.4}$$

Similarly for a (3-Dimensional) tensor field defined on the interface, the surface divergence is defined through the following relationship,

$$(\nabla_\Gamma.\boldsymbol{B}).\boldsymbol{a} = \nabla_\Gamma.(\boldsymbol{B}.\boldsymbol{a}). \tag{A.5}$$

A.1.1 Curvature Tensor and Invariants

The curvature tensor $\boldsymbol{L} = -\nabla_\Gamma \boldsymbol{n}$ provides information at the rate at which the normal changes direction. This tensor is related to the Weingarten map of differential geometry [164]. The invariants of the curvature tensor are then defined as the mean and the Gaussian curvature. The total curvature κ, twice the mean curvature is defined as

$$\kappa = \mathrm{tr}(\boldsymbol{L}) = -\nabla_\Gamma.\boldsymbol{n}. \tag{A.6}$$

The Gaussian curvature G is defined as the $\det \boldsymbol{L}$ .G is a useful quantity in models where the interfacial quantities depend on κ. It can be shown that,

$$\nabla_\Gamma.\boldsymbol{P} = \kappa \boldsymbol{n}. \tag{A.7}$$

Using the standard definition of the divergence of a tensor,

$$(\nabla_\Gamma.\boldsymbol{B})\,.\boldsymbol{a} = \nabla_\Gamma.\left(\boldsymbol{B}^T\boldsymbol{a}\right) \tag{A.8}$$

where $\boldsymbol{a}$ is a constant vector. Substituting the surface projection tensor $\boldsymbol{P} = \boldsymbol{I} - \boldsymbol{n}\otimes\boldsymbol{n}$ in Eq. (A.8)

$$(\nabla_\Gamma.(\boldsymbol{I} - \boldsymbol{n}\otimes\boldsymbol{n}))\,.\boldsymbol{a} = (\nabla_\Gamma.\boldsymbol{a}) - \nabla_\Gamma.((\boldsymbol{n}.\boldsymbol{a})\boldsymbol{n}) \tag{A.9}$$

$$(\nabla_\Gamma.(\boldsymbol{I} - \boldsymbol{n}\otimes\boldsymbol{n}))\,.\boldsymbol{a} = -\nabla_\Gamma.((\boldsymbol{n}.\boldsymbol{a})\,\boldsymbol{n}) \tag{A.10}$$

$$(\nabla_\Gamma.\boldsymbol{P})\,.\boldsymbol{a} = (\boldsymbol{n}.\boldsymbol{a})\,\kappa + (\nabla_\Gamma\boldsymbol{n}.\boldsymbol{n}).\boldsymbol{a} + (\nabla_\Gamma.\boldsymbol{a})\boldsymbol{n}.\boldsymbol{n}. \tag{A.11}$$

$\nabla_\Gamma.\boldsymbol{n} = -\kappa\boldsymbol{n}$ and $\nabla_\Gamma\boldsymbol{n}.\boldsymbol{n} = \boldsymbol{0}$, and $\nabla_\Gamma.\boldsymbol{a} = 0$

$$(\nabla_\Gamma.\boldsymbol{P})\,\boldsymbol{a} = \kappa(\boldsymbol{n}.\boldsymbol{a}) \implies \nabla_\Gamma.\boldsymbol{P} = \kappa\boldsymbol{n}. \tag{A.12}$$

Also, for tensor fields that are purely tangential (i.e. $\boldsymbol{n}.(\boldsymbol{B}.\boldsymbol{a}) = 0$, where $\boldsymbol{a}$ is a vector tangential to the interface)

$$\boldsymbol{n}.\nabla_\Gamma\boldsymbol{B} = \boldsymbol{B}.\boldsymbol{L}. \tag{A.13}$$

A.2 Surface Divergence Theorem

A divergence theorem can now be defined relating a loop integral on an interface to an integral over the area bounded by the loop. Defining $\boldsymbol{m}$ as the outward normal at every point on the bounding curve C of a section of a surface Γ, the surface divergence theorem for a tangential vector field $\boldsymbol{v}$ on an interface is defined as

$$\oint_C \boldsymbol{v}.\boldsymbol{m}dC = \int_\Gamma \nabla_\Gamma.\boldsymbol{v}d\Gamma. \tag{A.14}$$

For a tangential tensor $\boldsymbol{B}$, the surface divergence theorem is defined as,

$$\oint_C \boldsymbol{B}.\boldsymbol{m}dC = \int_\Gamma \nabla_\Gamma.\boldsymbol{B}d\Gamma. \tag{A.15}$$

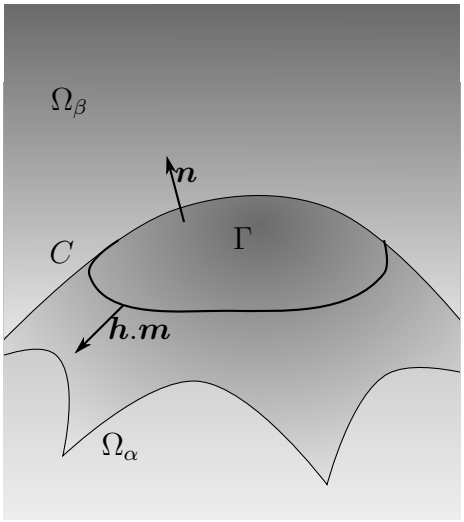

Figure A.1. Schematic showing the definition of various terms in the surface divergence theorem.

A.3 Material Derivative of an Interfacial Section

To derive balance laws for control volumes that are intersected by moving boundaries, the material derivative of a section $d\Gamma$ of the interface is needed. Consider the vector area differential $\boldsymbol{n}d\Gamma$. To compute the material derivative of this quantity, it is first transformed to an arbitrary reference domain through Nanson's formula [166].

$$\boldsymbol{n}d\Gamma = J\boldsymbol{F}^{-T}\boldsymbol{N}d\Gamma_0. \tag{A.16}$$

Using $\frac{D}{Dt}\boldsymbol{N}d\Gamma_0 = 0$

$$\frac{D}{Dt}\boldsymbol{n}d\Gamma = \left[\underbrace{\dot{J}\boldsymbol{F}^{-T}\boldsymbol{N}}_{I} + \underbrace{\Phi(\boldsymbol{X})J\dot{\boldsymbol{F}}^{-T}\boldsymbol{N}}_{II}\right] d\Gamma_0. \tag{A.17}$$

For term I, it is known that $\dot{J} = J\nabla.\boldsymbol{v}$. Hence, it can be written as $\nabla.\boldsymbol{v}J\boldsymbol{F}^{-T}\boldsymbol{N}$. The term II requires the computation of $\dot{\boldsymbol{F}}^{-T}$. To evaluate this, the following identity is considered,

$$\boldsymbol{F}^T\boldsymbol{F}^{-T} = \boldsymbol{I} \tag{A.18}$$

$$\dot{\boldsymbol{F}}^T\boldsymbol{F}^{-T} + \boldsymbol{F}^T\dot{\boldsymbol{F}}^{-T} = \boldsymbol{O} \tag{A.19}$$

Now, $\dot{\boldsymbol{F}} = \nabla\boldsymbol{v}\boldsymbol{F}$

$$\implies \dot{\boldsymbol{F}}^T = \boldsymbol{F}^T\nabla\boldsymbol{v}^T. \tag{A.20}$$

Substituting it back

$$\boldsymbol{F}^T\dot{\boldsymbol{F}}^{-T} = -\boldsymbol{F}^T\nabla\boldsymbol{v}^T\boldsymbol{F}^{-T} \tag{A.21}$$

Premultiplying both sides by $\boldsymbol{F}^{-T}$

$$\dot{\boldsymbol{F}}^{-T} = -\nabla\boldsymbol{v}^T\boldsymbol{F}^{-T}. \tag{A.22}$$

The derivative can therefore be rewritten as

$$\frac{D}{Dt}\boldsymbol{n}d\Gamma = \left(\nabla.\boldsymbol{v}\boldsymbol{I} - \nabla\boldsymbol{v}^T\right)J\boldsymbol{F}^{-T}\boldsymbol{N}d\Gamma_0 \tag{A.23}$$

or

$$\frac{D}{Dt}\boldsymbol{n}d\Gamma = \left(\nabla.\boldsymbol{v}\boldsymbol{I} - \nabla\boldsymbol{v}^T\right)\boldsymbol{n}d\Gamma_0. \tag{A.24}$$

As $\boldsymbol{n}.\boldsymbol{n} = 1$,

$$2\boldsymbol{n}.\frac{D}{Dt}\boldsymbol{n} = 0. \tag{A.25}$$

This implies that the normal $\boldsymbol{n}$ is orthogonal to $\frac{D}{Dt}\boldsymbol{n}$. Using $\frac{D}{Dt}\boldsymbol{n}d\Gamma = \frac{D}{Dt}\boldsymbol{n}d\Gamma + \boldsymbol{n}\frac{D}{Dt}d\Gamma$, and taking the dot product of Eq. (A.23) with $\boldsymbol{n}$

$$\frac{D}{Dt}d\Gamma = \boldsymbol{n}.\left(\nabla.\boldsymbol{v}\boldsymbol{I} - \nabla\boldsymbol{v}^T\right)\boldsymbol{n}d\Gamma \tag{A.26}$$

Expanding the above,

$$\frac{D}{Dt}d\Gamma = \left(\nabla.\boldsymbol{v} - \boldsymbol{n}.\nabla\boldsymbol{v}^T\boldsymbol{n}\right)d\Gamma \tag{A.27}$$

or,

$$\frac{D}{Dt}d\Gamma = \nabla\boldsymbol{v} : (\boldsymbol{I} - \boldsymbol{n}\otimes\boldsymbol{n})\,d\Gamma \tag{A.28}$$

$$\implies \frac{D}{Dt}d\Gamma = \nabla_\Gamma.\boldsymbol{v}d\Gamma. \tag{A.29}$$

Substituting this back into the expression for $\frac{D}{Dt}\boldsymbol{n}d\Gamma$, the material derivative of the normal can now be written as

$$\frac{D}{Dt}\boldsymbol{n} = \left(\nabla.\boldsymbol{v}\boldsymbol{I} - \nabla\boldsymbol{v}^T - \nabla_\Gamma.\boldsymbol{v}\boldsymbol{I}\right)\boldsymbol{n} \tag{A.30}$$

Writing $\nabla.\boldsymbol{v}\boldsymbol{I}$ as $\nabla_\Gamma.\boldsymbol{v}\boldsymbol{I} + \boldsymbol{n}\otimes\boldsymbol{n} : \nabla\boldsymbol{v}^T$

$$\frac{D}{Dt}\boldsymbol{n} = (\boldsymbol{n}\otimes\boldsymbol{n} - \boldsymbol{I})\,.\nabla\boldsymbol{v}^T\boldsymbol{n} \tag{A.31}$$

or

$$\frac{D}{Dt}\boldsymbol{n} = -\nabla_\Gamma \boldsymbol{v}^T \boldsymbol{n}. \tag{A.32}$$

Any velocity $\boldsymbol{v}$ for an interface can be decomposed into normal and tangential components as $V\boldsymbol{n}+\boldsymbol{P}.\boldsymbol{v}$. It is important to note that the tangential velocity components $\boldsymbol{P}.\boldsymbol{v}$ can not change the shape of the interface. Hence, in most physical problems, it is only the normal component V that plays an important part. Substituting the decomposed velocity $\boldsymbol{v}$ into Eq. (A.26) and letting $\boldsymbol{P}.\boldsymbol{v} = \boldsymbol{v}_t$,

$$\frac{D}{Dt}d\Gamma = \left(\nabla_\Gamma.(V\boldsymbol{n} + \boldsymbol{v}_t)\right) d\Gamma \tag{A.33}$$

$$\frac{D}{Dt}d\Gamma = \left(\nabla_\Gamma.(V\boldsymbol{n}) + \nabla_\Gamma.\boldsymbol{v}_t\right) d\Gamma \tag{A.34}$$

$$\frac{D}{Dt}d\Gamma = \left(\nabla_\Gamma V.\boldsymbol{n} + V\nabla_\Gamma.\boldsymbol{n} + \nabla_\Gamma.\boldsymbol{v}_t\right) d\Gamma \tag{A.35}$$

As $\nabla_\Gamma V$ is a vector tangent to the interface,

$$\nabla_\Gamma V.\boldsymbol{n} = 0 \tag{A.36}$$

Using Eq. (A.6), and the above

$$\frac{D}{Dt}d\Gamma = (-\kappa V + \nabla_\Gamma.\boldsymbol{v}_t)d\Gamma. \tag{A.37}$$

In variational treatments, as the tangential velocity components play no part, this relation is directly stated as,

$$\delta d\Gamma = -\kappa(\delta\boldsymbol{x}.\boldsymbol{n})d\Gamma. \tag{A.38}$$

Substituting the decomposed velocity into Eq. (A.30) leads to

$$\frac{D}{Dt}\boldsymbol{n} = -\nabla_\Gamma \left(V\boldsymbol{n} + \boldsymbol{v}_t\right)^T .\boldsymbol{n}. \tag{A.39}$$

Expanding the terms

$$\frac{D}{Dt}\boldsymbol{n} = -\nabla_\Gamma(V\boldsymbol{n})^T.\boldsymbol{n} - \nabla_\Gamma \boldsymbol{v}_t^T.\boldsymbol{n}. \tag{A.40}$$

Using $\nabla_\Gamma(V\boldsymbol{n}) = \nabla_\Gamma V \otimes \boldsymbol{n} + V\nabla_\Gamma \boldsymbol{n}$

$$\frac{D}{Dt}\boldsymbol{n} = -(\boldsymbol{n} \otimes \nabla_\Gamma V).\boldsymbol{n} - V\nabla_\Gamma \boldsymbol{n}^T.\boldsymbol{n} - \nabla_\Gamma \boldsymbol{v}_t^T.\boldsymbol{n}. \tag{A.41}$$

Again, $\nabla_\Gamma \boldsymbol{n}^T$ is an interfacial tensor, and hence $\nabla_\Gamma \boldsymbol{n}^T.\boldsymbol{n} = 0$ leading to

$$\frac{D}{Dt}\boldsymbol{n} = -(\boldsymbol{n} \otimes \nabla_\Gamma V).\boldsymbol{n} - \nabla_\Gamma \boldsymbol{v}_t^T.\boldsymbol{n}. \tag{A.42}$$

This can be further simplified into

$$\frac{D}{Dt}\boldsymbol{n} = -\nabla_\Gamma V - \nabla_\Gamma \boldsymbol{v}_t^T.\boldsymbol{n}. \tag{A.43}$$

In variational treatments, the above relation is stated as

$$\delta\boldsymbol{n} = -\nabla_\Gamma \left(\delta\boldsymbol{x}.\boldsymbol{n}\right). \tag{A.44}$$

This relation plays an important part in cases where the surface energy is anisotropic which is often captured by including a dependence on the direction of the normal. In this case, the variation or material derivative of the normal is required.

A.3.1 Material Derivative of Surface Integrals

The relations derived above can now be used to derive the material derivative of a surface integral. This relationship is useful in deriving local forms of interfacial transport theorems. Consider the material derivative of the integral of an interfacial field $\phi(\boldsymbol{x})$ over a part of the interface Γ, $\int_\Gamma \phi(\boldsymbol{x}) d\Gamma$. It is assumed that $\phi(\boldsymbol{x})$ can be extended into the bulk, such that $\nabla\phi(\boldsymbol{x}).\boldsymbol{n} = 0$ (Fig. A.2). Using Eq. (A.33),

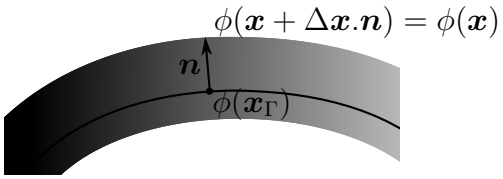

Figure A.2. Interfacial function with constant normal extension into the bulk.

$$\frac{D}{Dt}\int_\Gamma \phi(\boldsymbol{x})d\Gamma = \int_\Gamma \frac{D}{Dt}\phi(\boldsymbol{x})d\Gamma + \int_\Gamma \phi(\boldsymbol{x})\left(-\kappa V + \nabla_\Gamma.\boldsymbol{v}_t\right)d\Gamma. \tag{A.45}$$

Expanding $\frac{D}{Dt}\phi(\boldsymbol{x}) = \frac{\partial\phi(\boldsymbol{x})}{\partial t} + \nabla\phi(\boldsymbol{x}).\boldsymbol{v}$

$$\frac{D}{Dt}\int_\Gamma \phi(\boldsymbol{x})d\Gamma = \int_\Gamma \left(\frac{\partial\phi(\boldsymbol{x})}{\partial t} + \nabla\phi(\boldsymbol{x}).\boldsymbol{v} - \phi(\boldsymbol{x})\kappa V + \nabla_\Gamma.\boldsymbol{v}_t\right)d\Gamma. \tag{A.46}$$

Now, separating $\nabla\phi(\boldsymbol{x})$ as $\nabla_\Gamma\phi(\boldsymbol{x}) + \frac{\partial\phi(\boldsymbol{x})}{\partial n}\boldsymbol{n}$,

$$\nabla\phi(\boldsymbol{x}).\boldsymbol{v} = \nabla_\Gamma\phi(\boldsymbol{x}).(V\boldsymbol{n}+\boldsymbol{v}_t) + \frac{\partial\phi(\boldsymbol{x})}{\partial n}\boldsymbol{n}.(V\boldsymbol{n}+\boldsymbol{v}_t) \tag{A.47}$$

which gives, using the property of the constant normal extension

$$\nabla\phi(\boldsymbol{x}).\boldsymbol{v} = \nabla_\Gamma\phi(\boldsymbol{x}).\boldsymbol{v}_t. \tag{A.48}$$

Substituting this back into the expression

$$\frac{D}{Dt}\int_\Gamma \phi(\boldsymbol{x})d\Gamma = \int_\Gamma \left(\frac{\partial\phi(\boldsymbol{x})}{\partial t} + \nabla_\Gamma\phi(\boldsymbol{x}).\boldsymbol{v}_t - \phi(\boldsymbol{x})\kappa V + \phi(\boldsymbol{x})\nabla_\Gamma.\boldsymbol{v}_t\right)d\Gamma. \tag{A.49}$$

Using the identity, $\nabla_\Gamma.(\phi(\boldsymbol{x})\boldsymbol{v}_t) = \nabla_\Gamma\phi(\boldsymbol{x}).\boldsymbol{v}_t + \phi(\boldsymbol{x})\nabla_\Gamma.(\boldsymbol{v}_t)$,

$$\frac{D}{Dt}\int_\Gamma \phi(\boldsymbol{x})d\Gamma = \int_\Gamma \left(\frac{\partial\phi(\boldsymbol{x})}{\partial t} + \nabla_\Gamma.(\phi(\boldsymbol{x})\boldsymbol{v}_t) - \phi(\boldsymbol{x})\kappa V\right)d\Gamma. \tag{A.50}$$

Applying the surface divergence theorem (Eq. (A.14))

$$\frac{D}{Dt}\int_{\Gamma}\phi(\boldsymbol{x})d\Gamma = \int_{\Gamma}\left(\frac{\partial\phi(\boldsymbol{x})}{\partial t} - \kappa\phi(\boldsymbol{x})V\right)d\Gamma + \oint_{C}\phi(\boldsymbol{x})\boldsymbol{v}_t dC. \tag{A.51}$$

In the absence of an assumption of constant normal extension for $\phi(\boldsymbol{x})$ some authors [167], define an alternative time derivative $\mathring{\phi}(\boldsymbol{x}) = \frac{\partial\phi(\boldsymbol{x})}{\partial t} + \frac{\partial\phi(\boldsymbol{x})}{\partial n}V$, called the time derivative following the interface. Another point to note in the above derivation is that the velocity $\boldsymbol{v}$ is the velocity of the interface and not the velocity of particles that form part of the interface. In most cases, the tangential velocity of the interface doesn't play a part in the evolution of the interface. Hence it is possible to arbitrarily set $\boldsymbol{v}_t$ to 0, without losing any information.

A.4 Control Volumes with Accretion

In the derivation of the standard transport theorems for control volumes in Lagrangian frames of reference, the control is defined over a fixed set of material points and the evolution of fields over this fixed set of material points is related to fluxes through the boundaries of the control volume. The control volume Ω shown in Fig. A.3 contains a fixed set of material points.

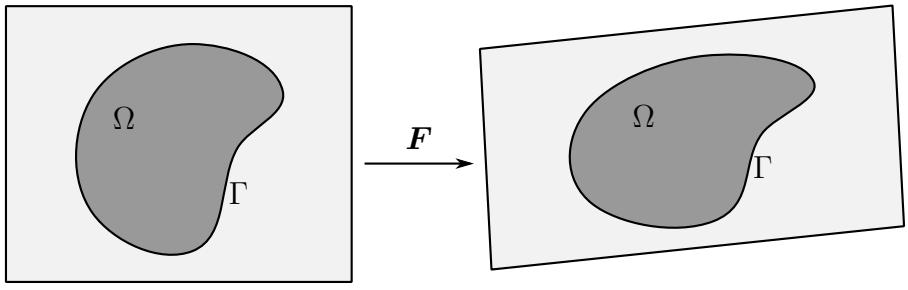

Figure A.3. Lagrangian control volume. The set of material points contained in the control volume don't change through the transformation.

Writing the transport theorem for an arbitrary quantity $\phi(\boldsymbol{x})$,

$$\frac{D}{Dt}\int_{\Omega}\phi(\boldsymbol{x})d\Omega = -\int_{\Gamma}\boldsymbol{J}.\boldsymbol{n}d\Gamma. \tag{A.52}$$

Expanding the material derivative, as the differentiation is in purely Lagrangian coordinates, the terms related to the convective velocities, as well as the term related to the $\frac{D}{Dt}d\Omega$ are zero. Using the divergence theorem on the right hand side

$$\frac{\partial\phi(\boldsymbol{x})}{\partial t} = -\nabla.\boldsymbol{J}. \tag{A.53}$$

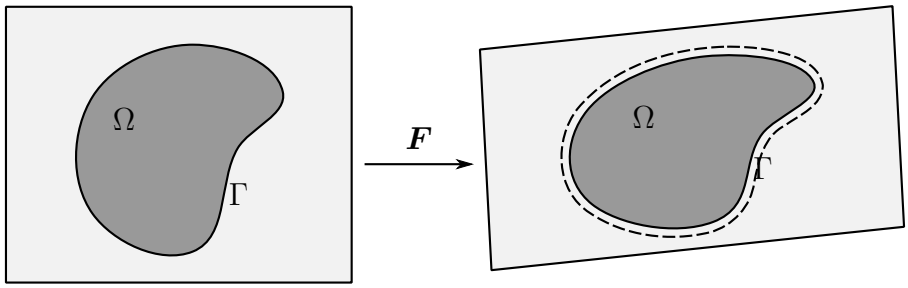

Figure A.4. Control volume with accretion. The set of material points that are contained in the control volume changes.

This control volume is insufficient to develop the equations of motion for moving boundary problems. In moving boundary problems, the total value of the field over the domain changes on account of the addition of material points to the control volume through accretion, as shown in Fig. A.4. To allow this to occur an additional term is added to Eq. (A.52), to account for the increase due to the volume swept by the motion of the boundaries of the control volume. The motion of the outer boundary of the control volume can be completely described by a normal velocity U. The additional contribution to the integral due to this swept volume is $\int_{\Gamma}\phi(\boldsymbol{x})Ud\Gamma$ and the balance law can be written as,

$$\frac{D}{Dt}\int_{\Omega}\phi(\boldsymbol{x})d\Omega = -\int_{\Gamma}\boldsymbol{J}.\boldsymbol{n}d\Gamma + \int_{\Gamma}\phi(\boldsymbol{x})Ud\Gamma. \tag{A.54}$$

In a more general Eulerian control volume Fig. A.6 the relation above can be written as

$$\int_{\Omega} \frac{\partial \phi(\boldsymbol{x})}{\partial t} d\Omega = -\int_{\Gamma} \boldsymbol{J}.\boldsymbol{n} d\Gamma + \int_{\Gamma} \phi(\boldsymbol{x})(U - \boldsymbol{v}.\boldsymbol{n}) d\Gamma. \tag{A.55}$$

While localizing the above integral it is assumed that the velocity field $\boldsymbol{u}$, with $\boldsymbol{u}.\boldsymbol{n} = U$ on Γ is uniformly 0 inside the domain. Eqs. (A.54) and (A.55) can now be used to derive a transport theorem for a domain divided by a moving interface.

A.5 Transport Theorem for an Interfacial Pillbox

Interfacial pillboxes Fig. A.5 formalize the process to derive local balance relations at interfaces. Consider the domain $\Omega = \Omega_\alpha \cup \Omega_\beta$ divided by the interface Γ shown in Fig. A.5. Ω_α and Ω_β are bounded otherwise by Γ_α and Γ_β. As usual, an arbitrary field $\phi(\boldsymbol{x})$ is considered, with the values in each of the phases specified by $\phi_\alpha(\boldsymbol{x})$ and $\phi_\beta(\boldsymbol{x})$. For the control volumes $\Omega_{\alpha,\beta}$ the boundaries of the control volumes $\Gamma, \Gamma_{\alpha,\beta}$ are allowed to move with an arbitrary normal velocity function U that is uniformly 0 inside the domain. The balance law for each phase can now be written as,

$$\begin{aligned}\frac{D}{Dt}\int_{\Omega_{\alpha,\beta}} \phi_{\alpha,\beta}(\boldsymbol{x}) d\Omega_{\alpha,\beta} = &-\int_{\Gamma_{\alpha,\beta}} \boldsymbol{J}_{\alpha,\beta}.\boldsymbol{n}_{\alpha\beta} d\Gamma_{\alpha,\beta} - \int_{\Gamma} \boldsymbol{J}.\boldsymbol{n}_{\Gamma_{\alpha,\beta}} d\Gamma + \\ &\int_{\Gamma_{\alpha,\beta}} \phi_{\alpha,\beta}(\boldsymbol{x}) U_{\alpha,\beta} d\Gamma_{\alpha,\beta} + \int_{\Gamma} \phi_{\alpha,\beta}(\boldsymbol{x}) U_{\Gamma_{\alpha,\beta}} d\Gamma.\end{aligned} \tag{A.56}$$

The interface is now considered as a separate domain, bounded by the curve C. A surface density $\phi_\Gamma(\boldsymbol{x}_\Gamma)$ is defined which is changed by inflows due to a flux h in the tangent plane of the interface. The normal to the curve C in the tangent plane of Γ is denoted $\boldsymbol{m}$. The balance law for the interface is now written as,

$$\frac{D}{Dt}\int_{\Gamma} \phi_\Gamma(\boldsymbol{x}_\Gamma) d\Gamma = -\oint_C \boldsymbol{h}.\boldsymbol{m} dC + \oint_C \phi_\Gamma(\boldsymbol{x}_\Gamma) W_\Gamma dC. \tag{A.57}$$

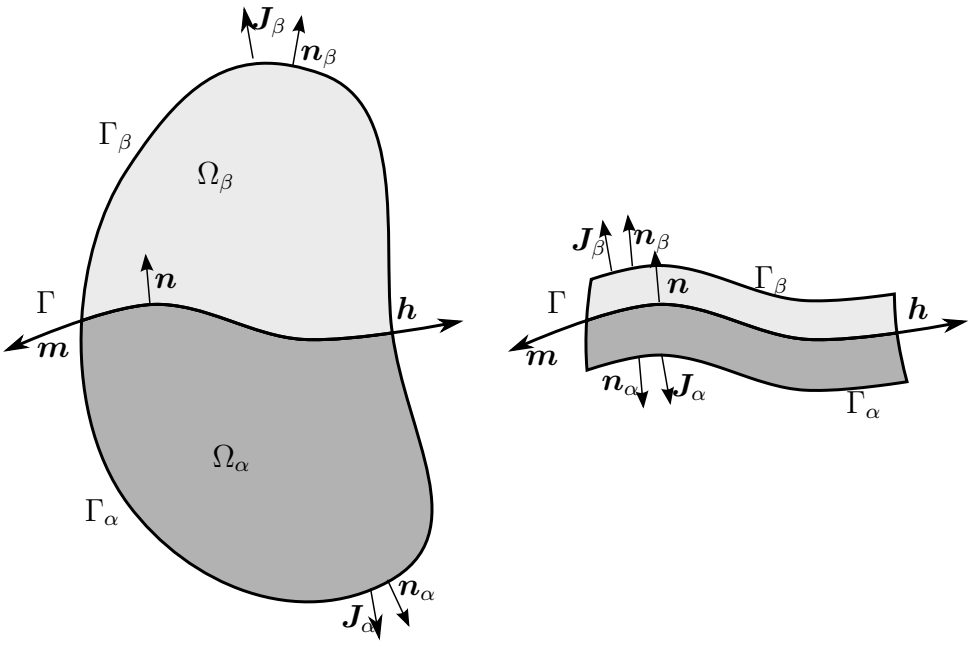

Figure A.5. Reducing an interfacial pillbox

In the above W_Γ is an accretive growth velocity of the control volume similar to U in Eq. (A.54). Using Eq. (A.45) and assuming that $\phi_\Gamma(\boldsymbol{x}_\Gamma)$ has a constant normal extension, the above can be written as

$$\int_\Gamma \left(\frac{\partial \phi_\Gamma(\boldsymbol{x}_\Gamma)}{\partial t} - \kappa \phi_\Gamma(\boldsymbol{x}_\Gamma) V_\Gamma \right) d\Gamma = - \int_\Gamma \nabla_\Gamma . \boldsymbol{h} d\Gamma + \oint_C \phi_\Gamma(\boldsymbol{x}_\Gamma)(W_\Gamma - \boldsymbol{v}_t . \boldsymbol{m}) dC. \tag{A.58}$$

To be able to define a transport theorem for the interfacial pillbox, Eqs. (A.56) and (A.57) need to be combined together. This leads to

$$\begin{aligned} \frac{D}{Dt} \left(\int_\Gamma \phi_\Gamma(\boldsymbol{x}_\Gamma) d\Gamma + \sum_{i=\alpha,\beta} \int_{\Omega_i} \phi_i(\boldsymbol{x}) d\Omega_i \right) = \sum_{i=\alpha,\beta} \Bigg(& - \int_{\Gamma_i} \boldsymbol{J}_i . \boldsymbol{n}_i d\Gamma_i - \int_\Gamma \boldsymbol{J} . \boldsymbol{n}_{\Gamma_i} d\Gamma \\ & + \int_{\Gamma_i} \phi_i(\boldsymbol{x}) U_i d\Gamma_i + \int_\Gamma \phi_i(\boldsymbol{x}) U_{\Gamma_i} d\Gamma \Bigg) \\ & - \int_\Gamma \nabla_\Gamma . \boldsymbol{h} d\Gamma + \oint_C \phi_\Gamma(\boldsymbol{x}_\Gamma) W_\Gamma dC. \end{aligned} \tag{A.59}$$

The following simplifications are made to Eq. (A.59).

1. The outer control surfaces $\Gamma_{\alpha,\beta}$ are now assumed to be infinitesimally close to the inner control surface Γ. As $\Gamma_{\alpha,\beta} \to \Gamma$, $\Omega \to 0$ and the bulk integral terms drop out.
2. The $\boldsymbol{n}_{\Gamma_\alpha}$ is set equal to $\boldsymbol{n}$. This implies that $\boldsymbol{n}_{\Gamma_\beta} = -\boldsymbol{n}$. Also, $\boldsymbol{n}_\alpha = -\boldsymbol{n}, \boldsymbol{n}_\beta = \boldsymbol{n}$.
3. The accretive normal velocities of the Γ interface from both sides, $\boldsymbol{u}_{\Gamma_{\alpha,\beta}}$ are set to be the same as the velocity of the interface $\boldsymbol{v}_\Gamma$. Together with the condition on the normals, this leads to,

$$V_\Gamma = U_{\Gamma_\alpha} = -U_{\Gamma_\beta}. \tag{A.60}$$

4. There is no flux that crosses the Γ interface. Hence $\int_\Gamma \boldsymbol{J}.\boldsymbol{n}_{\Gamma_i} d\Gamma = 0$.
5. The outer control loop for the interface Γ is held fixed, hence $W_\Gamma = 0$. It is also assumed that the accretion at the external boundaries can be neglected.
6. As the shape change of the interface is completely described by its normal velocity, the tangential velocity $\boldsymbol{v}_t = 0$.

These simplifications lead to,

$$\begin{aligned}\int_\Gamma \left(\frac{\partial \phi_\Gamma(\boldsymbol{x})}{\partial t} - \kappa \phi_\Gamma(\boldsymbol{x}) V_\Gamma \right) d\Gamma = &- \int_\Gamma (\boldsymbol{J}_\alpha - \boldsymbol{J}_\beta).\boldsymbol{n}_\Gamma d\Gamma \\ &+ \int_\Gamma \left(\phi_\alpha(\boldsymbol{x}) - \phi_\beta(\boldsymbol{x})\right) V_\Gamma d\Gamma \\ &- \int_\Gamma \nabla_\Gamma.\boldsymbol{h} d\Gamma.\end{aligned} \tag{A.61}$$

In the above, it is assumed that the derivatives are treated in a Lagrangian fashion. This leads to the absence of any convective terms, and consequently any fluxes across the boundary owing to the deformation motion of the system. The terms $(\boldsymbol{J}_\alpha - \boldsymbol{J}_\beta)$ and $(\phi_\alpha(\boldsymbol{x}) - \phi_\beta(\boldsymbol{x}))$ are replaced with $[\![\boldsymbol{J}]\!]$ and $[\![\phi(\boldsymbol{x})]\!]$. Using the fact that the domain

of integration Γ is arbitrary, and making the substitutions for the jump terms, a local form of the balance, valid at every point in the interface can be written as,

$$\frac{\partial \phi_\Gamma(\boldsymbol{x})}{\partial t} - \kappa \phi_\Gamma(\boldsymbol{x}) V_\Gamma = -\left[\!\left[\boldsymbol{J}\right]\!\right].\boldsymbol{n} + \left[\!\left[\phi(\boldsymbol{x})\right]\!\right] V_\Gamma - \nabla_\Gamma.\boldsymbol{h}. \tag{A.62}$$

While the above transport theorem was derived for a scalar field, similar relations can be defined for vector fields.

The above derivation is a reasonable transport theorem in the presence of evolution of interfaces in solids as accretion type processes are distinct from deformation type processes. The effect of deformation kinematics was limited in the previous derivation by using a purely Lagrangian approach, which eliminated all the convective terms. For a multiphase fluid, the same derivation can be carried out with the accretive velocities set to zero but with the convective components active.

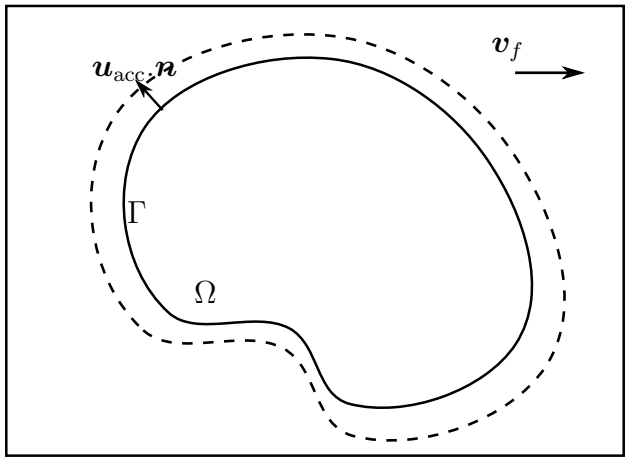

Figure A.6. Growing Eulerian control volume.

A.5.1 Interfacial Balance for Multiphase Fluids

Neglecting all the accretive velocities in Eq. (A.59), it can be rewritten as,

$$\frac{D}{Dt}\left(\int_{\Gamma}\phi_{\Gamma}(\boldsymbol{x}_{\Gamma})d\Gamma+\sum_{i=\alpha,\beta}\int_{\Omega_i}\phi(\boldsymbol{x})d\Omega_i\right)=\sum_{i=\alpha,\beta}\left(-\int_{\Gamma_i}\boldsymbol{J}_i.\boldsymbol{n}_i d\Gamma_i-\int_{\Gamma}\boldsymbol{J}.\boldsymbol{n}_{\Gamma_i}d\Gamma\right)-\int_{\Gamma}\nabla_{\Gamma}.\boldsymbol{h}d\Gamma. \tag{A.63}$$

Expanding the material derivatives in Eq. (A.63) and eliminating the bulk integrals in the limit as $\Gamma_{\alpha,\beta}\to\Gamma$, it can be rewritten as,

$$\begin{aligned}\int_{\Gamma}\left(\frac{\partial\phi_{\Gamma}(\boldsymbol{x}_{\Gamma})}{\partial t}-\phi_{\Gamma}(\boldsymbol{x}_{\Gamma})\kappa V_{\Gamma}\right)d\Gamma=\sum_{i=\alpha,\beta}\Bigg(&-\int_{\Gamma_i}\left(\boldsymbol{J}_i.\boldsymbol{n}_i-\phi(\boldsymbol{x})\boldsymbol{v}_i.\boldsymbol{n}_i\right)d\Gamma_i\\&-\int_{\Gamma}\left(\boldsymbol{J}.\boldsymbol{n}_{\Gamma_i}-\phi(\boldsymbol{x})\boldsymbol{v}_i.\boldsymbol{n}_{\Gamma_i}\right)d\Gamma\Bigg)\\&-\int_{\Gamma}\left(\nabla_{\Gamma}.\boldsymbol{h}+\nabla_{\Gamma}.(\phi_{\Gamma}(\boldsymbol{x}_{\Gamma})\boldsymbol{v}_{\Gamma t})\right)d\Gamma.\end{aligned} \tag{A.64}$$

The following simplifications are now applied Eq. (A.64)

1. There is no flux that goes across the interface Γ. Also there is no convective flux of $\phi(\boldsymbol{x})$ across the interface. This also implies $\boldsymbol{v}_{\alpha}=\boldsymbol{v}_{\Gamma}=\boldsymbol{v}_{\beta}$.
2. The normal points from α into β, and is the same as the normal to the interface.

$$\boldsymbol{n}_{\Gamma}=\boldsymbol{n}_{\Gamma_{\alpha}}=-\boldsymbol{n}_{\Gamma_{\beta}}. \tag{A.65}$$

$$\begin{aligned}\int_{\Gamma}\left(\frac{\partial\phi_{\Gamma}(\boldsymbol{x}_{\Gamma})}{\partial t}-\phi_{\Gamma}(\boldsymbol{x}_{\Gamma})\kappa V_{\Gamma}\right)d\Gamma=&-\int_{\Gamma}[\![\boldsymbol{J}\boldsymbol{n}_{\Gamma}]\!]\,d\Gamma-\int_{\Gamma}[\![\phi(\boldsymbol{x})V_{\Gamma}]\!]\,d\Gamma-\\&-\int_{\Gamma}\nabla_{\Gamma}.(\boldsymbol{h}+\nabla_{\Gamma}.(\phi_{\Gamma}(\boldsymbol{x}_{\Gamma})\boldsymbol{v}_{\Gamma t})d\Gamma.\end{aligned} \tag{A.66}$$

As the domain of integration is arbitrary, the following is true at every point on the interface

$$\frac{\partial \phi_\Gamma(\boldsymbol{x}_\Gamma)}{\partial t} - \phi_\Gamma(\boldsymbol{x}_\Gamma)\kappa V_\Gamma = [\![\boldsymbol{J}]\!] . \boldsymbol{n}_\Gamma - [\![\phi(\boldsymbol{x})]\!] V_\Gamma - \nabla_\Gamma . (\boldsymbol{h} + \phi_\Gamma(\boldsymbol{x}_\Gamma)\boldsymbol{v}_{\Gamma t}). \tag{A.67}$$

B. COORDINATE TRANSFORMATIONS FOR USE IN ASYMPTOTIC ANALYSIS

In phase field models dependent on a notional interfacial parameter thickness ϵ, and a bulk free energy function $F(\phi)$ that has only numerical meaning, it is necessary to show the equivalence of the phase field equations to corresponding sharp interface equations. This is done best when the differential equations are transformed into a moving coordinate system attached to an interface Γ moving with a normal velocity $V\boldsymbol{n}$ (Fig. B.1). This appendix describes the process of transforming the equations into this frame. The derivation here is based on the derivation in [68].

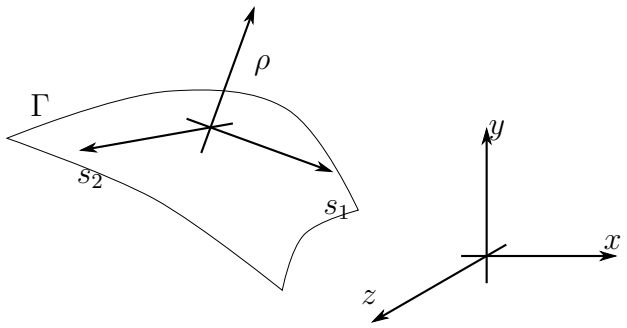

Figure B.1. Transformation of coordinate system from a global coordinate system to an interface attached coordinate system.

Consider a point $\boldsymbol{p}$ described as

$$\boldsymbol{p}_{\hat{\boldsymbol{e}}_{123}} = x_1\hat{\boldsymbol{e}}_{x_1} + x_2\hat{\boldsymbol{e}}_{x_2} + x_3\hat{\boldsymbol{e}}_{x_3}. \tag{B.1}$$

In an interface attached coordinate frame, this can be written as

$$\boldsymbol{p}_{\Gamma} = s_1\hat{\boldsymbol{e}}_{s_1} + s_2\hat{\boldsymbol{e}}_{s_2} + r\boldsymbol{n}. \tag{B.2}$$

In the above $\hat{\boldsymbol{e}}_{s_1,s_2}$ are two arbitrary directions in the plane tangential to the interface at an arbitrary origin on the interface at $\boldsymbol{O}_\Gamma$. $\boldsymbol{n}$ is the unit normal to the interface at $\boldsymbol{O}_\Gamma$, with the orientation as chosen. r is the normal signed distance from the interface. While working with the inner solution, the coordinate system is also scaled by $\frac{1}{\epsilon}$. Hence, the point p is written in the scaled coordinate system as

$$\boldsymbol{p}_\Gamma = s_1\hat{\boldsymbol{e}}_{s_1} + s_2\hat{\boldsymbol{e}}_{s_2} + \rho\boldsymbol{n}. \tag{B.3}$$

In the above,

$$\rho = \frac{r}{\epsilon}. \tag{B.4}$$

Given a scalar field $u(\boldsymbol{x}, t)$, it can be written in the transformed interface attached coordinate frame as $u(\boldsymbol{r}, t)$. The temporal and spatial derivatives of this field $u(\boldsymbol{r}, t)$ need to be written in terms of this moving coordinate frame.

B.1 Time Derivatives

The temporal derivative of the field $u(\boldsymbol{r}, t)$ can be written as,

$$\frac{\partial u(\boldsymbol{x}, t)}{\partial t} = \frac{\partial u}{\partial t} + \frac{\partial \boldsymbol{r}}{\partial t}.\nabla_{\boldsymbol{r}} u. \tag{B.5}$$

In the above $\frac{\partial \boldsymbol{r}}{\partial t}$ is the term associated with the evolution of the coordinate system, while $\nabla_{\boldsymbol{r}} u$ is the gradient of the field u in the coordinate system. The gradient of a function $f(\boldsymbol{r})$ in the coordinate system can be written as,

$$\nabla_{\boldsymbol{r}} f = \frac{\partial f}{\partial s_1}\hat{\boldsymbol{e}}_{s_1} + \frac{\partial f}{\partial s_2}\hat{\boldsymbol{e}}_{s_2} + \frac{\partial f}{\partial r}\boldsymbol{n} \tag{B.6}$$

The two tangential components of the gradient are referred to as the surface gradient of the function f, given by

$$\nabla_\Gamma f = \frac{\partial f}{\partial s_1}\hat{\boldsymbol{e}}_{s_1} + \frac{\partial f}{\partial s_2}\hat{\boldsymbol{e}}_{s_2}. \tag{B.7}$$

The other term in the time derivative (Eq. (B.5)) is the time derivative of the position vector $\boldsymbol{r}$. Instantaneously in the interface attached coordinate frame, this can be written as

$$\frac{\partial \boldsymbol{r}}{\partial t} = \frac{\partial s_1}{\partial t}\hat{\boldsymbol{e}}_{s_1} + \frac{\partial s_2}{\partial t}\hat{\boldsymbol{e}}_{s_2} + \frac{\partial r}{\partial t}\boldsymbol{n}. \tag{B.8}$$

The signed distance from the interface r satisfies the level-set equation. This is due to the fact that a point on the interface is always at 0 distance from the interface.

$$\frac{D}{Dt}r = \frac{\partial r}{\partial t} + \boldsymbol{v}.\nabla r = 0. \tag{B.9}$$

As the distance function is a linearly increasing function with no tangential variation

$$\nabla r = \frac{\partial r}{\partial r}\boldsymbol{n} = \boldsymbol{n}. \tag{B.10}$$

This allows the time derivative of the distance to be written as

$$\frac{\partial r}{\partial t} + \boldsymbol{v}.\boldsymbol{n} = 0, \tag{B.11}$$

or

$$\frac{\partial r}{\partial t} = -V. \tag{B.12}$$

Using Eqs. (B.8) and (B.12) in Eq. (B.5), the time derivative of $u(\boldsymbol{r}, t)$ can be written as,

$$\frac{D}{Dt}u = \frac{\partial u}{\partial t} - V\frac{\partial u}{\partial r} + \nabla_\Gamma u.\left(\frac{\partial s_1}{\partial t}\hat{\boldsymbol{e}}_{s_1} + \frac{\partial s_2}{\partial t}\hat{\boldsymbol{e}}_{s_2}\right). \tag{B.13}$$

In the scaled coordinate system,

$$\frac{\partial u}{\partial r} = \frac{\partial u}{\partial \rho}\frac{\partial \rho}{\partial r} = \frac{1}{\epsilon}\frac{\partial u}{\partial \rho}. \tag{B.14}$$

Hence,

$$\frac{D}{Dt}u = \frac{\partial u}{\partial t} - V\frac{1}{\epsilon}\frac{\partial u}{\partial \rho} + \nabla_\Gamma u.\left(\frac{\partial s_1}{\partial t}\hat{\boldsymbol{e}}_{s_1} + \frac{\partial s_2}{\partial t}\hat{\boldsymbol{e}}_{s_2}\right). \tag{B.15}$$

B.2 Spatial Derivatives

In this section the spatial derivatives of quantities are transformed from a coordinate system $\{x_1, x_2, x_3\}$ to a coordinate system $\{s_1, s_2, r\}$. First the gradient is derived, followed by the Laplacian. The derivation of the Laplacian is more relevant to the purposes of this document as it provides a way to introduce the effects of curvature into diffuse interface models.

B.2.1 Gradient of a Function

The gradient in the $\{x_1, x_2, x_3\}$ coordinate system can be related to the gradient in the $\{s_1, s_2, r\}$ coordinate system through the Jacobian of transformation as follows,

$$\nabla u = \left[\frac{\partial s_i}{\partial x_j}\right]^T .\nabla_\Gamma u + \frac{\partial u}{\partial r}\nabla r. \tag{B.16}$$

For vector functions, transforming the derivatives of a vector function $\boldsymbol{u}(x_1, x_2, x_3)$ to a co-ordinate system $\boldsymbol{u}(s_1, s_2, r)$, can be accomplished in the same manner.

$$\nabla \boldsymbol{u}(x_1, x_2, x_3) = \frac{\partial \boldsymbol{u}}{\partial r} \otimes \nabla r + \frac{\partial \boldsymbol{u}}{\partial s_1} \otimes \nabla s_1 + \frac{\partial \boldsymbol{u}}{\partial s_2} \otimes \nabla s_2, \tag{B.17}$$

$$= \frac{\partial \boldsymbol{u}}{\partial r} \otimes \boldsymbol{n} + \frac{\partial \boldsymbol{u}}{\partial s_1} \otimes \nabla s_1 + \frac{\partial \boldsymbol{u}}{\partial s_2} \otimes \nabla s_2. \tag{B.18}$$

The divergence of the function can now be defined as the trace of Eq. (B.17). This leads to,

$$\nabla . \boldsymbol{u}(x_1, x_2, x_3) = \frac{\partial \boldsymbol{u}}{\partial r} . \boldsymbol{n} + \frac{\partial \boldsymbol{u}}{\partial s_1} . \nabla s_1 + \frac{\partial \boldsymbol{u}}{\partial s_2} . \nabla s_2. \tag{B.19}$$

In the scaled co-ordinate system, the above can be written as,

$$\nabla . \boldsymbol{u}(x_1, x_2, x_3) = \frac{1}{\epsilon} \frac{\partial \boldsymbol{u}}{\partial \rho} . \boldsymbol{n} + \frac{\partial \boldsymbol{u}}{\partial s_1} . \nabla s_1 + \frac{\partial \boldsymbol{u}}{\partial s_2} . \nabla s_2. \tag{B.20}$$

The above relation is now used to derive a relation for the Laplacian of a function in the two coordinate systems.

B.2.2 Laplacian of a Function

The Laplacian $\nabla^2 u$ of a function u is defined as,

$$\nabla^2 u = \nabla . (\nabla u). \tag{B.21}$$

Using Eq. (B.16), the Laplacian in the $\{x_1, x_2, x_3\}$ coordinate system can be written as

$$\nabla^2 u = \nabla.(\nabla u) \tag{B.22}$$

$$= \nabla.\left(\left[\frac{\partial s_i}{\partial x_j}\right]^T.\nabla_\Gamma u + \frac{\partial u}{\partial r}\nabla r\right) \tag{B.23}$$

$$= \underbrace{\nabla.\left(\left[\frac{\partial s_i}{\partial x_j}\right]^T \nabla_\Gamma u\right)}_{I} + \underbrace{\nabla.\left(\frac{\partial u}{\partial r}\nabla r\right)}_{II}. \tag{B.24}$$

The terms I and II can now be evaluated separately. Term I can be expanded as follows,

$$I = \nabla.\left(\left[\frac{\partial s_i}{\partial x_j}\right]^T.\nabla_\Gamma u\right) \tag{B.25}$$

$$= \nabla.\left(\left[\frac{\partial s_i}{\partial x_j}\right]\right).\nabla_\Gamma u + \left[\frac{\partial s_i}{\partial x_j}\right]^T : \nabla(\nabla_\Gamma u). \tag{B.26}$$

In the above, the fact $\left[\frac{\partial s_i}{\partial x_j}\right]^T.\nabla r = 0$ is used. This is due to the fact that $\left[\frac{\partial s_i}{\partial x_j}\right]$ is a tensor that is tangential to the interface, while ∇r is normal to the interface. Hence any normal components drop out while evaluating the term and only tangential components remain. The term Eq. (B.26) is referred to as the surface laplacian of u. Evaluating the term II,

$$II = \nabla.\left(\frac{\partial u}{\partial r}\nabla r\right) \tag{B.27}$$

$$= \nabla(\frac{\partial u}{\partial r}).\nabla r + \frac{\partial u}{\partial r}\nabla^2 r \tag{B.28}$$

$$= \frac{\partial^2 u}{\partial r^2} + \frac{\partial u}{\partial r}\nabla^2 r. \tag{B.29}$$

As,

$$\nabla^2 r = \nabla.(\nabla r) = \nabla.\boldsymbol{n} \tag{B.30}$$

for interfaces with small curvature, $\nabla_\Gamma \approx \nabla$ and for small r

$$\nabla.\boldsymbol{n} \approx \nabla_\Gamma.\boldsymbol{n} + O(r) = -\kappa + O(r). \tag{B.31}$$

Hence II can be written as being approximately equal to,

$$II \approx \frac{\partial^2 u}{\partial r^2} - \frac{\partial u}{\partial r}\kappa + O(r). \tag{B.32}$$

Using Eq. (B.26) and § B.2.2, the Laplacian of u in the $\{s_1, s_2, r\}$ coordinate system can be written as

$$\nabla^2 u = \nabla_\Gamma^2 u + \frac{\partial^2 u}{\partial r^2} - \frac{\partial u}{\partial r}\kappa + O(r). \tag{B.33}$$

In the scaled coordinate system, can now be written as

$$\nabla^2 u = \nabla_\Gamma^2 u + \frac{1}{\epsilon^2}\frac{\partial^2 u}{\partial \rho^2} - \frac{1}{\epsilon}\frac{\partial u}{\partial \rho}\kappa + O(r). \tag{B.34}$$

In the above, the curvature is still being measured in the same length-scale as r.

C. MATCHING CONDITIONS FOR FORMAL ASYMPTOTIC ANALYSIS

Showing the equivalence of diffuse interface equations to sharp interface formulations derivable from continuum mechanics can be achieved in multiple ways. The first is through the means of Γ - convergence [60], where the equivalence is shown through the convergence of a series of minimizers to an energy functional in a phase field form to a sharp interface equation. This approach is very demanding mathematically, and becomes more involved with the addition of additional physics to the phase field equations.

The alternative approach is through the use of formal asymptotic analysis. In formal asymptotic analysis the solution to the phase field equation is *assumed to exist*. This solution to the phase field equation has a form where there is a rapid variation next to the interface and a more or less constant value is reached at distances which are *very far* from the interface. This allows the solution to be split into two parts, one which is valid close to the interface, called the *inner* solution and another that is valid at longer length scales called the *outer* solution (Fig. C.1).

These assumed solutions are substituted into the phase field equation and their behavior is studied as $\epsilon \to 0$. Care must be taken to choose a coordinate system for the analysis, where it is easy to solve the equations analytically. Typically for interface evolution processes, interfacial coordinate systems are best, especially when tangential variation is not expected to play a significant role. In the normal direction, the partial differential equations can be reduced to one-dimensional ordinary or partial differential equations. The main condition with which these solutions are tested is that the inner and outer solutions need to match in the domain where the two solutions overlap. This implies that the value of the inner solution at a point far away from the interface, should match with the value of the outer solution at a point close to the interface. Some essential matching relations are developed for 1-D systems in this

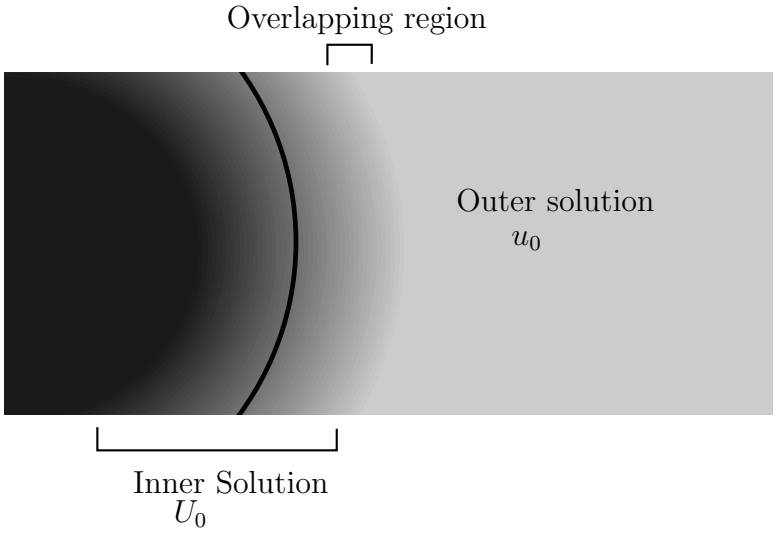

Figure C.1. Validity of the inner and outer solution in asymptotic analysis. In most cases the inner, outer and overlapping regions are only definable as limits.

appendix. More details can be found in [59, 168]. The approach here is based on the derivations in [59].

C.1 Inner and Outer Solutions

In this section, the distance from the interface is parametrized by r. In addition a length scale ϵ is specified so that the extent of the influence of the inner solution is $O(\epsilon)$. The outer solution is written as $u(r)$. The inner solution is written as $U(\rho)$, where $\rho = \frac{r}{\epsilon}$. As they are both solutions to the same equation, they should match in the overlapping region. This is expressed as,

$$\lim_{\rho \to \infty} U(\rho) = \lim_{r \to 0} u(r). \tag{C.1}$$

It is assumed that the solutions $U(\rho)$ and $u(r)$ are differentiable, and as they are describing the same function, the first derivatives of both functions should match in the overlapping region.

$$\lim_{\rho\to\infty} \frac{\partial U(\rho)}{\partial r} = \lim_{r\to 0} \frac{\partial u(r)}{\partial r} \tag{C.2}$$

Or, using the chain rule

$$\lim_{\rho\to\infty} \frac{1}{\epsilon}\frac{\partial U(\rho)}{\partial \rho} = \lim_{r\to 0} \frac{\partial u(r)}{\partial r}. \tag{C.3}$$

It is not possible to obtain the solutions U and u at the same time. Instead, as the functions are assumed to be differentiable, the solutions are written as an expansion in powers of ϵ. The outer solution is expanded as

$$u(r) = u_0(r) + \epsilon u_1(r) + \epsilon^2 u_2(r) + \epsilon^3 u_3(r) + \dots. \tag{C.4}$$

For the inner solution, the expansion is written as

$$U(\rho) = U_0(\rho) + \epsilon U_1(\rho) + \epsilon^2 U_2(\rho) + \epsilon^3 U_3(\rho) + \dots. \tag{C.5}$$

These solutions can be determined by substituting these into the differential equation (written in terms of r and ρ for the outer and inner solutions) and grouping terms by powers of ϵ. This will lead to an equation for each power of ϵ considered in the inner and outer solution. These equations need to be solved with boundary conditions derived from the matching conditions in the following section.

C.2 Derivation of Matching Conditions

The matching conditions for the function value are first derived. Substituting $r = \epsilon\rho$ into Eq. (C.1), and considering terms up to ϵ^2,

$$U_0(\rho) + \epsilon U_1(\rho) + \epsilon^2 U_2(\rho) = u_0(\epsilon\rho) + \epsilon u_1(\epsilon\rho) + \epsilon^2 u_2(\epsilon\rho) + O(\epsilon^3). \tag{C.6}$$

The terms on the right hand side are now each expanded in a Taylor series in r around $r = 0$. Keeping all terms up to the quadratic and grouping in terms of ϵ,

$$\begin{aligned} U_0(\rho) + \epsilon U_1(\rho) + \epsilon^2 U_2(\rho) =& u_0(0) + \epsilon \left(\frac{\partial u_0}{\partial r}\Big|_{r=0}\rho + u_1(0) \right) \\ &+ \epsilon^2 \left(\frac{1}{2}\frac{\partial^2 u_0}{\partial r^2}\Big|_{r=0}\rho^2 + \frac{\partial u_1}{\partial r}\Big|_{r=0}\rho + u_2(0) \right) \ldots \end{aligned} \tag{C.7}$$

Moving all the terms over to one side,

$$\begin{aligned} U_0(\rho) - u_0(0) + \epsilon \left(U_1(\rho) - \left(\frac{\partial u_0}{\partial r}\Big|_{r=0}\rho + u_1(0) \right) \right) \\ + \epsilon^2 \left(U_2(\rho) - \left(\frac{1}{2}\frac{\partial^2 u_0}{\partial r^2}\Big|_{r=0}\rho^2 + \frac{\partial u_1}{\partial r}\Big|_{r=0}\rho + u_2(0) \right) \right) \ldots = 0. \end{aligned} \tag{C.8}$$

As ϵ is a positive number, the co-efficients of each power of ϵ should be 0 in order for Eq. (C.8) to be 0. This leads to the following matching conditions for terms up to ϵ^2 as $\epsilon \to 0$ and $\rho \to \infty$,

$$U_0(\rho) = u_0(0) \tag{C.9a}$$

$$U_1(\rho) = u_1(0) + \frac{\partial u_0}{\partial r}\Big|_{r=0}\rho \tag{C.9b}$$

$$U_2(\rho) = u_2(0) + \frac{\partial u_1}{\partial r}\Big|_{r=0}\rho + \frac{1}{2}\frac{\partial^2 u_0}{\partial r^2}\rho^2\Big|_{\rho\to 0}. \tag{C.9c}$$

In the above approach, it is assumed that $\epsilon \to 0$ faster than $\rho \to \infty$. A similar approach is used to derive the matching conditions for the derivatives of the inner and the outer solution,

$$\frac{\partial U_0}{\partial \rho} + \epsilon \frac{\partial U_1}{\partial \rho} + \epsilon^2 \frac{\partial U_2}{\partial \rho} = \frac{\partial u_0(\epsilon\rho)}{\partial \rho} + \epsilon \frac{\partial u_1(\epsilon\rho)}{\partial \rho} + \epsilon^2 \frac{\partial u_2(\epsilon\rho)}{\partial \rho} + \dots \tag{C.10}$$

Again expanding the right hand side using a Taylor series around $r = 0$, and using $\frac{\partial u}{\partial \rho} = \frac{\partial r}{\partial \rho}\frac{\partial u}{\partial r} = \epsilon \frac{\partial u}{\partial r}$ the above can be written as

$$\frac{\partial U_0}{\partial \rho} + \epsilon \frac{\partial U_1}{\partial \rho} + \epsilon^2 \frac{\partial U_2}{\partial \rho} = \epsilon \frac{\partial u_0}{\partial r}\Big|_{r=0} + \epsilon^2 \left(\frac{1}{2} \frac{\partial^2 u_0}{\partial r^2}\Big|_{r=0} \rho + \frac{\partial u_1}{\partial r} \right) + \dots \tag{C.11}$$

By the same arguments as for the solution value, the matching conditions for the gradient can be written as,

$$\frac{\partial U_0}{\partial \rho} = 0 \tag{C.12a}$$

$$\frac{\partial U_1}{\partial \rho} = \frac{\partial u_0}{\partial r}\Big|_{r=0} \tag{C.12b}$$

$$\frac{\partial U_2}{\partial \rho} = \frac{1}{2} \frac{\partial^2 u_0}{\partial r^2}\Big|_{r=0} \rho + \frac{\partial u_1}{\partial r}\Big|_{r=0}. \tag{C.12c}$$

Usually, the leading and the first order terms are the ones of most interest.

D. NECESSARY INTEGRALS FOR ASYMPTOTIC ANALYSIS

In this appendix, the integrals necessary for asymptotic analysis for various choices of the regularized Heaviside and Dirac delta functions are specified. This is useful for deriving the constants necessary to scale the modified PDE appropriately to recover the sharp interface equations. The sinusoidal and hyperbolic tangent regularization functions are described here.

D.1 Sinusoidal Regularization

The sinusoidal regularization function is obtained as the solution to the phase field equations with the obstacle potential. This is due to the fact that they are the solutions to the differential equation,

$$\alpha\phi_{rr} + \beta\phi = 0. \tag{D.1}$$

The solutions to the above equation are of the form $\sin\sqrt{\frac{\beta}{\alpha}}r, \cos\sqrt{\frac{\beta}{\alpha}}r$. The Heaviside function associated with the solution to Eq. (D.1) can be written as,

$$h(r) = \begin{cases} 0, & \text{if } r \leq -\frac{\pi}{2}\sqrt{\frac{\alpha}{\beta}} \\ \frac{1+\sin\sqrt{\frac{\beta}{\alpha}}r}{2}, & -\frac{\pi}{2}\sqrt{\frac{\alpha}{\beta}} \leq r \leq \frac{\pi}{2}\sqrt{\frac{\alpha}{\beta}} \\ 1, & r \geq \frac{\pi}{2}\sqrt{\frac{\alpha}{\beta}}. \end{cases} \tag{D.2}$$

The first option for use as a Dirac δ function is,

$$g(r) = h'(r) = \begin{cases} 0, & |r| \geq \frac{\pi}{2}\sqrt{\frac{\alpha}{\beta}} \\ \frac{c}{2}\sqrt{\frac{\beta}{\alpha}}\cos\sqrt{\frac{\beta}{\alpha}}r, & |r| \leq \frac{\pi}{2}\sqrt{\frac{\alpha}{\beta}} \end{cases}. \tag{D.3}$$

This needs to be normalized so that $\int_{-\infty}^{\infty}\delta(r)=1$. For the function in Eq. (D.3), the integral is c and hence no further normalization is required. If instead of the $h'(r)$, $\phi'(r)$ is used as the Dirac δ function, the integral can be written as,

$$\int_{-\infty}^{\infty}\phi'(r)=\int_{-\frac{\pi}{2}\sqrt{\frac{\alpha}{\beta}}}^{\frac{\pi}{2}\sqrt{\frac{\alpha}{\beta}}}\sqrt{\frac{\beta}{\alpha}}\cos\sqrt{\frac{\beta}{\alpha}}r=2. \tag{D.4}$$

This implies that the normalization constant c is $\frac{1}{2}$. The most common Dirac δ function associated with the sinusoidal regularization is,

$$\delta(r)=c\left(1-\phi^2\right)=\begin{cases}0, & |r|\geq\frac{\pi}{2}\sqrt{\frac{\alpha}{\beta}}\\ c\cos^2\sqrt{\frac{\beta}{\alpha}}r, & |r|\leq\frac{\pi}{2}\sqrt{\frac{\alpha}{\beta}}.\end{cases} \tag{D.5}$$

The normalization constant for the above is derived by integration from $-\infty$, to ∞. This leads to,

$$\int_{-\infty}^{\infty}\delta(r)=c\int_{-\frac{\pi}{2}\sqrt{\frac{\alpha}{\beta}}}^{\frac{\pi}{2}\sqrt{\frac{\alpha}{\beta}}}\cos^2\sqrt{\frac{\alpha}{\beta}}r=\frac{c\pi}{2}\sqrt{\frac{\alpha}{\beta}}. \tag{D.6}$$

This leads to

$$\implies c=\frac{2}{\pi}\sqrt{\frac{\beta}{\alpha}}. \tag{D.7}$$

The final option for the Dirac δ function is,

$$\delta(r)=ch(r)(1-h(r))==\begin{cases}0, & |r|\geq\frac{\pi}{2}\sqrt{\frac{\alpha}{\beta}}\\ \frac{c}{4}\cos^2\sqrt{\frac{\beta}{\alpha}}r, & |r|\leq\frac{\pi}{2}\sqrt{\frac{\alpha}{\beta}}\end{cases}. \tag{D.8}$$

Integration of the above shows the normalization constant to be,

$$\implies c=\frac{8}{\pi}\sqrt{\frac{\beta}{\alpha}}. \tag{D.9}$$

D.2 Hyperbolic Tangent Regularization

The hyperbolic tangent regularization functions are obtained as solutions to the phase field equations with the biquadratic obstacle potential. The hyperbolic tangent functions are solutions to the differential equation,

$$-\alpha\phi_{rr} + f'(\phi) = 0. \tag{D.10}$$

Where

$$f(\phi) = \beta\left(1-\phi^2\right)^2 \tag{D.11}$$

or

$$f'(\phi) = -4\beta\left(\phi-\phi^3\right). \tag{D.12}$$

One of the solutions Eq. (D.10) is,

$$\phi(r) = \tanh\sqrt{\frac{2\beta}{\alpha}}r. \tag{D.13}$$

The Heaviside function associated with the solution in Eq. (D.13) can be written as,

$$h(r) = \frac{1+\phi(r)}{2}. \tag{D.14}$$

The Dirac δ functions associated with the above expressions for $\phi(r)$ and $h(r)$ are similar to the expressions in § D.1. The first one considered is $\delta(r) = ch'(r)$. Integrating $h'(r)$ from $-\infty$ to ∞,

$$c\int_{-\infty}^{\infty} h'(r)dr = c\int_{-\infty}^{\infty} \frac{1+\tanh\sqrt{\frac{2\beta}{\alpha}}r}{2}dr. \tag{D.15}$$

For Eq. (D.15), $c = 1$. Similar to the derivation in § D.1, for the Dirac δ function $\phi'(r)$, the factor $c = \frac{1}{2}$. The next Dirac δ function approximation that needs to be considered is,

$$\delta(r) = c(1 - \phi^2) = c\text{sech}^2\sqrt{\frac{2\beta}{\alpha}}r. \tag{D.16}$$

This can be integrated over $(-\infty, \infty)$ to get $c = \sqrt{\frac{\beta}{2\alpha}}$. For the Dirac δ function specified by,

$$\delta(r) = c(1 - \phi^2)^2 = c\text{sech}^4\sqrt{\frac{2\beta}{\alpha}}r \tag{D.17}$$

The value of the normalization constant for this version of the Dirac δ function is found by integration to be,

$$c = \frac{3}{2\sqrt{2}}\sqrt{\frac{\beta}{\alpha}}. \tag{D.18}$$

The final Dirac δ functions are in terms of $h(r)$. The simplest one is defined as $\delta(r) = c(h(r)(1 - h(r))$. This can also be written as,

$$\delta(r) = c(h(r)(1 - h(r)) = \frac{c}{4}\text{sech}^2\sqrt{\frac{2\beta}{\alpha}}r. \tag{D.19}$$

The constant c can be shown to be $2\sqrt{\frac{2\beta}{\alpha}}$. For the squared version of the above, written as, $\delta(r) = ch(r)^2(1 - h(r))^2$, the simplified version can be written as,

$$\delta(r) = \frac{c}{16}\text{sech}^4\sqrt{\frac{2\beta}{\alpha}}. \tag{D.20}$$

where the constant c can be shown to be equal to $12\sqrt{\frac{2\beta}{\alpha}}$.

D.3 Summary

The results in the above sections are summarized in terms of functions of r in Table D.1, and the Dirac δ functions in terms of the phase field function in Table D.2.

Table D.1. Summary of Heaviside and Dirac δ functions used in phase field models in terms of r.

	Sinusoidal	Hyperbolic Tangent
Solution $\phi(r)$	$\begin{cases} -1, & r \le -\frac{\pi}{2}\sqrt{\frac{\alpha}{\beta}} \\ \sin\sqrt{\frac{\beta}{\alpha}}r, & -\frac{\pi}{2}\sqrt{\frac{\alpha}{\beta}} \le r \le \frac{\pi}{2}\sqrt{\frac{\alpha}{\beta}} \\ 1, & r \ge \frac{\pi}{2}\sqrt{\frac{\alpha}{\beta}}. \end{cases}$	$\tanh\sqrt{\frac{2\beta}{\alpha}}r$
Dirac δ : $c\phi'(r)$	$\begin{cases} 0, & \lvert r\rvert \ge \frac{\pi}{2}\sqrt{\frac{\alpha}{\beta}} \\ \frac{1}{2}\sqrt{\frac{\beta}{\alpha}}\cos\sqrt{\frac{\beta}{\alpha}}r, & \lvert r\rvert \le \frac{\pi}{2}\sqrt{\frac{\alpha}{\beta}} \end{cases}$	$\frac{1}{2}\sqrt{\frac{2\beta}{\alpha}}\mathrm{sech}^2\sqrt{\frac{2\beta}{\alpha}}r$
Dirac δ : $c(1-\phi(r)^2)$	$\begin{cases} 0, & \lvert r\rvert \ge \frac{\pi}{2}\sqrt{\frac{\alpha}{\beta}} \\ \frac{2}{\pi}\sqrt{\frac{\beta}{\alpha}}\cos^2\sqrt{\frac{\beta}{\alpha}}r, & \lvert r\rvert \le \frac{\pi}{2}\sqrt{\frac{\alpha}{\beta}} \end{cases}$	”
Dirac δ : $c(1-\phi(r)^2)^2$	–	$\frac{3}{2\sqrt{2}}\sqrt{\frac{\beta}{\alpha}}\mathrm{sech}^4\sqrt{\frac{2\beta}{\alpha}}r$

Table D.2. Values of c for various Dirac δ functions in terms of $\phi(r)$ or $h(r)$.

Dirac δ	Sinusoidal	Hyperbolic Tangent
$c\phi'$	$\frac{1}{2}$	$\frac{1}{2}$
ch'	1	1
$c(1-\phi^2)$	$\frac{2}{\pi}\sqrt{\frac{\beta}{\alpha}}$	$\sqrt{\frac{\beta}{2\alpha}}$
$c(1-\phi^2)^2$	–	$\frac{3}{2\sqrt{2}}\sqrt{\frac{\beta}{\alpha}}$
$ch(1-h)$	$\frac{8}{\pi}\sqrt{\frac{\beta}{\alpha}}$	$2\sqrt{\frac{2\beta}{\alpha}}$
$ch^2(1-h)^2$	–	$12\sqrt{\frac{2\beta}{\alpha}}$

E. DIFFCODE: A SIMULATION SYSTEM TO STUDY DIFFUSION DRIVEN FAILURE IN INTERCONNECTS

The structure and use of the simulation tool, `DiffCode` developed in this thesis is described in this appendix. `DiffCode` is a C++ code developed using the `libMesh` finite element toolkit [137]. The `libMesh` finite element toolkit is developed in C++ on top of many well tested and widely used scientific software suites. It has the ability to use either the `PETSc`, [138, 169, 170] or the `Trilinos` [144] suite of linear and non-linear solvers. Other software packages that are used by `libMesh` are Metis and Parmetis for the construction of sparsity patterns and for partitioning the mesh for parallel simulations. `libMesh` allows the usage of the `Exodus II, VTK` and `Tecplot` tools for output and visualization. It has been used widely over the past 10 years for various large scale simulation tools, including the `MOOSE` [171] framework for the simulation of large scale multi-physics problems.

E.1 Code Structure

`DiffCode` has approximately 6000 lines of code built on top of `libMesh` and assumes that `PETSc` is available. At present, it is not possible to use `DiffCode` with other solver packages such as Trilinos. The problem information is stored in a main class called `DiffCode`. This class is derived from the `libMesh` `EquationSystems` class and acts as a container for all the classes corresponding to the solutions of the driving fields and the phase-field solver. The class also has methods to read the input files for material properties, geometry definition, time stepping and choice of output fields. The rest of the code consists of solver classes for the solution of the different fields. There is also an additional solver class for the computation of nodal approximations

to element quantities. Additionally there are classes which are used for storage of computed fields. The general structure of the code is described in Fig. E.1.

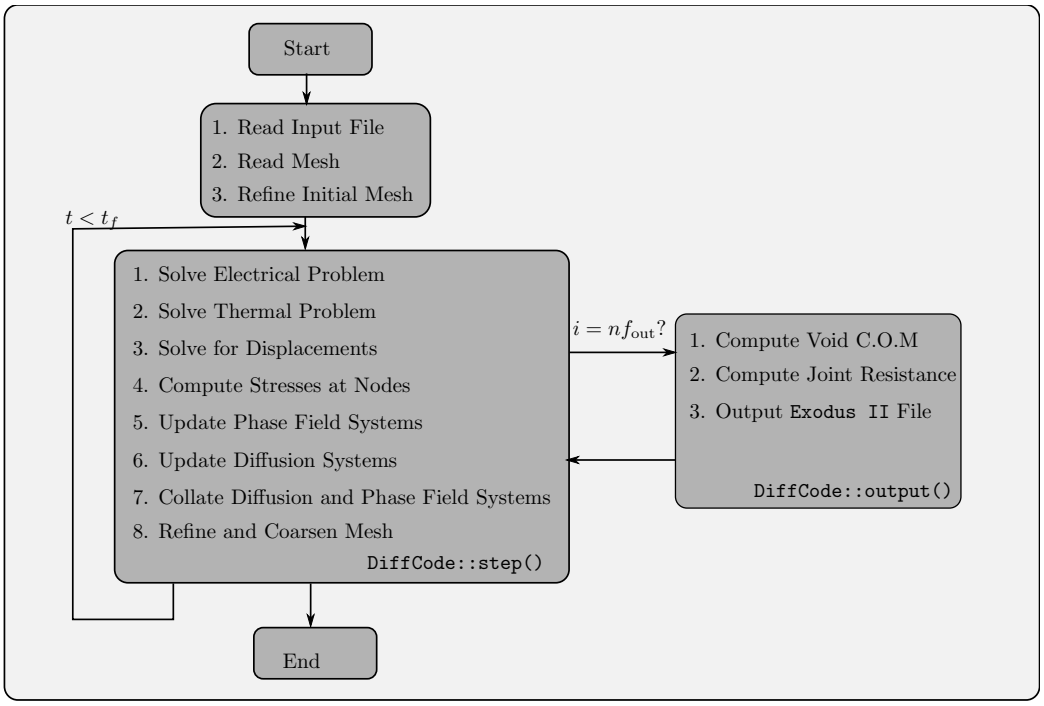

Figure E.1. General flow of `DiffCode`

E.1.1 Solver Classes

The solution to the electric potential and stress are implemented as friend classes of the `DiffCode` classes and are derived from the `libMesh` `LinearImplicitSystem` class. The dirichlet boundary conditions are applied using the `libMesh` `Dirichlet-Boundaries` framework. Additional `NeumannBoundary` classes are used to hold and apply the neumann boundary conditions. The heat transfer field solution is derived from `libMesh`'s `TransientLinearImplicitSystem` class. The `libMesh` transient systems allow the solution of time-stepping problems and to consider initial conditions. The Dirichlet and Neumann boundaries are applied in the same way.

AverageToNodes

In addition, there is an additional `AverageToNodes` class. The `AverageToNodes` class implements methods to take information that is available at gauss points and extrapolates it to the nodes. In addition, it also uses a small diffusive component to eliminate the noise that enters the solution when fields are extrapolated to the nodes. This is implemented as a `libMesh LinearImplicitSystem`. This class is also used for the computation of the stress fields. The stress fields and the stress invariants are computed at the gauss points and then averaged to the nodes using a global least squares solution, with the mentioned diffusive smoothing.

LinearCahnHilliard

The `LinearCahnHIlliard` class is derived from `libMesh`'s `TransientLinearImplicitSystem`. A `LinearCahnHilliard` object is created for each region which is indicated to be a phase-field region in the input file. `libMesh` allows the solution for the system to be restricted to a local region of the mesh. While there are no Dirichlet boundary conditions for the solution of the Cahn Hilliard system, contact angle conditions are needed. These are applied as Neumann boundary conditions which are implemented as C++ struct.

Diffusion

Similar to the `LinearCahnHilliard` object, there is a `Diffusion` object that corresponds to each of regions that is marked as a phase-field region. These are implemented as derived from `libMesh`'s `TransientLinearImplicitSystem`. Both Neumann and Dirichlet boundary conditions are implemented and can be applied.

E.1.2 Utility Classes

In addition to the solver classes, there are a couple of utility classes that are used for book-keeping and for organizing data. These are described in this section.

`Material`

The material properties for each material in the problem domain are stored as a `Material` object. The material object has methods to set and get all the material properties. The material properties are stored in a C++ `map` in the `DiffCode` class. The name of the material is used as the key in the `map`.

`ActiveRegion`

The next utility class that is implemented is the `ActiveRegion` class. The `ActiveRegion` object is equivalent to an ABAQUS section assignment. It holds the information of the elements and nodes corresponding to each of the components of the mesh. For example in an assembly with a solder joint, with an associated line and substrate, there is an active region for each of the three parts. In addition, if the active region has diffusion and the phase-field problem needs to be solved over the domain, it is marked as a phase-field region. Finally, if the active region is a phase-field region, the `ActiveRegion` object has the methods to create the initial void conditions.

`CollatedPhaseField`

It is inconvenient to access each `LinearCahnHilliard` separately while constructing the material properties for the solution of the electrical potential gradient and the stresses. Another place where access is needed to the phase-field variable in all regions is when the mesh is being refined. Hence, the values of the phase-field and the vacancy concentration are collated into an object of the `CollatedPhaseField`. This

is implemented as an extension of the `ExplicitSystem` class in `libMesh`. `ExplicitSystem` is the super class of `ImplicitSystem` in `libMesh`, and is similar except for a `solve()` method. This allows the value of the phase-field to be collected into a single system for output and for the purpose of computing material properties.

In addition, the `CollatedPhaseField` class has methods for mesh refinement with respect to the phase-field value. This is achieved by computing the average value of the phase-field variable over each element as,

$$\phi_{\text{average}} = \frac{\sum_{i=1}^{n_{\text{qp}}} \phi_{\text{qp}}}{n_{\text{qp}}}. \tag{E.1}$$

In the above n_{qp} is the number of quadrature points. ϕ_{average} is compared with the upper and lower limits for the phase-field, and if the value of ϕ_{average} lies between the two limits, the element is marked for refinement. Otherwise, the element is marked to be coarsened.

`StressSystem`

The solution of the diffusion and phase-field problems need the gradient of stress based quantities. This is achieved by using another class derived from `libMesh`'s `ExplicitSystem` class. The class has variables corresponding to all the stress and strain variables. In addition, there are variables for the stress invariants and strain energy. The values computed in the `AverageToNodes` object are stored in the `StressSystem` class.

E.2 Code Usage

Some details on the usage of the code are described in the following. In the first part of the section, the creation of geometry and the initial void configuration is described. Later the actual compilation and building of the code is discussed, as

well as the creation of input files and options files to pass information and material properties to the `DiffCode`.

E.2.1 Geometry Input

`DiffCode` gets geometry and mesh information from ABAQUS `.inp` files. While `libMesh` provides an `AbaqusIO` class which provides functions to read ABAQUS meshes. However, this is not capable of reading all ABAQUS `.inp` files. In particular the `libMesh` version of `AbaqusIO` is incapable of reading files generated by ABAQUS CAE. Instead, `DiffCode` uses a modified version of `AbaqusIO`, with features which are specific to the needs of `DiffCode`. The major differences are support for generated node and element sets. In addition, the modified `AbaqusIO` allows the selection of specific node and element sets for reading and allows them to be designated as active regions.

To create a mesh in ABAQUS CAE suitable for use with `DiffCode`, the different regions of the mesh for material assignment should be part of a consistent node and element set. The easiest way to construct this is through geometry sets in ABAQUS CAE, which constructs a node and element set of the same name. The boundaries of the geometry are to be created as ABAQUS surfaces. It is easier to apply Neumann boundary conditions on ABAQUS surfaces as opposed to standard ABAQUS node and element sets as it is easier to determine the direction of the surface elements.

Each of the geometry sets in the ABAQUS CAE input file corresponds to an `DiffCode` active region object. The code can at present not handle intersecting geometry sets, and the geometry sets need to be disjoint. `DiffCode` active regions correspond to ABAQUS section assignments. While defining an active region in the `DiffCode` input file, it is necessary to define the node and element set file corresponding to the active region, the material property associated with the region, and finally if the active region is a phase-field region.

E.2.2 Initial Conditions

The code allows arbitrary numbers of elliptical (in 2D) and ellipsoidal (in 3D) voids to be created as initial conditions. The voids are created by using the equations for the ellipse and the ellipsoid in plane polar or spherical polar co-ordinates. The equation for an ellipse with axes (a, b) in the plane polar co-ordinates (r, θ) can be written as,

$$r = ab\left(b^2\cos^2\theta + a^2\sin^2\theta\right)^{-\frac{1}{2}}. \tag{E.2}$$

In the above, a is the axis of the ellipse along $\theta = 0$, while b is the axis along $\theta = \frac{\pi}{2}$. Similarly, the equation for an ellipsoid with axes (a, b, c) in the spherical polar co-ordinates (r, θ, ψ) can be written as,

$$r = abc\left(b^2c^2\cos^2\theta\sin^2\psi + a^2c^2\sin^2\theta\sin^2\psi + a^2b^2\cos^2\psi\right)^{-\frac{1}{2}}. \tag{E.3}$$

In the above, $\theta \in [0, 2\pi]$ and $\psi \in [-\frac{\pi}{2}, \frac{\pi}{2}]$. a is the axis of the ellipsoid at $\theta = 0$,$\psi = 0$, b is axis of the ellipsoid at $\theta = \frac{\pi}{2}, \psi = 0$, while c is at $\psi = \pm\frac{\pi}{2}$.

If $a \approx b(\approx c)$, $r(\theta)$ or$r(\theta, \psi)$ can be used as an approximate distance function for the ellipse or ellipsoid. This can be used to construct phase-field versions of the ellipses and ellipsoid. The information needed for the construction of the ellipse or ellipsoid are the center of the ellipse/ellipsoid, (x_0, y_0, z_0) and the angles $(\theta_1, \theta_2, \theta_3)$. (Only θ_1 is required in the case of the ellipse.) $(\theta_1, \theta_2, \theta_3)$ are the angles of rotations applied to the a, b and c axes of the ellipsoid sequentially. To find the value of the phase-field corresponding to a given point (x, y, z), the point is first transformed into a rotated - translated co-ordinate system with origin at the center of the ellipse,

$$\{x, y, z\} \rightarrow R_1^{-1}R_2^{-1}R_3^{-1}\{x - x_0, y - y_0, z - z_0\}. \tag{E.4}$$

In the above, R is the standard rotation matrix,

$$R_i^{mn} = \begin{cases} \delta_{mn}, & m = i, \text{or } n = i \\ R_{\text{rot}}(\theta_i), & m, n \neq i. \end{cases} . \tag{E.5}$$

$R_{\text{rot}}(\theta)$ is the standard rotation matrix,

$$\begin{bmatrix} \cos\theta & \sin\theta \\ -\sin\theta & \cos\theta \end{bmatrix} . \tag{E.6}$$

The co-ordinates of the point in the transformed (x_t, y_t, y_t) co-ordinate systems are now used to compute the values of r_t, θ_t and ψ_t as,

$$r_t = \sqrt{x_t^2 + y_t^2 + z_t^2} \tag{E.7}$$

$$\theta_t = \tan^{-1} \frac{x_t}{y_t} \tag{E.8}$$

$$\psi_t = \cos^{-1} \frac{z_t}{r_t}. \tag{E.9}$$

These value of θ_t, ϕ_t are used to compute the distance of the ellipse from the center of the ellipse in the particular direction. This can be used to compute the value of the phase-field function, by substituting into the appropriate equilibrium phase-field profile for the potential function. For the bi-quadratic potential, the equilibrium profile can be written as,

$$\phi(d) = \tanh \frac{d}{\sqrt{2}\epsilon}. \tag{E.10}$$

where, d is the signed distance from the interface. The signed distance can be computed as, $d = r - r_t$, and the value of the phase-field is computed, $\phi(r - r_t)$.

Multiple Voids

The code allows the initial void shape to be specified as the Boolean union of an arbitrary number of voids. This is implemented by computing a vector with the value of the phase-field function for each of the voids. The final void geometry can then be specified as the minimum of these values,

$$\phi_{\cup} = \min\{\phi_1, \phi_2, \ldots\}. \tag{E.11}$$

This can be thought of in terms of the $R-$functions [172].

E.2.3 Input Files

An example of the input file used by `DiffCode` is presented here in Listing E.1, along with comments. More details on generating these input files are found in [173].

Listing E.1`DiffCode` input file example

```
# DiffCode input file.
#####################################################
jobname=multi_joint_test # name of the job
#####################################################
abqfile=2soldermodel.inp # name of the abaqus input file
dim=2 # dimension of problem
#####################################################
small_number=1e-8 # small number to prevent singular matrices
#####################################################
dt=1e-4 # timestep
dt0=1e-4 # initial timestep
tf =1 # final time
ofreq=20 # frequency of output
output_everything=false # switch to output working solutions
```

```
epsilon=1e-2 # notional interface thickness parameter
#####################################################
# Refinement information
#####################################################
init_refinement=3 # number of levels of initial refinement in the void
   region
init_uniform_refinement=1 # number of initial uniform refinement
refinement_levels=4# maximum number of refinement levels
refine_fraction=0.9 # fraction of elements that need refienement
coarsen_fraction=0.1 # fraction of elements that need to be coarsened
refinement_loops=1 #number of refinement loops
lower_pf=-0.95 # lower limit for phase field variable
upper_pf=0.95 # upper limit for phase field variable
error_based_refinement=false # switch between error based and value based
   refinement
#########################################
stabilization_param=5.0 # stabilization parameter for use with the cahn
   hilliard solver
second_order=true # switch to allow second order solution
#####################################################
# active region information
#####################################################
n_regions=5 # total number of regions
region_1=solder1
region_2=solder2
region_3=top1
region_4=top2
region_5=base # name for each of the region
#####################################################
# active regions
#####################################################
```

```
[regions] # regions section..
[./solder1] # first region
material=solder # material name
phase_field_region=true # whether the region needs the phase field equation
    to be solved
element_set=solder1 # abaqus element set corresponding to the element set
n_surfs=2 # number of surfaces
surfaces='solder1bottom solder1top' # names of the surfaces
n_voids=2 # number of voids
[./void_1] #info for first void
center='-3.10 .86 ' # center of void
size='0.06 0.06' # major and minor axis of ellipsoid
angles='0 0' # angle of void 1 angle for 2 d and 3 for 3 d
[../void_2] #info for second void
center='-3. .56 ' # center of void
size='0.04 0.06' # major and minor axis of ellipsoid
angles='0 0' # angle of void 1 angle for 2 d and 3 for 3 d
[]
.
. # information for second solder joint
.
[]
##############################################################################
[regions/top1]
material=copper
phase_field_region=false
element_set=top1
n_surfs=2
surfaces='left1 top1'
[]
##############################################################################
```

```
[materials] # material definition
n_mats=2 # no. of materials
name_1=solder # name of first material
name_2=copper # name of second material
[]
[materials/solder]
c=1.0 # electrical conductivity
E=1000.0 # young's modulus
nu=0.33 # poisson's ration
sZ=5.0 # surface electromigration parameter
sE=-1.0 # surface Elastic Energy parameter
sR=0.0 # surface reaction rate
sQ=1.0 # surface thermomigration parameter
dT='.25 .25 0.0' # bulk diffusivity tensor in Voigt form
sd=1.0 # surface diffusivity
gamma=1.0 # surface energy
Z=0.0 # bulk electromigration parameter
Q=1.0 # bulk thermomigration parameter
rt=10.0 # Gas constant times temperature
omega=0.0 # stress diffusion parameter
k=1.0# thermal conductivity
rhocp=1.0 # thermal mass
alpha=1e-6 # thermal expansivity
hf=1.0 # heat factor for joule heating
[]
[materials/copper]
#definition of other material
[]
# Boundary conditions
[cahn_hilliard/solder1]
n_nbcs='2 false false'
```

```
nbc1='solder1bottom 90 1'
nbc2='solder1top 90 1'
[]
# boundary conditions for other cahn hilliard
[]
[stress]
n_nbcs=1 #no. of neumann boundary conditions
nbc1='top 0.1 0.0' #surface followed by x,y values of traction
n_dbcs=1
dbc1='base_bottom 0.0 0.0 yes yes' #surface followed by values and whether
   the particular constraint is active (to allow for rollers)
invar='2 p ener vm' # invariants to compute (pressure energy, von-mises
   stress)
[]
### boundary conditions for diffusion problem
[diffusion/solder1]
n_dbcs=1
dbc1='solder1bottom 1.0'
[]
# boundary conditions for other diffusion parameters
[]
[int_av]
int_param=.01 # part of the interface to average quantities over
alpha=1.0 # direct average
beta=0.0001 # diffusional term
[]
```

Petsc Options

`DiffCode` assumes that `libMesh` is installed with `PETSc`. `PETSc` provides an easy way to configure the solvers and preconditioners through the command line. This

allows an easy way to drastically change the solvers being used without significant programming. There are multiple linear solvers that are called throughout a run of `DiffCode`, and they require very different options for efficient solution. This is accomplished by `PETSc` by assigning a prefix for the command line options. The prefixes for each of the solvers is tabulated in Table E.1.

Table E.1. Prefixes to set options for the various `PETSc` solvers.

Solver	Prefix
Electrical potential	`elec_`
Stress solver	`stress_solve_`
Temperature	`therm_`
Vacancy Diffusion	`diff_solve_`
Cahn Hilliard	`ch_solve_`

E.2.4 Making and Running `DiffCode`

To run the code, the system should have `libMesh` and `PETSc` installed. In the code folder (assuming `bash`),

```
EXPORT LIBMESH_DIR=/path/to/libmesh/installation
```

This will ensure the availability of `libMesh` variables while building the code. The code is best compiled with the `MPI` compilers with which `libMesh` and `PETSc` have been compiled. This is best achieved by adding the bin folder of the `PETSc` architecture with which `libMesh` has been to the `PATH`. This is done by,

```
EXPORT PATH=/path/to/petsc/architecture/bin:$PATH
```

The code can now be built by,

```
make
```

To run the code, the executable should be available in the path. This is done by,

```
EXPORT PATH=/path/to/code:$PATH
```

The executable is available in the system `PATH` and can be used for simulations. To run the code, the input file, the `PETSc` options file and the ABAQUS `.inp` file containing the mesh should be available in the system `PATH`. The `PETSc` options can also be directly supplied at the command lines. The code is run as

```
diff_code --inp=input_file -options_file petsc_options_file -
    other_petsc_options
```

In case the code is to be run in parallel, it is recommended that the same `mpirun` command that `PETSc` is compiled with be available on the `PATH`. The code can then be run as,

```
mpirun -n <np> diff_code --inp=input_file -options_file petsc_options_file
    -other_petsc_options
```

The code has currently been tested on upto 48 processors.

VITA

VITA

Subramanya was born in Hyderabad, India and spent his formative years in the plains and hills of North and West India. He got his bachelor's degree in Mechanical Engineering at the Indian Institute of Technology Madras, and has been working on his PhD at Purdue University ever since. Over the past few years, his hobbies at various times have been photography, modular origami and bread-making.

LIST OF PUBLICATIONS

LIST OF PUBLICATIONS

- Published
  - S. Sadasiva, G. Subbarayan, L. Jiang, and D. Pantuso. Numerical simulations of electromigration and stressmigration Driven void evolution in Solder interconnects. *Journal of Electronic Packaging*, 134(2):020907, 2012
  - S. Sadasiva, G. Subbarayan, L. Jiang, and D. Pantuso. Numerical simulations of electromigration and stress migration Driven void propagation in pb free Solder interconnects. In *ASME 2011 Pacific Rim Technical Conference and Exhibition on Packaging and Integration of Electronic and Photonic Systems*, pages 585–590. American Society of Mechanical Engineers, 2011
- In preparation for submission
  - A. Udupa, S. Sadasiva, and G. Subbarayan. Numerical simulations of late stage growth of intermetallics in pb free Solder microbumps. *in preparation for submission to Modelling and Simulations in Materials Science*, 2015
  - S. Sadasiva and G. Subbarayan. Multiphase field simulations of electromigration Driven intergranular void growth and evolution. *in preparation for submission to Modelling and Simulations in Materials Science*, 2015
  - S. Sadasiva and G. Subbarayan. Numerical simulations of the effect of anisotropic diffusivity in tin on electromigration failure in Solder interconnects. *in preparation for submission to Journal of Electronics Packaging*, 2015
  - S. Sadasiva, G. Subbarayan, and D. Pantuso. 3 dimensional simulations of electromigration Driven void growth and failure in Solder joints. *in preparation for submission to Modeling and Simulations in Material Science*, 2015